

→ LIBRARY (Research)

1404

UILU-ENG-89-2006

AISC E&R Library



## ENGINEERING STUDIES

Research Series No. 547

*key words:*  
1- optimization  
2- frames, multi-story



ISSN: 0069-4274

# OPTIMAL DESIGN OF FRAMED STRUCTURES UNDER MULTIPLE LOADING CONDITIONS BASED ON A STABILITY CRITERION

By

Shahram Pezeshk

and

Keith D. Hjelmstad

*primary author*

A Report to  
The National Science Foundation  
Research Grant ECE 86-58019, and  
The American Institute of Steel Construction

Department of Civil Engineering  
University of Illinois at Urbana-Champaign  
Urbana, Illinois

August 1989

RR1404

7548

**Optimal Design of Framed Structures  
Under Multiple Loading Conditions  
Based on a Stability Criterion**

By  
**Shahram Pezeshk**  
and  
**Keith D. Hjelmstad**

A Report to  
**The National Science Foundation**  
Research Grant ECE 86-58019,  
and  
**The American Institute of Steel Construction**

**Department of Civil Engineering**  
**University of Illinois at Urbana-Champaign**  
**Urbana, Illinois**

**August 1989**

<b>REPORT DOCUMENTATION PAGE</b>	1. REPORT NO. UIUL-ENG-87-2005	2.	3. Recipient's Accession No.
4. Title and Subtitle OPTIMAL DESIGN OF FRAMED STRUCTURES UNDER MULTIPLE LOADING CONDITIONS BASED ON A STABILITY CRITERION		5. Report Date August 1989	6.
7. Author(s) S. Pezeshk and K. D. Hjelmstad		8. Performing Organization Rept. No. SRS 547	
9. Performing Organization Name and Address Department of Civil Engineering University of Illinois 205 N. Mathews Avenue Urbana, IL 61801		10. Project/Task/Work Unit No.	
12. Sponsoring Organization Name and Address National Science Foundation American Institute of Steel Construction		11. Contract(C) or Grant(G) No. (C) (G) ECE 86-58019	
		13. Type of Report & Period Covered	
15. Supplementary Notes		14.	
16. Abstract (Limit: 200 words)			
<p>An optimization-based design methodology is presented for improving the strength and overall stability of framed structures. The design methodology is a multiple-objective optimization procedure whose objective functions involve the buckling eigenvalues and eigenvectors of the structure. Designs are constrained to have constant weight. An iterative optimality criterion method is used to solve the optimization problem. The method provides a general tool for <b>designing complex structures with nonlinear behavior</b> and generally leads to <b>designs with better limit strength and stability while avoiding nonlinear analysis in the optimization cycle</b>. The approach is indirect, but is effective and efficient.</p> <p>The design procedure is developed for two and three dimensional framed structures which have limit states governed by inelastic limit loads. The method presented as two main novelties: (a) frequency weighting functions are introduced and incorporated into the objective function to control the vibration characteristics of the designs, and (b) the new design methodology includes an effective way to combine multiple loading conditions. Several examples are presented to evaluate the validity of the underlying assumptions and to examine the performance of the procedure.</p>			
17. Document Analysis a. Descriptors			
Optimization, Steel Structures, Stability			
b. Identifiers/Open-Ended Terms			
c. COSATI Field/Group			
18. Availability Statement	19. Security Class (This Report) Unclassified	21. No. of Pages 193	
	20. Security Class (This Page) Unclassified	22. Price	



## TABLE OF CONTENTS

CHAPTER	Page
<b>1 INTRODUCTION .....</b>	<b>1</b>
1.1 Introduction .....	1
1.2 Stability .....	2
1.3 Multiple Loading Conditions .....	3
1.4 Optimization Algorithm .....	4
1.5 Report Organization .....	6
1.6 Acknowledgements .....	7
<b>2 OPTIMAL DESIGN OF PLANAR FRAMED STRUCTURES BASED ON A STABILITY CRITERION .....</b>	<b>8</b>
2.1 Introduction .....	8
2.2 Motivation .....	8
2.3 Formulation .....	10
2.4 Sensitivity Analysis .....	13
2.5 Solution Procedure .....	15
2.5.1 Recurrence Relations .....	15
2.5.2 Equation to Determine Lagrange Multiplier .....	17
2.5.3 Active/Passive Set Strategies .....	18
2.5.4 Scaling Procedure .....	18
2.5.5 Convergence Criterion .....	19
<b>2.A CROSS SECTIONAL PROPERTIES .....</b>	<b>20</b>
2.A.1 Overview .....	20
<b>3 APPLICATION OF 2-D OPTIMIZATION TO FRAMED STRUCTURES .....</b>	<b>26</b>
3.1 Introduction .....	26
3.2 Analysis Procedure .....	26
3.2.1 Damping Matrix Used for Dynamic Analyses .....	26
3.2.2 Time Interval Used for Dynamic Analyses .....	28
3.2.3 Damage Estimates .....	28
3.3 Three Story Frame .....	30
3.3.1 Preliminary Design .....	30
3.3.1.1 Code Lateral Loads .....	30
3.3.1.2 Base Shear .....	31
3.3.1.3 Code Distribution .....	31



	Page
3.3.2 Optimization .....	33
3.3.3 Analysis .....	34
3.3.4 Optimization with Frequency Weighting Function .....	39
3.4 Eight Story Frame .....	42
3.4.1 Preliminary Design .....	42
3.4.2 Optimization .....	43
3.4.3 Analysis .....	44
3.5 Conclusions .....	50
<b>4 MULTIPLE OBJECTIVE OPTIMAL DESIGN OF 3-D FRAMED STRUCTURES BASED ON A STABILITY CRITERION WITH MULTIPLE LOADING CONDITIONS .....</b>	<b>51</b>
4.1 Overview .....	51
4.2 Multicriterion Optimization .....	51
4.2.1 Noninferiority .....	52
4.3 Formulation and Development .....	54
4.4 Eigenvalue and Eigenvector Sensitivity Analysis .....	57
4.5 Recurrence Relations .....	63
4.6 Equation to Determine Lagrange Multiplier .....	64
4.7 Specialization to Specific Cross Sectional Types .....	65
4.8 Convergence Criteria .....	66
4.9 Scaling Procedure .....	66
<b>5 APPLICATION OF 3-D OPTIMIZATION ALGORITHM TO FRAMED STRUCTURES .....</b>	<b>68</b>
5.1 Overview .....	68
5.2 3-D Analysis Procedure .....	68
5.3 Description of MRF Example Problem .....	69
5.3.1 Single Loading .....	71
5.3.1.1. Four Design Variables Under Single Loading (2M-1L) ...	71
5.3.1.2. Six Design Variables Under Single Loading (3M-1L) ...	73
5.3.2 Final Observations for Optimization Under One Loading Condition .	74
5.3.3 Multiple Loading .....	87
5.3.3.1. Four Design Variables Under Two Loading Conditions (2M-2L) & N=6 .....	87
5.3.3.2 Six Design Variables Under Two Loading Conditions (3M-2L) & N=6 .....	97
5.3.3.3 Eight Design Variables Under Two Loading Conditions (4M-2L) & N=6. ....	99
5.3.4 Final Observation on the Proposed Optimization Technique Under Multiple Loading .....	102

	Page
5.4 Displacement Constraint Optimization .....	113
5.4.1 Introduction .....	113
5.4.2 Example Problems .....	113
5.4.3 Performance of the Optimized Designs Under an Unexpected Loading Condition .....	114
<b>6 APPLICATION OF 3-D OPTIMIZATION ALGORITHM TO IRREGULAR FRAMED STRUCTURES .....</b>	<b>118</b>
6.1 Introduction .....	118
6.2 Description Of SETBACK Example Problem .....	118
6.2.1 Seismic Coefficients .....	120
6.2.2 Modal Base Shear .....	121
6.2.3 Modal Forces .....	121
6.2.4 A Note on Analysis Procedure .....	123
6.3 Discussion of the Optimization Algorithm as Applied to SETBACK Frame ....	124
6.4 Displacement Constraint Optimization .....	128
6.5 General Comments .....	129
<b>7 APPLICATION OF 3-D OPTIMIZATION ALGORITHM TO HIGH-RISE FRAMED STRUCTURES .....</b>	<b>145</b>
7.1 Overview .....	145
7.1 Application of the Optimization to KORN Frame .....	145
<b>8 SUMMARY, CONCLUSIONS, AND RECOMMENDATIONS FOR FUTURE RESEARCH .....</b>	<b>149</b>
8.1 Summary .....	149
8.2 Conclusions .....	150
6.2 Recommendations for Future Research .....	152
<b>APPENDIX .</b>	
A 3-D DISPLACEMENT CONSTRAINT OPTIMIZATION PROBLEM .....	154
B SOME PRACTICAL IMPLEMENTATION ISSUES NECESSARY TO SOLVE THE BUCKLING EIGENVALUE PROBLEM .....	158
C APPROXIMATE ANALYSIS OF THE POST-LIMIT RESPONSE OF FRAMES .....	161
D SENSITIVITY OF GEOMETRIC STIFFNESS MATRIX .....	183
<b>LIST OF REFERENCES .....</b>	<b>186</b>



# LIST OF TABLES

Table	Page
3.1 Properties of the Optimized Designs Without Frequency Penalty .....	33
3.2 Frequency and the Buckling Eigenvalue of the Initial and the Optimized Designs .	33
3.3 Properties of the Optimized Designs with Frequency Penalty .....	39
3.4 Properties of the 8-Story Initial Design and Code Lateral Force Distribution ....	43
3.5 Properties of the 8-Story Optimized Design .....	43
5.1 Properties of the Optimized Designs for Case (2M-1L) .....	76
5.2 Properties of the Optimized Designs for Case (3M-1L) .....	81
5.3 Properties of the Optimized Design for Case (2M-2L) & N=6 .....	91
5.4 Properties of the Optimized Designs Using Three Material Sets, Two Loading Cases and Six Eigenpairs (3M-2L) & N=6 .....	103
5.5 Properties of the Optimized Designs Using Four Material Sets, Two Loading Conditions, and Six Eigenpairs (4M-2L) with N=6 .....	109
5.6 Properties of the Optimum Design for the Displacement Constraint Optimization Method .....	115
6.1 Mass Properties .....	120
6.2 Properties of the Final Design .....	122
6.3 Mode Shapes of the Final Design .....	122
6.4 Periods of the Final Design .....	123
6.5 Parameter Properties of the Example Problems .....	124
6.6 Dynamic Properties of the Applied Sinusoidal Loading .....	128
6.7 Properties of the Optimized Designs for the Case (5M-1L) & N=5, and $\underline{b} = 4.0, \underline{h} = 4.0$ and Case (5M-1L) & N=10, and $\underline{b} = 4.0, \underline{h} = 4.0$ .....	132
6.8 Properties of the Optimized Design for the Case (8M-1L) & N=5, and $\underline{b} = 4.0, \underline{h} = 4.0$ .....	135
6.9 Properties of the Optimized Designs for the Case (5M-1L) & N=5, and $\underline{b} = 1.8, \underline{h} = 7.5$ and Case (5M-1L) & N=10, and $\underline{b} = 1.8, \underline{h} = 7.5$ .....	137



	Page
6.10 Properties of the Optimized Design for the Case (5M-2L) & N=5, and $\underline{b} = 1.8, \underline{h} = 7.5$ .....	140
6.11 Properties of the Optimized Design Using a Displacement Constraint Approach to Minimize Volume under a Top Displacement Constraint of 1.2 Inches .....	143
7.1 Properties of the Initial and Optimized Designs ( $\underline{b} = 3.0, \underline{h} = 3.0$ ) under Single Loading Case .....	147
B.1 Subspace Iteration .....	160
C.1 Member Properties .....	177
C.2 Frame MRF-4 Properties .....	177
C.3 Summary of Results .....	178

## LIST OF FIGURES

Figure	Page
2.1 Possible Weighting Functions: (a) Bell Shaped Response Spectra; (b) Uniform Building Code; (c) Sinusoidal Response Spectra; (d) Mexico's Federal District Code .....	12
2.A.1 Empirical Relationship Between Moment of Inertia and Column Depth .....	21
2.A.2 Empirical Relationship Between Moment of Inertia and Column Depth and the Actual Members Identified by AISC .....	22
2.A.3 Different Cross Sectional Types .....	23
2.A.4 Flange Thickness Versus Web Thickness for Wide Flange Sections Identified by AISC .....	24
3.1 Topology of the 3-Story Frame .....	30
3.2 Code Shear Distribution for 3-Story Frame .....	31
3.3 Static Analysis of 3-Story Frame .....	34
3.4 Dynamic Analysis of 3-Story Frame Under Sinusoidal Base Acceleration .....	36
3.5 3-Story Frame under Pacoima Dam 1971 Earthquake Base Acceleration .....	37
3.6 Average Element Damage Statistics for 3-Story Frame .....	38
3.7 Maximum Element Damage Statistics for 3-Story Frame .....	38
3.8 Sinusoidal Response Spectra .....	40
3.9 Static Analyses of the Initial and Optimized Designs With and Without Frequency Penalty .....	40
3.10 3-Story Frame under Pacoima Dam 1971 Earthquake Base Acceleration .....	41
3.11 Topology of the 8-Story Frame .....	42
3.12 Static Analysis of 8-Story Frame .....	44
3.13 Dynamic Analysis of 8-Story Frame Under Sinusoidal Base Acceleration .....	46
3.14 Dynamic Analysis of 8-Story Frame Under Pacoima Dam 1971 Earthquake Base Acceleration .....	47
3.15 Dynamic Analysis of 8-Story Frame Under El Centro 1941 Earthquake Base Acceleration .....	48

	Page
3.16 Average Damage Statistics for 8-Story Frame .....	49
3.17 Maximum Element Damage Statistics for 8-Story Frame .....	49
4.1 Rectangular Cross Sectional Properties .....	65
4.2 I-beam Cross Sectional Properties .....	65
4.3 Scaling of Two Design Variable Design Space .....	67
5.1 Topology of the MRF Frame .....	70
5.2 Applied Loading Conditions for MRF Frame .....	70
5.3 Case (2M-1L) & N=6 and $\Pi=\{1\}$ .....	77
5.4 Case (2M-1L) & N=8 and $\Pi=\{1\}$ .....	78
5.5 Case (2M-1L) & N=10 and $\Pi=\{1\}$ .....	79
5.6 Summary of Load-Deformation Curves for the Optimized Designs Under Category (3M-1L) .....	80
5.7 Case (3M-1L) & N=6 and $\Pi=\{1\}$ .....	82
5.8 Case (3M-1L) & N=8 and $\Pi=\{1\}$ .....	83
5.9 Case (3M-1L) & N=10 and $\Pi=\{1\}$ .....	84
5.10 Summary of Load-Deformation Curves for the Optimized Designs Under Category (3M-1L) .....	85
5.11 Magnitude of Dominant Mode Eigenvalues of the Optimized Design Cases (2M-1L) and (3M-1L) .....	85
5.12 Buckling Mode Shapes of the Initial Design and the Optimized Design Using Six Design Variables and Eight Eigenpairs [(3M-1L) & N=8] .....	86
5.13 Case (2M-2L) & N=6 with $\Pi=\{1,1\}$ .....	92
5.14 Case (2M-2L) & N=6 and $\Pi=\{1,1\}$ Using NLC=2 to Formulate the Buckling Eigenvalue Problem .....	93
5.15 Case (2M-2L) & N=6 and $\Pi=\{1,2\}$ .....	94
5.16 Case (2M-2L) & N=6 and $\Pi=\{2,3\}$ .....	95
5.17 Case (2M-2L) & N=6 and $\Pi=\{1,3\}$ .....	96



	Page
5.18 Case (3M-2L) & N=6 with $\Pi=\{1,1\}$ , and $\underline{b} = 5.0$ , $\underline{h} = 3.0$ .....	104
5.19 Case (3M-2L) & N=6 with $\Pi=\{1,2\}$ , and $\underline{b} = 5.0$ , $\underline{h} = 3.0$ .....	105
5.20 Case (3M-2L) & N=6 with $\Pi=\{1,2\}$ , and $\underline{b} = 4.5$ , $\underline{h} = 3.0$ .....	106
5.21 Case (3M-2L) & N=6 with $\Pi=\{1,3\}$ , and $\underline{b} = 5.0$ , $\underline{h} = 3.0$ .....	107
5.22 Case (3M-2L) & N=6 with $\Pi=\{3,3\}$ , NLC=2, and $\underline{b} = 5.0$ , $\underline{h} = 3.0$ .....	108
5.23 Case (4M-2L) & N=6 with $\Pi=\{1,1\}$ .....	110
5.24 Case (4M-2L) & N=6 with $\Pi=\{1,2\}$ .....	111
5.25 Distribution of the Material Sets for Case (4M-2L) .....	112
5.26 Limit Load Comparisons .....	112
5.27 Imperfection Loading .....	115
5.28 Load-Deformation Curves for Displacement Control Optimization Technique Under Loading Case I and II .....	116
5.29 Load-deformation Curves Using Different Optimization Techniques Under Load Case I Plus a Load of 0.5 kips Applied in Z-direction at the Top of One of the Second Story Columns .....	117
6.1 Topology of the SETBACK Frame .....	119
6.2 Load Case I (100% $Q_E$ in X-direction plus 30% $Q_E$ in Y-direction) .....	130
6.3 Load Case II (100% $Q_E$ in Y-direction plus 30% $Q_E$ in X-direction) .....	130
6.4 Nonlinear Static Analysis of the Initial Design: (a) Load Factor Versus Norm of Nodal Displacements; (b) Load Factor Versus Lateral Top Displacement ....	131
6.5 Case (1): with (5M-1l) & N=5, and $\underline{b} = 4.0$ , $\underline{h} = 4.0$ .....	133
6.6 Case (2): with (5M-1) & N=10, and $\underline{b} = 4.0$ , $\underline{h} = 4.0$ .....	134
6.7 Distribution of Material Sets for (8M-1L) & N=5 .....	135
6.8 Case (3): with (8M-1L) & N=5, and $\underline{b} = 4.0$ , $\underline{h} = 4.0$ .....	136
6.9 Case(4): with (5M-1L) & N= 5, and $\underline{b} = 1.8$ , $\underline{h} = 7.5$ .....	138
6.10 Case (5): with (5M-1L) & N=10, and $\underline{b} = 1.8$ , $\underline{h} = 7.5$ .....	139

	Page
6.11 Case (6): with (5M-2L) & $N=5$ , $\Pi=[1,1]$ , and $\underline{b} = 1.8$ , $\underline{h} = 7.5$ .....	141
6.12 SETBACK Frame under Sinusoidal Base Acceleration with Amplitude and Frequency of the Base Acceleration Chosen to Give the Same Dynamic Magnification Factor for Both Designs .....	142
6.13 Analyses of Optimized Design Based on Stability Criterion and Optimized Design Based on Displacement Constraint; (a) Under Load Case I; (b) Under Load Case II .....	144
7.1 Topology of KORN Frame and Loading Conditions .....	146
7.2 Spectral Evolution and the Load Deformation Curves for Frame KORN .....	148
C.1 Idealized Structural Behavior for Rankine-Type Estimate .....	171
C.2 Response of MRF-1 .....	179
C.3 Response of MRF-2 .....	179
C.4 Response of MRF-3: (a) Estimates Based on Eqn. (2.13); (b) Estimates Based on Eqn. (2.18) Using Mode One; (c) Estimates Based on Eqn. (2.18) Using Other Modes; (d) Evolution of Participaton Factors: (P+D) Case; (e) Evolution of Participation Factors: (D) Case; (f) Evolution of Participation Factors: (P) Case .....	180
C.5 Response of MRF-4: (a) Estimates Based on Eqn. (2.13); (b) Estimates Based on Eqn. (2.18) Using Mode One; (c) Estimates Based on Eqn. (2.18) Using Other Modes; (d) Evolution of Participaton Factors: (P+D) and (D) Cases; (e) Evolution of Participation Factors: (P) Case .....	181
C.6 Response of EBF-1 .....	182
C.7 Response of EBF-2 .....	182

## LIST OF SYMBOLS

The important symbols and notations used in this dissertation are defined where they are first appear in the text and given below:

- $()^a$  = (superscript "a") indicates an active design variable;
- $()^p$  = (superscript "p") indicates a passive design variable;
- $A_i$  = area of element in group  $i$ ;
- $b$  = width of a rectangular cross section;
- $B$  = strain displacement operator;
- $\beta$  = period ratio of the structure to the applied loading;
- $\beta_{ij}$  = weighted modal participation of the applied loading;
- $C(x)$  = constraint function;
- $C$  = structural damping matrix;
- $D$  = elastic moduli;
- $D$  = dead loads;
- $D_j$  = nodal displacements for  $j$ th constraint;
- $\bar{D}_j$  =  $j$ th assigned nodal displacement constraint;
- $\delta_m$  = maximum deformation obtained during cyclic loading;
- $\delta_u$  = maximum attainable monotonic deformation ;
- $\epsilon_{ij}$  = strain;
- $\dot{\epsilon}_{ij}^p$  = plastic strain rate;
- $F_b$  = allowable bending stress;
- $F_i$  = the lateral force applied to level  $i$ ;
- $F_t$  = the portion of  $V$  considered concentrated at the top of the structure;
- $f_i$  =  $i$ th applied loading;
- $\phi_i$  =  $i$ th buckling mode shape;
- $G, G_1, G_1$  = geometric stiffness matrices;
- $\Gamma$  = given volume or initial cost of the structure;
- $h$  = height of a rectangular cross section;
- $H$  = variation of discrete nodal displacements;
- $K$  = structural elastic stiffness matrix;



- $K_p^A$  = axial plus shear contribution to stiffness for element  $p$  with cross sectional areas factored out;
- $K_p^M, K_p^m, K_p^T$  = major axis bending, minor axis bending, and torsional contribution to stiffness for element  $p$  with relevant cross sectional properties factored out;
- $I$  = Occupancy importance factor;
- $L_i$  = length of  $i$ th element;
- $L$  = live loads;
- $L[]_x$  = linearizing about the configuration  $x$ ;
- $\lambda_L$  = geometrically linear load factor;
- $M$  = number of element groups;
- $M_0$  = flexural capacity;
- $M$  = structural mass matrix;
- $m$  = applied moment;
- $M_{aa}$  = set of groups with both design variables active;
- $M_{ap}$  = set of groups with height passive and width active;
- $M_{pa}$  = set of groups with width passive and height active;
- $M_{pp}$  = set of groups with both height and width passive;
- $\mu_i$  =  $i$ th elastic critical buckling eigenvalue;
- $N$  = axial force;
- $N_0$  = axial capacity;
- $N$  = number of eigenpairs used in the objective function;
- $N_v$  = number of independent design variables defining a cross section ( $N_v=3$  for I-beam, and  $N_v=2$  for a rectangular cross section);
- $N_L$  = number of loading conditions considered;
- $\omega$  = vibration frequency;
- $\Omega_i$  = specific mass of group  $i$ ;
- $p$  = applied axial force;
- $p_j(\omega)$  = vibrational weighting function;
- $\Pi_j$  = vector containing a set of index numbers with one-to-one correspondence with the bucking eigenvalues;
- $q$  = applied forces;
- $q$  = applied transverse force;

- $Q$  = earthquake Loads;  
 $\hat{R}, \hat{R}_0, \hat{R}_1$  = internal shear and axial forces, proportional load, dead load;  
 $\rho$  = mass density;  
 $\sigma_{ij}$  = stress;  
 $\psi_i$  =  $i$ th vibration mode shape;  
 $S$  = Coefficient for site-structure resonance;  
 $T$  = fundamental natural frequency;  
 $u$  = cross sectional displacements;  
 $u$  = axial displacements;  
 $V$  = shear force;  
 $V_0$  = shear capacity;  
 $x$  = total design vector;  
 $x_i$  = design vector for group  $i$ ;  
 $x_{ij}$  = design variable  $j$  from group  $i$ ;  
 $x_i$  =  $i$ th design variable;  
 $\underline{x}_i$  = minimum permissible design variable of the group  $i$ ;  
 $\bar{x}_i$  = maximum permissible design variable of the group  $i$ ;  
 $\xi$  = Lagrange multiplier;  
 $\xi_1, \xi_2$  = percentage of the critical damping;  
 $\Xi$  = strain gradient;  
 $\eta_f$  = yield function;  
 $w_i$  = the portion of total dead load which is located at or is assigned to level  $i$   
 $Z$  = objective function;  
 $Z$  = seismicity zone (Chapter 3);  
 $\zeta$  = scaling factor.

## CHAPTER 1

### INTRODUCTION

#### 1.1. Introduction

Recent advances in computational mechanics and nonlinear analysis have provided structural engineers with general and systematic procedures for modeling and analyzing complicated structures. Almost any complex structure can be analyzed using a finite element approach considering geometric and material nonlinearities, under both static and dynamic loads. In spite of the achievements in analysis, the design procedure has not evolved. Most of today's designs are based on traditional trial and error procedures wherein a structure is designed, analyzed, and checked for compliance with the design criteria. If the performance of the structure does not meet the defined design criteria, then the structure is redesigned. This process of design, analysis, and checking continues until a design is achieved. The final design is generally not optimal in any sense. The method of trial and error is especially ineffective for complex designs that are beyond the experience and intuition of the designer. Furthermore, the designer usually unable to account for global aspects of design such as overall stability, ductility, and strength.

The objective of this study is to understand and gain knowledge about the nonlinear behavior of framed structures from analyses and incorporate the knowledge into the framework of an optimization-based design methodology to enhance the overall stability, ductility, and strength of framed structures. Traditionally, stability and ductility have played a secondary role in design process or have been ignored completely. However, these issues are fundamentally important to robust structural performance and they must be included in the design process.

Many algorithms have been developed to improve the limit strength of structures. In most of these applications geometrically linear analysis is employed with the consequence that overall strength of the design is overestimated. Directly optimizing the limit load of the structure would require a full nonlinear analysis at each iteration which would be prohibitively expensive. The objective of this research is to develop an algorithm that can improve the limit-load of geometrically nonlinear framed structures while avoiding the nonlinear analysis.



## 1.2. Stability

Based on observations made on the limit and post-limit behavior of elasto-plastic frames, Hjelmstad and Pezeshk (1988) developed an approximate model of the nonlinear behavior of this type of structure. From the model it can be observed that the overall stability and strength of a structure can be improved by maximizing its linearized buckling eigenvalues. The design methodology developed in this study exploits this observation and suggests an optimization-based procedure whose objective function involves a linear combination of the buckling eigenvalues of the structure. A constant volume constraint with bounds on the design variables is used in conjunction with an optimality criterion approach for search.

The design procedure is formulated to improve the overall performances of both planar and space framed structures using rectangular or I-beam cross sections. Three-dimensional design problems are computationally more expensive to consider than the planar design problems, but they yield insight into the real behavior of the structure and can help avoid some of the problems that might appear in planar design procedure such as the need for out-of-plane buckling constraint.

There are different types of instability that can occur in a structure. Among these are local buckling of the thin elements (e.g. flange and web) of a member, single member buckling in a complex structure, and buckling of the structure as a whole. Buckling of a structure depends both upon the constitution of the structure and on the loading, which has some spatial variation and is either static or time dependent. In this study we are primarily concerned with the global stability of structures under static loads. It is up to the designer to select a representative spatial variation of loads with which to carry out the design. The resulting structure will be most robust in resisting those loads. We demonstrate, by way of examples, that in general improving the overall stability characteristics of structure under static loading also improves the dynamic performance.

The earliest attempt to optimize structures subjected to stability constraint was considered by Clausen (1851) where he found that for columns whose cross sections are of prescribed shape the optimal tapering will increase the buckling load by one third over that of a uniform column. Lagrange (1773) had treated the same problem earlier but arrived at the wrong result due to computational errors. The result obtained by Clausen was independently found and generalized by Nikolai (1955) for additional limit on stresses. Keller (1960) found that the strongest column among all columns having a given length and volume has a cross section in the shape of an equilateral triangle shape. Further, Tadjbakhsh and Keller (1962) derived the optimal solutions for columns clamped at one end and simply

supported at the other, and for clamped-clamped columns. The solution in the latter case was obtained with respect to the first buckling mode. Later on Olhoff and Rasmussen (1976) discovered this solution was incorrect and a bimodal solution gives the optimal shape.

Keller (1960), Tadjbakhsh and Keller (1962), Keller and Niordson (1966), and Taylor (1967) developed one-dimensional models with one design variable to maximize the buckling load of a structure with a volume constraint. The approach was based on continuum theory and not readily extendible to complex structures such as frames.

A recurrence relation based on a optimality criterion was employed by Simites, Kamat, and Smith (1973) to design a column subjected to a distributed load. An exponential recurrence relation based on an optimality criterion was proposed by Venkayya *et al.* (1973, 1974), and Khot *et al.* (1973, 1976) to design portal frames and truss structures. Khot (chapter 3 of Atrek *et al.* 1984) proposed a method based on the optimality criterion approach to minimize weight of truss structures under stability constraints. In this paper the stability constraints were stated with the requirement that the critical eigenvalues be separated by a specific interval and the critical buckling mode be the preselected one. Khot and Kamat (1983) discussed an optimization method based on optimality criterion to minimize the design weight under displacement, system stability, and element stresses for truss structures considering geometric nonlinear behavior. Kamat and Ruangsilasingha (1985) and Kamat (1987) addressed the problem of maximization of the critical load of shallow space trusses and shallow truss arches of given configuration and volume. Levy and Perng (1988) discussed the optimal design of trusses to withstand nonlinear stability requirements. In a recent paper by Lin and Liu (1989), they discussed the optimal minimum weight design of linear-elastic truss and beam elements under static loads subjected to size, stress, displacement and system buckling constraint. Finally, a recent book by Gajewski and Zyczkowski (1989) provides a complete review of optimal structural design under stability constraints with a bibliography having over 2000 entries.

### 1.3. Multiple Loading Conditions

Multiple loads and load combinations are a fundamental aspect of structural design because the structure will be expected to survive in a diverse environment. The selection of these loads and the method used to combine them constitute one of the most important aspects of the design process. One of the principal novelties of the method presented in this study is that it can efficiently design a structure



with multiple loading conditions. The formulation proposed here weights the various load cases in accordance with their level of participation in potentially important buckling events.

In recent years there have been only a few papers on the subject of multiple loading cases. Turner and Raymond (1980) used the optimality criterion approach to design columns and portal frames under multiple loading conditions. They optimized the structural buckling load for different load ratios, plotted the result in a loading space, and came up with an envelope which they referred to as the stability envelope. Chibani (1987) developed a minimum weight optimal design method for truss structures under alternate loading cases. He used a geometric programming algorithm and developed a new decomposition method to handle multiple loading cases.

Reliability-based structural optimization under stochastic loads is another approach to considering multiple loading cases. Work in this area has been done by Wen (1977, 1980a, and 1980b), and Wen and Pearce (1980) where they developed procedures for handling combinations of loads and load effects. Kim and Wen (1987) developed a method for reliability-based structural optimization under time varying random loadings with emphasis on realistic modeling of the loadings and the effect of the uncertainties of loadings on the design. In a recent recent paper, Tada and Seguchi (1989) formulated a method for the determination of the shape of structures under multiple loading cases when the direction, the magnitude, and the position of the loads vary with a known probability law. This method finds the shape which makes the total potential energy stationary under constant volume.

#### 1.4. Optimization Algorithm

The optimization procedure used for this study is based on optimality criteria method (OCM). The goal of the method is to generate a design that satisfies specified criteria, and in doing so maximize the objective function. The criteria are based on the nature of the problem and are derived by differentiating the Lagrangian with respect to the design variables. OCM is an iterative method because the constraints and the objective are nonlinear in the design variables. In deriving the optimality criteria and developing the algorithm, full use is made of the knowledge of the behavior of the constraints imposed on the structure. The algorithms are efficient because the effort is proportional to the number of constraints not the number of design variables.

Prager (1968, 1971, and 1973), Prager and Prager (1979), Prager and Taylor (1968), Sheu and Prager (1968), Prager and Shield (1968), Martin (1969, 1970), Chern and Prager (1970, 1971),



Chern (1971), Chern and Matin (1971) have done extensive work in developing a rigorous optimality criteria approach for various design problems. Most of these papers are concerned with generalized compliance constraints. Generalized compliance is defined as the virtual work of a fictitious loading system when it is subjected to the displacement field of the actual loading. For example, a single displacement constraint at a point of the structure can be treated as a compliance constraint. Compliance in this case is the virtual work of a unit load at the point of displacement constraint going through the actual displacement. When the fictitious loading coincides with the actual loading, the compliance represents the generalized stiffness of the structure.

Barnett (1961) discussed the optimal design of determinate structures for a given deflection. The OCM was formulated in terms of virtual strain energy due to a unit dummy load at the point of prescribed displacement.

Prager (1968) presented a description of the general problem of optimality criteria in structural design. Prager and Taylor (1968) discussed the specific problems associated with optimal structural design where they discussed the optimal design for maximum stiffness, maximum fundamental frequency, and maximum buckling. Sheu and Prager (1968) considered the optimal design of frames with piecewise constant specific stiffness requirement. Prager (1971 and 1973) discussed the optimal design of statically determinate beams and trusses with deflection, compliance, and stress constraint. Prager and Shield (1968) discussed optimal design of a beam-tie with two stiffness requirements. Optimal design of sandwich beams with compliance requirements under alternative loads was presented by Chern and Prager (1970). Chern and Prager (1971) developed a procedure for minimum weight design of statically determinate trusses subject to multiple constraints. Martin (1970) discussed optimal design of elastic structures for multipurpose loading. Martin (1969) discussed the optimal design of beams and frames with compliance constraints. Chern (1971) discussed optimal design of beams for alternative loads and constrains on generalized compliance and bending stiffness. He also established the necessary and sufficient conditions for global optimality for determinate structures and they can be used in an iterative fashion for indeterminate beams.

Some of the other discussions on the optimality criteria method can be found in Allwood and Weaver (1984), Atrek *et. al.* (1984), Fluery (1983), Khot (1976), Khot, Berke, and Venkayya (1979), and Khot (1981).

There are two main approaches to solve the structural optimization problem: one is based on the many rigorous numerical methods of nonlinear mathematical programming (MP) and one is based on

intuitive concepts of the optimality criteria method (OCM). There are advantages and disadvantages claimed for each method. It is claimed that MP methods are guaranteed convergence properties and are general in the sense that any type of constraints can be considered. The disadvantage of MP is the computing time which increases rapidly with the size of the problem whereas in the OCM the computing time does not increase with the number of the design variables, which makes it very effective method in solving problems with large number of design variables. The disadvantage of using OCM is the lack of generality and sound mathematical foundations (Chapter 5 of Morris (1982). Fluery and Sanders (1977 and 1983) attempted to reconcile MP and OCM and they showed that, based on a primal solution scheme, a mixed method can be described which permits a continuous transition between a strict mathematical programming method and a pure optimality criterion technique. The generalized optimality criterion is shown to be equivalent to a mathematical programming linearization method using reciprocals of the design variables. In another words MP and OCM can be considered as the two ends of the same spectrum.

### 1.5. Report Organization

Chapter 2 starts with the development of design methodology improving the limit and post-limit performances of two-dimensional frames. The motivation of the study is discussed. The optimization problem is solved using optimality criteria. A frequency weighting function is introduced and is formulated for the optimization algorithm.

The strengths and limitations of the optimization design methodology, developed in chapter 2, are investigated through its application to two building frames in chapter 3. The two design problems are optimized and then analyzed under various static and dynamic loading cases and the their quality of performance is examined.

Chapter 4 discusses the development and formulation of a multiple-objective optimal design of three-dimensional framed structures based on a stability criterion to improve their strength and stability characteristics. A efficient procedure is developed to handle multiple loading conditions. The mathematical formulation and the general concepts are presented in detail.

In chapter 5 the applicability of the proposed three-dimensional optimal design procedure with multiple loading cases is investigated by applying the method developed in chapter 4 to a two-story space frame structure. Parameter studies are performed on the size of subspace, minimum design variable



sizes, method of formulating the buckling eigenvalue problem, and the number design variables. Detail discussion of the optimization procedure and a physical interpretation of the results of the optimization method is given.

In chapter 6 the application of three-dimensional optimization design procedure to an setback structure is discussed. Parameter studies are performed to investigate the effect of different parameters on the overall performance of the optimization procedure and optimized designs under single and multiple loading conditions. The loading cases considered are the equivalent lateral static loads that are obtained following ATC-3-06 recommendations.

In chapter 7 the three-dimensional optimization procedure is applied to a high-rise building with 15 stories. The performance of the optimization and the optimized design is investigated and discussed.

Chapter 8 gives a summary of the study, conclusions, and recommendations for future research.

#### 1.6. Acknowledgments

This study was supported by the National Science Foundation under grant number ECE 86-58019 and American Institute of Steel Construction. The support from these organizations gratefully acknowledged. The results, opinions, and conclusions expressed in this report are solely those of the authors and do not necessarily represent those of the sponsors.

This report was prepared as a doctoral dissertation by Shahram Pezeshk under the supervision of Professor K.D. Hjelmstad. Professors N. Khachaturian, J.P. Murtha, D.A. W. Pecknold, and A.R. Robinson are thanked for reviewing the manuscript.



## CHAPTER 2

### OPTIMAL DESIGN OF PLANAR FRAMED STRUCTURES BASED ON A STABILITY CRITERION

#### 2.1. Introduction

The present chapter suggests an objective function to use as the basis for a design methodology for improving the strength and the overall stability characteristics of framed structures whose capacities are governed by limit-load behavior. Attention is focused on planar structures. The objective function is a linear combination of the critical buckling eigenvalues of the structure with each eigenvalue weighted by a frequency penalty function. An iterative optimality criterion method is used to solve the optimization problem.

#### 2.2. Motivation

The choice of the objective function to improve the limit and post-limit behavior of planar framed structures is motivated by observations on the nonlinear behavior of this type of structure. Hjelmstad and Pezeshk (1988) have developed an approximate model to demonstrate the effect of geometric nonlinearities on the performance of framed structures through an approximate relation which gives the full nonlinear response of a structure in terms of its geometrically linear response. A brief sketch of the approximation is presented below to justify the subsequent choice of objective function for the optimization.

Hjelmstad and Pezeshk (1988) considered the general case of a structure subjected to a combination of proportional ( $\lambda R_0$ ) and non-proportional loads ( $R_1$ ), where  $\lambda$  is the proportionality factor of the proportional loads. To facilitate the derivation they introduce an associated buckling eigenvalue problem

$$K\phi = \mu G\phi \tag{2.1}$$

where  $K$  is the linear structure stiffness matrix,  $\{\mu, \phi\}$  is the fundamental eigenpair, and  $G$  is the geometric stiffness matrix defined in terms of the two loading cases as

$$G = G_0 + \frac{1}{\mu} G_1 \quad (2.2)$$

in which  $G_0$  is the linearized geometric stiffness matrix for the proportional loads with  $\lambda = 1$ , and  $G_1$  is the linearized geometric stiffness matrix for the non-proportional loads. Assume that the eigenvector is normalized such that  $\phi^T G \phi = 1$  and let  $\alpha \equiv \mathbf{u}^T G \phi$  be a parameter which measures the magnitude of the displacement vector  $\mathbf{u}$ . Assuming that first mode behavior dominates the nonlinear response, the nonlinear load factor can be expressed in terms of the geometrically linear load factor,  $\lambda_L$ , as

$$\lambda(\alpha) = \frac{\lambda_L(\alpha) a_0 \mu - \alpha \gamma_1}{a_0 \mu + \alpha \gamma_0} \quad (2.3)$$

where  $a_0 = \mathbf{u}_0^T G \phi$  is the value of  $\alpha$  for the displacements under proportional loads only with  $\lambda = 1$ ,  $\gamma_0 \equiv \phi^T G_0 \phi$ , and  $\gamma_1 \equiv \phi^T G_1 \phi$ . From Eq. (2.2) and the above definitions, we note that  $\gamma_0 + \frac{1}{\mu} \gamma_1 = 1$ . Consequently Eq. (2.3) takes the simplified form

$$\lambda(\hat{\alpha}) = \frac{\lambda_L(\hat{\alpha}) - \hat{\alpha}(1 - \gamma_0)}{1 + \hat{\alpha} \gamma_0 / \mu} \quad (2.4)$$

where  $\hat{\alpha} \equiv \alpha / a_0$  is a normalized displacement measure. From its definition it is clear that  $\gamma_0$  is a number in the range  $\{0, 1\}$ . The case  $\gamma_0 \rightarrow 0$  indicates greater relative importance of the dead loading to the eigenvalue problem, while the case  $\gamma_0 \rightarrow 1$  indicates greater relative importance of the proportional loading. With a few modest assumptions, the limit load can be approximated by a Rankine-type estimate as

$$\lambda_{cr} \approx \frac{\lambda_p \gamma_0}{1 + \lambda_p \gamma_0 / \mu} \quad (2.5)$$

where  $\lambda_p$  is the geometrically linear plastic capacity of the structure.

It is clear from Eq. (2.5) that the larger is  $\mu$ , the larger will be the limit capacity of the structure. In the post-limit regime, the geometrically linear capacity  $\lambda_L(\alpha)$  is generally constant or nearly constant. Therefore, the slope of the post-limit response curve is  $-(1 - \gamma_0 + \gamma_0 \lambda_L / \mu)$ . Thus, the larger  $\mu$



is, the smaller will be the post-limit loss of carrying capacity. In each case, it is apparent from this simple model that maximizing the buckling eigenvalue will lead to a more robust structure.

**Remark.**— As is shown in the examples in Hjelmstad and Pezeshk (1988) and Appendix C the buckling mode which dominates the response of the structure is not known *a priori*. For planar moment-resisting frames it is likely that the fundamental mode dominates the response, but for eccentrically-brace and three-dimensional frames, mode one might not be the dominant one. One can easily demonstrate that the above argument holds for any eigenpair  $\{\mu, \phi\}$ . Hence, one must endeavor to maximize the eigenvalue corresponding to the dominant mode. Because the dominant mode is generally not known in advance, one might maximize a weighted sum of eigenvalues. This approach is adopted in the sequel.

The rest of the present chapter and the following chapters exploit the above ideas and develop optimization criteria which have the goal of improving the stability characteristics of a structure. The validity of the observations made on the role of the eigenvalues in improving the limit and post-limit of structure is investigated through several example applications.

### 2.3. Formulation

The optimization problem to be solved is a combination of buckling and frequency eigenvalues as the following:

$$\begin{aligned}
 & \text{MAXIMIZE} \quad \sum_{j=1}^N \mu_j(\mathbf{x}) p_j(\omega(\mathbf{x})) \\
 & \text{SUCH THAT} \quad \sum_{i=1}^M A(x_i) \sum_{v \in i} \rho_v L_v = \Gamma \\
 & \quad \underline{x}_i < x_i < \bar{x}_i
 \end{aligned} \tag{2.6}$$

where  $\mu_j$  is the  $j$ th elastic critical buckling eigenvalue,  $\omega(\mathbf{x})$  is a vector of vibration frequencies,  $p_j(\omega)$  is a frequency weighting function (some of the  $p_j$  could be zero and may or may not depend on  $\omega$ ),  $\mathbf{x}$  is the vector of design variables,  $\Gamma$  is the given weight of the structure, and  $i$  is the group number (elements in each group have identical properties).  $A(x_i)$  is the area of element in group  $i$  (these relationships can be found in appendix 2.A),  $L_v$  is the length of element  $v$  in group  $i$ , and  $\rho_v$  is the mass density of the element  $v$  in group  $i$ . The  $i$ th design variable,  $x_i$  (moment of inertia in the



present development) has a minimum permissible value  $\underline{x}_i$ , and a maximum permissible value of  $\bar{x}_i$ .  $M$  is the number of groups, and  $N$  is the number of the eigenvalues and eigenvectors considered in the objective function.

To simplify the formulation we define the specific mass of the group  $i$  to be:

$$\Omega_i \equiv \sum_{v \in i} \rho_v L_v \quad (2.7)$$

Using Eqn. (2.6) the Lagrangian functional can be cast as:

$$L(x, \xi) = \sum_j \mu_j p_j(\omega) - \xi \left[ \sum_{i=1}^M A(x_i) \Omega_i - \Gamma \right] \quad (2.8)$$

where  $\xi$  is the Lagrange multiplier. It should be pointed out here that the constraints on the size of the elements given in Eq. (2.6) are not included in deriving Eq. (2.8). Normally, in structural optimization algorithms, the size constraints can be handled more efficiently by treating them as active/passive constraints. Whenever an element violates a size constraints, the design variable associated with that element is set to its limiting value and removed from the active set. A more detailed discussion of active and passive set strategy is given in section 2.5.3.

Taking the derivative of the Lagrangian with respect to the design variable  $x_i$  and setting the corresponding equation to zero results in:

$$\frac{\partial L(x, \xi)}{\partial x_i} = \sum_{j=1}^N \left[ \frac{\partial \mu_j}{\partial x_i} p_j(\omega) + \mu_j \frac{\partial p_j(\omega)}{\partial x_i} \right] - \xi \frac{\partial A(x_i)}{\partial x_i} \Omega_i = 0 \quad (2.9)$$

Rearranging Eqn. (2.9) and using chain rule to expand the second term in the brackets gives the following *optimality criteria*:

$$\frac{\sum_{j=1}^N \left[ \frac{\partial \mu_j}{\partial x_i} p_j(\omega) + \mu_j \sum_k \frac{\partial p_j(\omega)}{\partial \omega_k} \frac{\partial \omega_k}{\partial x_i} \right]}{\xi \frac{\partial A(x_i)}{\partial x_i} \Omega_i} = 1 \quad (2.10)$$

The weighting functions  $p_j(\omega)$  introduce information about the vibrational characteristics of the structure. These functions can be used to avoid undesirable dynamic effects such as resonance by pushing the structure away from it. The weighting function can be considered as a constraint on the frequencies of the structure which is introduced in the form of a penalty function in the objective. The choice of weighting function is dependent on the type of problem considered. Some of the possible weighting functions are given in Fig. 2.1. If the curve of the inverse of the frequency weighting function has a positive slope then the design is pushed toward having smaller period whereas when the slope of the weighting function is negative the design is pushed toward having a larger period. Weighing functions with steeper slopes result in a bigger encouragement to change the frequency of the design. If the weighting function is flat then there is no encouragement for design to change its frequency content.

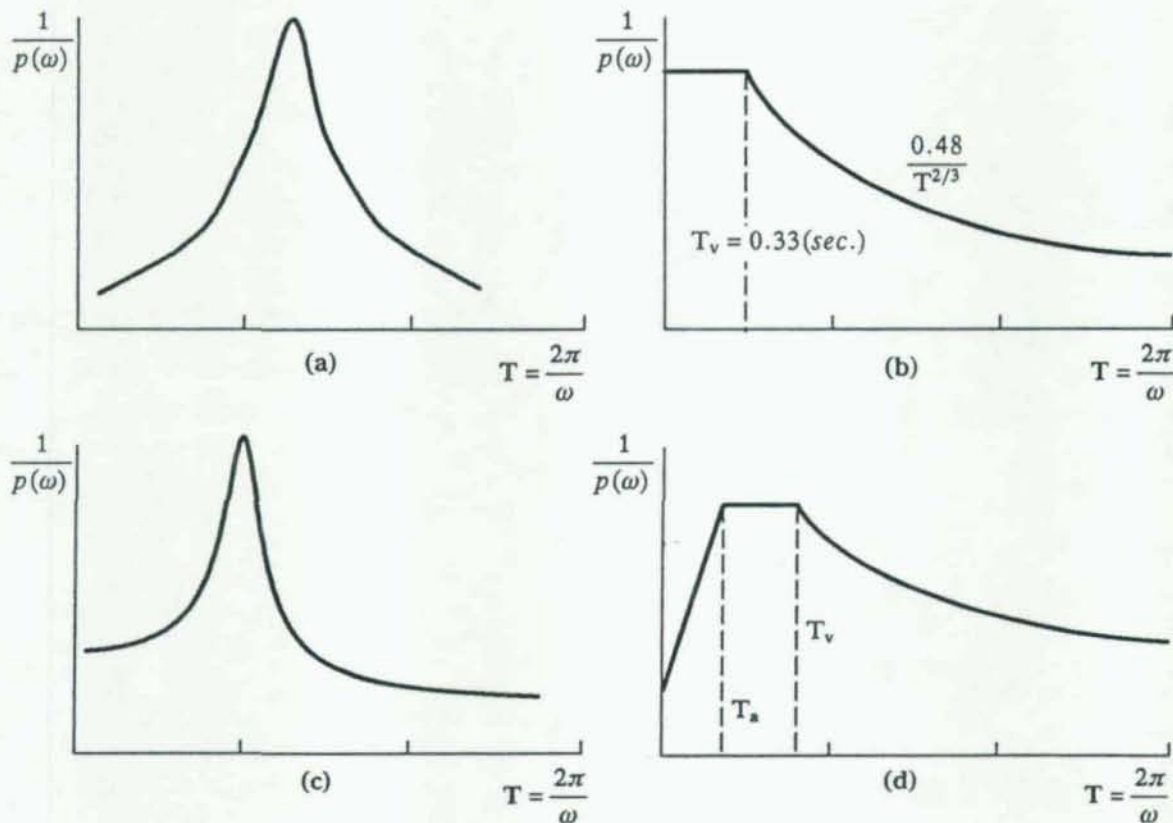


Fig. 2.1. Possible Weighting Functions: (a) Bell Shaped Response Spectra; (b) Uniform Building Code; (c) Sinusoidal Response Spectra; (d) Mexico's Federal District Code

## 2.4. Sensitivity Analysis

In order to evaluate the optimality criterion given in Eqn. (2.10), one needs to determine the sensitivities of the buckling loads and vibration frequencies of the structure with respect to the design variables. To determine the sensitivity of the buckling eigenvalues with respect to the design variables  $x_i$ , consider the following eigenvalue problem:

$$\mathbf{K}\phi_j = \mu_j \mathbf{G}\phi_j \quad (2.11)$$

where  $\phi_j$  and  $\mu_j$  represent the  $j$ th eigenvector and eigenvalue respectively,  $\mathbf{K}$  represents the elastic stiffness, and matrix  $\mathbf{G}$  is the geometric stiffness.

Differentiating Eqn. (2.11) with respect to design variable  $x_i$  gives:

$$\frac{\partial \mathbf{K}}{\partial x_i} \phi_j + \mathbf{K} \frac{\partial \phi_j}{\partial x_i} = \frac{\partial \mu_j}{\partial x_i} \mathbf{G} \phi_j + \mu_j \frac{\partial \mathbf{G}}{\partial x_i} \phi_j + \mu_j \mathbf{G} \frac{\partial \phi_j}{\partial x_i} \quad (2.12)$$

The gradient of the eigenvalue is then given by:

$$\frac{\partial \mu_j}{\partial x_i} = \frac{\phi_j^t \left[ \frac{\partial \mathbf{K}}{\partial x_i} + \mu_j \frac{\partial \mathbf{G}}{\partial x_i} \right] \phi_j}{\phi_j^t \mathbf{G} \phi_j} \quad (2.13)$$

Solving for the second term in parentheses given in Eqn. (2.13) numerically for several example problems, it was concluded that this term was negligible compared to the other terms (Appendix D presents the formulation for computing this term in detail).

The linear elastic structural stiffness  $\mathbf{K}$  exhibits the following explicit form in terms of cross sectional properties

$$\mathbf{K} = \sum_{i=1}^M \left[ A(x_i) \sum_{m \in i} \mathbf{K}_m^A + I(x_i) \sum_{m \in i} \mathbf{K}_m^I \right] \quad (2.14)$$

where  $\mathbf{K}_i^A$  is the element axial plus shear stiffness matrix, and  $\mathbf{K}_i^I$  is the element bending stiffness matrix of group  $i$  with either area or the moment of inertia factored out.

Differentiating the structural stiffness matrix (Eqn. (2.14)) with respect to the design variable  $x_i$  and by noting that  $\frac{\partial I(x_i)}{\partial x_i} = 1$  gives:



$$\frac{\partial K}{\partial x_i} = \frac{\partial A(x_i)}{\partial x_i} \sum_{m \in i} K_m^A + \sum_{m \in i} K_m^I \quad (2.15)$$

Therefore, Eqn. (2.13) can be computed as:

$$\frac{\partial \mu_j}{\partial x_i} = \frac{\phi_j^T \left[ \frac{\partial A(x_i)}{\partial x_i} \sum_{m \in i} K_m^A + \sum_{m \in i} K_m^I \right] \phi_j}{\phi_j^T G \phi_j} \quad (2.16)$$

Similarly, the sensitivity of the frequencies with respect to the design variable  $x_i$  can be determined by taking the derivative of the frequency eigenvalue problem:

$$K\psi_k = \omega_k^2 M\psi_k \quad (2.17)$$

where  $\psi_k$  and  $\omega_k$  represent the  $k$ th mode shape and frequency respectively and  $M$  represents the mass matrix of the structure. Differentiating the characteristic Eqn. (2.17) with respect to design variable  $x_i$  and simplifying and collecting terms results in:

$$\frac{\partial \omega_k}{\partial x_i} = \frac{1}{2\omega_k} \frac{\psi_k^T \frac{\partial K}{\partial x_i} \psi_k}{\psi_k^T M \psi_k} = \frac{1}{2\omega_k} \frac{\psi_k^T \left[ \frac{\partial A(x_i)}{\partial x_i} \sum_{m \in i} K_m^A + \sum_{m \in i} K_m^B \right] \psi_k}{\psi_k^T M \psi_k} \quad (2.18)$$

Note that in deriving Eqn. (2.18) the derivative of the mass matrix with respect to the design variables is assumed to be zero. This is true because the mass distribution of the structure is often assumed to be independent of the design variables for framed structures since most of the mass is associated with non-structural elements.

Having all the sensitivity terms determined, the optimality criterion can be calculated by substituting Eqn. (2.16) and Eqn. (2.18) into Eqn. (2.10). To simplify notation we write the optimality criterion as:

$$\frac{Q_i}{\xi \Omega_i} = 1 \quad i=1, \dots, M \quad (2.19)$$

where

$$Q_i \equiv \frac{\sum_{j=1}^N \left[ \frac{\partial \mu_j}{\partial x_i} p_j(\omega) + \mu_j \sum_k \frac{\partial p_j(\omega)}{\partial \omega_k} \frac{\partial \omega_k}{\partial x_i} \right]}{\frac{\partial A(x_i)}{\partial x_i}} \quad i=1, \dots, M \quad (2.20)$$

## 2.5. Solution Procedure

The optimum structure must satisfy the optimality criterion and the weight constraint. Since these equations are nonlinear, they can be solved only by an iterative scheme. The iterative algorithm suggested here consists of using a set of recurrence relationships based on the optimality criteria. The recurrence relations are the optimality criteria written in a form that can be used in an iterative fashion. Repeated use of the recurrence relation will move the initial design toward a design which satisfies the optimality criteria and the constraints. The iteration is split between two sets of unknowns. The first set contains the coefficients  $Q_i$ , and the second set contains the Lagrange multiplier  $\xi$ . The coefficients  $Q_i$  can be evaluated by solving the linearized buckling and vibration eigenvalue problems and determining the sensitivity of the buckling and frequency eigenvalues with respect to the design variables. The Lagrange multiplier is determined by using the condition that the design lies on the constraint surface at the end of each iteration. Because of the nonlinearity of the problem, when one moves the design to satisfy the optimality criteria the constraint surface moves. Conversely, when one moves the design to satisfy the constraint, the optimality criteria will not be satisfied. This behavior necessitates a repeated analysis of the structure, evaluation of the flexibility coefficients, determination of the Lagrange multiplier, and use of the recurrence relations. In the next sections the recurrence relations are derived and the method to determine the Lagrange multiplier is discussed.

### 2.5.1. Recurrence Relations

There have been various forms of recurrence relations developed and used. Berke (1970) derived a recursion relation based on a virtual strain energy criterion for problems with prescribed displacements. The recursion relation eliminated the need for determining the Hessian matrix for nonlinear programming, which is computationally expensive. The same recurrence relation was effectively used by Gellatly and Berke (1971) for a displacement constraint algorithm combined with stress ratio algorithm for design problems with stress and displacement constraints.



Later, Venkayya, Khot, and Berke (1973); Khot, Venkayya, and Berke (1973); and Khot, Venkayya, and Berke (1976) derived different forms of the recurrence relations for displacement constraints, stress constraints, and dynamic stiffness requirements as follows: write the optimality criteria in general form as

$$\eta_i = 1 \quad i = 1, \dots, M \quad (2.21)$$

multiply both sides by the design variable  $x_i^r$  and take the  $r$ th root. The optimality criterion can now be written in recurrence form as:

$$x_i^{\kappa+1} = x_i^{\kappa} (\eta_i^{\kappa})^{1/r} \quad (2.22)$$

where  $\kappa$  denotes the iteration number and  $r$  is the step size parameter. In Eqn. (2.22)  $\eta_i^{\kappa}$  is evaluated at the  $\kappa$ th iteration and is used to determine the new design variable  $x_i^{\kappa+1}$ . The Eqn. (2.22) is referred to as the exponential recurrence relation. At optimum the optimality criterion Eqn. (2.21) will be satisfied, therefore, the design variables will be unchanged with any additional iterations at optimum.

Eqn. (2.22) can be rewritten as:

$$x_i^{\kappa+1} = x_i^{\kappa} [1 + (\eta_i^{\kappa} - 1)]^{1/r} \quad (2.23)$$

Near the optimum, the term  $(\eta_i^{\kappa} - 1)$  will be small compare to unity, therefore, Eqn. (2.23) can be expanded by using the binomial theorem. Considering only the linear terms one obtains:

$$x_i^{\kappa+1} = x_i^{\kappa} [1 + \frac{1}{r} (\eta_i^{\kappa} - 1)] \quad (2.24)$$

This equation is referred to as the linear recurrence relation for the design variables. In Eqn. (2.24) the term  $(\eta_i^{\kappa} - 1)$  is the error in satisfying the optimality criterion and is equal to zero at the optimum.

Khot (1981) showed that the linear recurrence relations and the equations used to estimate the Lagrange multipliers derived by using the optimality criterion approach can also be obtained using the projection method of nonlinear programming.

In this study, the optimality criteria are used to modify the design variables. The recurrence relations proposed by Eqn. (2.24) is used as:

$$x_i^{\kappa+1} = x_i^{\kappa} \left[ 1 + \frac{1}{r} \left[ \frac{Q_i}{\xi \Omega_i} - 1 \right] \right] \quad i = 1, \dots, M \quad (2.25)$$

where  $\kappa$  denotes the iteration number and  $r$  is the step size parameter. The convergence behavior depends on the parameter  $r$ . Depending on the behavior of the constraint, it may be necessary to increase  $r$  in order to prevent divergence. If the optimization problem is run in a non-interactive environment a large value of step length such as  $r=8$  or  $r=10$  is recommended to ensure that there is no problem with divergence. Of course, this choice will result in slower convergence.

Another approach to controlling convergence is to generate an intermediate design vector whenever the objective function starts to deviate from the decreasing or increasing trend in the previous iterations. The intermediate design vector can be generated by taking the average of the variables in the previous iteration and the present iteration. It can be shown that this averaging process is equivalent to redoing the last iteration with  $r$  doubled.

A parameter study on the magnitude of step length and its effect on the convergence of the optimization can be found in paper by No and Aguinagalde (1987).

### 2.5.2. Equation to Determine Lagrange Multiplier

The Lagrange multiplier  $\xi$  must be determined in order to use the recurrence Eqn. (2.25). An equation to determine the Lagrange multiplier can be obtained by linearizing constraint about the current iterate.

The weight constraint can be expanded as:

$$C(x) = \sum_{i=1}^M A(x_i) \Omega_i - \Gamma = 0 \quad (2.26)$$

Linearizing about the configuration  $x^{\kappa}$  one obtains:

$$L[C]_{x=x^{\kappa}} = C(x^{\kappa}) + \sum_{i=1}^M \frac{\partial C}{\partial x_i} (x_i - x_i^{\kappa}) \quad (2.27)$$

where

$$\frac{\partial C}{\partial x_i} = \frac{\partial A(x_i)}{\partial x_i} \Omega_i \quad (2.28)$$



Thus the linearized constraint becomes:

$$\sum_{i=1}^M A(x_i^r) \Omega_i - \Gamma + \sum_{i=1}^M \frac{\partial A(x_i^r)}{\partial x_i} \Omega_i (x_i - x_i^r) = 0 \quad (2.29)$$

In Eqn. (2.29),  $C(x^r) \approx 0$  since the design variables are updated by the recurrence relationship after the Lagrange multiplier is estimated. We estimate the Lagrange multiplier by satisfying the linearized constraint at the new iterate  $x^{r+1}$ . Substituting  $x = x^{r+1}$  into Eqn. (2.29) and solving for the Lagrange multiplier we get

$$\xi = \frac{\sum_{i=1}^M Q_i(x^r) \frac{\partial A(x_i^r)}{\partial x_i} x_i^r}{\sum_{i=1}^M \frac{\partial A(x_i^r)}{\partial x_i} x_i^r \Omega_i - r \left[ \sum_{i=1}^M A(x_i^r) \Omega_i - \Gamma \right]} \quad (2.30)$$

since the constant weight constraint is an equality,  $\xi$  can be either positive or negative.

### 2.5.3. Active/Passive Set Strategies

After each iteration a set of new design variables is obtained. If the design variables are in the permissible range, they are considered active elements, otherwise, they are considered passive elements. Allwood and Chung (1984) suggested that in general if a design variable is passive in two consecutive iterations, it will stay passive until convergence. The method suggest by Allwood and Chung is implemented here.

It is generally more efficient to keep a passive element passive until the end. The program is set up so that the designer can change a passive element to an active element or vice versa. Thus, if a designer's judgment suggests that a design variable should be active, he can turn the passive design set to active and check its status at every iteration. One benefit of keeping a design variable in the passive set once it become passive is that this can expedite convergence.

### 2.5.4. Scaling Procedure

Since the weight constraint is not exactly enforced at each iteration, it is necessary to scale the design variables to keep the design feasible. The weight of the structure after each iteration can be

split into two parts: one part is the weight of the members in the active set,  $W^A$ , and the other is the weight of the members in the passive set,  $W^P$ .

$$W^A + W^P = \Gamma \quad (2.31)$$

In order to scale the weight of a structure after each iteration, the area of each active element is scaled by  $\zeta$  as  $x_i \leftarrow x_i \zeta$  with

$$\zeta = \frac{\Gamma - W^P}{W^A} \quad (2.32)$$

Since only the active set is scaled, iteration is necessary only if a variable becomes passive as a consequence of scaling.

#### 2.5.5. Convergence Criterion

The optimization theoretically converges when all the optimality criteria are satisfied. After each iteration the deviation of the optimality criteria from unity is calculated and if the Euclidean norm of the deviation is less than a specified tolerance the iteration is terminated. The tolerance is specified by the designer.



## 2.A. APPENDIX

### CROSS SECTIONAL PROPERTIES

#### 2.A.1. Overview

Member properties are assumed to be composed of the collection of all regular series wide flange rolled steel shapes as identified by the American Institute of Steel Construction (AISC). This set is clearly discrete. Many researchers have tried to come up with continuous models to define the discrete set of member properties. In general optimization on a continuous domain is more efficient than optimization on a discrete domain. The continuous relationship between cross sectional area and moment of inertia used in chapter 2 were obtained from empirical relations derived by Walker (1977) for economy wide flange steel sections. These relationships are as follows:

For columns with  $I \leq 429 \text{ in}^4$

$$D = 1.470I^{0.368}$$

$$A = 2.95I^{0.23456}$$

For columns with  $I > 429 \text{ in}^4$

$$D = 10.5I^{0.0436}$$

$$A = 0.0494I^{0.9093}$$

For girders

$$D = 2.660I^{0.287}$$

$$A = 0.61124I^{0.4719}$$

(2.A.1)

Where  $D$  is the section depth in *inches* and  $A$  is the area (*inches*)<sup>2</sup>. The limits of the model are shown in Fig. 2.A.2.

The program written for the optimization algorithm is set to select column sections (as is defined in Eqn. (2.A.1)) for column members, and girder sections (as is defined in Eqn. (2.A.1)) for

girder members. Where depth restrictions do not apply and member instability problem (out-of-plane buckling) are unlikely to be critical, beam sections may be used with advantage for column members. Conversely, an option is included in the program whereby one may stipulate column sections for beam members if desired.

The empirical relationship given by Eqn. (2.A.1) has a discontinuity of slope at a moment of inertia of 429 in<sup>4</sup>. This discontinuity can cause difficulty in convergence of the optimization algorithm if some of the design variables are near 429 in<sup>4</sup>. To solve this problem a continuous curve was fit between the two curves proposed by Walker (Eqn.(2.A.1)). The method of matching tangents, described by Menegotto and Pinto (1973), yields the following relationship

$$D = 0.00042 I + \frac{5.872 + 0.022377 I}{1 + (0.4253 + 0.00162 I)^{(1/7)}} \quad (2.A.2)$$

and the cross section area can be determined as

$$A = \frac{I}{0.1521 D^{2.08}} \quad (2.A.3)$$

For comparison purposes, the curves given by Eqn. (2.A.1) and Eqn. (2.A.2) are plotted in Fig. 2.A.1.

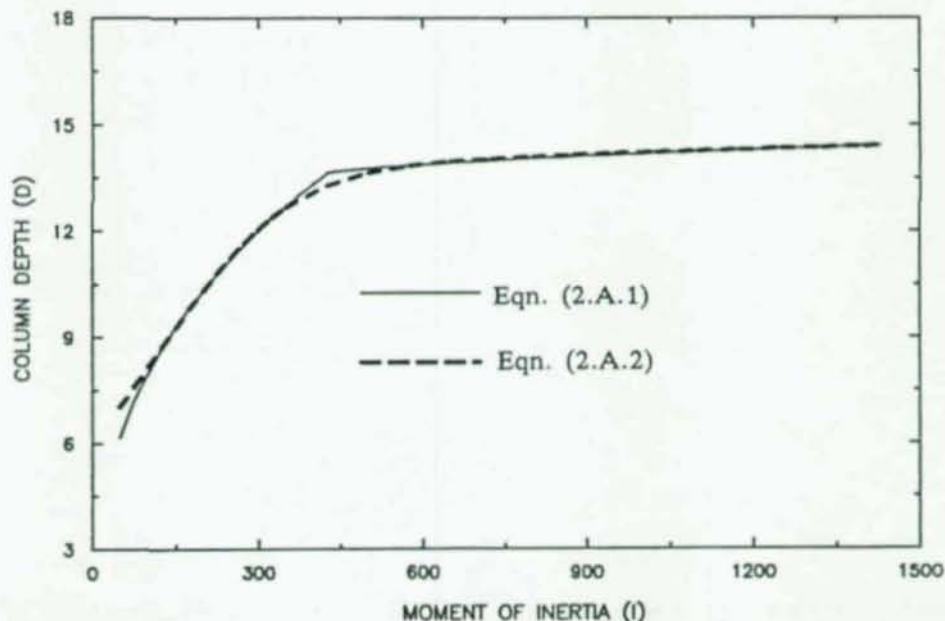


Fig. 2.A.1. Empirical Relationship Between Moment of Inertia and Column Depth



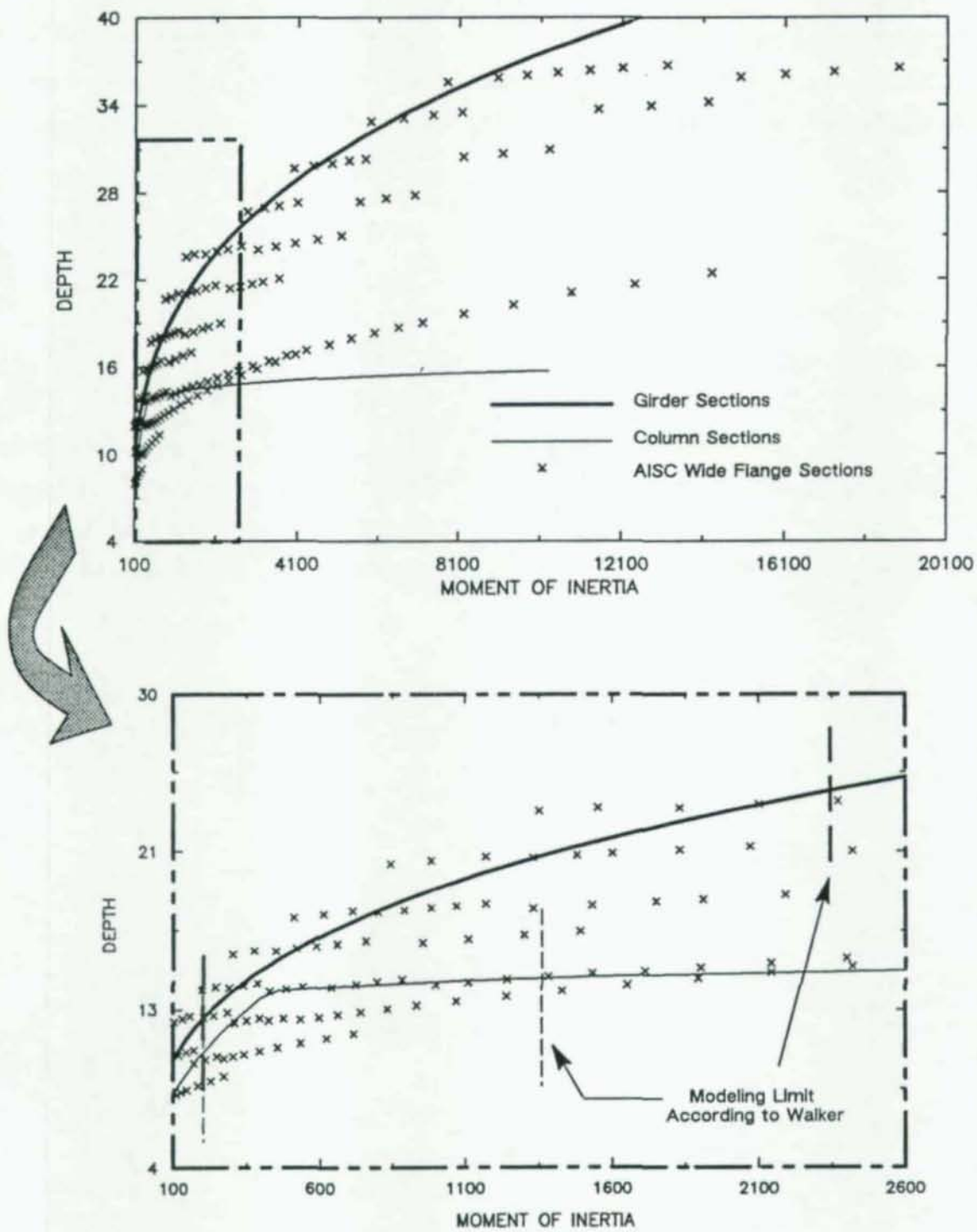


Fig. 2.A.2. Empirical Relationship Between Moment of Inertia and Column Depth and the Actual Members Identified by AISC

It is important to note that the empirical relationship given in (2.A.2) is only good for a certain range and covers only a small portion of the discrete set as given in AISC. To see where the empirical relationship of Eqn. (2.A.2) stands in the whole discrete set, Fig. 2.A.2 is presented. From this figure it is obvious that the continuous function covers a very small and specific range of the discrete members. Therefore, it is important to come up with a method that can model the discrete set with more generality. One way of handling the problem is to use more than one design variable to represent the cross sectional properties of a member and let the optimization algorithm find the best relationships among the cross sectional components as needed to achieve an optimal design. In this way, one is not bounded to the curve given by Eqn. (2.A.2) and can move in the discrete set freely and the optimization will assign the necessary relationship. Using more than one design variable in defining the cross sectional properties makes the problem more complicated to handle but gives more realistic representation of the optimal cross sectional types. Using more variables to identify a cross section will allow the optimization to be more flexible and the design need not be chosen from a pre-assigned set. This freedom is, of course, a blessing to the researcher and a curse to the designer who must, in the end, select from the discrete set.

The two types of cross sections that are most widely used are rectangular and wide flange sections as shown in Fig. 2.A.3 below.

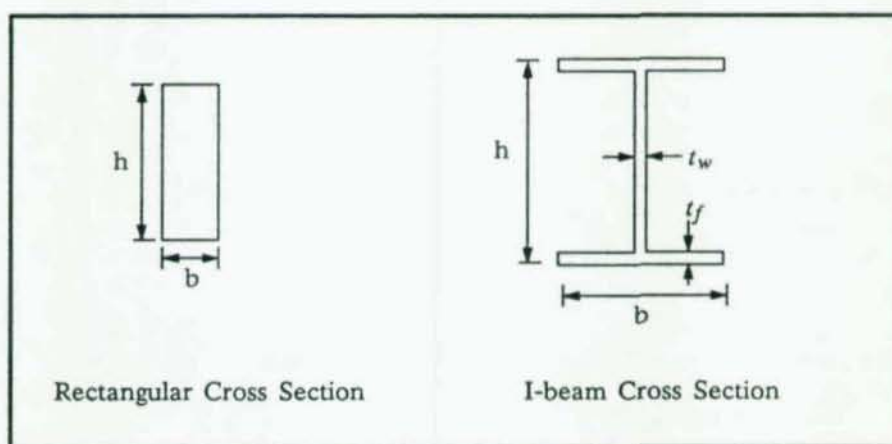


Fig. 2.A.3. Different Cross Sectional Types

Properties of rectangular cross section can be expressed in terms of width ( $b$ ) and height ( $h$ ) and properties of the wide flange sections can be expressed in terms of the parameters ( $h, b, t_f, t_w$ ); where  $h$  is the height,  $b$  is the width,  $t_w$  is the web thickness, and  $t_f$  is the flange thickness. There-



fore, there are four variables necessary to represent the properties of the I-beam members. One can observe a relationship between the flange thickness and the web thickness of available (AISC) I-beam sections. They are very closely related to one another by  $t_f \approx 1.6t_w$ . Fig. 2.A.4 presents a plot of  $t_w$  versus  $t_f$ . Thus, there are only three independent variables needed to describe an I-beam cross section accurately. These three independent parameters can be used as design variables for the optimization.

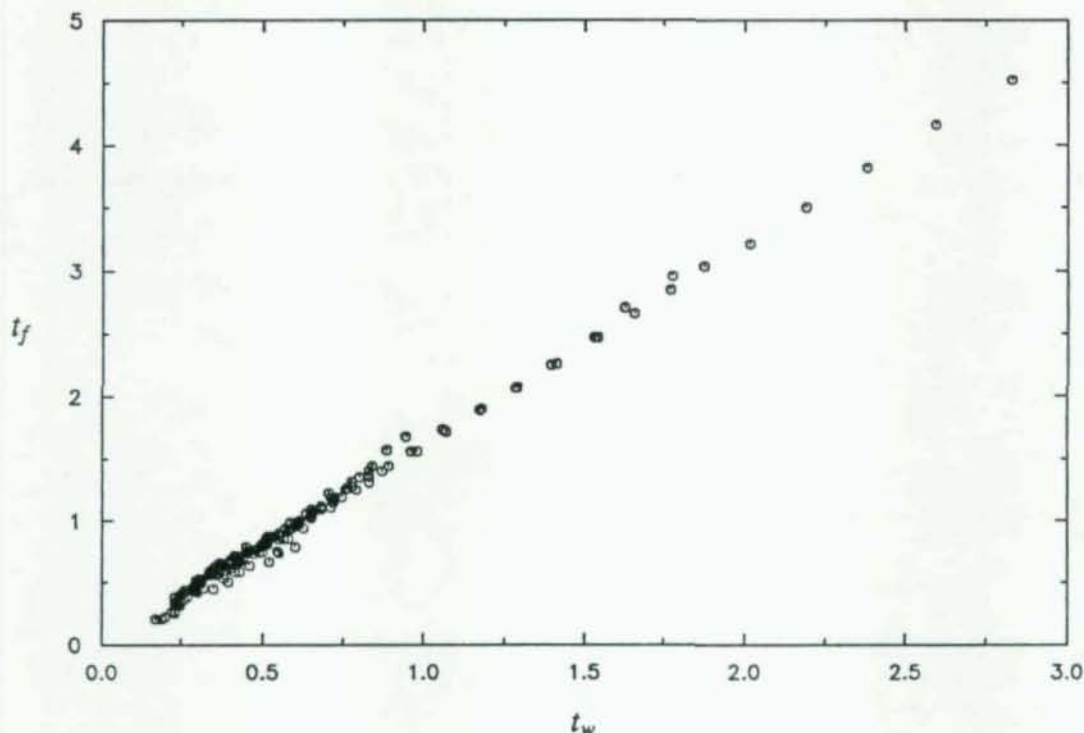


Fig. 2.A.4. Flange Thickness Versus Web Thickness for Wide Flange Sections Identified by AISC

One must be careful when multiple design variables are used to define the member cross sectional properties because the objective function may be insensitive to certain unmodeled phenomenon. Under such circumstances the design variables will generally move toward their extreme permissible sizes. For example, if a planar frame is optimized to maximize the fundamental buckling eigenvalue with a volume constraint, the cross section tends toward having the highest moment of inertia in the plane of the structure. The cross sections will tend to have the smallest possible width with the largest possible height. The resulting structure would have no resistance to out-of-plane buckling.

This problem could be solved in two ways. One way is to put an additional constraint on the design variables to prevent out-of-plane instability if it becomes important. Another way is to consider a three-dimensional frame in which case the objective will provide the necessary constraint among the three cross sectional variables. It may be impossible to write an explicit constraint for global out-of-plane buckling, except for simple cases like single member buckling, hence, the later approach is more promising than the former, and will be investigated in the sequel.

Another example of an unmodeled phenomenon concerns local buckling of flange and web elements. Because the analytical model does not include local buckling modes, these will not be represented in the objective function. One could use a model which incorporates local buckling, but the interaction between local and global buckling for most structures is small and thus the resulting algorithm would probably not be robust. On the other hand, since local and global buckling are lightly coupled, local buckling constraints in the form of width-to-thickness limitation would be relatively simple to describe and implement.



## CHAPTER 3

### APPLICATION OF 2-D OPTIMIZATION TO FRAMED STRUCTURES

#### 3.1. Introduction

This chapter is devoted to application of the methods developed in previous chapter to two framed structures. The examples will serve to demonstrate the effectiveness of the design procedure. Presentation of the examples include three parts: (1) discussion of the initial design method; (2) discussion of the optimization process, and (3) analyses and discussion of the quality of the initial and the optimized designs under static and dynamic environment.

To start the chapter it is necessary to discuss some of the analysis procedures employed.

#### 3.2. Analysis Procedure

The approach to analyzing the 2-D frames considered in this study is that proposed by Simo, Hjelmstad, and Taylor (1983). A finite element discretization of the structure in conjunction with the standard Newton-Raphson iteration scheme, is employed to solve the nonlinear equations of motion.

The finite element discretization of the frames analyzed throughout this chapter consists of two elements between each structural joint. Quadratic interpolation was employed for all the elements. The norm of the local constitutive residual was forced to be within a tolerance of  $10^{-10}$  at each global iteration. A global iteration tolerance of  $10^{-8}$ , measured as ratio of the the Euclidean norm of the nodal force unbalance to the Euclidean norm of the initial configuration was used.

Displacement control load incrementing, as described by Batoz and Dhatt (1979), was used throughout the analyses. Lateral displacement of the top story was used as the control point. Lateral top displacement is used throughout this study to characterize structural deformation.

##### 3.2.1. Damping Matrix used for Dynamic Analyses

The damping matrix is modeled as a linear combination of the mass and stiffness matrix. This type of damping matrix is known as Rayleigh damping and has the form

$$C = \alpha M + \beta K \quad (3.1)$$

Where  $M$  is the mass matrix, and  $K$  is the stiffness matrix. The multipliers  $\alpha$  and  $\beta$  can be determined from modal damping with any pair of natural frequencies. For the present study these multipliers are determined from the first and the second natural vibration frequencies ( $\omega_1$  and  $\omega_2$ ). To find the parameters  $\alpha$  and  $\beta$  multiply both sides of Eqn. (3.1) by the eigenvector

$$\psi_i^T C \psi_i = \psi_i^T (\alpha M + \beta K) \psi_i \equiv 2\omega_i \xi_i \quad i = 1, 2 \quad (3.2)$$

Using the orthonormality of the eigenvector, Eqn. (3.2) can be rewritten as

$$\alpha + \beta \omega_i^2 = 2\omega_i \xi_i \quad i = 1, 2 \quad (3.3)$$

Using this relation for  $\omega_1, \xi_1$  and  $\omega_2, \xi_2$ , we obtain two equations for  $\alpha$  and  $\beta$

$$\alpha + \beta \omega_1^2 = 2\omega_1 \xi_1 \quad \text{and} \quad \alpha + \beta \omega_2^2 = 2\omega_2 \xi_2 \quad (3.4)$$

Solving for  $\alpha$  and  $\beta$  we get

$$\alpha = \frac{2(\xi_2 \omega_1 - \xi_1 \omega_2) \omega_1 \omega_2}{\omega_1^2 - \omega_2^2} \quad (3.5)$$

$$\beta = \frac{2(\xi_1 \omega_1 - \xi_2 \omega_2)}{\omega_1^2 - \omega_2^2} \quad (3.6)$$

where  $\xi_1$  and  $\xi_2$  are the percentage of the critical damping of first and second modes. One observation about Rayleigh damping is that the mass proportional damping term increase the effect of damping in the lower modes, while the stiffness proportional damping increases the effect of damping in the higher modes.

In nonlinear analysis, the stiffness matrix is updated after each iteration and may not be constant. Therefore, the initial stiffness matrix or the tangent stiffness matrix can be saved to use in calculation of the damping matrix. Alternatively, after the damping matrix is determined once, it can be stored and used throughout the analysis.



### 3.2.2. Time Interval Used for Dynamic Analyses

There are two factors that must be considered in employing an appropriate time steps: (1) stability of the numerical integration scheme, and (2) proper representation of the input ground motion function. Using constant-average-acceleration method (*i.e.*, Newmark method with  $\beta=0.25$ ) for a linear system, the first requirement is satisfied automatically, since the method is unconditionally stable. Ground motions are normally digitized at 0.02 second intervals, therefore, for the linear analyses of problems a time interval of  $\Delta t=0.02$  seconds can be used. For the time interval different than 0.02 seconds the ground acceleration is obtained by linear interpolation between two coordinate points.

Although the numerical integration scheme used is unconditionally stable for linear systems, the method might become unstable for a nonlinear system if the time step is large (Adeli, et al., 1978). Unlike conditionally stable methods in linear analysis, for nonlinear analysis a stability criterion to control the time step is not established yet. However, it is apparent that only for a small time step the implicit procedures are stable (Belytschko *et. al.*, 1976). Time steps of  $\Delta t = 0.005$  seconds were used for most of the analyses presented here.

### 3.2.3. Damage Estimates

Different designs can be compared with respect to the damage sustained during a dynamic excitation. One of the most widely used damage model was developed by Park and Ang (1985) from 403 tests on reinforced concrete members. The model assumes that the damage may be expressed in terms of a damage index,  $D$ , which is computed from the sum of the normalized maximum deformation and normalized hysteretic energy dissipated during cyclic loading. The damage index can be expressed as

$$D = \frac{\delta_m}{\delta_u} + \frac{\beta}{Q_y \delta_u} \int dE \quad (3.7)$$

where  $D > 1$  signifies complete collapse of the member;  $\delta_m$  is the maximum deformation obtained during cyclic loading;  $dE$  is the incremental absorbed hysteretic energy,  $Q_y$  is the shear force at first yielding of the member;  $\delta_u$  is the maximum attainable monotonic deformation; and  $\beta$  is a normalization parameter.  $\beta$  was determined by evaluating the parameter in Eqn. (3.3) at failure point ( $D=1$ ) for 261 cyclically loaded specimens and solving for  $\beta$ .

In the present study we adopt a simplified damage model which is indexed by plastic strain energy dissipation only. Although this model is simple, it should provide a good qualitative indication of structural distress. The plastic strain energy dissipation can be computed as

$$D(t) = \int_V \int_0^t \sigma_{ij} \dot{\epsilon}_{ij}^p dV \quad (3.8)$$

where  $\dot{\epsilon}_{ij}^p$  is the plastic strain rate and  $\sigma_{ij}$  is the stress and  $V$  is the volume of the structure and numerically can be determined as

$$D(t_{n+1}) = D(t_n) + [(\eta - 1)\sigma_{ij}(t_{n+1}) + \eta\sigma_{ij}(t_n)][\epsilon_{ij}^p(t_{n+1}) - \epsilon_{ij}^p(t_n)] \quad (3.9)$$

where for backward Euler  $\eta=1$ , for forward Euler  $\eta=0$ , and for midpoint formulation  $\eta = 1/2$ .

In the following examples the damage statistics for initial and optimized designs under different dynamic excitations are determined and the results are discussed.



### 3.3. Three Story Frame

#### 3.3.1. Preliminary Design

The first example is a three story frame with topology as given in Fig. 3.1. This frame was designed based to meet the Uniform Building Code (1979) specification.

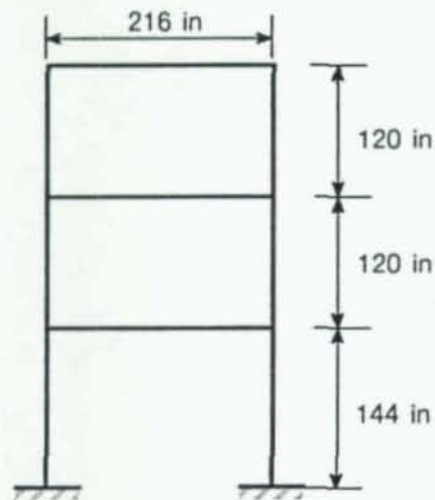


Fig. 3.1. Topology of the 3-Story Frame

The loads on the structure were:

Dead load:	80 psf	
Live load:	40 psf	for a typical floor
	20 psf	for the roof
Exterior walls	50 lb/ft	

Lateral loads and their distribution were computed for zone 4 following the code recommendation. A preliminary design was performed using full dead and live load to determine maximum moments in girder sections.

##### 3.3.1.1. Code Lateral Loads

Dead load on girders:	77.6 kips
Dead load on columns	57.6 kips
Dead load of the columns and girders	4.0 kips
Total	139.2 kips

### 3.3.1.2. Base Shear

$$V = ZIKCSW$$

$$S = 1 \quad (\text{Coefficient for site-structure resonance})$$

$$I = 1 \quad (\text{Occupancy importance factor})$$

$$Z = 1 \quad (\text{High seismicity zone})$$

$$K = 0.67 \quad (\text{Moment resisting frame})$$

$$CS = \frac{1}{\sqrt{[(1-\beta^2)^2 + (2\beta\xi)^2]}} \quad \text{where } \beta = \frac{T}{T}$$

$$\text{Assume } \beta = 1.5 \rightarrow CS = 0.78$$

$$V = (0.67)(0.78)(139.2) = 72.74 \text{ (Kips)} \quad \text{Base Shear}$$

### 3.3.1.3. Code Distribution

The UBC force distribution is given as

$$F_i = \frac{w_i h_i}{\sum_j w_j h_j} (F_t - V) \quad i = 1, \dots, N \quad (3.10)$$

$$F_t = 0 \text{ for } T \leq 0.7 \text{ sec.}$$

where  $F_i$  is the lateral force applied to level  $i$ ,  $w_i$  is the portion of total dead load which is located at or is assigned to level  $i$ ,  $F_t$  is the portion of  $V$  considered concentrated at the top of the structure. Using Eqn. (3.9) results in the lateral force distribution given in Fig. 3.2.

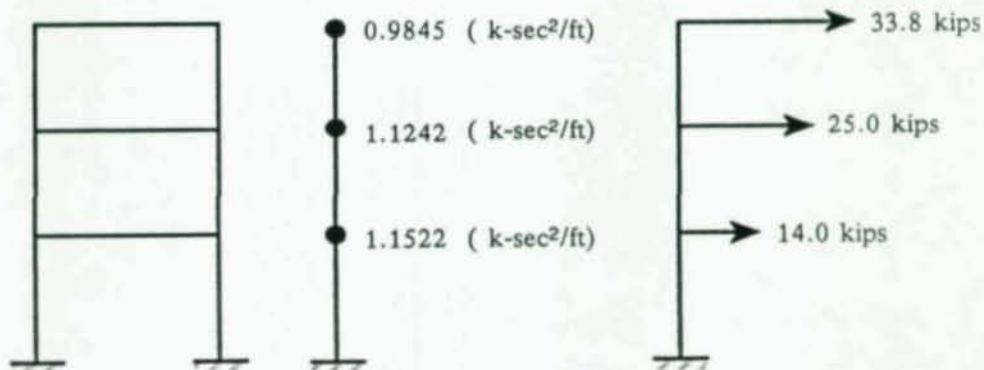


Fig. 3.2. Code Shear Distribution for 3-Story Frame



The AISC specification was used for the design requirements on steel sections. Yield stress was 36 ksi for all sections and frames. The sections were assumed properly braced against lateral buckling. For girders the allowable bending stress of  $F_b = 24$  ksi was used.

For combination of dead plus live load plus earthquake (D+L+Q) the allowable increase in working stress of 33% was followed (Section 2303 UBC code). L stands for live loading, D stands for dead loading, and Q stands for earthquake loading.

Analyses of the preliminary design were done for load combinations (D+L) and  $0.75(D+L+Q)$ .

For girders, the maximum moments were used to proportion the sections and then checked for shear and deflections (due to live load) limitations. For column design, the frame was assumed to be fully braced in the out-of-plane direction (Y-direction), and  $K_x$  was computed according to the AISC procedure.

After checking all the requirements and going through several iteration of design and analysis, the following members were chosen for the design:

W24X55 → *Girders*

W12X96 → *Columns*

Lateral deflections were computed under lateral loads from earthquake to check against drift requirements. No changes were necessary.

### 3.3.2. Optimization

The design achieved based on the UBC specification was used as the initial design for the optimization. The initial design is optimized maximizing the first critical eigenvalue of the structure under combined lateral and dead loads with no frequency penalty. Six design variables were used: three design variables for columns and three design variables for girders. The optimization converged in 35 iterations resulting in an optimized design with the properties given in Table 3.1., which lists the cross sectional area ( $A$ ), the bending moment of inertia ( $I$ ), the axial capacity ( $N_0$ ), the shear capacity ( $V_0$ ), and the flexural capacity of ( $M_0$ ). The shear coefficient used for of the members was  $\kappa = 0.33$ .

Table 3.1. Properties of the Optimized Designs Without Frequency Penalty

Member	Stiffness Properties		Yield Properties		
	$A$ (in <sup>2</sup> )	$I$ (in <sup>4</sup> )	$N_0$ (kips)	$V_0$ (kips)	$M_0$ (kips)
1st story columns	38.2	1500	1376	795	7484
2nd story columns	21.6	807	777	449	4122
3rd story columns	12.3	385	443	256	2143
1st story girders	23.9	2360	859	496	6875
2nd story girders	22.9	2163	825	476	6462
3rd story girders	13.4	698	484	279	2884

The fundamental period and buckling eigenvalues of the both initial and the optimized design are given in Table 3.2. The fundamental buckling eigenvalue of the design increased from 98.7 to 141.5.

Table 3.2. Frequency and the Buckling Eigenvalue of the Initial and the Optimized Designs

Design	$\lambda$	$T(sec)$
Initial Design	98.7	0.538
Optimum Design	141.5	0.444

### 3.3.3. Analysis

**Static Analysis.**— In order to investigate the performance of the optimized design, both the initial design and the optimized designs were analyzed under statically applied lateral and dead loadings. Full nonlinear analyses were performed in order to evaluate the overall stability of the initial and the optimized designs. Statically applied loads considered herein are not strictly applicable to dynamically applied loads such as occur during an earthquake, but the nonlinear static behavior provides a reasonably realistic indication of the response of the structures to earthquake loadings and represents a useful step toward understanding the dynamic response of the structure and gives some insight into the general integrity of a structure (Galambos and Maxwell, 1965; Bertero and Kamil, 1975). The results of the analyses are given in Fig. 3.3. One can observe that the load carrying capacity of the optimized structure was increased by 44% without any increase in the rate of post-limit load degradation. The conclusion from static analysis is that the optimized design is better than the initial design as far as overall strength and stability is concerned.

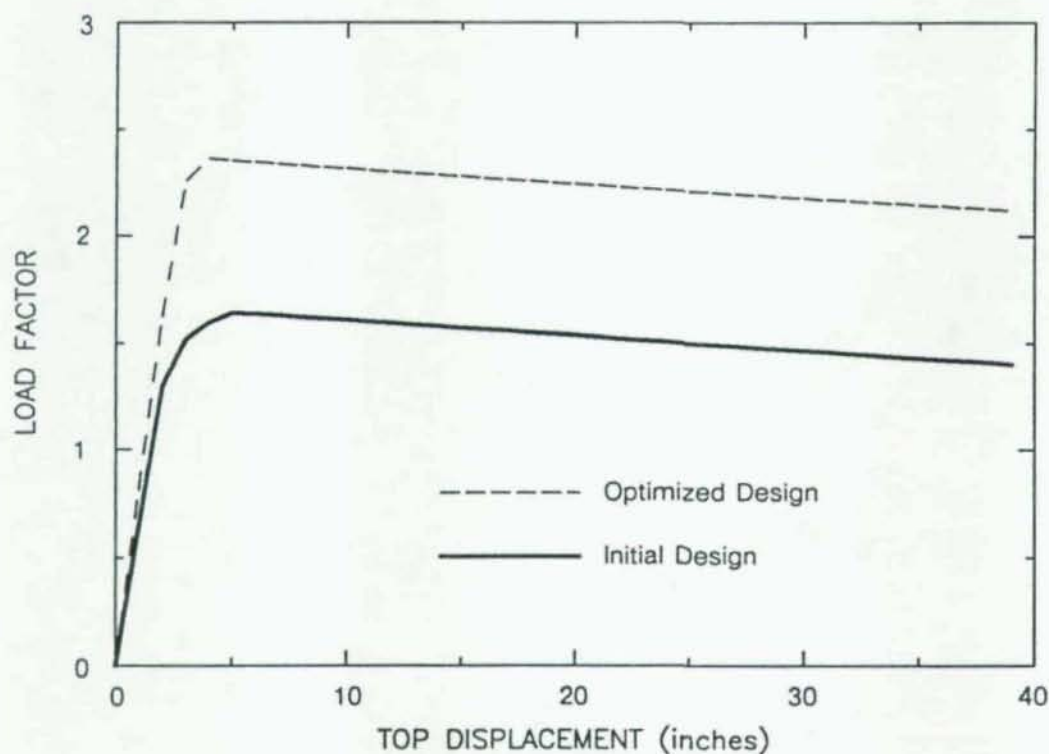


Fig. 3.3. Static Analysis of 3-Story Frame



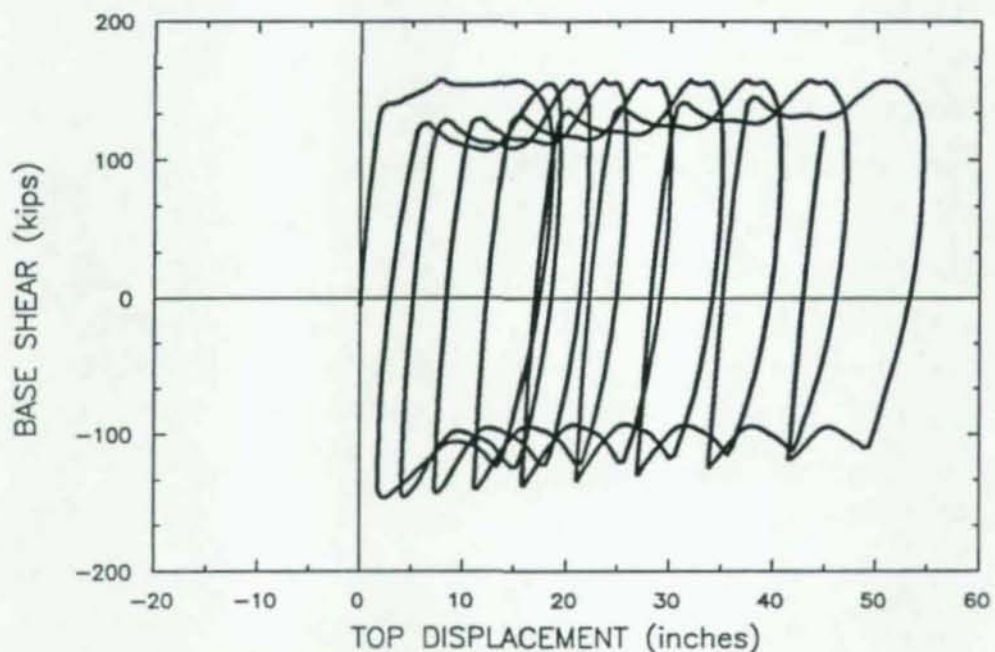
**Sinusoidal Base Acceleration.**— To demonstrate that the optimized design is better under dynamically applied loads, both the initial and the optimized designs were analyzed and compared under sinusoidal base acceleration and earthquake base acceleration.

The performance of the both initial and the optimized designs under sinusoidal base acceleration is given in Fig. 3.4. To make the comparison more fair, the sinusoidal base acceleration was applied in the two cases with the same frequency but different amplitude. The amplitude of the applied base acceleration was chosen such that both initial design and the optimized design had the same elastic dynamic magnification factors. A damping ratio of 3% of critical was used for the first and the second modes. The base shears obtained from time history analysis and plotted against the lateral top displacement of the frames in Fig. 3.4. One can see that the initial design tends to drift cyclically whereas the optimized design does not, making the latter a more attractive design.

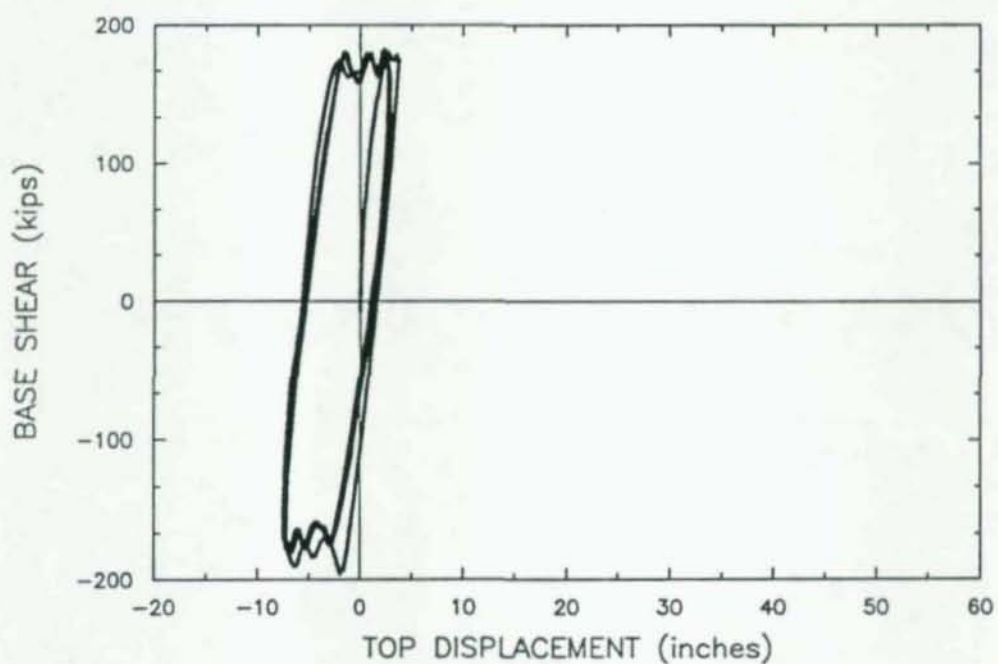
**Pacoima Dam Earthquake.**— Both the initial and the optimized design were analyzed under the 1971 Pacoima Dam earthquake. The response history and base shear history of both initial and the optimized designs are given in Fig. 3.5. One can see that the initial design drifts a great deal. The optimized design has controlled drift even though the base shears are higher. Although no failure is predicted for the initial design under Pacoima Dam earthquake, the optimized design is more desirable because of its ability to control drift.

**Maximum Element Damage Statistics.**— Fig. 3.7 shows the maximum element damage statistics, wherein one can observe that maximum element damage is less for the optimized design than the initial design. Location of the maximum damage is not under our control.

**Average Element Damage Statistics.**— Fig. 3.6 represents the average element damage statistics which is obtained by taking the norm of damage in each element during the time history analyses. Observe that the average damage is less for the optimized design than the initial design.



(a) Initial Design, Amplitude of Sinusoidal Base Acceleration  $A_{\max}=500$



(b) Optimized Design, Amplitude of Sinusoidal Base Acceleration  $A_{\max}=228$

Fig. 3.4. Dynamic Analysis of 3-Story Frame Under Sinusoidal Base Acceleration

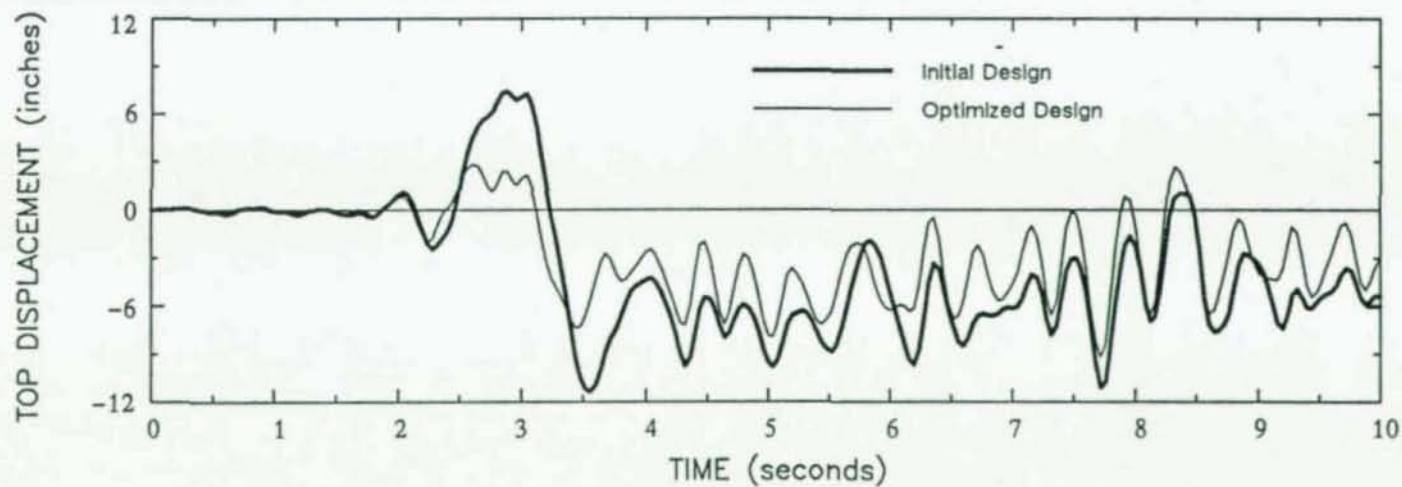
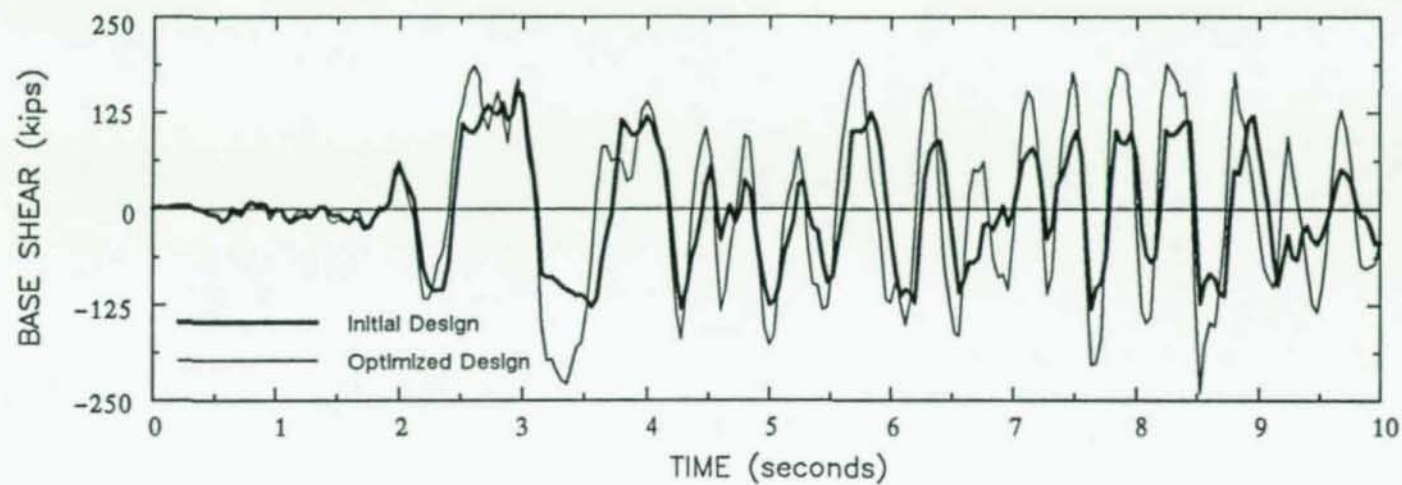


Fig. 3.5. 3-Story Frame under Pacoima Dam 1971 Earthquake Base Acceleration



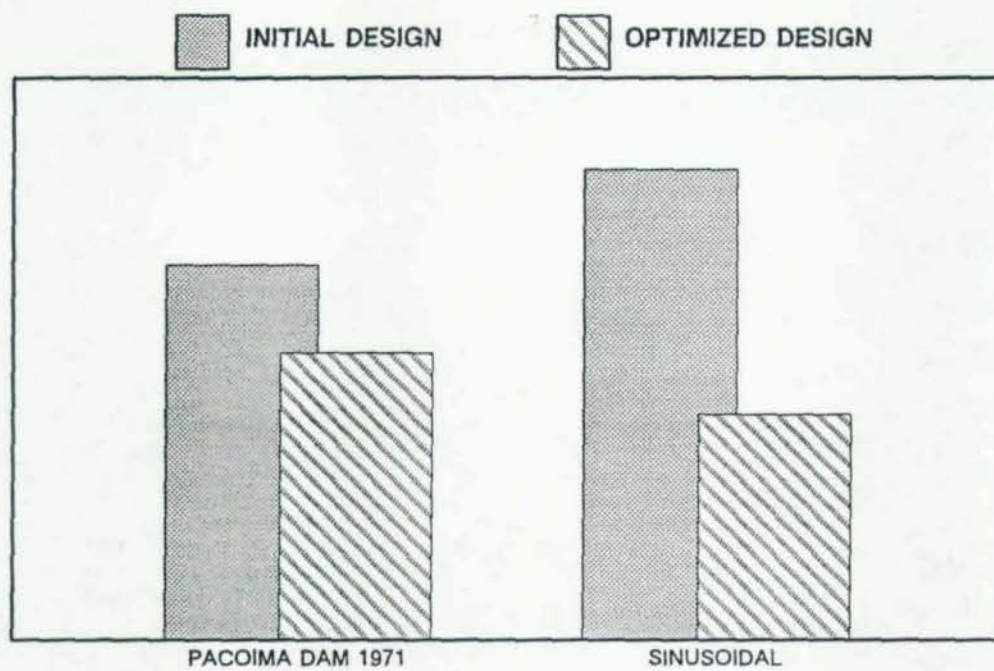


Fig. 3.6. Average Element Damage Statistics for 3-Story Frame

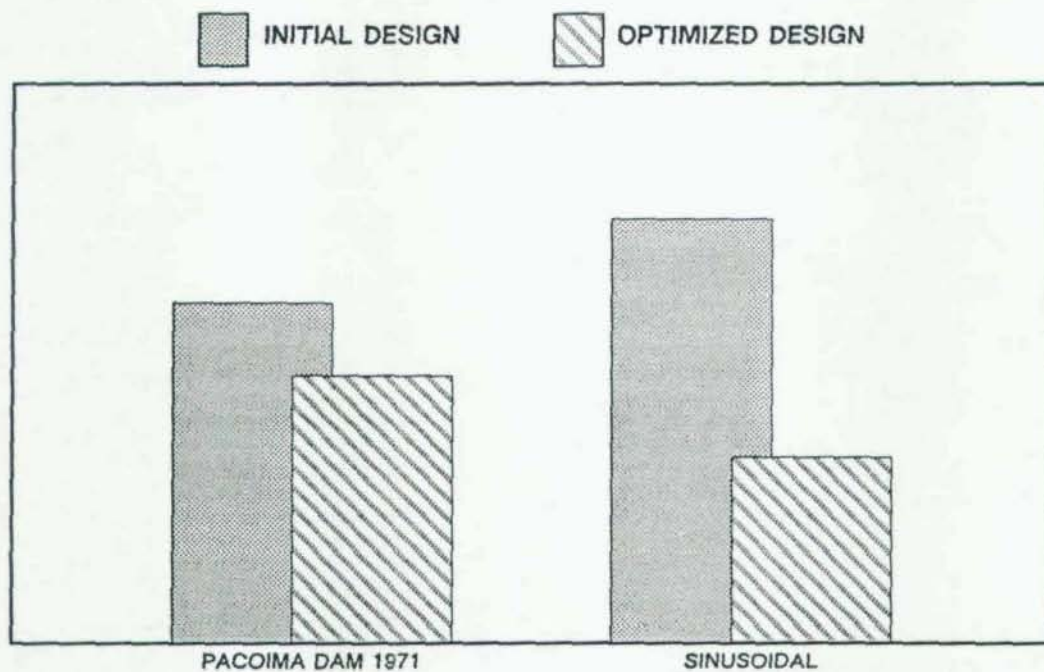


Fig. 3.7. Maximum Element Damage Statistics for 3-Story Frame

### 3.3.4. Optimization with Frequency Weighting Function

So far nothing has been said about the frequency penalty. The performance of the optimized 3-story frame (opt) was better than the initial design under static and dynamic excitation without considering any frequency penalties. The structure can also be optimized using a frequency weighting function. To demonstrate how the weighting function operates on a design, the 3-story frame is optimized again with a frequency weighting. Suppose that the structure is to be designed to resist a sinusoidal loading of frequency  $\bar{\omega}$ . We will take the frequency weighting function to be the sinusoidal response spectrum

$$p(\omega) = [(1 - \beta^2)^2 + (2\beta\xi)^2]^{a/2} \quad (3.11)$$

where  $\beta = \bar{\omega}/\omega$  and the exponent  $a$  is an arbitrary parameter. For simplicity,  $a = 1$  was used and the initial design was optimized with the weighting function given above. The properties of the resulting optimized design (optf) are given in Table 3.3. The first buckling eigenvalue of the optf is 155.6 with the fundamental period of 0.48 seconds. Fig. 3.8 gives a view of where the fundamental periods of all the designs are relative to each other. From this figure, one can see that the period of the optf has elongated compared to opt because of downhill curve of penalty function. Using a larger number for  $a$  will enhance the effect of the penalty resulting in a larger change of frequency content of the design. The optf is a compromise between the initial design and the optimized design opt.

Frame optf was analyzed under static loading with the results as shown in Fig. 3.9. The performance of opt is similar to optf, and both have higher load carrying capacities compared to the initial design. The post-limit slopes are almost the same as the initial design.

Frame optf was also analyzed under Pacoima Dam earthquake and the resulting base shear response histories of both initial and the optimized designs are plotted in Fig. 3.10. Again, from this picture, one can see that both opt behaves similarly to optf and both behave better than the initial design as far as controlling the drift is concerned.

Table 3.3. Properties of the Optimized Designs with Frequency Penalty

Member	Stiffness Properties		Yield Properties		
	A (in <sup>2</sup> )	I (in <sup>4</sup> )	N <sub>0</sub> (kips)	V <sub>0</sub> (kips)	M <sub>0</sub> (kips)
1st Story Column	39.4	1550	1282	740	6947
2nd story columns	31.9	1230	715	413	3774
3rd story columns	12.4	389	465	268	2099
1st story girders	23.6	2311	1049	606	9295
2nd story girders	15.8	992	863	498	6918
3rd story girders	7.7	217	427	246	2390



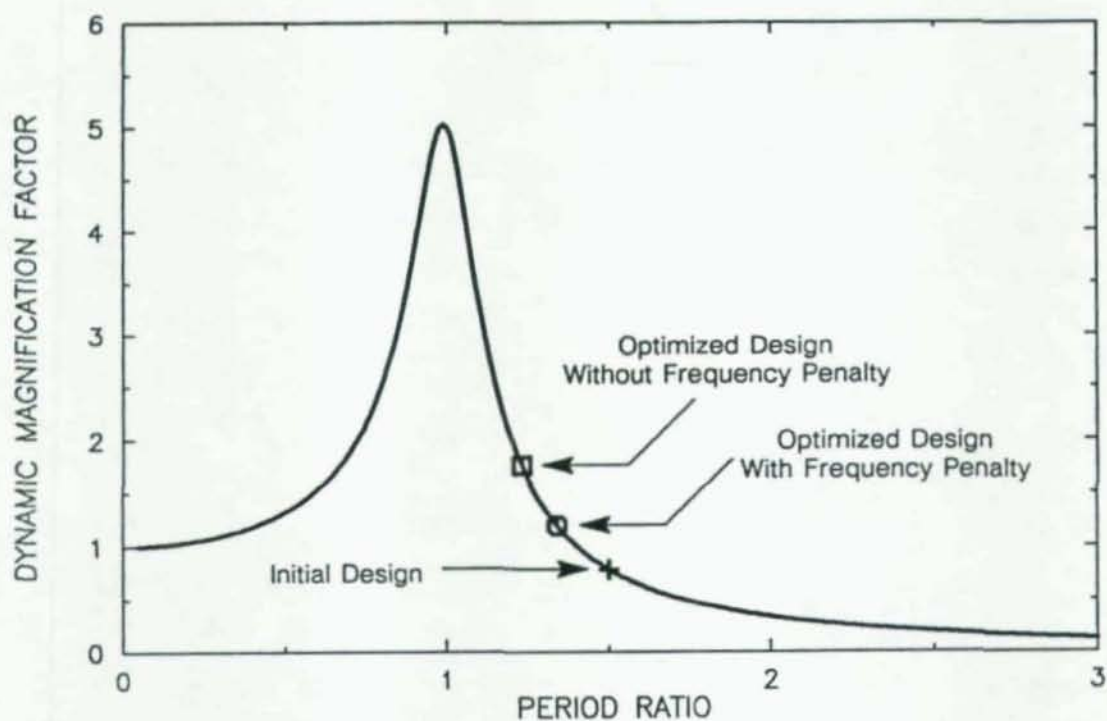


Fig. 3.8. Sinusoidal Response Spectra

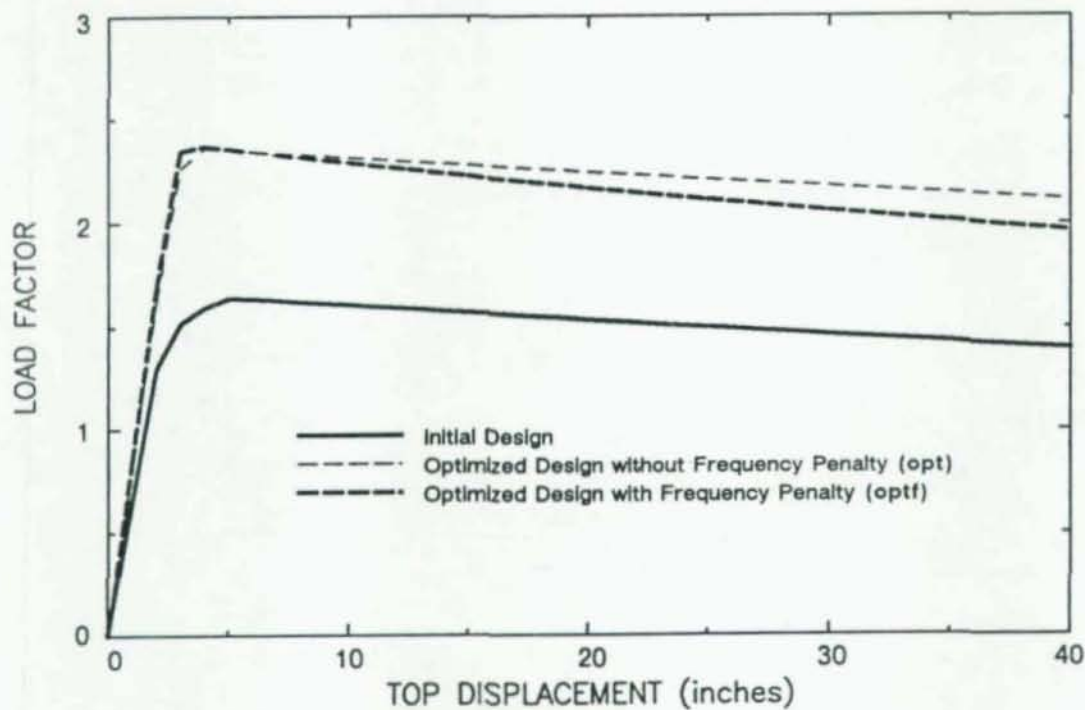


Fig. 3.9. Static Analyses of the Initial and Optimized Designs With and Without Frequency Penalty



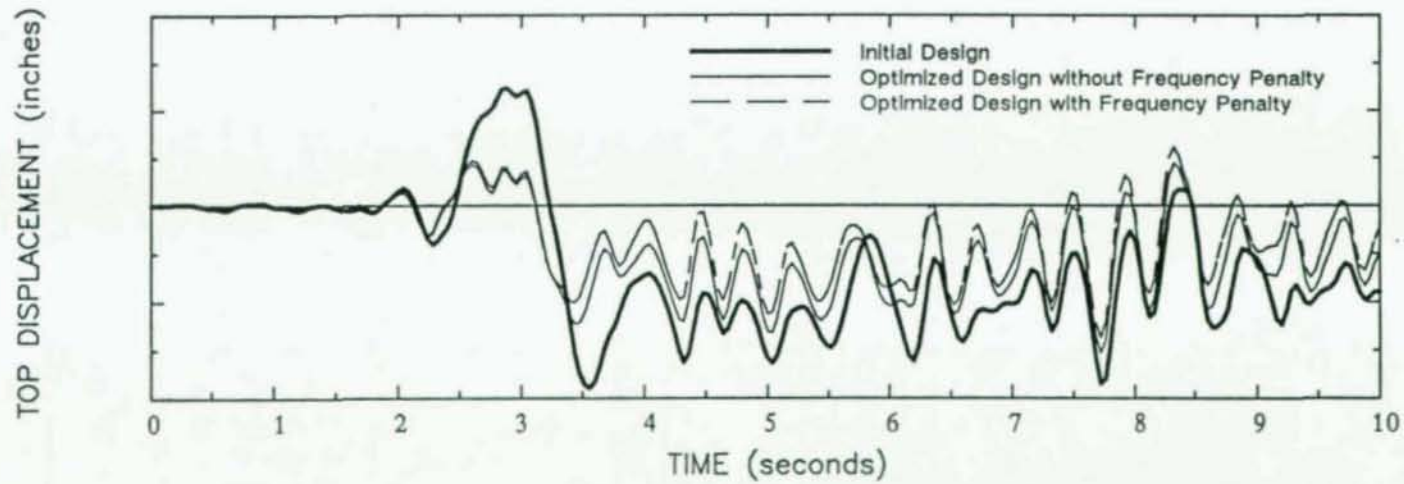
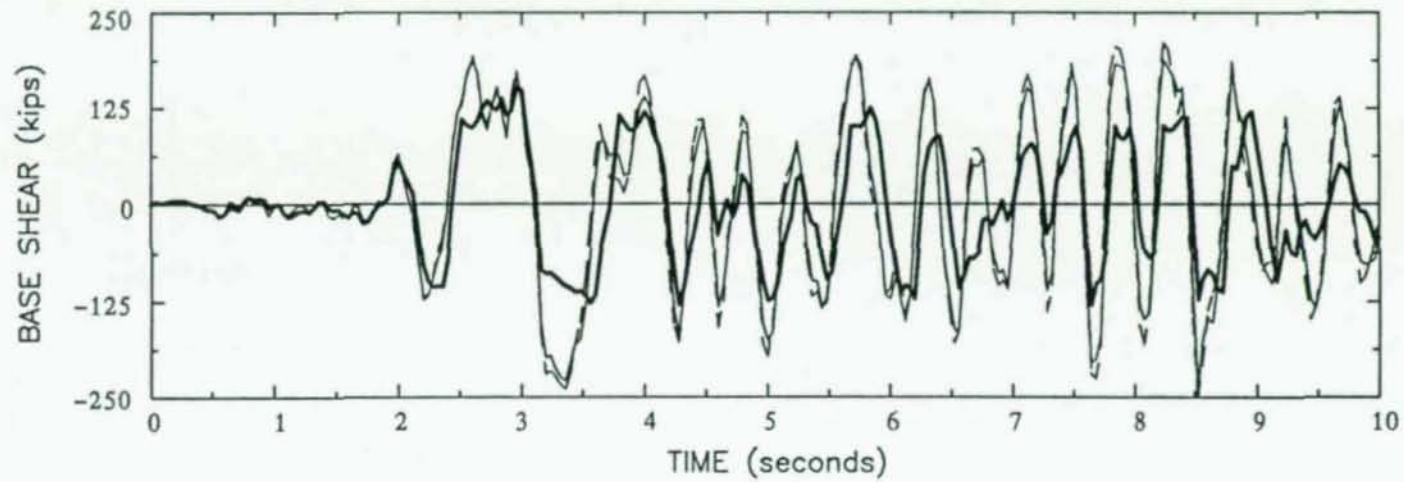


Fig. 3.10. 3-Story Frame under Pacoima Dam 1971 Earthquake Base Acceleration

### 3.4. Eight Story Frame

#### 3.4.1. Preliminary Design

The 8-story frame with topology given in Fig. 3.11 is a modified version of a design given by Korn and Galambos (1968). The properties of the structure are given in Table 3.4. This design was checked with UBC lateral load provisions (1979) and the AISC specification (1978). All the requirements were satisfied.

The loading on the structure consisted of:

*Dead load:*

*0.25 kips/lin for roof level*

*0.30 kips/lin for typical floor*

The lateral force distribution on the structure was obtained following the UBC lateral load provisions. The calculated lateral force distribution along with the story mass of the structure is given in Table 3.4.

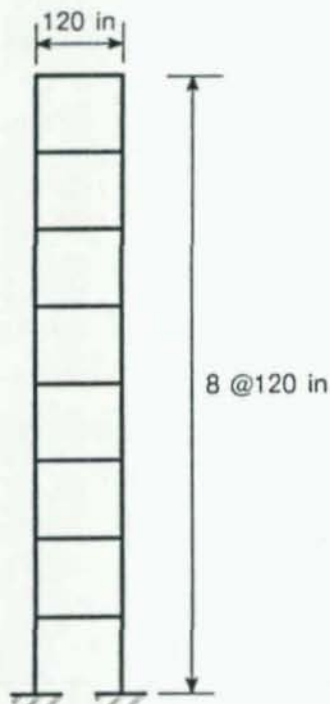


Fig. 3.11. Topology of the 8-Story Frame

Table 3.4. Properties of the 8-Story Initial Design and Code Lateral Force Distribution

Story	Column	Girder	Mass ( <i>k-sec<sup>2</sup>/in</i> )	<i>F<sub>l</sub></i> ( <i>kips</i> )
1	W14X99	W14X38	0.056	0.315
2	W14X99	W14X38	0.056	0.629
3	W14X90	W14X38	0.056	0.943
4	W14X90	W14X38	0.056	1.258
5	W12X79	W14X30	0.056	1.572
6	W12X79	W14X30	0.056	1.888
7	W10X49	W12X26	0.056	2.200
8	W10X49	W12X26	0.045	2.984

#### 3.4.2. Optimization

The 8-story frame was optimized by maximizing the first buckling eigenvalue of the structure under dead loading only, keeping the volume of the structure constant. There were 16 design variables: 8 representing the moments of inertia of the columns and 8 representing the moments of inertia of the girders. The properties of the optimized design is given in Table 3.5.

Table 3.5. Properties of the 8-Story Optimized Design

Story	Column	Girder
1	W14X99	W24X76
2	W14X99	W24X76
3	W14X74	W24X76
4	W14X74	W24X76
5	W14X48	W21X57
6	W14X48	W21X57
7	W12X35	W12X35
8	W12X35	W12X35



### 3.4.3. Analysis

**Static Analysis.**— The result of the static analyses are given in Fig. 3.12. Observe that the load carrying capacity of the optimized structure increased from a load factor of 5.0 for the initial design to 9.8 for the optimized design (an increase of about 100%) with only a very slight increase in the rate of post-limit load degradation. The conclusion from static analysis is that the optimized design is better than the initial design as far as overall strength and stability is concerned.

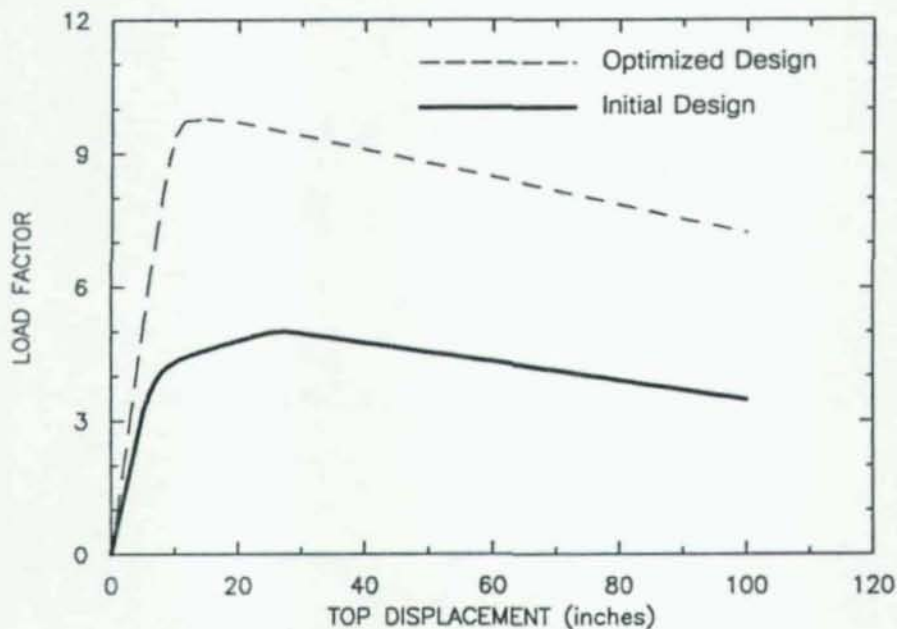


Fig. 3.12. Static Analysis of 8-Story Frame

**Sinusoidal Base Acceleration.**— To make the comparison of the initial and optimized designs fair, each design was analyzed under a sinusoidal base acceleration of the same amplitude at their respective resonant frequencies. Again, the dynamic magnification factors for both case are the same. A damping ratio of 5% of critical was used for the first and the second modes. Fig. 3.13 presents the base shear versus the lateral top displacement under the sinusoidal base acceleration. Observe that the initial design has tendency to drift whereas the optimized design has stable drift, which making it a more attractive design.

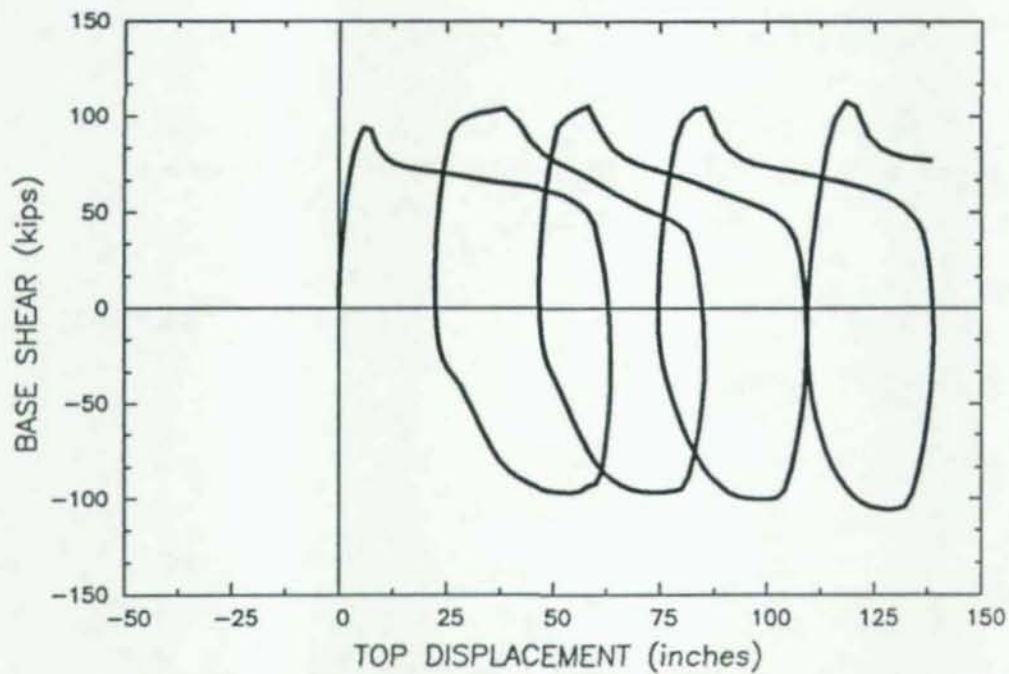
**Pacoima Dam Earthquake.**— Both the initial and the optimized design were analyzed under the 1971 Pacoima Dam earthquake. The response history and base shear history of both initial and the optimized designs are given in Fig. 3.14. Observe the severe drift of the initial design versus the

controlled drift of the optimized design. The base shears are higher for the optimized design as expected due to the fact that the optimized design is stiffer and stronger.

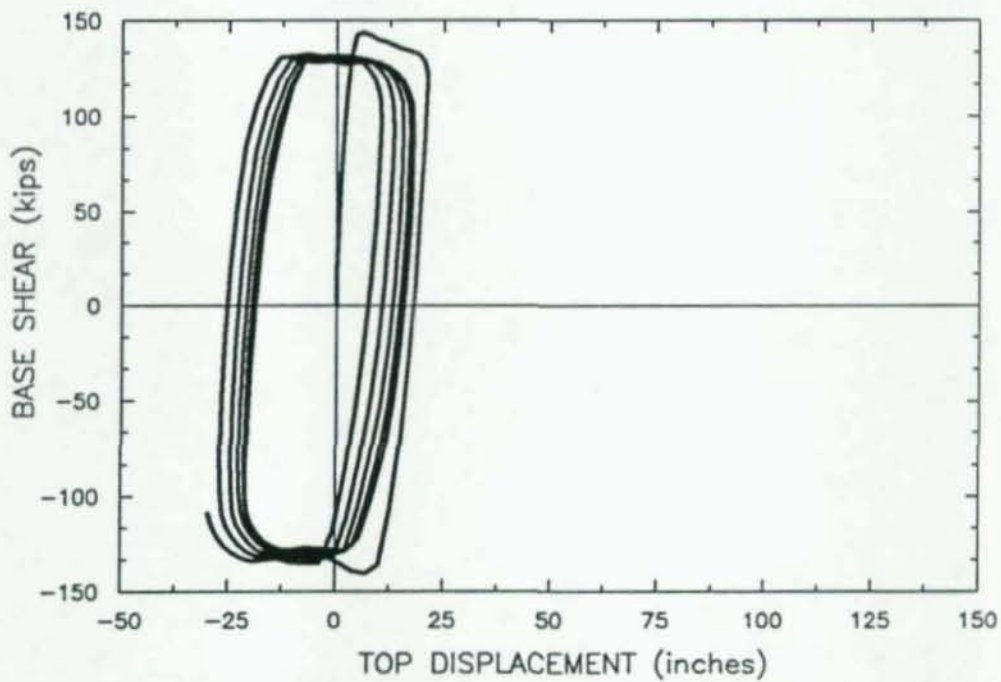
**El Centro Earthquake.**— Both the initial and the optimized designs were analyzed under the 1940 El Centro earthquake. The response history and base shear history of both initial and the optimized designs are given in Fig. 3.15. The maximum drift of both the initial design and the optimized design roughly the same magnitude. It is difficult to distinguish quality of performance based upon the response history.

**Damage Statistics.**— Fig. 3.17 represents the maximum element damage statistics. The maximum element damage is reduced for optimized design under sinusoidal base acceleration but increased under Pacoima Dam and El Centro earthquake. The question is whether the failure of a single member is thought to cause general failure of the structure. Bear in mind that more damage for an element does not necessary mean the failure of the element. In general, a single element failure does not result in general failure of a structure.

The average element damage statistics is given in Fig. 3.16 where one can see that for the optimized design the average element damage is reduced.



(a) Initial Design, Amplitude of Sinusoidal Base Acceleration  $A_{\max}=500$



(b) Optimized Design, Amplitude of Sinusoidal Base Acceleration  $A_{\max}=500$

Fig. 3.13. Dynamic Analysis of 8-Story Frame Under Sinusoidal Base Acceleration



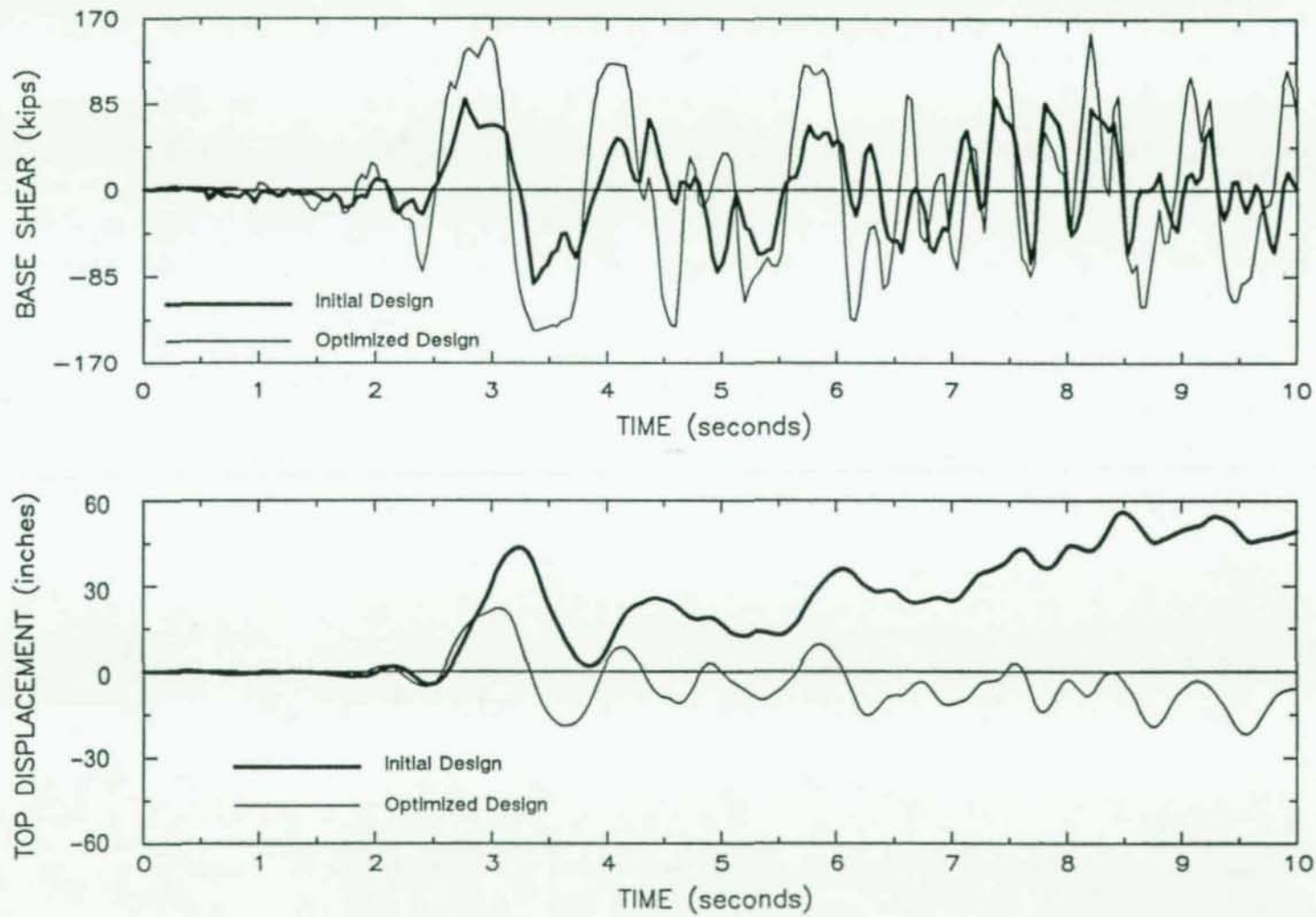


Fig. 3.14. Dynamic Analysis of 8-Story Frame Under Pacoima Dam 1971 Earthquake Base Acceleration

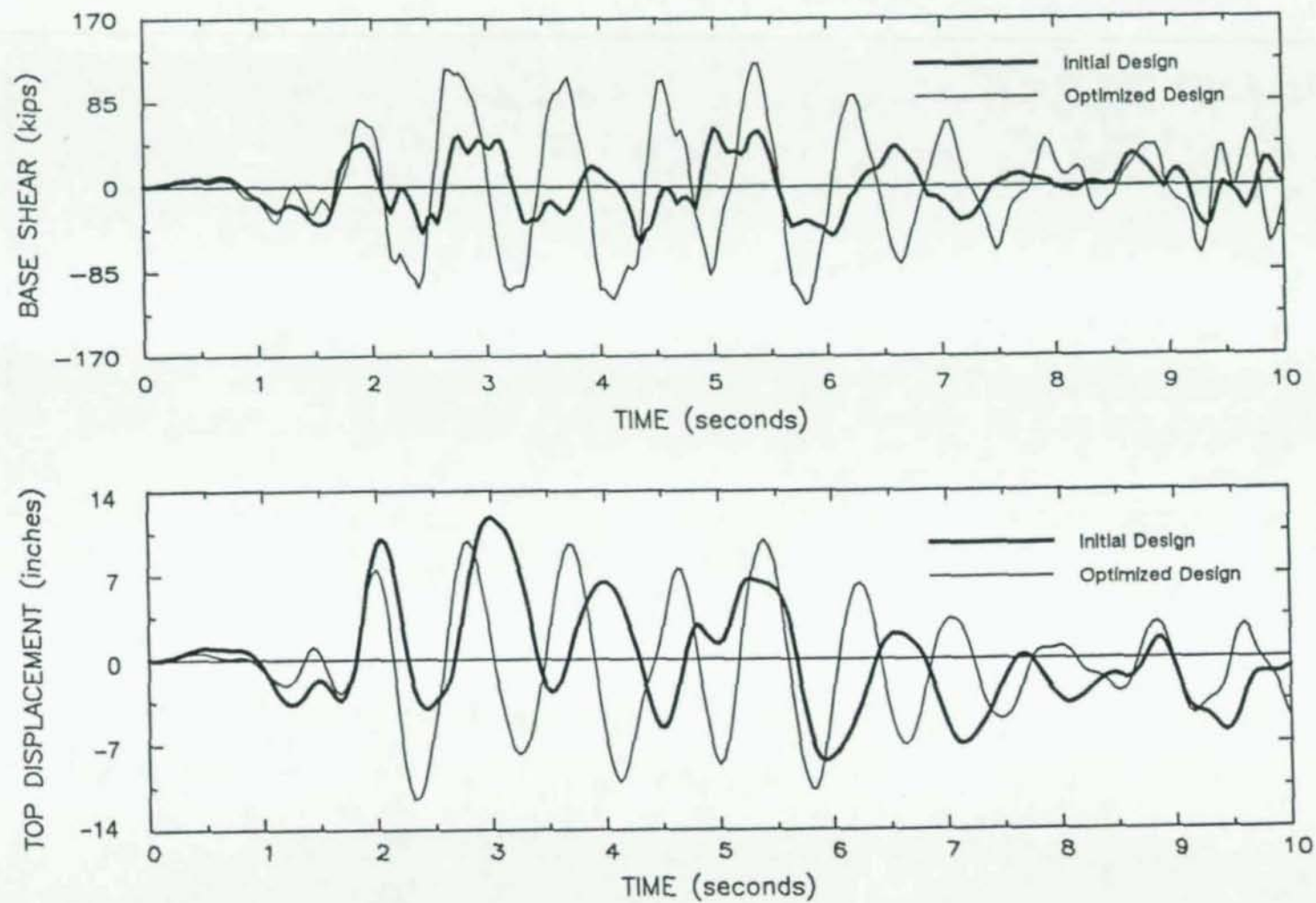


Fig. 3.15. Dynamic Analysis of 8-Story Frame Under El Centro 1941 Earthquake Base Acceleration

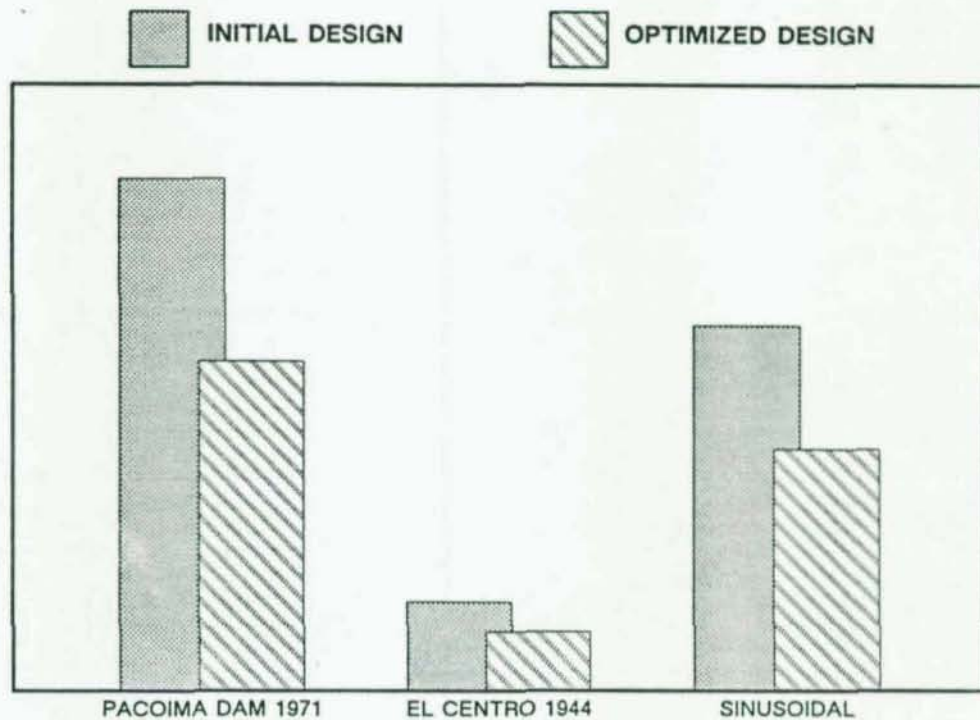


Fig. 3.16. Average Damage Statistics for 8-Story Frame

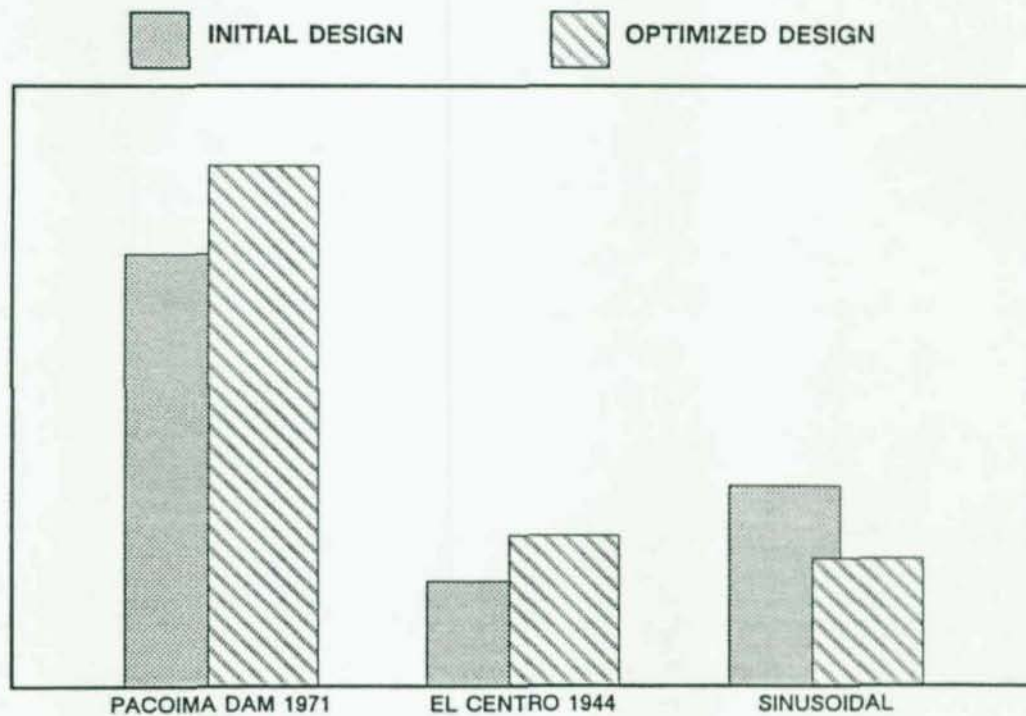


Fig. 3.17. Maximum Element Damage Statistics for 8-Story Frame



### 3.5. Conclusions

The following conclusions can be drawn from the preceding chapter:

- Maximizing the buckling eigenvalue increases the static limit-load of a laterally loaded structure without degrading the post-limit behavior, increasing overall toughness. The elastic buckling eigenvalue of 3-story frame was increased, using the optimization method, from 98.7 to 141.5 and as a result the limit-load of the design was improved by 44%.
- Slender buildings are particularly well suited to the proposed optimization method. Since their behavior is more greatly influenced by geometric effects ( $P-\Delta$  effect). Thus, stability, which is the basis of the optimization methodology, becomes more important. For example, the 8-story frame which is a tall and slender building the optimization method improved the limit-load of the design by 100%.
- Statically based optimal design results in an optimized design that behaves well under dynamically applied loads. The optimization method is directly aimed at improving the limit-load and post-limit slope response of a statically loaded structure but has the consequence of improving the performance of the structure under dynamic loads.
- The frequency penalty function can help control the vibration spectrum and can be thought of as a flexible constraint imposed on a design. The examples demonstrated that even without the vibration penalty, the static based design procedure improves dynamic performance of the structures. Nevertheless the frequency penalty may be important in some applications.
- Under dynamically applied loads it was noticed that the optimal structure controlled cyclic drift better than the initial design.
- Based on the few examples optimized one might conclude that the optimal structure tends toward to having less element damage on average than the initial design. However, more study needs to be done to substantiate such a claim.

## CHAPTER 4

### MULTIPLE OBJECTIVE OPTIMAL DESIGN OF 3-D FRAMED STRUCTURES BASED ON A STABILITY CRITERION WITH MULTIPLE LOADING CONDITIONS

#### 4.1. Overview

Much of present design methods are based on experience gained over several decades, largely using two-dimensional idealization of structures. However, such information may be of little use for the design of special structures. Three-dimensional design problems are more complicated to carry out, but they yield insight into the real behavior of the structure. Today with the help of the new generation of the computer systems and different optimization methodologies one can solve complex and unprecedented static and dynamic design problems. Although researchers in the field of structural engineering generally agree that optimum design of three-dimensional building frames especially in the seismic regions would be beneficial, methods have been slow to emerge. Most of the research in this area has dealt with the optimization of truss and plane frame structures.

The design methodology to be presented here is a multiple-objective optimization procedure whose objective functions involve the buckling eigenvalues and eigenvectors of the structure. A constant weight with bounds on the design variables is used in conjunction with an optimality criterion approach. The method provides a general tool for solving complex design problems and generally leads to structures with better limit strength and stability.

One of the novelties of the new design methodology is its ability to efficiently model and design structures under multiple loading conditions. These loading conditions can be different factored loads or any kind of loads that can be applied to the structure simultaneously or independently.

The following is a short presentation of the multiple objective optimization problem, followed by the formulation of the optimization algorithm.

#### 4.2. Multicriteria Optimization

In many of structural design problems, there exist several often conflicting criteria to be considered by the designer. It has been a common practice to cast design problems in the framework of a



single objective function optimization problem. But, in recent years more attention has been paid to multiobjective optimization problems. Multiobjective optimization where the objective function is vector-valued offers a promising method for considering different and mutually conflicting requirements in a design problem. Some of the recent work using multicriteria optimization in the area of structural mechanics can be found in the work of researchers such as Koski (1979) and Koski and Silvenninen (1982) where they studied multicriteria optimization of trusses by choosing weight and several displacement criteria as design criteria. A constraint method to solve a structural design problem was applied by Carmichael (1980). Austin and Pister (1985) applied the multicriteria optimization technique to design earthquake-resistant steel buildings where minimum weight, minimum story drifts and maximum dissipated energy were used as the objective functions.

Multicriteria optimization has been used by many researchers in such areas as operations research, control theory, water resources, and many others. A comprehensive discussion on the topic of multicriteria optimization can be found in Cohon (1978), Goicoechea (1982), and Dlesk and Liebman (1983).

#### 4.2.1. Noninferiority

Some mathematical background and terminology are given here to make the reader familiar with concepts frequently used in this and future chapters.

Mutliobjective programming deals with optimization problem with two or more objective functions. The general multiobjective optimization is stated as:

$$\text{Maximize } Z(x) \quad (4.1)$$

Where  $Z$  is the multicriteria objective function given by

$$Z(x) = \{Z_1(x) \ Z_2(x) \ \cdot \cdot \cdot \ Z_m(x)\} \quad (4.2)$$

where  $Z_i$  is the  $i$ th individual objective function.

In single-objective problems, the goal of solving the optimization problem is to identify an optimal solution which is feasible and to come up with the best value of the objective function. In the



case of multiple-objective optimization there exists no unique optimal value which would result in an optimum for all criteria at the same time.

In the context of multiobjective optimization a new concept called *noninferiority* serves a similar purpose as the optimum for a single optimization problem. The idea of noninferiority as defined by Cohen (1978) is also called *nondominance* or *Pareto optimality* by different researchers in different fields of research.

Definition: A vector  $x^* \in X$  is called *noninferior* or *Pareto optimal* if and only if there exists no  $x \in X$  such that  $Z_i(x) \geq Z_i(x^*)$  for  $i=1, 2, \dots, m$  with  $Z_j(x) > Z_j(x^*)$  for at least one  $j$ . Here  $X$  is the feasible set. The definition of noninferiority simply says that  $x^*$  is noninferior if there exists no feasible vector  $x$  which would increase some objective functions without causing a simultaneous decrease in at least one objective. The corresponding vector  $Z^* = Z(x^*)$  in the objective space is called a noninferior solution.

There are many different generating techniques to determine the noninferior set. A good survey of different generating techniques can be found in chapter 22 of Atrek, *et al.* (1984) and Cohon (1975). The most popular generating techniques are weighting methods and constraint methods. A weighting method is used in this study because it is the most natural way of combining objective functions when they are of the same type.

The optimization problem considered in this study is atypical of multiobjective optimization problems because all of the objective functions have the same nature and yet are conflicting. For example, maximizing one buckling eigenvalue might result in a decrease in another one. Since all the objective functions are of the same nature, a weighting technique is the best method to produce the noninferior set. One of the advantages of the formulation developed here is that all the weighting factors are determined automatically, eliminating the principal difficulty inherent in a general weighting solution technique.

The current formulation developed is an optimization problem consisting of set of objectives  $\{\mu_1^2, \mu_1\mu_2, \dots, \mu_N^2\}$ . The objectives are combined using a weighting technique as  $\sum \sum w_{ij}\mu_i\mu_j$  where there are infinite number of different combinations of weighting factors that can be used. The whole noninferior set can be obtained by using all the possible combinations of weighting factors. For the multiple objective optimization problem concerned here, we as the decision maker can put preference on a set of the objective functions based on our knowledge of the structural mechanics by

choosing the weighting factors accordingly. For example, mode 25 has negligible participation in the response of the structure and by maximizing it, no advantage is gained. Therefore, the importance of mode 25 can be put to zero by choosing its weighting factor zero. Usually the first few eigenvalues dominate and more weight needs to be put on them. Therefore there is no need to obtain the whole noninferior set. The number of different combination of weighting factors can be reduced to only a few by knowing the mechanics of the structures and our judgment.

#### 4.3. Formulation and Development

To improve the limit behavior and stability characteristics of the three-dimensional framed structure under multiple loading cases, one needs to mix several different ingredients to generate an objective function. Similar to Chapter 2 one should include the buckling eigenvalues in the objective. To handle multiple loading conditions, we also purpose including the loading conditions directly in the objective function. We further hypothesize that the loading conditions should become important to the objective function if they cause displacements similar to a buckling eigenvector which is in the design subspace. This observation was made clear in development of the approximate method in appendix C. The proposed formulation then, seeks to maximize buckling eigenvalues of the structure using the work of the various load cases going through modal displacements as weighting factors.

One natural way to put all these ingredients in the framework of an objective function is to combine them in a linear form as:

$$\sum_i^N \sum_j^{NL} \mu_i |f_j \cdot \phi_i| \quad (4.3)$$

or in a quadratic form as:

$$\sum_i^N \sum_j^{NL} \mu_i |f_j \cdot \phi_i + f_i \cdot \phi_j| \mu_j \quad (4.4)$$

The only shortcoming of using a quadratic form such as Eqn. (4.4) is that the number of the buckling eigenpairs used in the objective function is not necessary equal to the number of the loading



conditions. Therefore, to make a compromise it is best to use an alternate form which has quadratic terms only for some terms such as:

$$\sum_{i=1}^N \sum_{j=1}^{NL} \mu_i |f_j \cdot \phi_i| \mu_{\Pi_j} \quad (4.5)$$

where  $\Pi_j$  is a vector containing a set of index numbers with values in the range  $[1, N]$  with one-to-one correspondence with the buckling eigenvalues. The dimension of the set is equal to the number of the loading conditions ( $NL$ ). For example,  $\Pi = \{2, 3\}$  leads to  $\sum_{i=1}^N \mu_i [(f_1 \cdot \phi_i) \mu_2 + (f_2 \cdot \phi_i) \mu_3]$ .

Equation (4.5) can be considered as a quasi-quadratic form with  $\mu_{\Pi_j}$  used to put more emphasis and importance on some of the eigenvalues. How to choose  $\Pi_j$  will be discussed in the future chapters where the application of the design procedure is presented.

Choosing Eqn. (4.5) as the objective function, we define the multiple objective optimization problem to be:

MAXIMIZE

$$\sum_{i=1}^N \sum_{j=1}^{NL} \mu_i(x) \beta_{ij}(x) \mu_{\Pi_j}(x) \quad (4.6)$$

SUCH THAT

$$\begin{aligned} \sum_{i=1}^M A_i(x_i) \Omega_i &= \Gamma \\ \underline{x}_{ij} &< x_{ij} < \bar{x}_{ij} \end{aligned} \quad (4.7)$$

where  $N$  = number of eigenpairs used;  $L_v$  = length of  $v$ th element;  $NL$  = number of loading conditions considered;  $\mu_i$  =  $i$ th elastic critical buckling eigenvalue;  $\Gamma$  = given weight of the structure;  $A_i$  = area of group  $i$  (elements in each group have identical cross sectional properties);  $x$  = total design vector where  $x = \{x_1, x_2, \dots, x_M\}$ ;  $x_i$  = design vector for group  $i$  where  $x_i = \{x_{i1}, x_{i2}, \dots, x_{iN_v}\}$  where  $N_v$  is the total number of independent design variables;  $x_{ij}$  =  $j$ th design variable for  $i$ th group;  $\underline{x}_{ij}$  = minimum permissible  $j$ th design variable for  $i$ th group;  $\bar{x}_{ij}$  = maximum permissible  $j$ th design variable for  $i$ th group;  $M$  = number of element groups;  $\rho_v$  = specific mass of  $v$ th element;  $\Omega_i = \sum_{v \in i} \rho_v L_v$  = specific mass of group  $i$ .

An I-beam can be identified by three independent design variables ( $N_v=3$ ) such as:  $x_{m1} = b_m$ ,  $x_{m2} = h_m$ ,  $x_{m3} = t_m$  where the three design variables represent width, height, and flange



thickness of an I-beam cross section respectively. A rectangular cross section can be identified by two independent design variables ( $N_v=2$ ) such as:  $x_{m1} = b_m$ ,  $x_{m2} = h_m$  where are the two design variables represent height and width of a rectangular cross section.

The factor  $\beta_{ij} = |\phi_i \cdot f_j|$  is the weighted modal participation of the applied loading in which  $\phi_i$  is  $i$ th elastic buckling mode shape of the structure, and  $f_i$  is the  $i$ th loading case. If an applied loading does a lot of work going through a certain modal displacement, the factor  $\beta_{ij}$  will dictate the maximization of that mode. The noninferior set for the multiple-objective optimization problem (Eqn. (4.6)) is generated using a weighting method that incorporates preferences. The factor  $\beta_{ij}$  is a preference found automatically to determine the importance of each eigenvalue in the chosen subspace. For multiple loading cases, one can give preference to the importance of the loading condition by factoring the loading cases accordingly. Thus, factors used to scale the loading cases can serve as a weighting factor introduced by the designer.

Note that the form and the number of the objective functions change as the number of the eigenpairs chosen, or the number of the loading cases, or the load magnification factor change, resulting in a multiple objective optimization problem.

Using Eqn. (4.6) and Eqn. (4.7) the Lagrangian functional can be cast as:

$$L(x, \xi) = \sum_{i=1}^N \sum_{j=1}^N \mu_i(x) \beta_{ij}(x) \mu_{nj}(x) - \xi \left[ \sum_{i=1}^M A_i(x_i) \Omega_i - \Gamma \right] \quad (4.8)$$

where  $\xi$  is the Lagrange multiplier. It should be pointed out here that the constraints on the size of the elements given in Eq. (4.7) are not included in deriving Eq. (4.8). Constraint on the permissible sizes can be handled efficiently by treating them as passive constraints in the sense that whenever an element violates the size constraints, the design variable associated with that element adopts the minimum or the maximum permissible sizes and is placed in the passive set. A more detailed discussion of active/passive design set strategy is given in section 2.5.3.

Differentiating Eq. (4.8) with respect to design variable  $x_{mn}$  and setting the corresponding equation to zero results in:

$$\frac{\partial L}{\partial x_{mn}} = \sum_{i=1}^N \sum_{j=1}^N \left[ \frac{\partial \mu_i}{\partial x_{mn}} \beta_{ij} \mu_{nj} + \mu_i \frac{\partial \beta_{ij}}{\partial x_{mn}} \mu_{nj} + \mu_i \beta_{ij} \frac{\partial \mu_{nj}}{\partial x_{mn}} \right] - \xi \frac{\partial A_m}{\partial x_{mn}} \Omega_m = 0 \quad (4.9)$$

Rearranging Eqn. (4.9) results in the *optimality criteria*

$$\frac{\sum_{i=1}^N \sum_{j=1}^N \left[ \frac{\partial \mu_i}{\partial x_{mn}} \beta_{ij} \mu_{\pi_j} + \mu_i \frac{\partial \beta_{ij}}{\partial x_{mn}} \mu_{\pi_j} + \mu_i \beta_{ij} \frac{\partial \mu_{\pi_j}}{\partial x_{mn}} \right]}{\xi \frac{\partial A_m}{\partial x_{mn}} \Omega_m} = 1 \quad \begin{matrix} m = 1, \dots, M \\ n = 1, \dots, N_v \end{matrix} \quad (4.10)$$

In Eqn. (4.10) there exist two sensitivity terms: sensitivity of  $\beta_{ij}$ , and  $\mu_i$  with respect to the design variables. The sensitivity of the  $\beta_{ij}$  is a function of sensitivity of eigenvectors. Thus, sensitivities of both eigenvalues and eigenvectors are needed. Determination of these sensitivities is discussed in the following section.

#### 4.4. Eigenvalue and Eigenvector Sensitivity Analysis

Evaluation of the optimality conditions require knowledge of the sensitivity, or rate of change, of the buckling eigenvalues and eigenvectors with respect to the design variables. Procedures for computing these sensitivities have been known for some time, but efficient methods of computation continue to be of interest to researchers. A complete and detailed discussion of the problem has been given recently by Dailey (1989). Some of the basic ideas are outlined below.

Consider the following eigenvalue problem

$$K\phi = \mu G\phi \quad (4.11)$$

where  $K$  is the (positive definite) elastic stiffness matrix and  $G$  is the (possibly indefinite) geometric stiffness matrix. Both of matrices are symmetric and depend on design variables  $x$ . If the dimension of the matrices  $K$  and  $G$  is  $N$ , then Eqn. (4.11) gives rise to solution pairs  $(\mu_i, \phi_i)$ ,  $i=1, \dots, N$ . The eigenvectors are orthogonal and hence span  $N$ -dimensional space. Further assume that the eigenvectors are normalized such that  $\phi_i^T G \phi_i = \text{constant}$ . The value of the constant, which may be negative since matrix  $G$  is possibly indefinite, is not important to the present derivation. There exists the possibility that  $\phi_i^T G \phi_i = 0$ , so one must be careful when dividing this constant out in the following derivations. For practical purposes we can constrain our vectors to be perpendicular to the nullspace of  $G$  to avoid the problem since the infinite eigenvalues are of no interest in the present setting.

Consider that the matrices  $K$  and  $G$  depend upon a parameter; possibly, but not necessarily, a design variable or a linear combination of design variables. The eigenvalues and eigenvectors must



also depend implicitly upon the same parameter. Differentiating Eqn. (4.11) with respect to the parameter yields

$$K'\phi + K\phi' = \mu'G\phi + \mu G'\phi + \mu G\phi' \quad (4.12)$$

where a prime indicates differentiation with respect to the parameter. Collecting terms gives

$$[K' - \mu G']\phi + [K - \mu G]\phi' - \mu'G\phi = 0 \quad (4.13)$$

which holds for all pairs of eigenvalues and eigenvectors. The derivative of the  $i$ th eigenvector can be expanded in terms of eigenvectors, which form a basis

$$\phi'_i = \sum_{k=1}^N \gamma_{ik} \phi_k \quad (4.14)$$

substituting Eqn. (4.14) into Eqn. (4.13) and multiplying by  $\phi_j^t$  yields

$$\phi_j^t [K' - \mu_i G']\phi_i + \sum_{k=1}^N \gamma_{ik} \phi_j^t [K - \mu_i G]\phi_k - \mu'_i \phi_j^t G\phi_i = 0 \quad (4.15)$$

or, noting the orthogonality of the eigenvectors

$$\phi_j^t [K' - \mu_i G']\phi_i + \gamma_{ij} (\mu_j - \mu_i) \phi_j^t G\phi_j - \mu'_i \phi_j^t G\phi_i = 0 \quad (4.16)$$

If  $i=j$ , the second term disappears and Eqn. (4.16) gives an expression for the derivative of the eigenvalue

$$\mu'_i = \frac{\phi_i^t [K' - \mu_i G']\phi_i}{\phi_i^t G\phi_i} \quad (4.17)$$

If  $i \neq j$ , Eqn. (4.16) allows the determination of the coefficient  $\gamma_{ij}$

$$\gamma_{ij} = \frac{\phi_j^t [K' - \mu_i G']\phi_i}{(\mu_i - \mu_j) \phi_j^t G\phi_j} \quad (4.18)$$

The coefficient  $\gamma_{ii}$  is obtained by differentiating the normality condition

$$\phi_i^t G\phi_i + \phi_i^t G\phi'_i + \phi_i^t G'\phi_i = 0 \quad (4.19)$$

Substituting the eigenvector expansion and solving for the only unknown coefficient



$$\gamma_{ii} = -\frac{1}{2} \frac{\phi_i^t G' \phi_i}{\phi_i^t G \phi_i} \quad (4.20)$$

By placing the coefficients found into Eqn. (4.14), one obtains the sensitivity for the  $i$ th eigenvector and eigenvalue as

$$\begin{aligned} \mu'_i &= \frac{\phi_i^t [K' - \mu_i G'] \phi_i}{\phi_i^t G \phi_i} \\ \phi'_i &= \sum_{j=1} \frac{\phi_j^t [K' - \mu_i G'] \phi_i}{(\mu_i - \mu_j) \phi_j^t G \phi_j} \phi_j - \frac{1}{2} \frac{\phi_i^t G' \phi_i}{\phi_i^t G \phi_i} \phi_i \end{aligned} \quad (4.21)$$

Clearly, the parameter with respect to which differentiation is done can be any of the design variables. Hence, Eqn. (4.21) can be used to compute the rate of change of the eigenproperties with respect to the design variables. The derivative of the geometric stiffness matrix is usually nearly zero and is therefore generally neglected in practical computations. Numerical derivation of the geometric stiffness matrix can be found in Appendix D. The matrix  $G'$  is identically zero for statically determinate structures since the distribution of force through the structure does not depend upon the element rigidities.

The sensitivity of the  $\beta_{ij}$  is easily computed from the eigenvector sensitivity as

$$\beta'_{ij} = \phi'_i \cdot f_j \quad (4.22)$$

The eigenvector sensitivity derived in Eqn. (4.21) is theoretically correct and the derivation is instructive, but the formula suffers from some practical drawbacks. The expression for the sensitivity of an eigenvector requires the knowledge of all of the eigenvectors and eigenvalues of the system. The method becomes prohibitively expensive for large systems since the determination of all  $N$  eigenpairs becomes practically impossible. The approach followed in solving practical problems in the present study is to truncate the sum after a finite (small) number of terms. Specifically, the eigenvector derivatives are determined from Eqn. (4.21) by including only those eigenvectors in the subspace used to define the objective function. Although using only a few eigenvectors in Eqn. (4.21) does not give the exact eigenvector derivative, computational experience has shown that the results are adequate for the optimization algorithm.

Nelson (1976) presented a powerful algorithm for computing eigenvector and eigenvalue derivatives of general matrices with nonrepeated eigenvalues in which the derivatives of any mode require only the eigenvalue and eigenvector of that mode. Nelson's method is succinctly derived by Dailey (1989), and the main features of the method are described below. From Eqn. (4.13) one can see that the eigenvector derivative can be obtained by solving the following system of equations

$$[K - \mu G]\phi' = \mu' G\phi - [K' - \mu G']\phi \quad (4.23)$$

where the quantities on the right-hand-side can all be considered known since the derivative of the eigenvalue is easily obtained from Eqn. (4.17). The coefficient matrix matrix  $K - \mu G$  is one degree rank deficient (for a distinct eigenvalue), and the nullspace is spanned by the eigenvector  $\phi$ . Thus, the solution the Eqn. (4.23) is given by the sum of a particular solution,  $v$ , plus a component in the nullspace as

$$\phi' = v + c\phi \quad (4.24)$$

The particular solution is found by setting one component of  $v$  to zero (usually the one corresponding to the largest component of  $\phi$ ) and solving the resulting equations. The constant  $c$  is determined from the normality condition given by Eqn. (4.19). Substituting Eqn. (4.24) into Eqn. (4.19) one gets

$$(v + c\phi)^T G \phi_i + \phi_i^T G (v + c\phi) + \phi_i^T G' \phi_i = 0 \quad (4.25)$$

Solving for  $c$  there results

$$c = -\frac{1}{2} \frac{2\phi^T G v + \phi^T G' \phi}{\phi^T G \phi} \quad (4.26)$$

thereby defining the eigenvector derivative.

Many of the equations derived thus far are valid only for distinct eigenvalues; in particular, Eqn. (4.21) and Nelson's method. In the last decade there has been a great deal of interest in systems having repeated eigenvalues since they occur naturally in many symmetric structures. Olhoff and Rasmussen (1977) and Masur and Mroz (1980) have shown that in a certain clamped columns, optimized to maximizing the buckling load, a repeated eigenvalue may occur. Prager and Prager (1979) used a finite dimensional model to demonstrate that repeated eigenvalue can occur in an



optimal column. Indeed, many optimization problems lead to symmetric structures which often have multiple eigenvalues.

The sensitivity properties of the repeated eigenvalue problems have been studied by researchers in the disciplines of system identification, structural control, and optimization. Some of the related work done on the design sensitivity of the repeated eigenvalues can be found in Haug and Rousselet (1980), Haug and Choi (1986), Zhong and Cheng (1986), and Wardi and Polak (1982). Ojalvo (1986 and 1987) extended Nelson's algorithm to handle repeated eigenvalues. Recently, Dailey (1989) found that the method presented by Ojalvo was correct only for certain special cases and he extended the method to handle general eigenvalue and eigenvector derivative of real symmetric matrices for the case of repeated eigenvalues. Dailey's method not only leads to an algorithm for computing the derivatives of eigenvalues and eigenvectors for the degenerate case, but also gives insight into the difficulties associated with using the information.

An eigenvalue of multiplicity  $m$  is characterized by an  $m$ -dimensional subspace in which all vectors are eigenvectors. If the system is perturbed, the multiple eigenvalue splits into up to  $m$  distinct eigenvalues. From this observation it is clear that there are  $m$  eigenvalue derivatives (some of which may come out to be repeated) even though there is only one eigenvalue. For each eigenvalue derivative there is an eigenvector derivative. The problem arises from the fact that, while the eigenvectors are not unique, the derivatives are unique (except for repeated eigenvalue derivatives). Put another way, the derivatives of the eigenvectors only exist in certain directions. Define matrices  $A$  and  $B$  as

$$A \equiv \Phi' [K' - \mu G'] \Phi \quad B \equiv \Phi' G \Phi \quad (4.27)$$

where  $\Phi = [\phi_1, \phi_2, \dots, \phi_m]$  ( $n \times m$ ) is a matrix of the eigenvectors corresponding to the repeated eigenvalue. Now consider the following auxiliary eigenvalue problem

$$A\psi = \lambda B\psi \quad (4.28)$$

The eigenvalues  $\lambda_1, \lambda_2, \dots, \lambda_m$  of Eqn. (4.28) are the eigenvalue derivatives,  $\mu'_1, \mu'_2, \dots, \mu'_m$ , of the original system. The eigenvectors,  $\psi$ , of Eqn. (4.28) determine the directions in which the derivatives of the eigenvectors exist. Let  $\Psi = [\psi_1, \psi_2, \dots, \psi_m]$  ( $m \times m$ ) be a matrix whose columns are the eigenvectors of Eqn. (4.28). The directions in which eigenvector derivatives exist are the columns of the matrix  $Z$  which is given in terms of the eigenvalues of the original system as  $Z = \Phi \Psi$  ( $n \times m$ ). Note



that because  $\Psi$  is square and its columns are orthonormal, operation with  $\Psi$  represents pure rotation in  $m$ -dimensional space. Thus, the directions in which eigenvector derivatives exist are simply rotations of the original eigenvectors.

The matrix  $A$  depends on the derivatives of the matrices  $K$  and  $G$ . Therefore, the directions in which eigenvector derivatives exist will be different for each different design variable, complicating the evaluation of the eigenvector sensitivities. Repeated eigenvalues in an unfortunately chosen symmetric initial design can be easily diagnosed and easily cured. For the optimization problems solved here the solutions will, at worst, converge to a configuration with a repeated eigenvalue. In those cases convergence of the optimization algorithm is generally achieved before numerical difficulties set in. As a consequence of the preceding observations, the implementation used for the computations presented in subsequent chapters treats the spectrum as completely distinct. Later, through some examples, the accuracy and validity of that assumption will be examined.

To determine Eqn. (4.22), one needs to find the gradient of the stiffness matrix with respect to the design variables. The linear elastic structural stiffness  $K$  exhibits the following explicit form in terms of cross sectional area, moment of inertia, and torsional constant

$$K(x) = \sum_{i=1}^M \left[ A_i(x_i) \sum_{p \in i} K_p^A + I_i^M(x_i) \sum_{p \in i} K_p^M + I_i^m(x_i) \sum_{p \in i} k_p^m + J_i(x_i) \sum_{p \in i} K_p^T \right] \quad (4.29)$$

where  $K_p^A$ ,  $K_p^M$ ,  $K_p^m$ , and  $K_p^T$  are respectively, axial plus shear, major axis bending, minor axis bending, and torsion contributions to stiffness for element  $p$  with the relevant cross sectional parameter factored out.

Differentiating the structural stiffness matrix given in Eqn. (4.29) with respect to design variable  $x_{mn}$  results in

$$\frac{\partial K}{\partial x_{mn}} = \frac{\partial A_m}{\partial x_{mn}} K_m^A + \frac{\partial I_m^M}{\partial x_{mn}} K_m^M + \frac{\partial I_m^m}{\partial x_{mn}} K_m^m + \frac{\partial J_m}{\partial x_{mn}} K_m^T \quad (4.30)$$

where the partials in Eqns. (4.30) can easily be calculated using the cross sectional properties. The relationship between moment of inertias and areas and design variables can be determined based on the type of the cross section as presented for rectangular and I-beam cross sections in section 4.7.

Having the partial derivative of  $K$  with respect to the design variables, the sensitivity of the  $\beta_{ij}$  with respect to the design variables can be calculated from Eqn. (4.22).

Note terms such as  $K_p^A$  are extremely sparse, involving non-zero elements only in the slots associated with degree-of-freedom of element  $p$ . Consequently the element contributions  $\phi_k^t K_p^A \phi_i$  required in Eqn. (4.21) can efficiently be efficiently computed.

Now all sensitivity terms in the *optimality criteria* Eqns. (4.10) are determined. To make the formulation easier to follow Eqn. (4.10) can be simplified as:

$$\frac{Q_{mn}}{\xi} = 1 \quad \begin{matrix} m=1, \dots, M \\ n=1, \dots, N_v \end{matrix} \quad (4.31)$$

where  $m$  represents the group number,  $n$  represents the design variable within that group, and  $Q_{mn}$  is given by:

$$Q_{mn} = \frac{\sum_{i=1}^N \sum_{j=1}^N \left[ \frac{\partial \mu_i(x)}{\partial x_{mn}} \beta_{ij}(x) \mu_{nj}(x) + \mu_i(x) \frac{\partial \beta_{ij}(x)}{\partial x_{mn}} \mu_{nj}(x) + \mu_i(x) \beta_{ij}(x) \frac{\partial \mu_{nj}(x)}{\partial x_{mn}} \right]}{\frac{\partial A_m(x)}{\partial x_{mn}} \Omega_m} \quad (4.32)$$

The term  $Q_{mn}$  is the buckling strain energy density in the group  $m$ .

#### 4.5. Recurrence Relations

The optimality criteria are used to modify the design variables in each iteration in terms of recurrence relations similar to that proposed by Khot et al. [1981]:

$$x_{mn}^{\kappa+1} = x_{mn}^{\kappa} \left[ 1 + \frac{1}{r} \left[ \frac{Q_{mn}}{\xi} - 1 \right] \right] \quad (4.33)$$

where  $\kappa$  is the iteration number and  $r$  is the step size parameter. The convergence behavior depends on the parameter  $r$ . The method of choosing the step length to speed convergence was explained in detail in section 2.5.1.

#### 4.6. Equation to Determine Lagrange Multiplier

In order to be able to use the recurrence Eqn. (4.33), the Lagrange multiplier  $\xi$  has to be determined. The Lagrange multiplier is determined by using the condition that after each iteration the design moves on the constraint surface so that the constraint is satisfied. A set of equations to determine the Lagrange multiplier can be obtained by linearizing the constraint equation about current iterate.

The weight constraint can be expanded as:

$$C(x) = \sum_{m=1}^M A_m(x_m) \Omega_m - \Gamma = 0 \quad (4.34)$$

Linearizing about the configuration  $x^e$  one obtains:

$$L[C]_{x=x^e} = C(x^e) + \sum_{m=1}^M \sum_{n=1}^{N_y} \frac{\partial C}{\partial x_{mn}} (x_{mn} - x_{mn}^e) \quad (4.35)$$

where the partial derivative of constraint with respect to the design variable  $x_{mn}$  can be evaluated by taking derivative of Eqn. (4.34):

$$\frac{\partial C}{\partial x_{mn}} = \frac{\partial A_m}{\partial x_{mn}} \Omega_m \quad (4.36)$$

The Lagrange multiplier can be obtained by satisfying the linearized constraint equation at the new iterate  $x^{e+1}$ . Substituting Eqn. (4.33) and Eqn. (4.36) into Eqn. (4.35) and solving for Lagrange multiplier one gets:

$$\xi = \frac{\sum_{m=1}^M \sum_{n=1}^{N_y} \frac{\partial A_m}{\partial x_{mn}} x_{mn} \Omega_m}{\sum_{m=1}^M \left[ r A_m + \sum_{n=1}^{N_y} \frac{\partial A_m}{\partial x_{mn}} x_{mn} \right] \Omega_m - r \Gamma} \quad (4.37)$$

since the constant weight constraint is an equality,  $\xi$  can be either positive or negative.



#### 4.7. Specialization to Specific Cross Sectional Types

The design vector,  $\mathbf{x}_i$ , used in the preceding sections is a vector of independent variables identifying a cross section for group  $i$ . For example, the  $\mathbf{x}_i$  vector for a rectangular cross section would be

$$\mathbf{x}_i = \left\{ \begin{matrix} b \\ h \end{matrix} \right\}_i \quad (4.38)$$

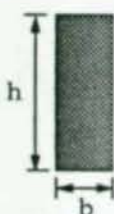
where  $b$  and  $h$  are the width and the height of the cross section. The cross sectional properties of rectangular section are:

$$I^M = \frac{1}{12}bh^3$$

$$I^m = \frac{1}{12}b^3h$$

$$A = bh$$

$$J = \frac{1}{3}hb^3 \left[ 1 - \frac{192b}{\pi^5 h} \tanh \frac{\pi h}{2b} \right]$$



where  $b < h$

(4.39)

Fig. 4.1. Rectangular Cross Sectional Properties

For an I-beam cross section the vector  $\mathbf{x}_i$  would be

$$\mathbf{x}_i = \left\{ \begin{matrix} b \\ h \\ t \end{matrix} \right\}_i \quad (4.40)$$

where  $b$ ,  $h$ , and  $t$  are the width, height, and the flange thickness respectively. The cross sectional properties of an I-beam are given below:

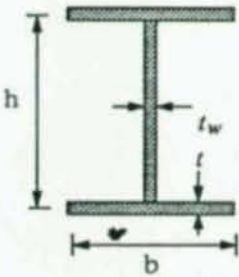
$$A = ht_w + 2bt$$

$$I^M = \frac{1}{12}t_w h^3 + \frac{1}{2}bt^2$$

$$I^m = \frac{1}{12}(b^3t + ht_w^3)$$

$$J = \frac{1}{3}(2bt^3 + ht_w^3)$$

$$t_w = \text{constant} \cdot t$$



(4.41)

Fig. 4.2. I-beam Cross Sectional Properties

#### 4.8. Convergence Criteria

The optimization problem theoretically is converged when all the optimality criteria as given in Eqns. (4.10) is satisfied with a specified tolerance. After each iteration the deviation of the optimality criteria from unity is calculated and if the norm of the deviation is less than the specified tolerance the iteration is terminated. The tolerance is specified by the designer.

#### 4.9. Scaling Procedure

After each iteration to satisfy the constraint relationship, it is necessary to scale the design variables to bring the weight of the structure to the level of the assigned weight constraint  $\Gamma$ . Scaling is necessary to insure that the design at each iteration is feasible. The following is a development of the scaling procedure for rectangular members. The same procedure can be developed for I-beam cross sections.

The weight of the structure after each iteration can be divided to three groups depending on which design variables are passive and which are active. Thus the total weight is given by:

$$\Gamma = W^{aa} + W^{ap} + W^{pp} \quad (4.41)$$

where  $W$ 's are various weights. A superscript "a" indicates an active design variable, superscript "p" indicates a passive design variable, and there is one superscript for each design variable in the group. Let  $M_{aa}$  be the set of groups with both design variables active,  $M_{ap}$  be the set of groups with height passive and width active,  $M_{pa}$  be the set of groups with width passive and height active, and  $M_{pp}$  be the set of groups with both height and width passive.

$$W^{aa} = \sum_{i \in M_{aa}} h_i^a b_i^a \Omega_i \quad (4.42)$$

$$W^{ap} = \sum_{i \in M_{ap}} h_i^p b_i^a \Omega_i + \sum_{i \in M_{pa}} h_i^a b_i^p \Omega_i \quad (4.43)$$

$$W^{pp} = \sum_{i \in M_{pp}} h_i^p b_i^p \Omega_i \quad (4.44)$$

The weight of the structure is scaled after each iteration by scaling only the active design variables. The scaling factor  $\zeta$ , such that  $x_{ij} \leftarrow x_{ij}\zeta$ , is determined by the equation:

$$\zeta^2 W^{aa} + \zeta W^{ap} + W^{pp} - \Gamma = 0 \quad (4.45)$$

solving for  $\zeta$  gives:

$$\zeta = \sqrt{\frac{\Gamma - W^{pp}}{W^{aa}} + \left(\frac{W^{ap}}{2W^{aa}}\right)^2} - \frac{W^{ap}}{2W^{aa}} \quad (4.46)$$

The scaling equation for  $n$  design variables per group is an  $n$ th order polynomial. Higher order polynomials can be easily solved by Newtons method.

A graphic presentation of the scaling procedure for a case with two design variables is given in Fig. 4.3. After each iteration, a design in the design space, such as point A, is achieved. After scaling the design moves from point A to point B where the weight constraint is satisfied. After each iteration the design gets closer to the optimum design point C.

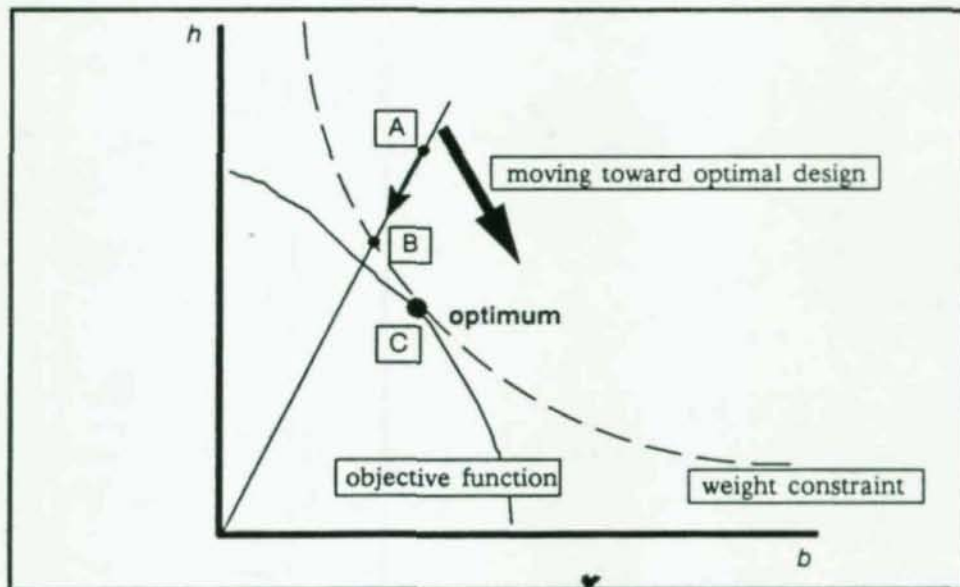


Fig. 4.3. Scaling of Two Design Variable Design Space



## CHAPTER 5

### APPLICATION OF 3-D OPTIMIZATION ALGORITHM TO FRAMED STRUCTURES

#### 5.1. Overview

To demonstrate the performance and the strength of the proposed optimization methodology several frames are optimized. Different framed structures, under single and multiple loading conditions, are optimized and analyzed. Parameter studies are carried out to examine the effect of the number of eigenpairs used in the objective function, the number of design variables carried, different choices for the objective function, and different ways of formulating the linearized buckling eigenvalue problem. The parameter studies show the effect of each parameter on the final optimal design.

#### 5.2. 3-D Analysis Procedure

The approach employed in the analyses of the 3-D frames of this study is that proposed by Simo (1984), Simo and Vu-Quoc (1986), and Molhem (1989). The theoretical background related to this method can be found in Simo (1984) and the computational aspects are treated in Simo and Vu-Quoc (1986). Simo (1984) introduced the concept of attaching an orthogonal basis to each cross section and used that basis to develop material and spatial statements of a fully nonlinear 3-D beam theory. The theory allows the use of incremental rotations of the moving frame as rotational degrees of freedom. Simo and Vu-Quoc (1986) employed Euler parameters to represent finite rotation to avoid the singularity typically associated with the use of Euler angles.

The elasto-plastic model used here is a stress resultant model. The yield function, taking into account isotropic and kinematic hardening considered was such that the yield surface formed an ellipsoid in stress resultant space. Specifically it had the form

$$\mathcal{Y}(\mathbf{z}, K) = \sum_{i=1}^6 \left( \frac{z_i}{z_{0i}} \right)^2 - K(W^p) \quad (5.1)$$

where  $z = \{N, V_1, V_2, T, M_1, M_2\}$  is the vector of stress resultants including axial force ( $N$ ), major and minor axis shear ( $V_1, V_2$ ), torque ( $T$ ), and major and minor bending moments ( $M_1, M_2$ ). The normalized factors  $z_0$  are the fully plastic values of the stress resultant. The plastic work  $W^p$  is defined as

$$W^p = \int_0^{\epsilon} z \cdot d\epsilon^p \quad (5.2)$$

and the effective stress is

$$z = q - a \quad (5.3)$$

where  $q$  is the material stress resultant vector,  $\epsilon^p$  is the plastic strain vector conjugate to  $q$ , and  $a$  is the back stress resultant vector.  $K$  is the isotropic hardening function with  $K(0)=1$  which is generally nonlinear in  $W^p$ .

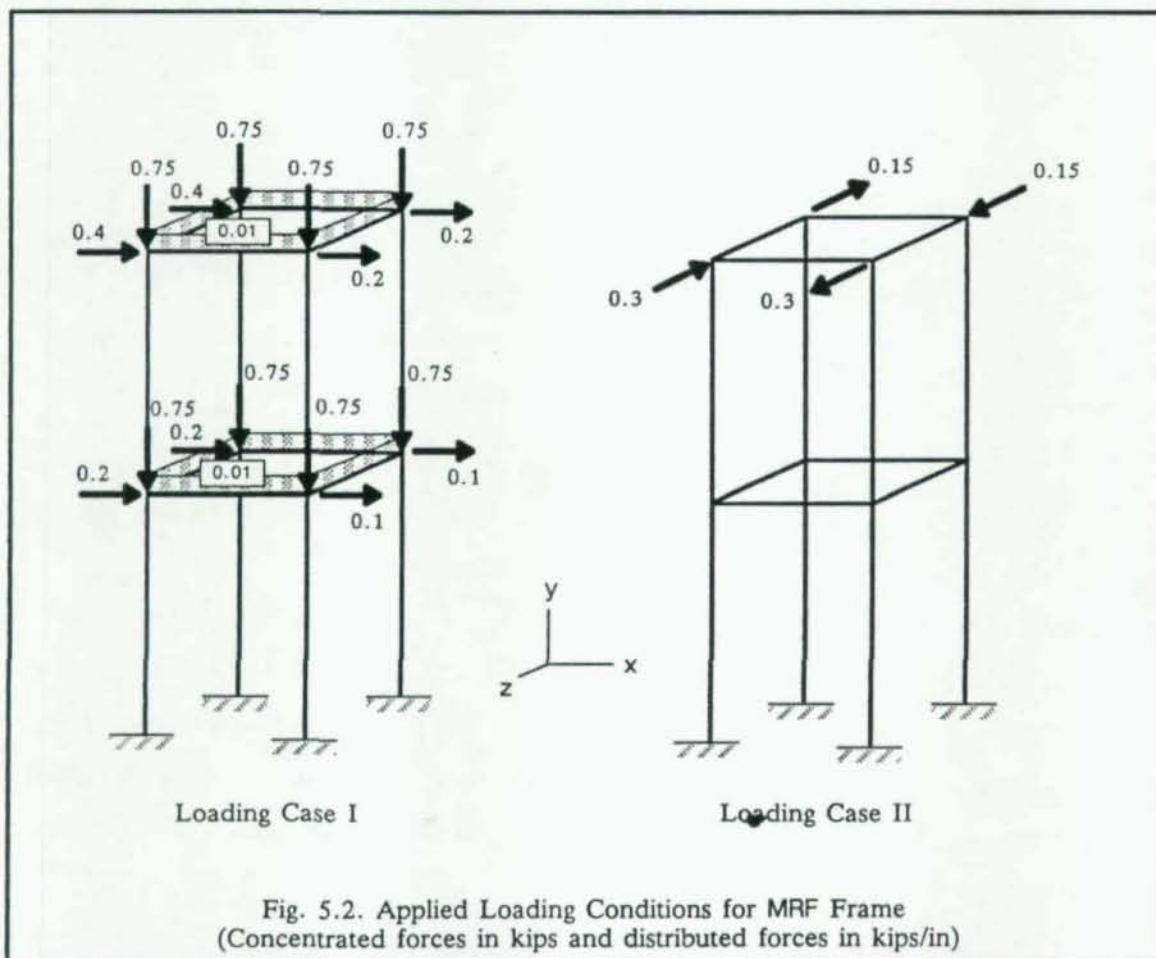
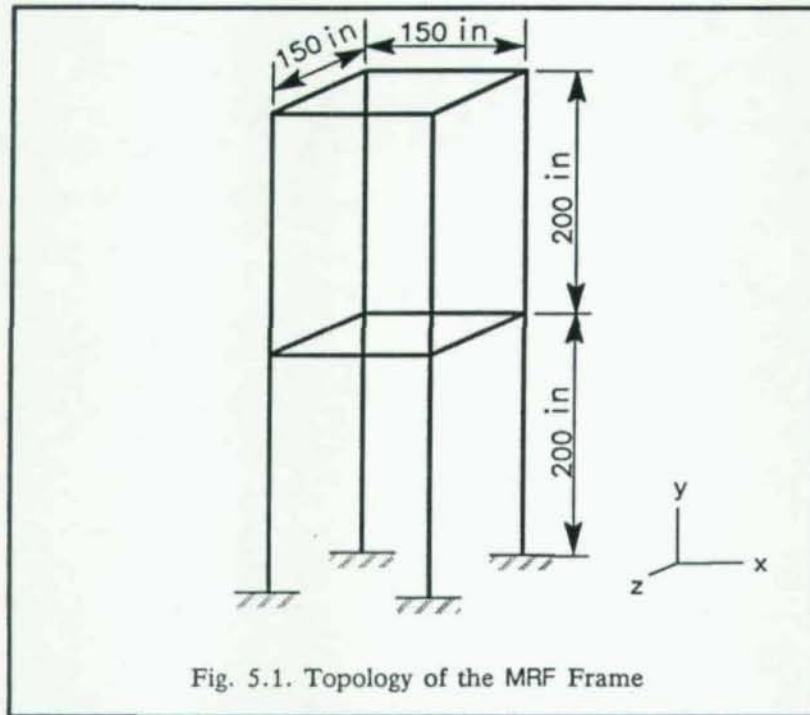
The computation scheme uses the return mapping algorithm with a consistent tangent operator to do rate independent plasticity (Simo and Taylor, 1985; and Molhem, 1989).

### 5.3. Description of MRF Example Problem

MRF is a two-story, single bay, three-dimensional, moment-resisting frame with tall stories. Stories were chosen tall to highlight stability as an important design criterion. The topology of the frame is given in Fig. 5.1 where one can note that the width in both directions is 150 inches and the total height is 400 inches.

Frame MRF will be designed under one or two different loading conditions. One loading case is applied in X-direction and one is applied in Z-direction. Each load case models a different phenomenon such as an earthquake, a wind, or a geometric imperfection. The first load case (load case I) consists of proportionally applied triangular shaped load in the X-direction along with a distributed non-proportional loading applied on the girders and proportional vertical loading applied at the column levels. Lateral loads are obtained following UBC specifications. The second type of load case (load case II) consists of torsional loads applied at the top story level in Z-direction.

Load cases I and II are mutually exclusive loading conditions and not necessarily applied at the same times. The two types of loadings are shown in Fig. 5.2.





For each optimization problem solved, a figure is presented displaying the evolution of the buckling eigenvalues during the course of optimization. This spectral evolution allows one to easily observe how the eigenvalues shift and how their magnitudes alter, and gives insight into the behavior of the structure as the optimization progresses. The mode that has the highest participation or has the highest  $\beta_{ij}$  factor is singled out with a cross marker. The eigenvalues at each iteration are connected with lines. If different step sizes are used during the optimization, the step size will be displayed on this figure also.

Two types of load-deformation curves are presented: one with top displacement in X-direction and one with top displacement in Z-direction. The one with top displacement in X-direction is analyzed under loading case I. Similarly, the one with top displacement in Z-direction is analyzed under load case II. For each figure the load-deformation is given for both the initial design and the optimal design.

MRF is used as an initial design and is optimized in the subsequent sections. The following is the discussion of the different optimization procedure and the performance of the optimized designs.

### 5.3.1. Single Loading

#### 5.3.1.1. Four Design Variables Under Single Loading (2M-1L)

The notation (2M-1L) stands for two material sets and one loading condition. First the MRF frame is optimized under single loading using the objective function given below:

Objective Function      Maximize $\sum_{i=1}^N \mu_i \beta_{i1} \mu_1$
--

Each material set has two design variables: width ( $b$ ) and height ( $h$ ) of the rectangular cross section. For the problems optimized under category (2M-1L), all the columns have identical material properties; so do the girders. To understand the effect of the number of eigenpairs on the optimization, three different numbers of eigenpairs (6, 8, and 10) were used. The following is a summary of the optimization procedure and the performance of the optimized designs using different eigenpairs in the objective function. The properties of the optimized design are given in Table 5.1.

(1) N=6

The spectral evolution during the optimization for N=6 is given in Fig. 5.3. Although, optimization continued until iteration 22, it practically converged in 10 iterations. During the initial iterations the magnitude of each of the eigenvalues changed by large factors until iteration 7 where one of the girder's design variables became passive. Subsequently, the optimization converged smoothly.

Mode 3 had the highest participation factor ( $\beta_{ij}$ ) at optimum. This behavior was expected because mode 3 was a sidesway mode. The sidesway mode started as mode 2 and as it was maximized through optimization it switched place with mode 3 and stayed as mode 3 until convergence. The initial design and the optimized design were both analyzed under loading case I and the resulting load-deformation curves are given in the Fig. 5.3, in which one can see that the optimized design had higher load carrying capacity than the initial design with the same post-limit slope compared to the initial design.

(2) N=8

The member properties of the final optimized design for N=8 is similar to previous case with N=6. The spectral evolution and the load-deformation of the initial and the optimum design are given in Fig. 5.4. The optimization practically converged in 15 iterations.

(3) N=10

The spectral evolution for N=10 (Fig. 5.5) shows a lot of activity until iteration 32 where the algorithm settles and finds its way toward convergence at iteration 45. Before iteration 27 all the design variables were active and the algorithm was somewhat aimless. At iteration 27 one of the girder design variables became passive and was kept passive until convergence.

The algorithm is set to keep design variables passive as once they become passive. The designer has the option to change the passive design variables to active design variables if desired. Because of the random activity in the first few iterations a design variable might be set to passive artificially. Therefore, for the case N=10 after each iteration all the design variables are set to active for first 20 iterations.



It is worth noting that as the optimization approached convergence, modes 3 and 4 coalesced. The optimization algorithm had no problem reaching the optimum design even in the presence of the multiple eigenvalue.

To better compare the three example problems under category (2M-1L), the load deformation curves found in Fig. 5.3 through Fig. 5.5 are plotted in Fig. 5.6. From this figure, one can see that the case with  $N=10$  results in a better design than the other two cases. Load-deformation curves for  $N=6$  and  $N=8$  cases are practically the same. One might conclude that a bigger subspace of eigenpairs will lead to a better design.

#### 5.3.1.2. Six Design Variables Under Single Loading (3M-1L)

The designation (3M-1L) is short for three material sets under a single loading condition. Again, there are two design variables assigned to each material set making the total number of the design variables 6. The three material sets consist of first story columns, second story columns, and all girders grouped.

The same objective function,  $\sum_{i=1}^N \mu_i \beta_{i1} \mu_1$ , that was used for case (2M-1L) is also considered here. Three different cases are studied here with the number of eigenpairs varied among the numbers 6, 8, and 10. The following is the discussion of the results of the optimization of these three cases. The property of the optimized designs are presented in Table 5.2.

##### (1) $N=6$

The spectral evolution and load-deformation for  $N=6$  is given in Fig. 5.7. Optimization starts with step length  $r=8$  and all the design variables active. After iteration 10 the height of the girders became passive and adopted the minimum allowable value of 3 inches ( $\underline{h} = 3$ ). Starting from iteration 10 the algorithm suffered from zigzagging around the optimum solution. To solve this problem the size of step length parameter was increased from 8 to 20. This solved the zigzag problem and the algorithm converged quickly. The load-deformation curves given in Fig. 5.7 shows that the optimized design is a better design than the initial design both in terms of strength and stability.



(2)  $N=8$

Eight eigenpairs ( $N=8$ ) were used to optimize the initial design. The result of optimizing is given in Fig. 5.8. Comparing the result for this case with the  $N=6$  case, one can see that both resulted in practically identical optimized designs. One can observe that modes 7 and 8 do not participate in the objective function, and as a result, have no effect on the optimization. In general, a designer can not decide *a priori* if the eigenvalues are important to the optimal design because a lot of mode shifting occurs during the course of optimization. A designer can choose a smaller subspace size to reduce the final computational time require to reach an optimal design. However, as shown in the next example (case (3)), a large subspace will often help improve design. Mode shifting will be discussed in more detail in section 4.3.2.

(3)  $N=10$

The spectral evolution for the case  $N=10$  is shown in Fig. 5.9. One can see that during the first 25 cycles of optimization a lot of mode shifting takes place, with eigenvalues changing size by a large amount from one iteration to another. The reason for this behavior is that the chosen step length  $r=6$  is too small for this problem. Thus, after iteration 20 the step length was increased to  $r=20$ . Using  $r=20$  caused smaller change in design variables which helped keep the iterates in the feasible region.

At iteration 41 the height of the girders became passive design variables with a value of 3.0 inches ( $\underline{h} = 3$ ). The optimization converged at iteration 75. After iteration 40, although the optimality criteria are not exactly unity, the change in objective function is very small. Therefore, convergence can be assumed prior to a global convergence. What is suggested here is that there are some convergence tolerances in the program which could be liberalized for some problem to speed up solution without an important change in the outcome of the optimized design.

### 5.3.2. Final Observations for Optimization Under One Loading Condition

To better understand the performance of the three optimized structures found under category (3M-1L), all the load-deformation curves are plotted together in Fig. 5.10. Exactly the same type of behavior can be observed here as it was observed for case (2M-1L).

- The more eigenpairs used in the objective function, the better was the performance of the optimized design.

- Using more independent design variables resulted in a better design. For example, the magnitude of the load factor at the limit points for the case (2M-1L) &  $N=10$  was 37.9 compared to the magnitude of the limit point for the case (3M-1L) &  $N=10$  which was 45.9, about a 20% improvement in the strength of design without a significant change in computational time to achieve the optimized design.
- As the optimization progresses a large amount of mode shifting takes place. Therefore, one can not inspect the eigenvectors of the initial design to choose the number of modes. To show that this is true, consider Fig. 5.12 where the mode shapes of the optimized design for case (3M-1L) &  $N=8$  and the initial design are plotted. Looking at the mode shapes of the initial design it seems that mode 7 (the second mode in direction of loading) will have a high participation in the objective function. But, when using 8 eigenpairs for optimization, mode 7 of the initial design shifts to mode 9 of the optimized design which is out of the range initially chosen. Consequently, mode 7 of the initial design does not participate in the objective function at all. If a designer desires to have a specific mode of the initial design in the final design, it is recommended to choose at least several eigenpairs more than the desired eigenvalue for the optimization problem.
- The bigger was the magnitude of the dominant eigenvalue of the optimized design, the better the final optimized design behaved. The eigenvalues of the dominant mode at the optimized design for the under category (2M-1L) are 455, 541, and 580 for cases of 6, 8 and 10 eigenpairs respectively. Similarly, the eigenvalues for the case (3M-1L) at the optimized design are 579, 583, and 607 which again agrees with the assumption. The magnitude of the dominant buckling eigenvalues of the optimum designs (2M-1L) and (3M-1L) are presented in Fig. 5.11.
- For some design problems, the optimality criterion can vary from the optimal value of unity while still providing a small change in the objective function. Therefore, optimization can be terminated prior to reaching a global convergence.
- During course of optimizing a structure, the designer cannot change the number of the eigenpairs used in the objective function since doing so would change the optimization problem thereby causing problem with convergence.



Table 5.1. Properties of the Optimized Designs for Case (2M-1L)

ONE LOADING CONDITION WITH FOUR DESIGN VARIABLES			
PROPERTY	6 EIGENPAIRS	8 EIGENPAIRS	10 EIGENPAIRS
<b>Columns</b>			
Width	6.497 (6.388)	6.505	7.079
Height	5.586 (5.494)	5.518	4.976
Area	35.6 (35.7)	35.9	35.2
Strong Moment of Inertia	125.4 (121.5)	126.6	147.1
Weak Moment of Inertia	89.4 (93.2)	91.1	76.7
Torsion	180.6 (181.9)	183.3	169.5
<b>Girders</b>			
Width	7.271 (7.231)	7.158	7.454
Height	3.000 (3.000)†	3.000†	3.000
Area	21.8 (21.7)	21.5	22.4
Strong Moment of Inertia	96.1 (94.5)	91.7	103.6
Weak Moment of Inertia	16.4 (16.3)	16.1	16.8
Torsion	49.0 (48.6)	48.0	50.6

( ) Eigenpairs Obtained From the Nonlinear Stiffness Matrix

† Passive Design Variable

Mode No	Eigenvalue at Optimum			Participation at Optimum		
	No. of Eigenpairs Used			No. of Eigenpairs Used		
	6	8	10	6	8	10
1	285(246)	276	230	0	0	0
2	423(327)	416	358	0	0	0
3	455(354) ‡	457	494	12.8(11.7)	0	0
4	547(448)	541 ‡	495 ‡	0	13.639	12.619
5	693(634)	679	580	0	0.0897	0.0302
6	695(635)	700	688	0.03(0.09)	0	0
7	*	-742	732	*	0.2215	0
8	*	754	753	*	0	0.1283
9	*	*	-760	*	*	0
10	*	*	-787	*	*	0.0886

‡ Dominant Mode at Convergence



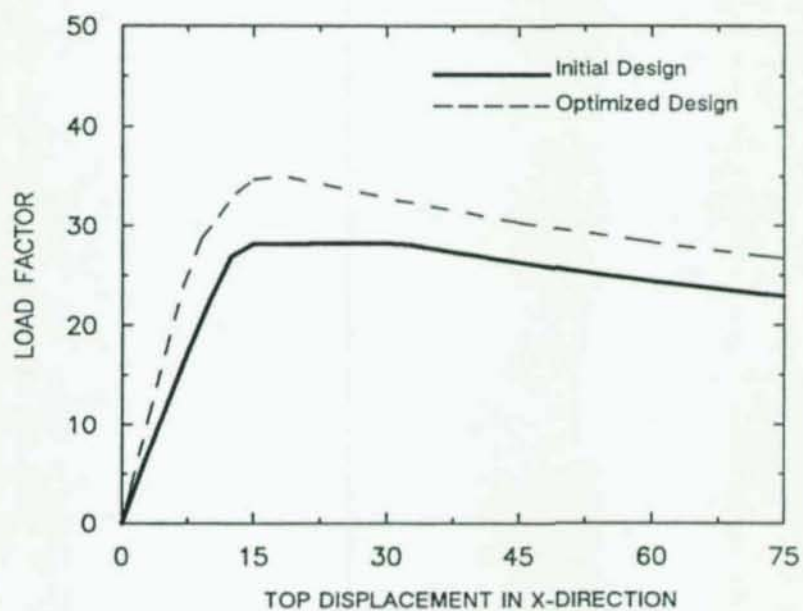
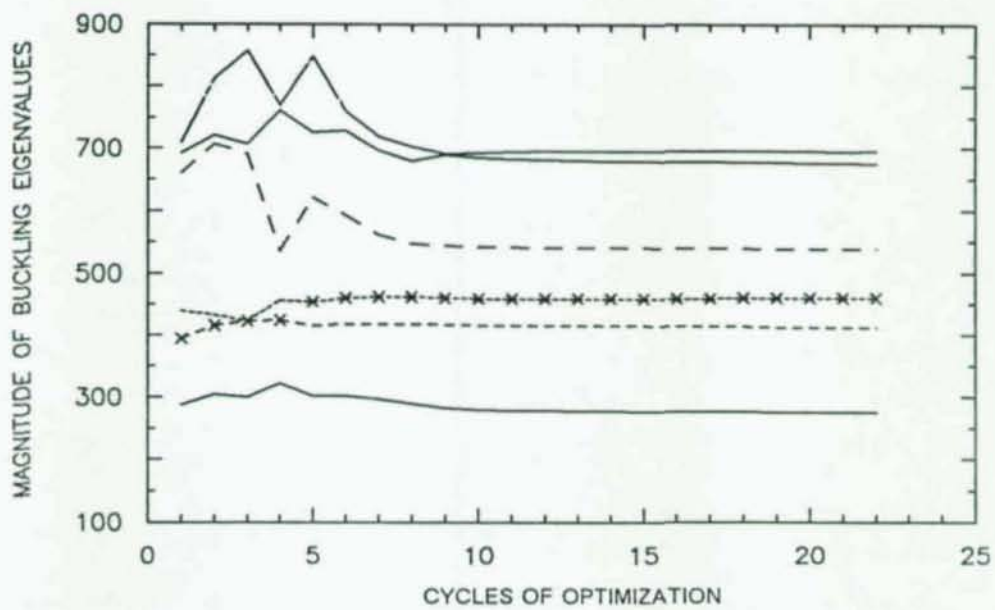


Fig. 5.3. Case (2M-1L) &  $N=6$  and  $\Pi=\{1\}$

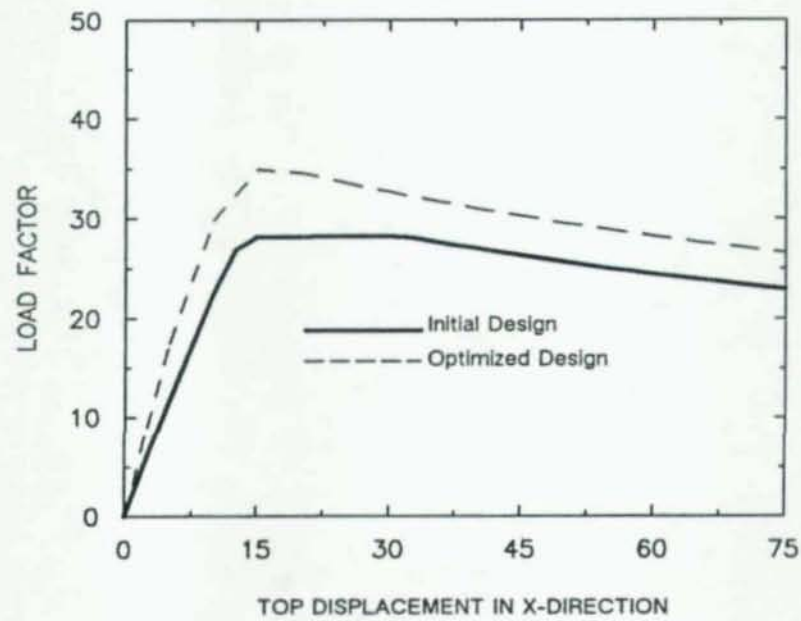
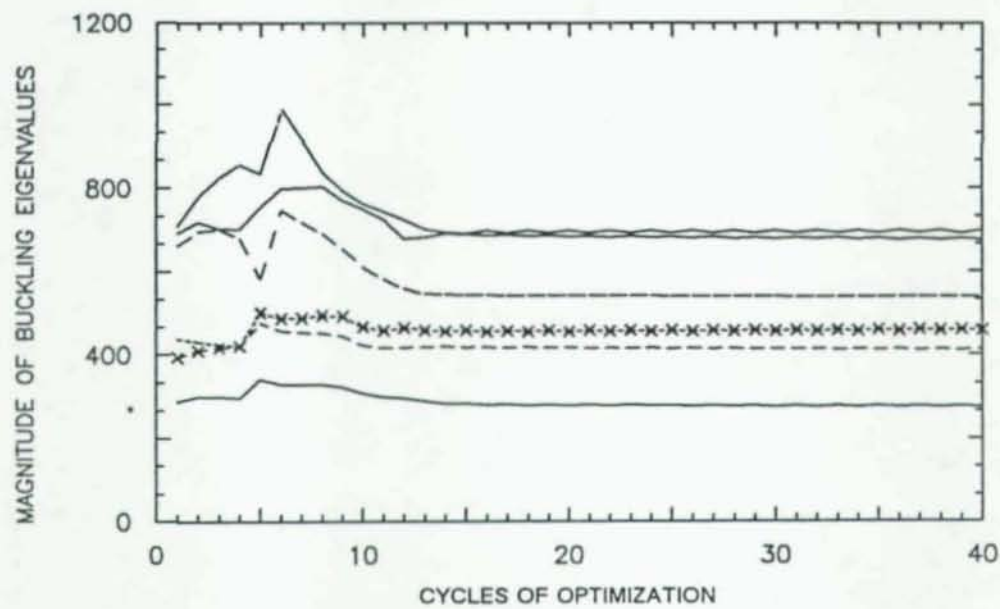


Fig. 5.4. Case (2M-1L) &  $N=8$  and  $\Pi=\{1\}$

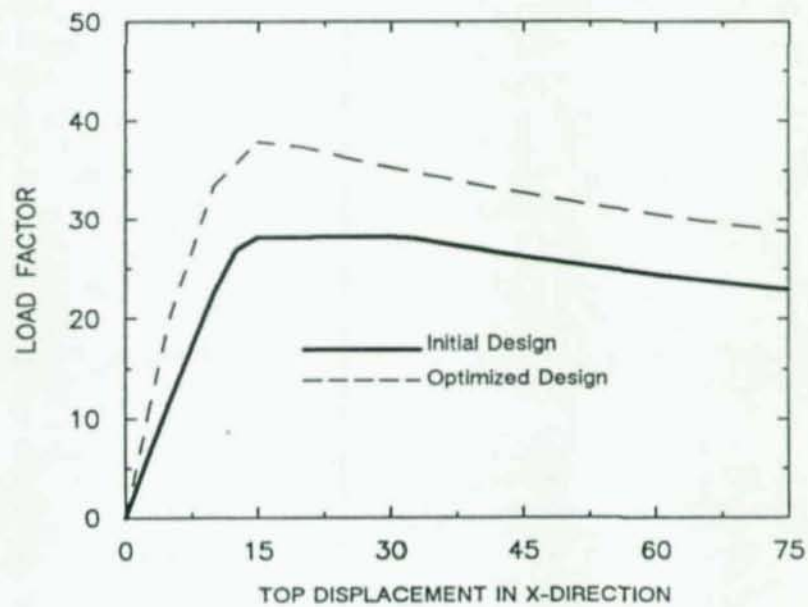
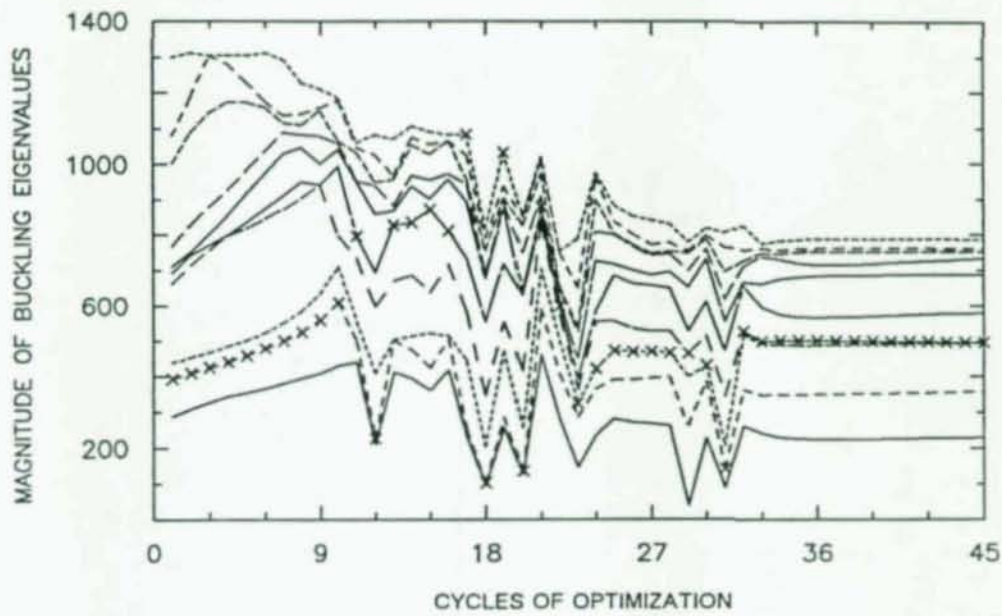


Fig. 5.5. Case (2M-1L) &  $N=10$  and  $\Pi=\{1\}$



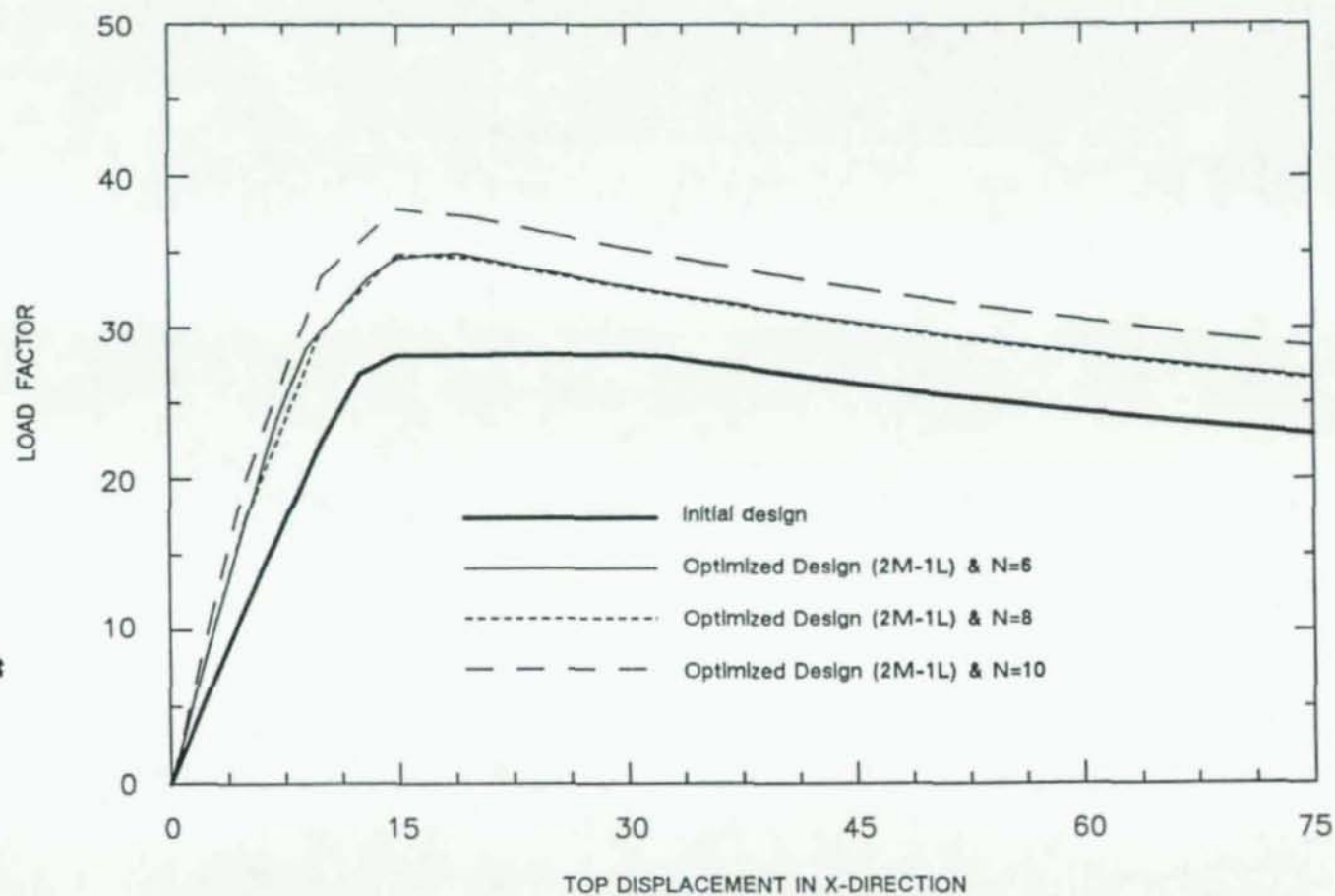


Fig. 5.6. Summary of Load-Deformation Curves for the Optimized Designs Under Category (3M-1L)

Table 5.2. Properties of the Optimized Designs for Case (3M-1L)

ONE LOADING CONDITION WITH SIX DESIGN VARIABLES			
PROPERTY	6 EIGENPAIRS	8 EIGENPAIRS	10 EIGENPAIRS
<b>First Story Columns</b>			
Width	7.763	7.606	8.278
Height	5.509	5.338	5.040
Area	42.8	40.6	41.7
Strong Moment of Inertia	214.7	195.76	238.3
Weak Moment of Inertia	108.1	96.4	88.3
Torsion	250.5	225.03	54.97
<b>Second Story Columns</b>			
Width	5.884	5.962	6.376
Height	4.348	4.242	4.080
Area	25.6	25.247	26.0
Strong Moment of Inertia	73.8	74.5	88.1
Weak Moment of Inertia	40.3	37.6	36.1
Torsion	90.7	87.4	21.8
<b>First and Second Story Girders</b>			
Width	7.923	8.478	8.089
Height	3.000	3.000	3.000
Area	23.7	25.4	24.176
Strong Moment of Inertia	124.4	152.3	131.8
Weak Moment of Inertia	17.8	19.1	18.0
Torsion	54.8	59.8	13.8

Mode No	Eigenvalues at Optimum			Participation at Optimum		
	No. of Eigenpairs Used			No. of Eigenpairs Used		
	6	8	10	6	8	10
1	292	269	250	0	0	0
2	336	319	288	0	0	0
3	444	427	408	0	0	0
4	579 <sup>†</sup>	583 <sup>†</sup>	582	13.897	13.639	0.0932
5	651	631	607 <sup>†</sup>	0.0410	0.0897	13.508
6	720	729	683	0	0	0
7	*	803	761	*	0.2215	0
8	*	909	785	*	0	0.4733
9	*	*	-848	*	*	0
10	*	*	-863	*	*	0.0724

† Dominant Mode at Convergence

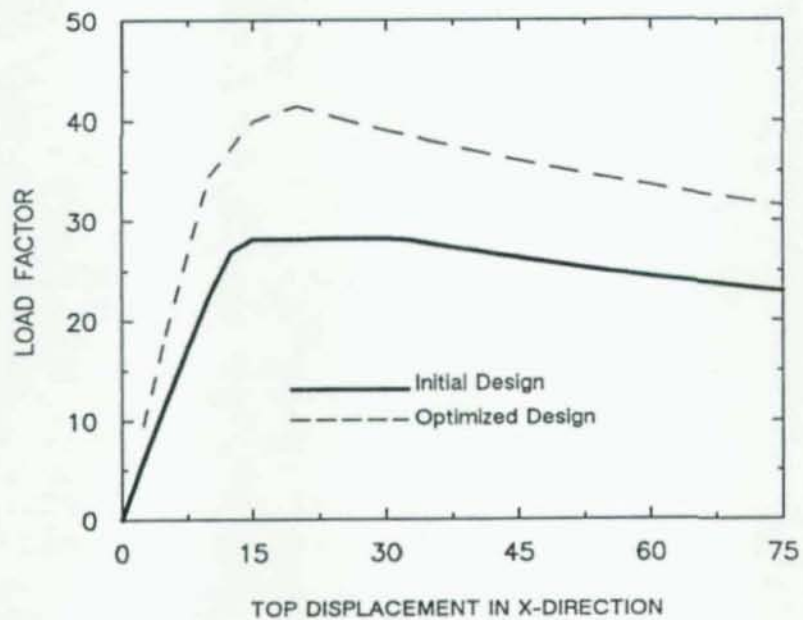
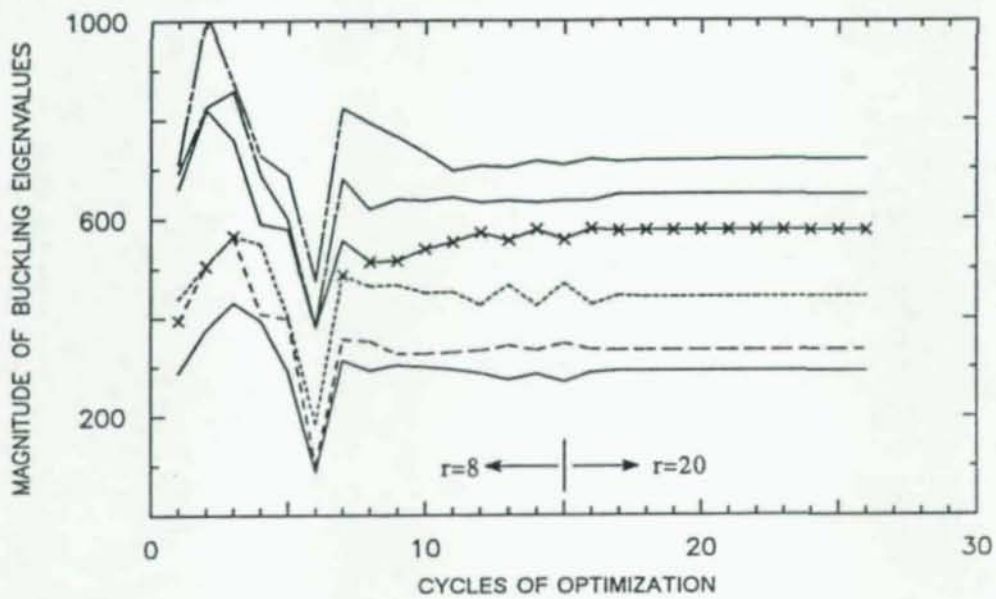


Fig. 5.7. Case (3M-1L) &  $N=6$  and  $\Pi=\{1\}$



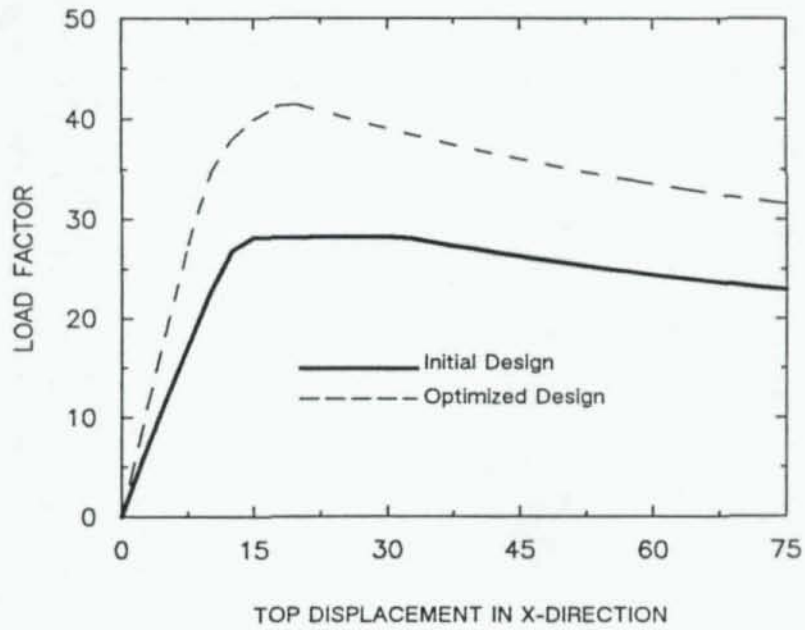
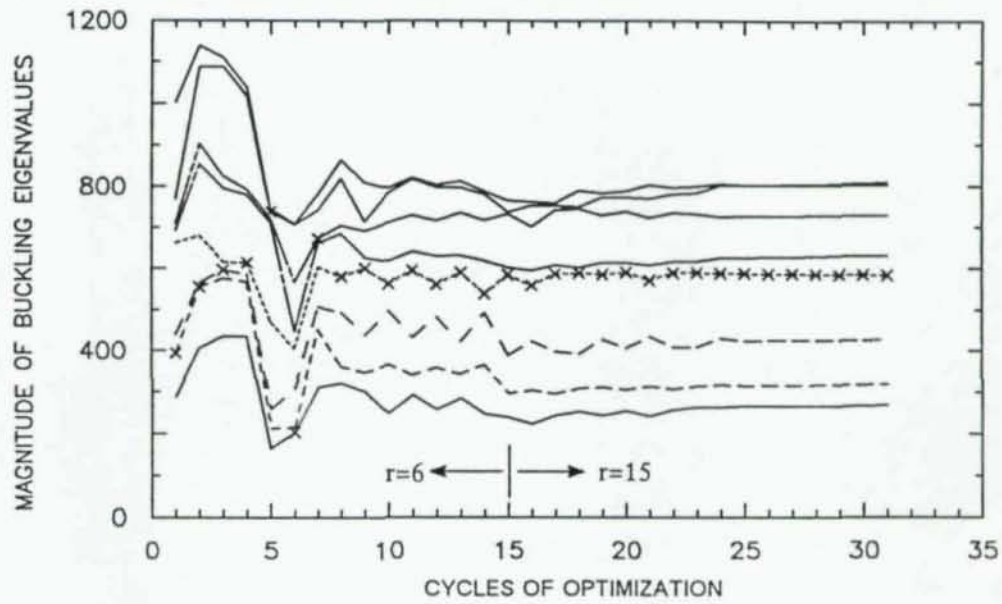


Fig. 5.8. Case (3M-1L) &  $N=8$  and  $\Pi=\{1\}$

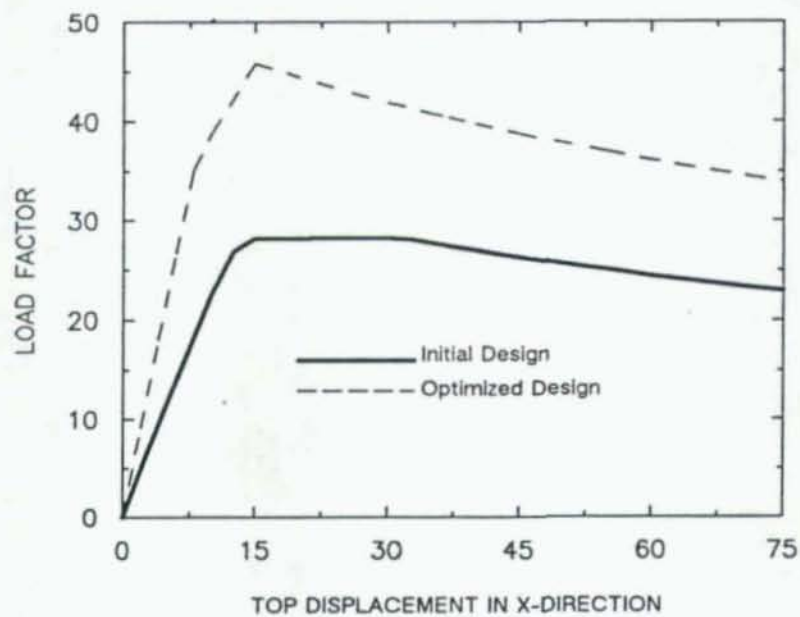
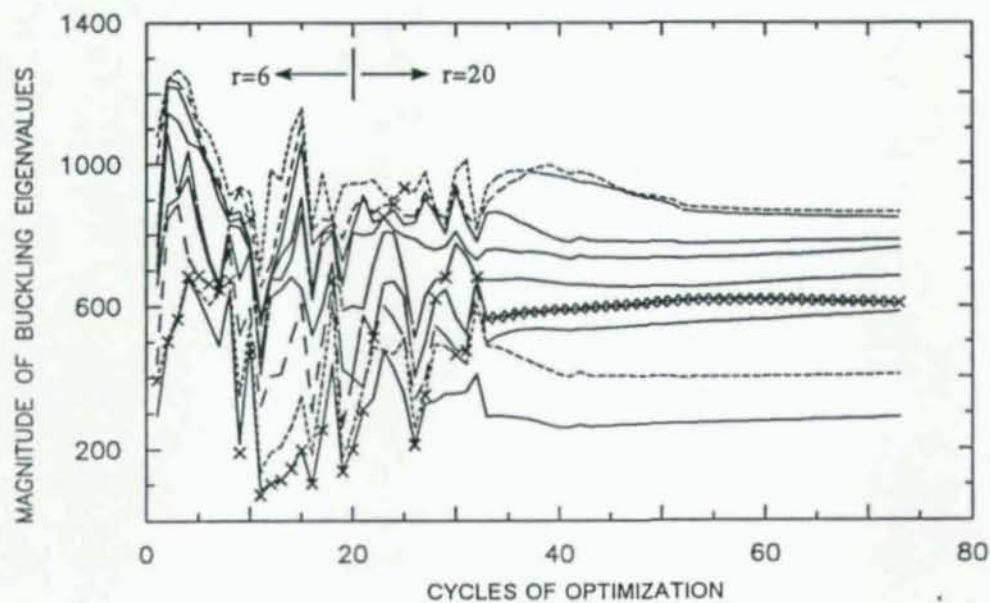


Fig. 5.9. Case (3M-1L) &  $N=10$  and  $\Pi=\{1\}$

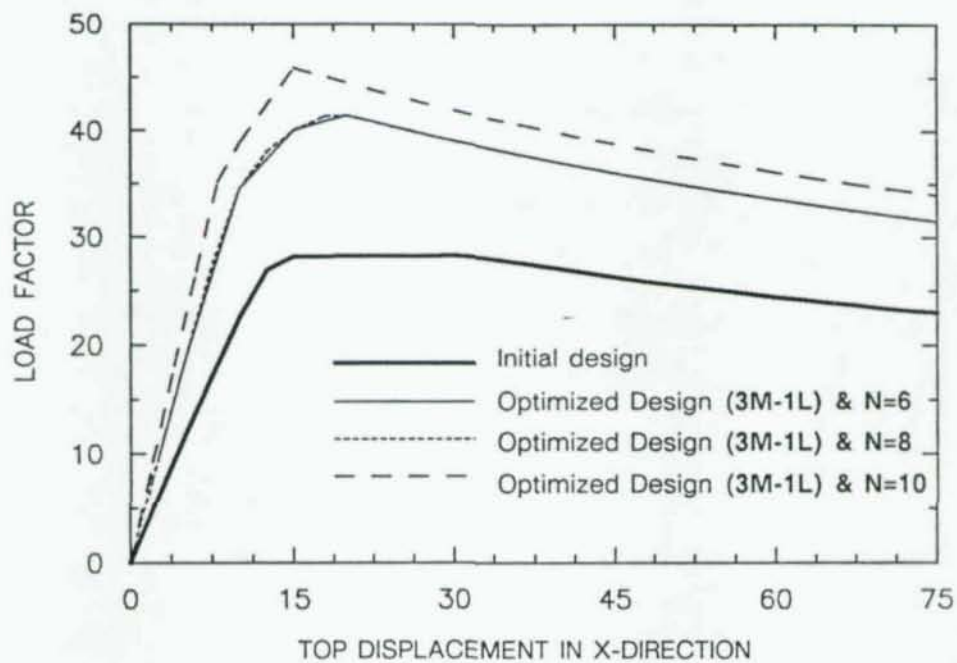


Fig. 5.10. Summary of Load-Deformation Curves for the Optimized Designs Under Category (3M-1L)

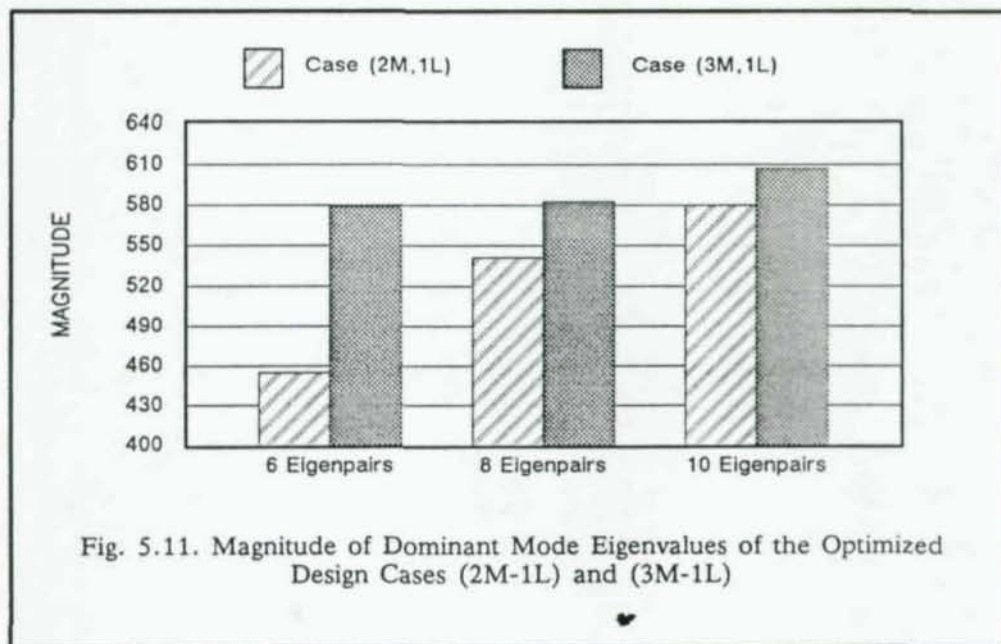


Fig. 5.11. Magnitude of Dominant Mode Eigenvalues of the Optimized Design Cases (2M-1L) and (3M-1L)



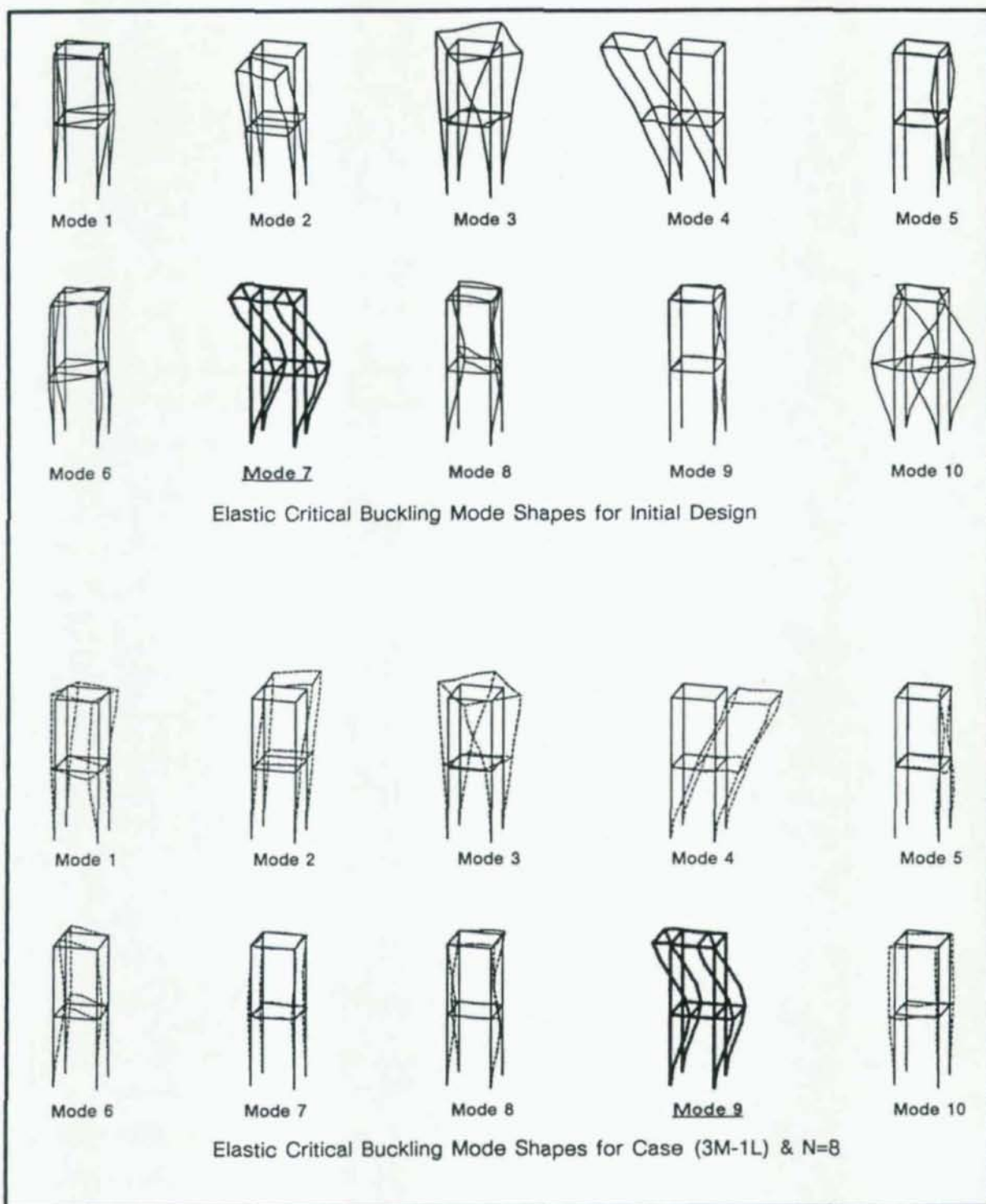


Fig 5.12. Buckling Mode Shapes of the Initial Design and the Optimized Design Using Six Design Variables and Eight Eigenpairs [(3M-1L) & N=8]

### 5.3.3. Multiple Loading

The following three sections are the application of the optimization methodology to multiple loading conditions.

#### 5.3.3.1. Four Design Variables Under Two Loading Conditions (2M-2L) & N=6.

The notation (2M-2L) stands for two material sets and two loading cases. For the following design problems, different objective functions are considered, the optimization is carried out, and the results are discussed. All the following example problems are under category (2M-2L) with N=6. Many of the optimization problems considered use common parameters during the optimization. In order to prevent repetition, common parameters will be noted and can be assumed the same for each problem unless otherwise stated.

All the following optimization problems, except case (2) start from the designs that were obtained under a single loading case instead of starting from the initial design. Since optimized designs under single loading case are available it is better to use them because they are probably closer to the optimal design than the initial design under multiple loading condition. Using the initial design as the starting design for multiple loading optimization problem will probably reach the same optimal design. The properties of the optimized design under category (2M-2L) & N=6 is given in Table 5.3.

The two different loading cases considered for this problem are shown in Fig 5.2. One loading condition is of sidesway type and one is of torsional type. Final optimized designs are analyzed under both loading conditions and the results are presented and discussed. A minimum allowable design variable of 3.0 inches is used for both height and width ( $\underline{b} = \underline{h} = 3.0$  inches). The eigenvalue problem is formulated from load case I unless otherwise mentioned.

Finally, the optimal designs found here are by no means the only possible optimized designs under the category (2M-2L) with N=6. An infinite number of different optimized designs can be found just by changing the importance parameters, the number of eigenpairs in the objective function, or the method of formulating the buckling eigenvalue problem. The examples generated should illustrate these different possibilities. In practice it will not be feasible to determine the whole noninferior optimal set. Therefore, several different cases are considered to come up with a subset of the whole noninferior optimized set. Finally, from the determined subset of the noninferior set a design is chosen as the best design.



(1)  $N=6$  &  $\Pi=\{1,1\}$

The spectral evolution for the present case (standard case) is given in Fig. 5.13. The algorithm converged in 25 iterations. Initially, mode 2 had the highest participation factor (until iteration 10). After iteration 10 mode 3 dominated and again after iteration 13 mode 2 and 3 shifted places and mode 2 remained dominant until convergence. Mode two at convergence is a sidesway buckling mode which is similar to static deflected shape under applied load case I. It is interesting to note that at the optimum modes 1 and 2 coalesced as did modes 4 and 5. Mode 1 is torsional mode and mode 2 is sidesway mode. As it can be seen from the spectral evolution figure, the algorithm had no problem reaching the optimized design.

The analysis of the resulting optimized design is given in Fig. 5.13. There are two load-deformation curves presented in this figure: one under load case I and one under load case II. From these two plots, it is obvious that the optimized design is a better design under both loading conditions. The optimized design has a higher load carrying capacity than initial design under both loading conditions. Post-limit strength degradation is about the same for both initial and the optimized designs under load case I and it is better for the optimized design compared to the initial design under load case II. Since the dominant mode throughout the optimization process was the sidesway mode, in the same direction and shape as the load condition I, it is expected that the optimized design to perform better under the load condition I.

(2)  $N=6$  &  $\Pi=\{1,1\}$ , Alternate Buckling Eigenvalue Problem (NLC=2)

Problem definition for this case is exactly the same as the case (1), except the buckling eigenvalue problem is formulated differently. For the case of multiple loading cases, it is not clear what loading conditions to use in formulating the buckling eigenvalue problem, therefore, the same example problem that was optimized in case (1) is also optimized here by considering a combination of load case I and II for the buckling eigenvalue problem. Comparison of the results from the present case with case (1) will give an understanding of the effect of the loading conditions as used in the formulation of the buckling eigenvalue problem in the overall performance of the optimization.

The spectral evolution and the load-deformation curves for the optimized design are presented in Fig. 5.14. The optimization problem converged in 11 iterations without much changes in the magnitude of the eigenvalues. The optimized design has distinct eigenvalues, and they are almost uniformly spread.



The optimized design performed better under both loading conditions than the initial design. The optimized design for this case had higher load carrying capacity in both direction compared to the previous optimized design obtained in case (1). The slope of the post-limit curve under lateral loading case is steeper compared to previous optimized design which makes this design less attractive.

Note that by incorporating the load case II in conjunction with the load case I in the formulation of the buckling eigenvalue problem improved the performance of the optimized design under load case II and worsened the performance of the optimized design under load case I compared to the case (1).

(3)  $N=6$  &  $\Pi=\{1,2\}$

The spectral evolution and the load-deformation curves for the present case are given in Fig. 5.15. There is not a significant difference between the design obtained under multiple loading condition compared to the optimized design under single loading condition. The design starts with a multiple eigenvalue (mode 1 & 2) which persists until convergence. At optimum, mode 1 and 2 are sidesway modes and mode 3 is the torsional mode. Looking at the load-deformation curves one can observe the improvement of the limit-load under both loading conditions.

The final optimized design for this problem and the optimized design obtained in the previous problem are very similar (see the properties given in Table 5.3). The design obtained here has repeated eigenvalues whereas the previous example with practically the same properties had distinct eigenvalues. The difference between these cases is that the eigenvalue problem was formulated differently for the two cases. In previous case the eigenpairs were obtained using a combination of both load cases while for the present example only load case I was used.

(4)  $N=6$  &  $\Pi=\{2,3\}$

In the previous case it was noticed that the second buckling eigenvector at optimum was a sidesway mode and the third buckling eigenvector at optimum was a torsional mode. Thus, to improve the performance of the design under both load cases I and II, which are of sidesway and torsional type, it was decided to put more importance on mode 2 and 3 by choosing an objective function with  $\Pi=\{2,3\}$ .

Optimization problem with the objective function of  $N=6$ ,  $\Pi=\{2,3\}$  converged in 19 iterations with modes 3 and 4 coalescing. At optimum mode 3 is a torsional mode and mode 4 is a sidesway mode.

Spectral evolution and load-deformation curves for this case are given in Fig. 5.16. As the optimization progressed, one can observe that the magnitude of all the eigenvalues except mode 3 decreased slightly. The magnitude of mode 3 increased until it became repeated eigenvalue with mode 4. Looking at the load-deformation curves, one can observe that the optimized design is much better design than initial design. In fact, this design is arguably the best design among all the optimized designs found under multiple loads.

(5)  $N=6$  &  $\Pi=\{1,3\}$

In previous two cases mode 3 of the optimized designs was found to be a torsional mode, thus, it was decided to put more importance on mode 3 by using the  $\Pi=\{1,3\}$  for the objective function to improve the performance of the optimized designs under load case II.

The plots of spectral decomposition and load-deformation curves for the case having  $N=6$  and  $\Pi=\{1,3\}$  are presented in Fig. 5.17. The optimization problem converged quickly in 9 iterations with small changes in the magnitude of the eigenvalues without any mode shifting. The dominant mode at optimum was the torsional mode. The optimization converged with no repeated eigenvalues.

Looking at the load-deformation curves, one can see that the optimized design has a better load carrying capacity than the initial design under both loading conditions. Under load case II the optimized design is obviously an improvement over the initial design which just shows that by putting more emphasis on mode 3 which is a torsional mode helped improving the performance under load case II. Improving the performance under load case II resulted in the opposite effect on the performance of the optimized design under load case I compared to the optimized design in case (2) which is expected. The optimal design has a higher limit load under load case I. The post-limit curve has a steeper slope than the initial design but it always bounds the initial design from above.

Table 5.3. Properties of the Optimized Design for Case (2M-2L) &amp; N=6

TWO LOADING CONDITION WITH FOUR DESIGN VARIABLES					
Properties	$\sum_{i=1}^N \sum_{j=1}^2 \mu_i \beta_{ij} \mu_1$	$\sum_{i=1}^N \sum_{j=1}^2 \mu_i \beta_{ij} \mu_1$	$\sum_{i=1}^N \mu_i (\beta_{i1} \mu_1 + \beta_{i2} \mu_2)$	$\sum_{i=1}^N \mu_i (\beta_{i1} \mu_2 + \beta_{i2} \mu_3)$	$\sum_{i=1}^N \mu_i (\beta_{i1} \mu_1 + \beta_{i2} \mu_3)$
<b>Columns</b>					
Width	5.044	5.870	5.910	6.944	5.591
Height	6.919	5.426	5.426	4.899	5.668
Area	34.9	31.9	32.1	34.0	31.7
Strong Moment of Inertia	139.3	78.1	78.7	68.0	84.8
Weak Moment of Inertia	74.0	91.5	93.3	136.7	82.6
Torsion	168.3		146.5	158.2	142.1
<b>Girders</b>					
Width	7.598	8.956	8.859	7.992	9.026
Height	3.000	3.000	3.000	3.000	3.000
Area	27.8	26.9	26.6	23.98	27.1
Strong Moment of Inertia	17.1	20.15	19.9	17.98	20.3
Weak Moment of Inertia	109.7	180.0	173.8	127.6	183.8
Torsion	51.9	64.1	61.4	55.45	64.3
<b>Optimization Parameters</b>					
Step Size Parameter	8	8	8	10	8
Method to Formulate EVP	1	2	1	1	1
Number of iterations	25	11	12	19	9
<b>Eigenvalues at Optimum</b>					
Mode 1	409.7	280	257.1	219.5	267.8
Mode 2	417.0 <sup>†</sup>	413 <sup>†</sup>	419.5 <sup>†</sup>	355.7	400.7 <sup>†</sup>
Mode 3	572.2	472	422.5	491.4 <sup>†</sup>	450.5
Mode 4	704.7	533	549.7	493.0	582.1
Mode 5	-709.5	-659	670.0	566.6	715.9
Mode 6	718.1	687	756.9	695.9	755.9

† Dominant mode at convergence



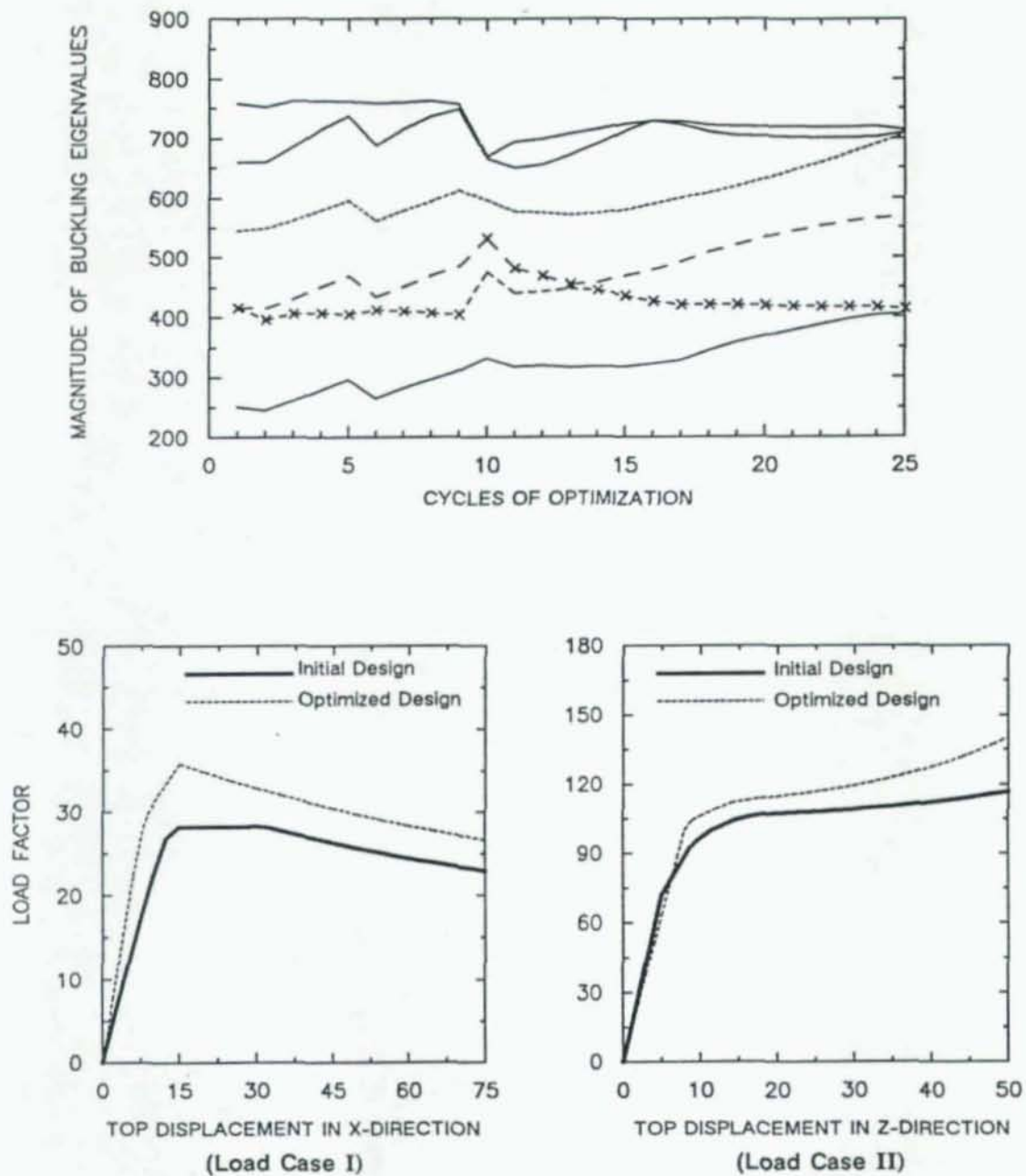


Fig. 5.13. Case (2M-2L) & N=6 with  $\Pi=\{1,1\}$

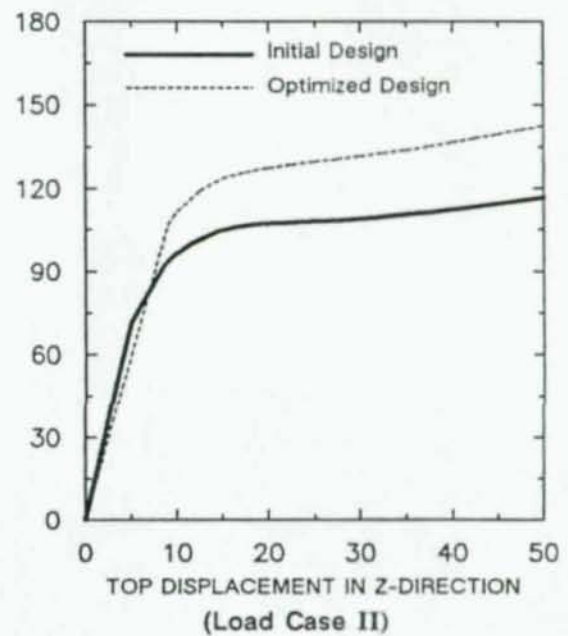
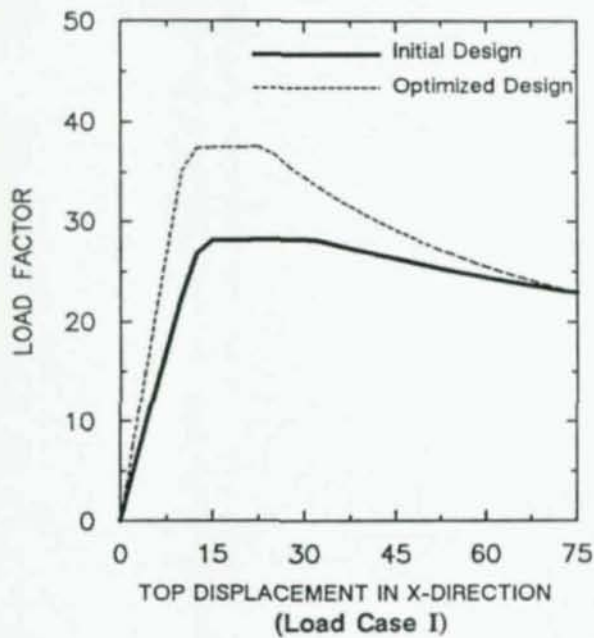
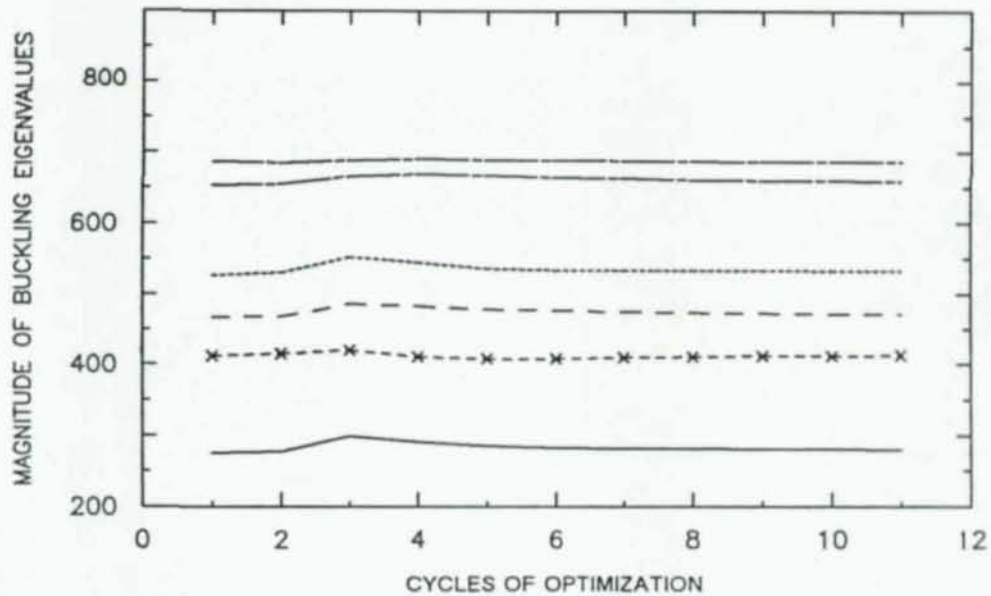


Fig. 5.14. Case (2M-2L) &  $N=6$  and  $\Pi=\{1,1\}$  Using  $NLC=2$  to Formulate the Buckling Eigenvalue Problem

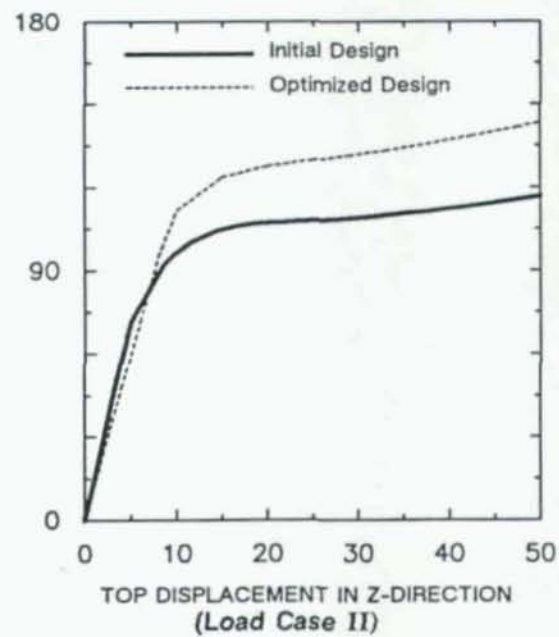
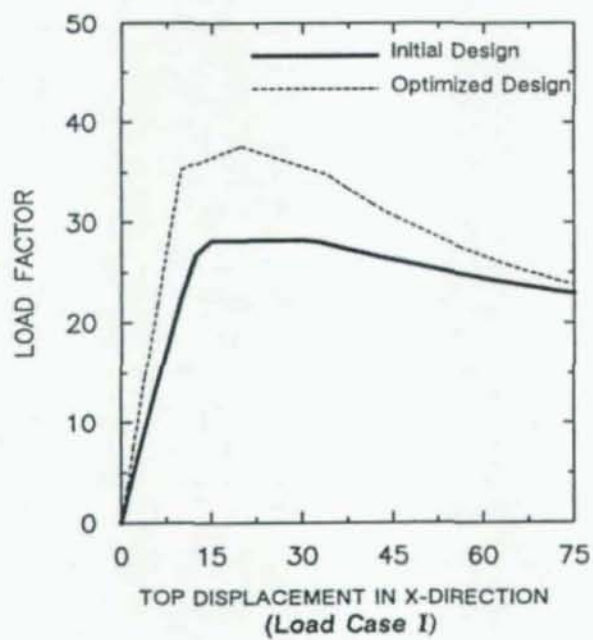
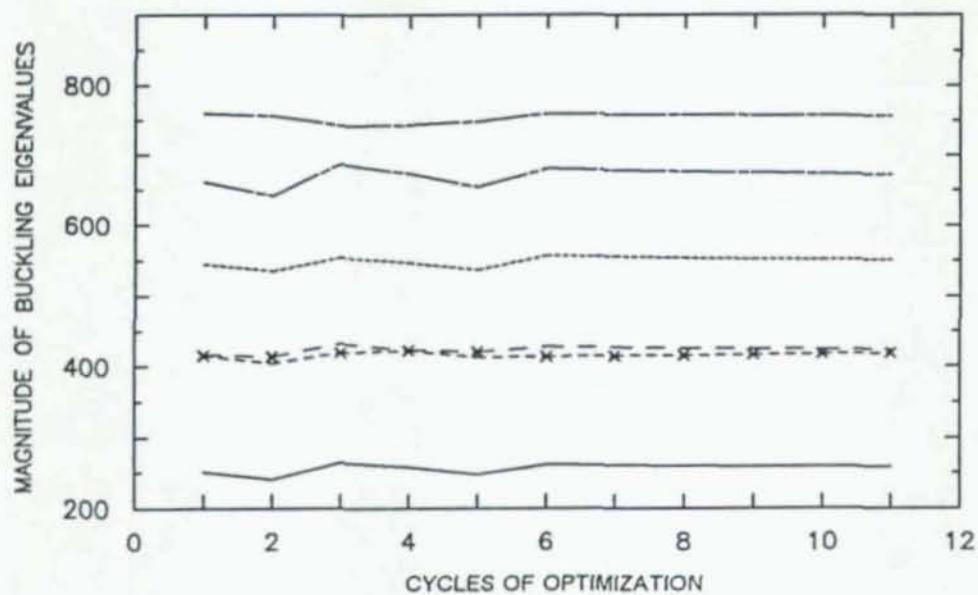


Fig. 5.15. Case (2M-2L) &  $N=6$  and  $\Pi=\{1,2\}$



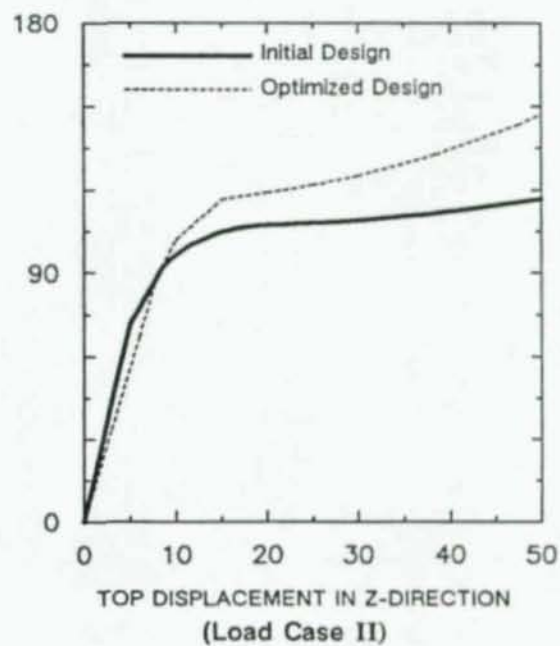
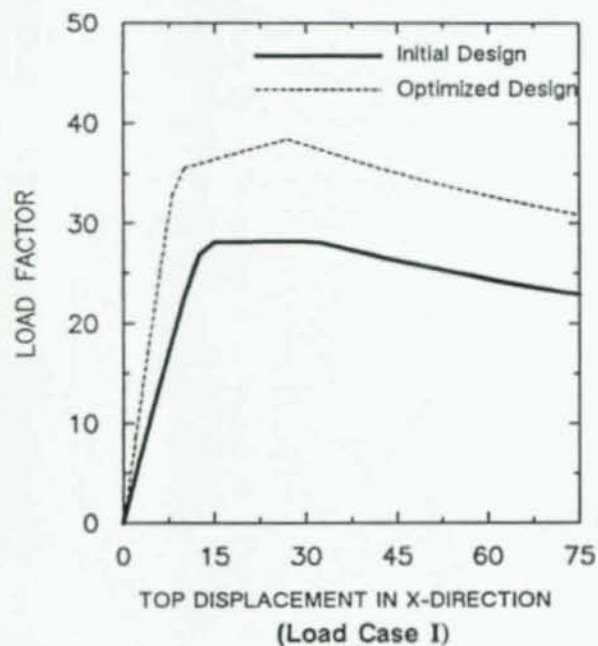
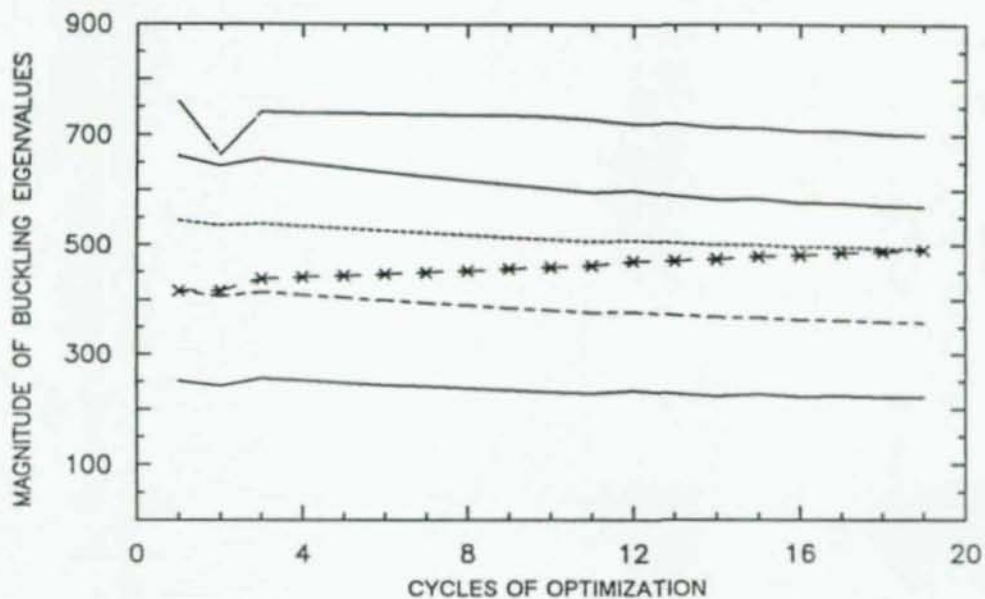


Fig. 5.16. Case (2M-2L) &  $N=6$  and  $\Pi=\{2,3\}$

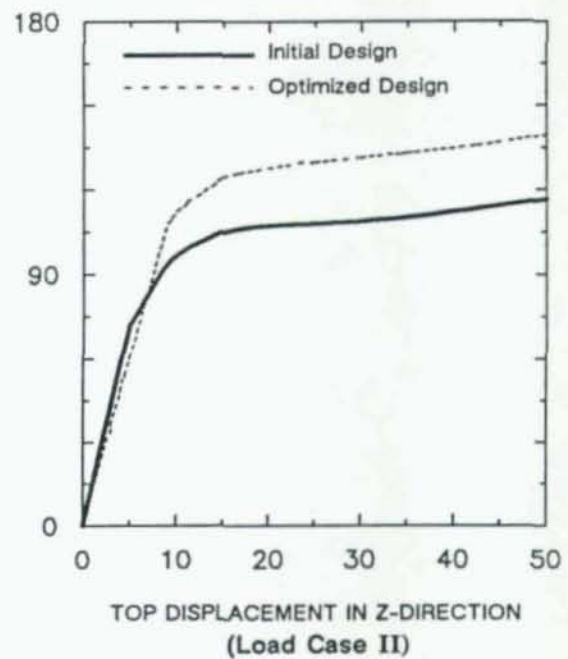
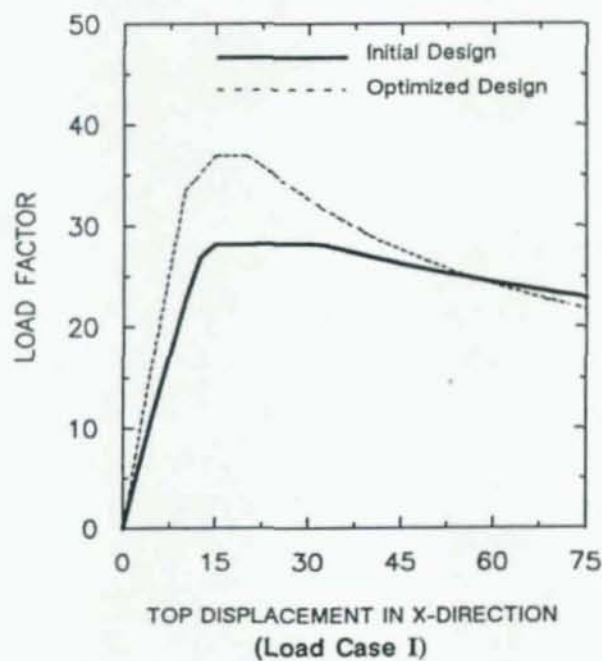
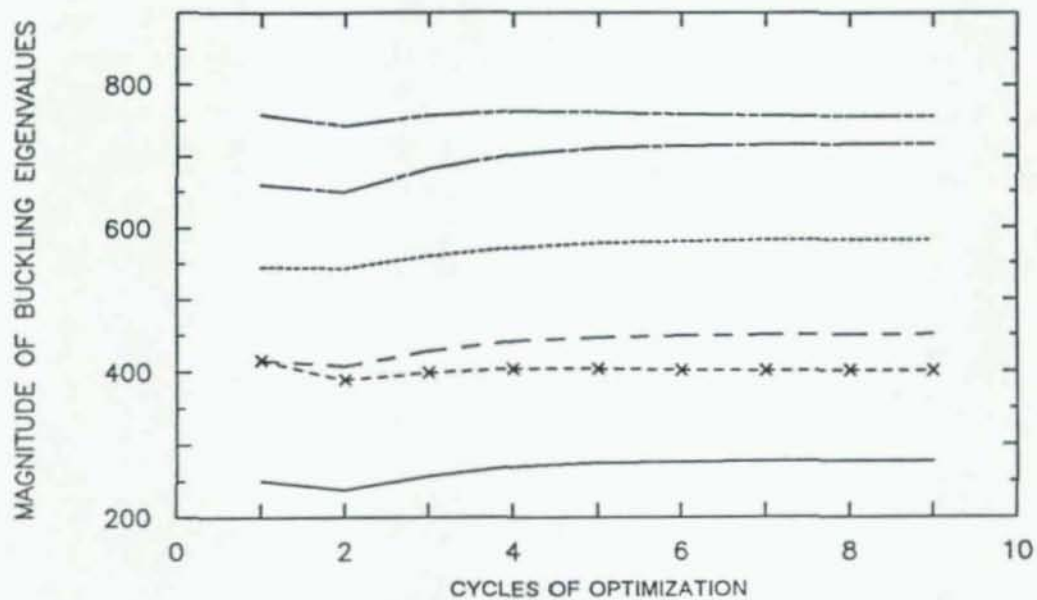


Fig. 5.17. Case (2M-2L) &  $N=6$  and  $\Pi=\{1,3\}$

### 5.3.3.2. Six Design Variables Under Two Loading Conditions (3M-2L) & N=6.

The notation (3M-2L), N=6 stands for 3 material sets, 2 loading cases, and 6 eigenpairs. All the following example problems are in the category (3M-2L) with N=6. All the assumptions made in sections 5.3.3.1 are made here also. Six different design problems are optimized in this section. The six optimized designs all have the same initial design but are optimized with different objective functions and use different methods for formulating the associated buckling eigenvalue problem. The performance of the optimization method and the behavior of the optimized designs are discussed below. A summary of properties of the optimized designs is given in Table 5.4.

#### (1) N=6, and $\Pi=\{1,1\}$

The spectral evolution and load-deformation curves for the case N=6, and  $\Pi=\{1,1\}$  are given in Fig. 5.18. The optimization converged in 27 iterations. The dominant mode starts as mode 4; as the optimization proceeds it swaps with mode 3, an ordering which persists until convergence. At the optimum the width of the second story columns and the height of the girders are passive, meaning that they have attained the minimum allowable width of  $\underline{b} = 5.0$  and height of  $\underline{h} = 3.0$  inches.

Looking at the load-deformation curves it is obvious that the optimized design is a better design than the initial design under loading case I and the initial design is a better design than the optimized design under load case II. Since the dominant mode (mode 3) has the same shape as the linear displacement under load case I, the optimized design is expected to behave better under load case I. To improve the design under load case II one should either increase the importance factor associated with the second load case or use more eigenpairs in the objective function. Choosing more eigenpairs might be helpful if one of the modes in the chosen range is a torsional mode, the same shape as load case II.

Another way of improving the performance of the design for load case II would be to choose four material sets: two for columns and two for girders. This choice would allow a better distribution of material throughout the structure. The optimized design would be expected to have collapse mechanism with hinges forming in the girders, thereby improving the nonlinear performance of the structure under load case II. This case is studied later.



(2)  $N=6$  &  $\Pi=\{1,2\}$

There are two different cases studied under the objective function  $\sum_{i=1}^6 \mu_i(\beta_{i1}\mu_1 + \beta_{i2}\mu_2)$ : One with the minimum allowable design variable for width of  $\underline{b} = 5.0$  and one with  $\underline{b} = 4.5$ . The parameter studies are performed to see the effect of changing the minimum permissible design variables. In a way a limit on the design variable sizes could be viewed as incorporating unmodeled constraints such as member local buckling. Because we are concerned with improvement of global buckling characteristics of the designs, the problem of local buckling can be circumvented by assuming appropriate allowable sizes for the design variables.

The result of the optimization and the load-deformation curves for these two cases are presented in Fig. 5.19 and Fig. 5.20. The optimization problem for both cases converged with modes 2 and 3 having repeated eigenvalues. At optimum, mode 2 was torsional and mode 3 was sideways for both cases. In both cases the dominant mode was the sideways mode in direction of loading I (X-direction). For the case with smaller allowable width it was necessary to choose a larger step length after the 10th iteration to achieve convergence. The eigenvalues of the optimized designs were 503 and 530 respectively. The first case had a much better load carrying capacity compared with the initial design under both loading conditions and overall is a superior design. Using  $\underline{b} = 5.0$  resulted in better design under both loading cases and using  $\underline{b} = 4.5$  resulted in a better design under load case I. The second case also under load case I, had much higher load carrying capacity had a steeper post-limit slope compared with the initial design. Between the two designs, the first one is more desirable.

The study on the minimum design variables exposes the fact that minimum column permissible dimension is important to the post-limit degradation. The study has revealed that the observation is of fundamental importance.

Notice that the optimization algorithm will change the orientation of the members if it finds them to improve the stability of the design. Looking at Table 5.4, one can see that the optimization resulted in a change in the orientation of the first story columns.

(3)  $N=6$  &  $\Pi=\{1,3\}$

In case (2) it was found that mode 3 was a sideways mode with the same shape as the displaced configuration of the design under loading case I. To improve the behavior of the optimized design under

load case one, the importance of mode 3 was increased by including it in  $\Pi$  with the hope that it will remain as mode 3.

The spectral evolution and load-deformation curves for the case  $N=6$ , and  $\Pi=\{1,3\}$  are given in Fig. 5.21. The optimization problem converged in 20 iterations with the optimized design having repeated eigenvalues (modes 3 and 4) at the optimum. The minimum allowable width of  $\underline{b} = 5.0$  was used for this problem. Looking at the load-deformation curves under both loading conditions it appears that the optimized design is much better than the initial design, having higher load carrying capacity with the same post-limit slope as the initial design. Also notice that the performance of the design under load case I improved compared to the case (1) by choosing  $\Pi=\{1,3\}$  in the objective function.

#### (4) $N=6$ & $\Pi=\{3,3\}$

To solve the optimization problem the buckling eigenvalue problem was formulated using a combination of loading cases I and II.  $\Pi=\{3,3\}$  was used for the objective function to put emphasis on mode 3 to improve the performance of the design under load case I (from previous cases it was observed that mode 3 at optimum had been a sidesway mode).

The optimization problem converged in 37 iterations, although, as one can see in Fig. 5.22, the magnitude of the objective function or the eigenvalues did not change by much after iteration 10. The optimization resulted in a design with stronger girder and weaker columns compared to the previous four cases. The optimized design did not have any repeated eigenvalues.

Looking at the load-deformation curves given in Fig. 5.22, one can observe that the optimized design behaves much better under load case I and is comparable with the initial design under load case II. Therefore, putting more importance on mode 3 which was a sidesway mode and stayed as a sidesway mode until convergence helped improving the performance of the optimized design under load case I.

#### 5.3.3.3. Eight Design Variables Under Two Loading Conditions (4M-2L) & $N=6$ .

The notation (4M-2L) &  $N=6$  stands for four material sets, two loading cases, and 6 eigenpairs. Each material set consists of two design variables: one height and one width of a rectangular cross section. The distribution of the material sets are given in the Fig. 5.25, where there are two material sets allocated



for the columns and two material sets allocated for the girders. There are two design problems discussed in this section. All the assumptions made in section 5.3.3 are made here also. Result of optimization method and the nonlinear behavior of the optimized designs are summarized and discussed. Summary of properties of the optimized designs is presented in Table 5.5.

(1)  $N=6$  &  $\Pi=\{1,1\}$

The same objective function used in section 5.3.4-(1) is applied here except that there are four material sets used instead of three material sets. The optimized design under similar objective function as was used for the (3M-2L) case did not perform as well as the initial design under loading case II. This case is considered here to demonstrate that a proper selection of design variables is important in overall performance of the optimized design.

The result of the load-deformation curves and the spectral evolution for this case is given in Fig. 5.23. The optimization problem converged in 23 iterations with final optimized design having multiple eigenvalues. Looking at the load-deformation curves, one can observe that the optimized design is a much better compared to the initial design under loading case I and slightly better under load case II.

To see how the load carrying capacities of the optimized designs of cases (3M-2L) &  $N=6$  and (4M-2L) &  $N=6$  compare with the initial design let us look at the Fig. 5.26. One can see that the optimized design using four material sets has a much higher load carrying capacity than the optimized design (3M-2L) &  $N=6$  or the initial design. The load carrying capacity of the optimized design improved 100% under load case I and improved slightly under load case II. For case of (3M-2L) &  $N=6$  the initial design was better under load case II, but as is shown here, choosing a better distribution of material allows a global improvement under both loading cases.

(2)  $N=6$  &  $\Pi=\{1,2\}$

The objective function used for this problem is the same as the optimization problem solved in section 5.3.4-(2). The reason for the present case study is to show that even though the design with three material sets resulted in an optimized design with improved performance, it is possible to achieve better performance by increasing the number of design variables for the optimization. The minimum allowable design variable for width is chosen to be  $\underline{b} = 5.0$  inches. The result of the spectral evolution and the load-deformation curves are given in Fig. 5.24.



One can see from the spectral evolution that the optimization problem converged in 40 iteration with the eigenvalues of modes 5 and 6 coalescing. Again, the optimization algorithm had no problem reaching an optimal solution with the repeated eigenvalues. Mode 5, a sideways mode, was the dominant mode at convergence. The same problem with the same objective function using three material sets converged with the eigenvalues of modes 2 and 3 coalescing. Mode 3 was the dominant mode. The magnitude of the dominant mode for this problem is 777 and for the case with three material sets was 503. Since the magnitude of the dominant eigenvalue for the present optimized design is much higher, it is expected to behave better. The load-deformation curves given in Fig. 5.24 show that under load case I the design with four material sets performed much better than the optimized design obtained using three. Under load case II all three designs: initial design, optimized design (3M-2L) & N=6, and the present optimized design performed almost the same.

#### 5.3.4. Final Observation on the Proposed Optimization Technique Under Multiple Loading

- In general, using more design variables will result in a better behaved optimized design. But from practical point view it makes sense to group elements together to save on labor, detailing, and fabrication costs.
- The larger the magnitude of the dominant eigenvalue of the optimized design (one with maximum  $\beta_{ij}$ ), the better the final optimized design will behave.
- The proposed optimization technique is a multiple objective optimization method that is solved using a weighting method. The weighting parameters  $\beta_{ij}$  are automatically generated from the loading conditions and the buckling modes. Multiple objective design optimization results in set of optimized designs that are called the noninferior design set. The designer can then choose the best design from the noninferior design set. This choice is generally made using information which is not included in the objective function; for example nonlinear and dynamic analyses. The best design among all the optimized designs found under multiple loading condition would be the optimized design to maximize  $\sum_{j=1}^2 \sum_{i=1}^6 \mu_i \beta_{ij} \mu_1$  given in section 5.3.5 under category (4M-2L) & N=6. This design improved the load carrying capacity of the initial design by a factor of more than two under load case I and slightly under load case II.
- If a combination of the loading conditions was used to formulate the eigenvalue problem, the final modes came out distinct. However, if one loading condition was used to formulate the buckling eigenvalue problem, then the optimum had multiple eigenvalues. In general, eigenvalues will likely coalesce when there is equality of the weighting factors, for example if  $\phi_1 \cdot f_1 = \phi_2 \cdot f_2$ . The tendency toward repeated eigenvalues in the examples suggests that the occurrence is more than coincidental.
- The optimized designs are interesting in the sense that they almost always have passive girder depth. The tendency is probably due to the tall story heights; deep girders do not add much to the lateral stiffness of the structure. Physically, the structure is telling us that the optimum configuration is similar to a structure having columns tied together with simple beams.
- The study of the minimum permissible design variables exposes that fact that the minimum dimension is important for the post-limit degradation of the structures. The observation reveals the fact that the post-limit robustness might be sacrificed with a poor choice of the minimum design variables.

Table 5.4. Properties of the Optimized Designs Using Three Material Sets, Two Loading Cases and Six Eigenpairs (3M-2L) & N=6

Properties	$\sum_{i=1}^N \sum_{j=1}^2 \mu_i \beta_{ij} \mu_1$	$\sum_{i=1}^N \mu_i (\beta_{i1} \mu_1 + \beta_{i2} \mu_2)$		$\sum_{i=1}^N \mu_i (\beta_{i1} \mu_1 + \beta_{i2} \mu_3)$	$\sum_{i=1}^N \sum_{j=1}^2 \mu_i \beta_{ij} \mu_3$
<b>1st Story Columns</b>					
Width	6.159	6.390	6.604	7.634	7.898
Height	7.564	6.119	5.848	4.954	4.589
Area	46.6	39.1	38.6	37.8	36.2
Strong Moment of Inertia	222.2	122.0	110.1	77.3	63.6
Weak Moment of Inertia	147.3	133.1	140.4	183.7	188.4
Torsion	300.0	216.1	209.4	185.4	162.0
<b>2nd Story Columns</b>					
Width	5.000	5.000	4.500	5.000	6.213
Height	4.775	5.596	5.723	5.540	4.13
Area	23.9	28.0	25.6	27.7	25.7
Strong Moment of Inertia	45.4	73.0	70.3	70.8	36.5
Weak Moment of Inertia	49.7	58.3	43.5	57.7	82.6
Torsion	80.1	110.0	91.2	107.9	86.0
<b>Girders</b>					
Width	7.453	8.209	8.874	8.560	9.354
Height	3.000	3.000	3.000	3.000	3.000
Area	22.4	24.6	26.6	25.7	28.1
Strong Moment of Inertia	16.8	18.5	20.0	19.3	21.1
Weak Moment of Inertia	103.5	138.3	174.7	156.8	204.6
Torsion	50.1	57.0	62.9	601.1	67.0
<b>Properties &amp; Parameters</b>					
Step Size Parameter	6	8	8 & 20	8 & 10	8
Method to Formulate EVP	1	1	1	1	2
Number iterations	27	17	15	20	37
$\frac{b}{h}$	5.0	5.0	4.5	5.0	5.0
$\frac{h}{h}$	3.0	3.0	3.0	3.0	3.0
<b>Eigenvalues at Optimum</b>					
Mode 1	433.	342.	317.	240.	211.
Mode 2	485.	502.	530.	433.	301.
Mode 3	523.†	503.†	540.†	585.†	309.
Mode 4	593.	602.	675.	592.	545.
Mode 5	787.	757	783.	639.	620.†
Mode 6	-791.	775	786.	751.	641.

† Dominant Mode at Optimum



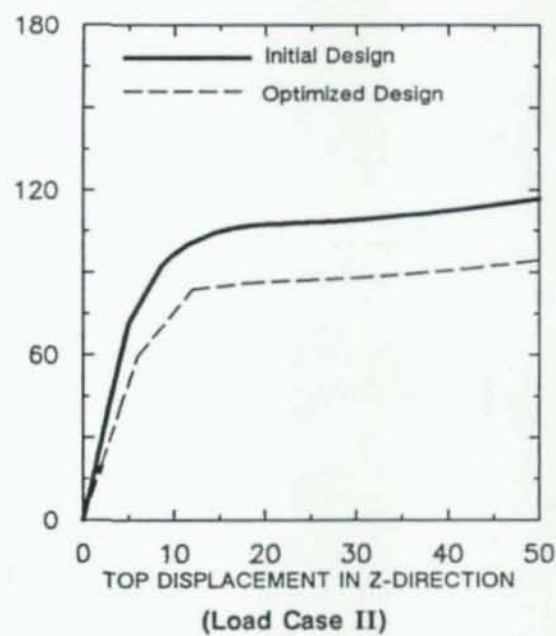
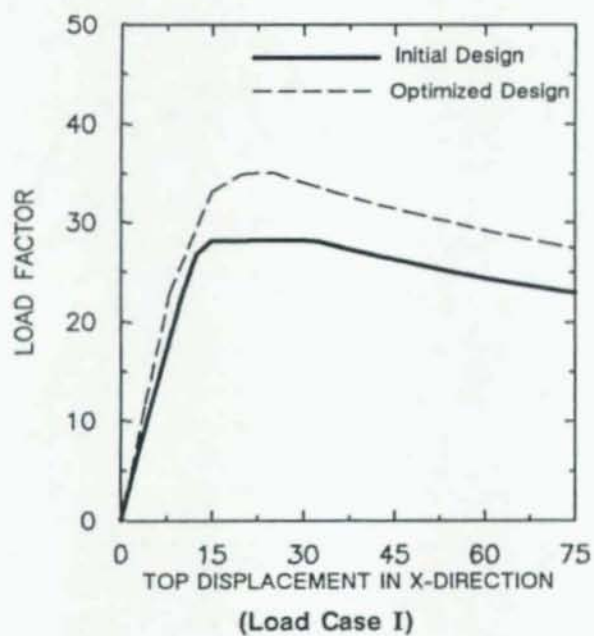
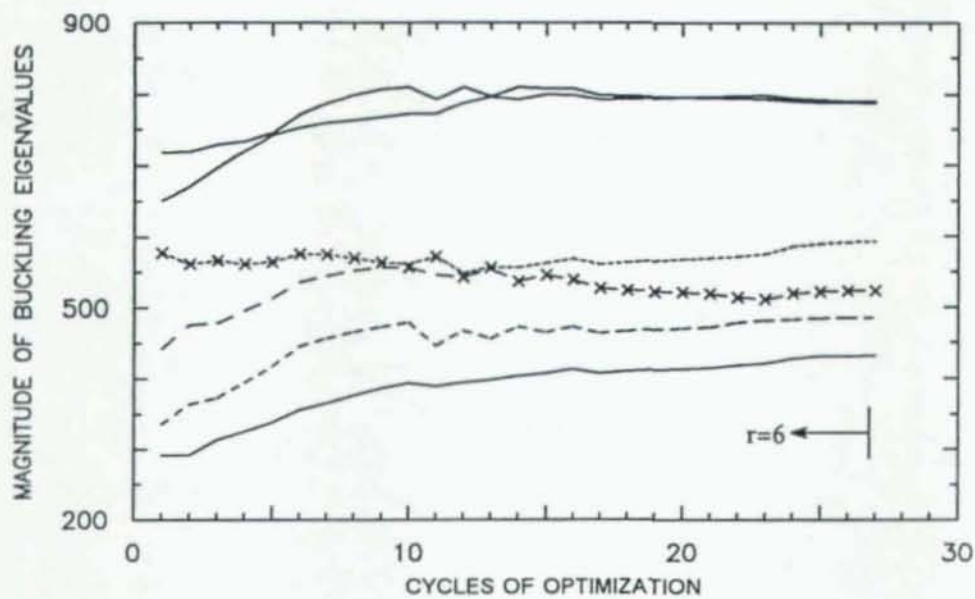


Fig. 5.18. Case (3M-2L) &  $N=6$  with  $\Pi=\{1,1\}$ , and  $\underline{b} = 5.0$ ,  $\underline{h} = 3.0$

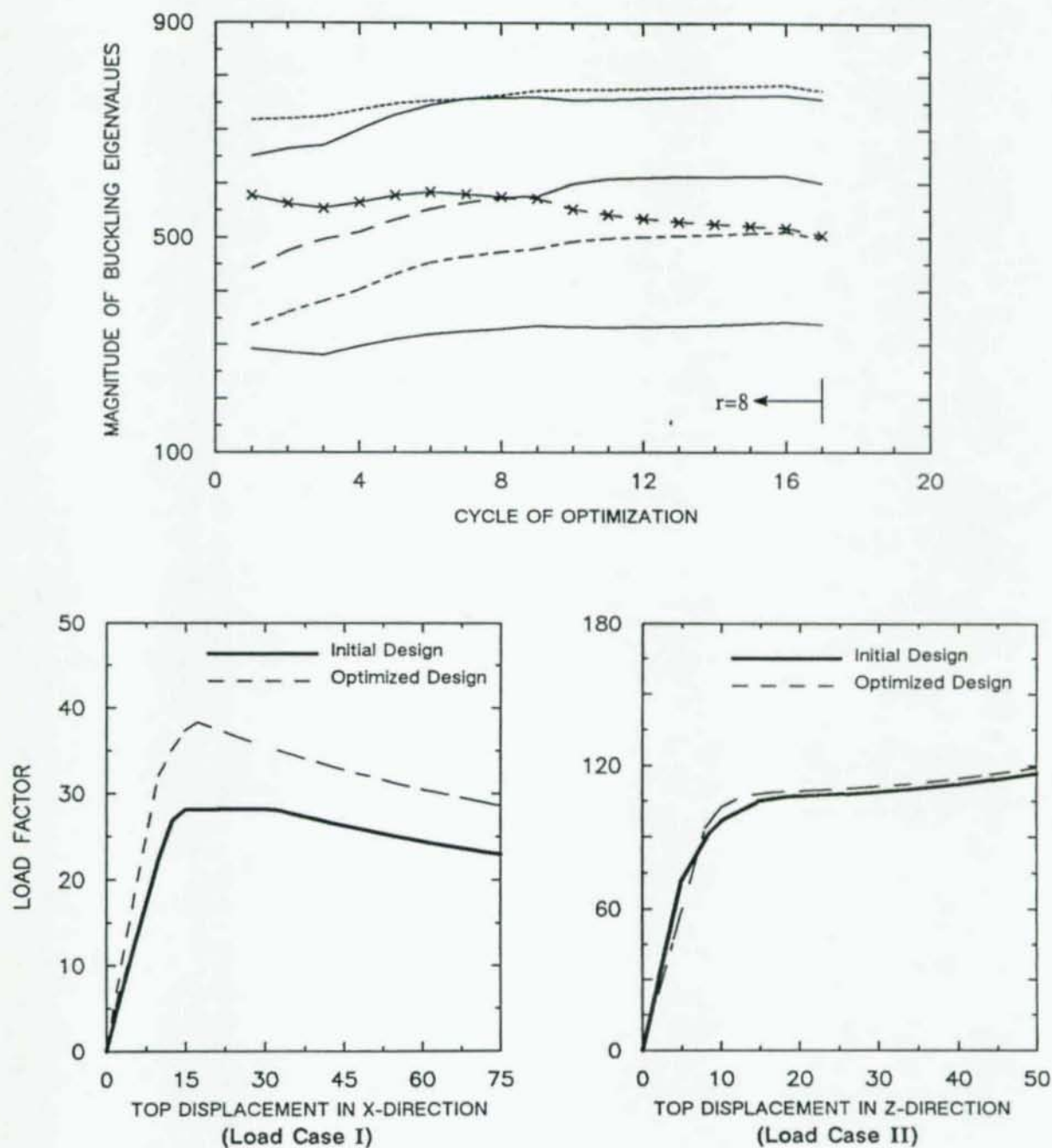


Fig. 5.19. Case (3M-2L) & N=6 with  $\Pi=\{1,2\}$ , and  $\underline{b} = 5.0$ ,  $\underline{h} = 3.0$

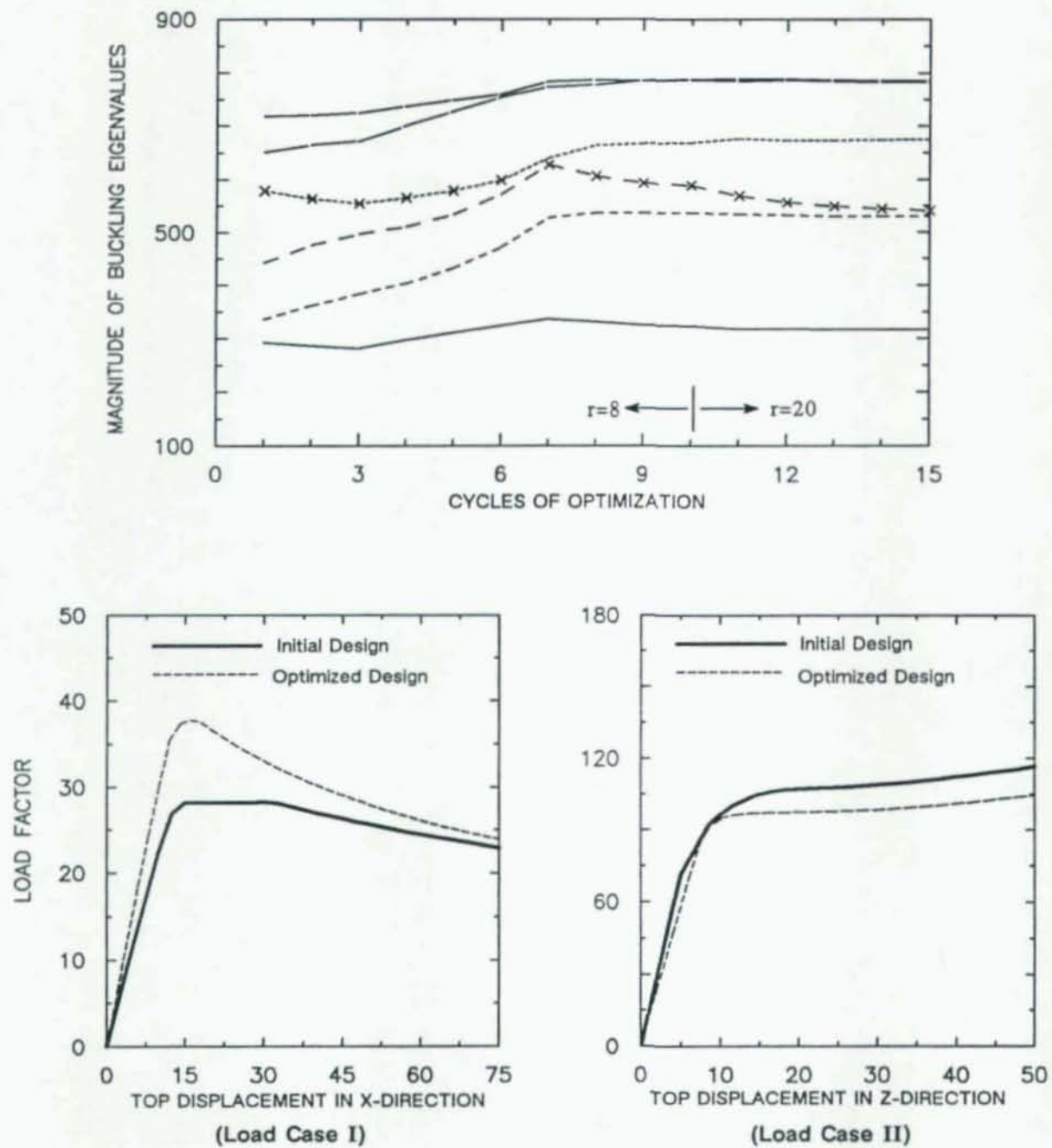


Fig. 5.20. Case (3M-2L) &  $N=6$  with  $\Pi=\{1,2\}$ , and  $\underline{b} = 4.5$ ,  $\underline{h} = 3.0$



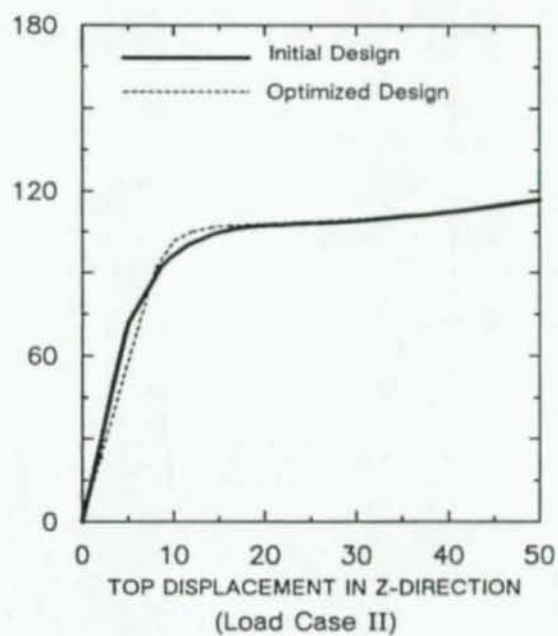
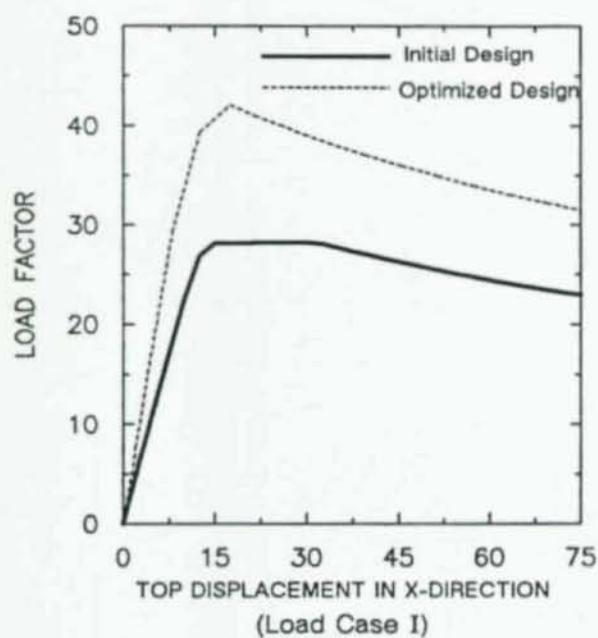
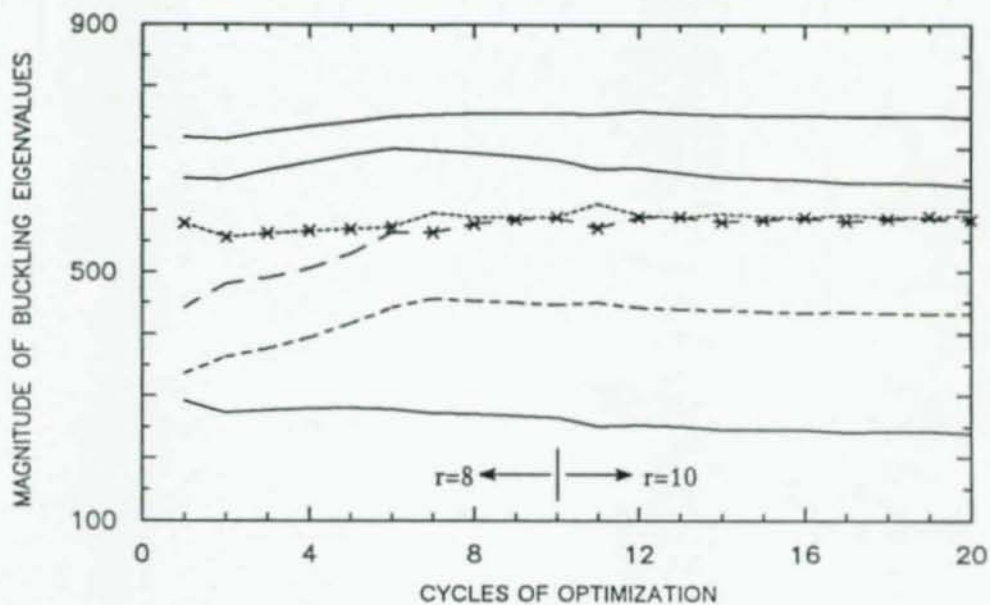


Fig. 5.21. Case (3M-2L) &  $N=6$  with  $\Pi=\{1,3\}$ , and  $\underline{b} = 5.0$ ,  $\underline{h} = 3.0$

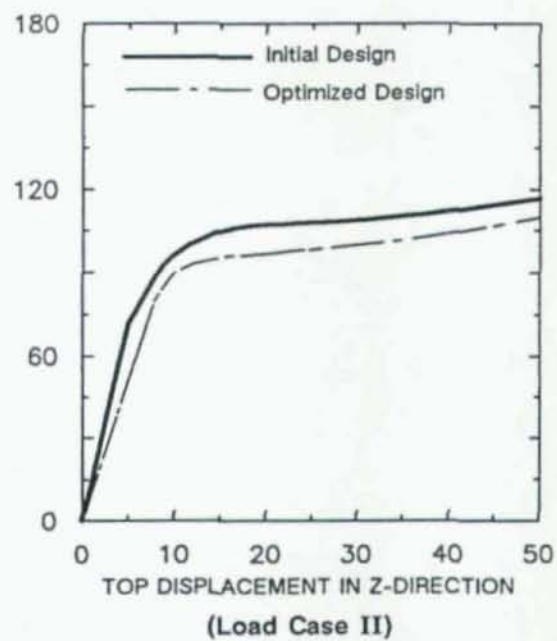
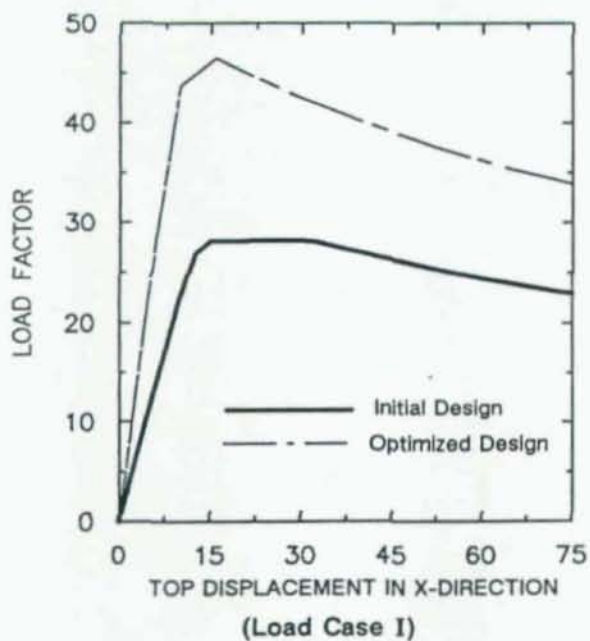
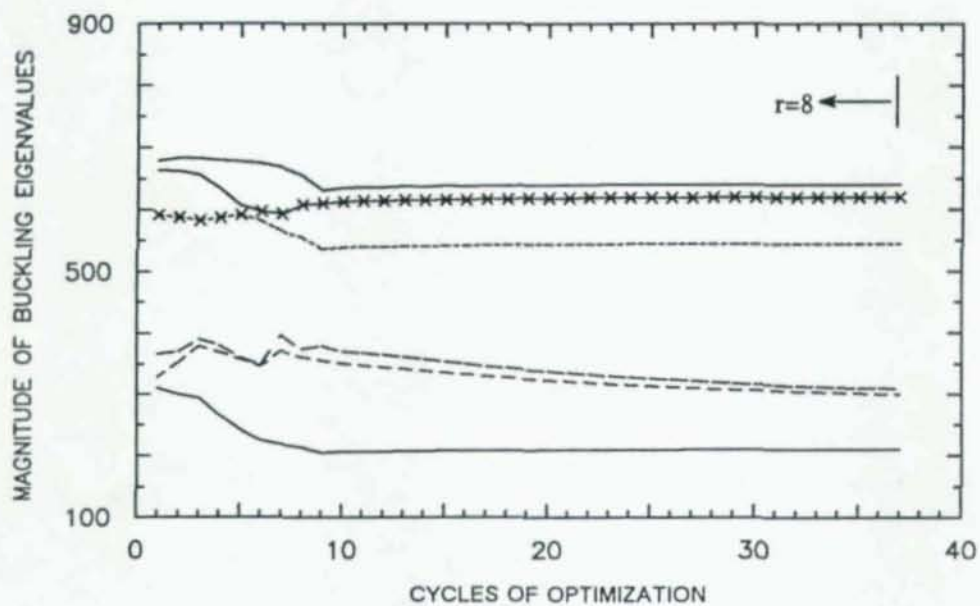


Fig. 5.22. Case (3M-2L) &  $N=6$  with  $\Pi=\{3,3\}$ ,  $NLC=2$ , and  $\underline{b} = 5.0$ ,  $\underline{h} = 3.0$

Table 5.5. Properties of the Optimized Designs Using Four Material Sets, Two Loading Conditions, and Six Eigenpairs (4M-2L) with N=6

PROPERTIES	$\sum_{i=1}^N \sum_{j=1}^2 \mu_i \beta_{ij} \mu_j$	$\sum_{i=1}^N \mu_i (\beta_{i1} \mu_1 + \beta_{i2} \mu_2)$
<b>1st Story Columns</b>		
Width	7.544	7.499
Height	5.459	5.528
Area	41.2	41.5
Strong Moment of Inertia	102.2	105.57
Weak Moment of Inertia	195.3	194.3
Torsion	288.1	232.4
<b>2nd Story Columns</b>		
Width	7.627	6.819
Height	3.691	3.882
Area	28.3	26.5
Strong Moment of Inertia	32.1	33.2
Weak Moment of Inertia	138.9	102.6
Torsion	89.9	85.9
<b>1st Story Girders</b>		
Width	10.334	9.746
Height	3.000	3.000
Area	31.0	29.2
Strong Moment of Inertia	23.3	21.9
Weak Moment of Inertia	275.9	231.5
Torsion	76.1	62.113
<b>2nd Story Girders</b>		
Width	5.000	6.287
Height	3.000	3.000
Area	15.0	18.9
Strong Moment of Inertia	11.25	14.1
Weak Moment of Inertia	31.25	62.1
Torsion	28.2	39.7
<b>Properties:</b>		
Step Size Parameter	8	8 & 20
Method to Solve for EVP	1	1
Cycles to Convergence	23	40
$\frac{b}{h}$	5.0	5.0
$\frac{h}{b}$	3.0	3.0
<b>Eigenvalues at Optimum:</b>		
Mode 1	282	272
Mode 2	345	287
Mode 3	444	390
Mode 4	700	649
Mode 5	777 <sup>†</sup>	774 <sup>†</sup>
Mode 6	-788 <sup>†</sup>	777 <sup>†</sup>

† Dominant Mode at Optimum



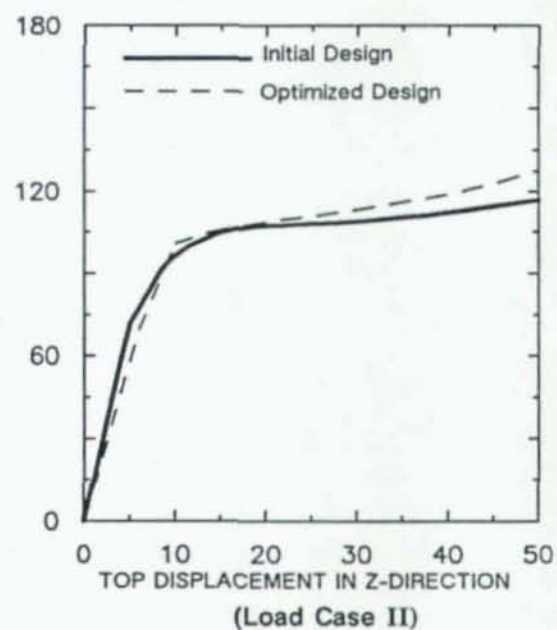
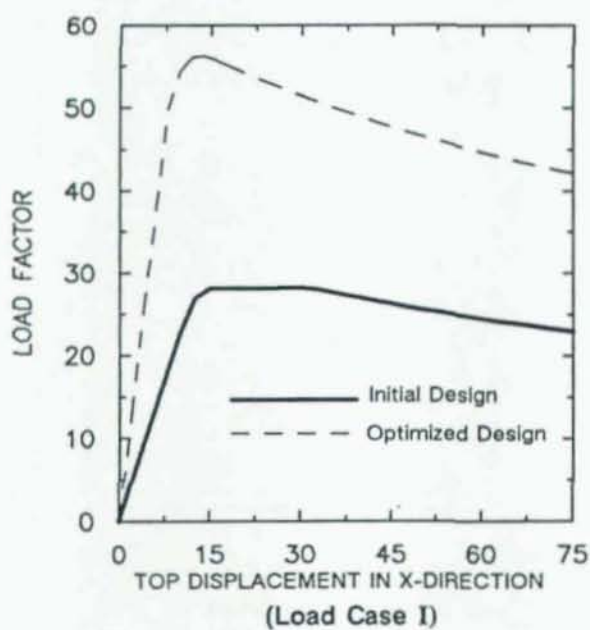
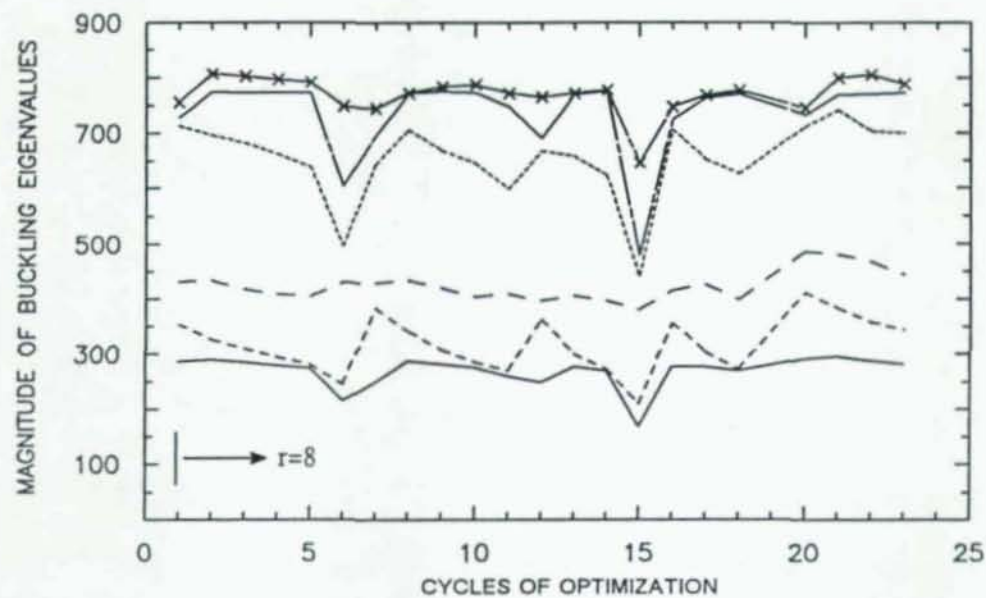


Fig. 5.23. Case (4M-2L) &  $N=6$  with  $\Pi=\{1,1\}$

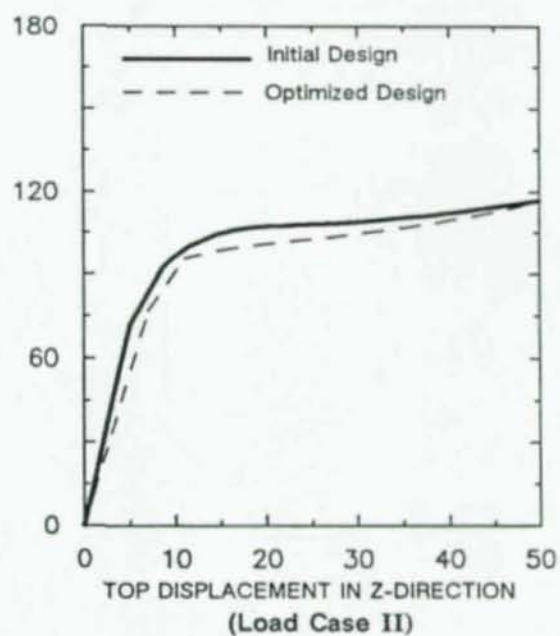
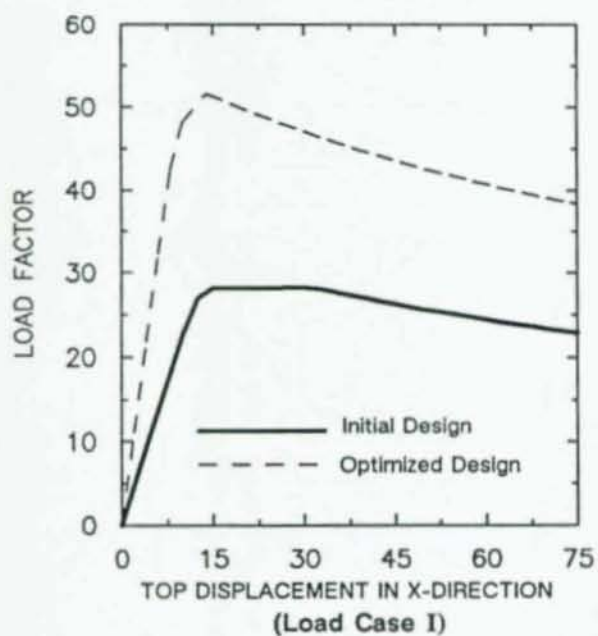
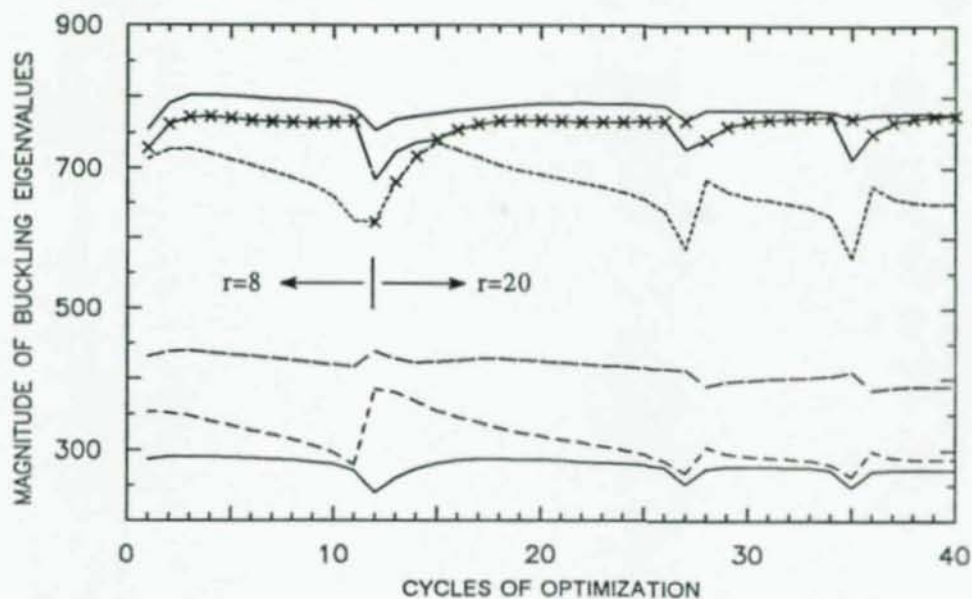
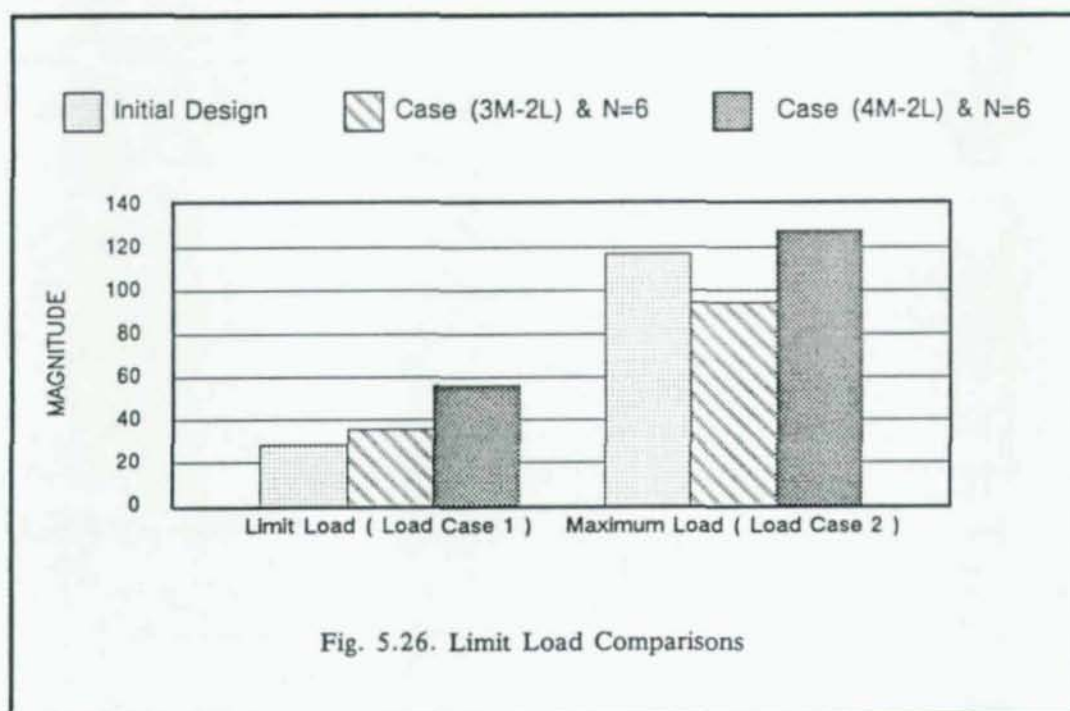
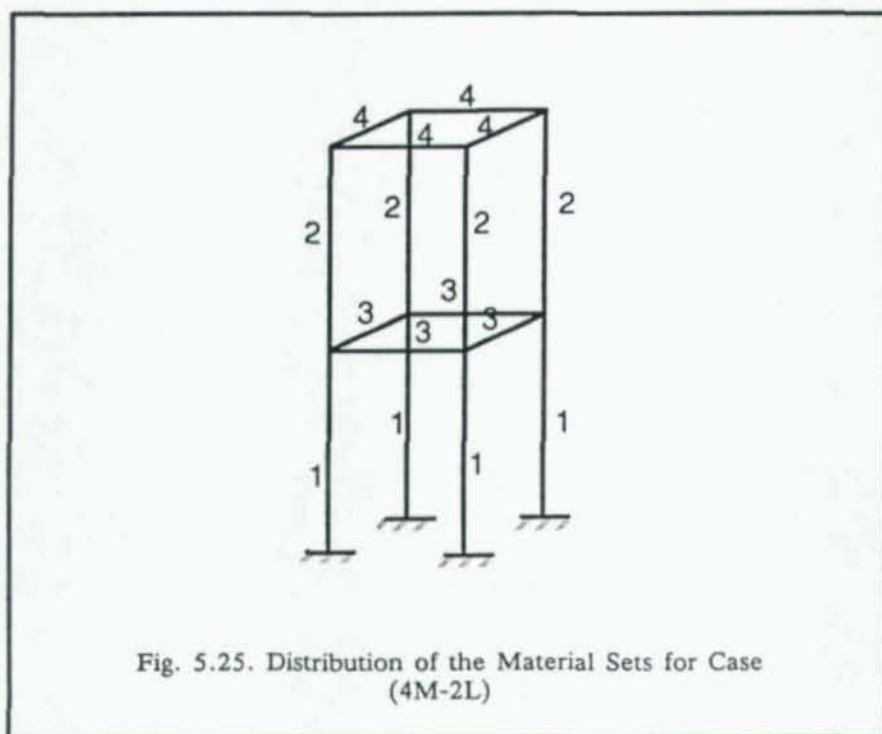


Fig. 5.24. Case (4M-2L) & N=6 with  $\Pi=\{1,2\}$





## 5.4. Displacement Constraint Optimization

### 5.4.1. Introduction

The essence of the proposed optimization technique is to enhance the global stability of a framed structure and consequently to upgrade the structure's performance. In particular, structures having inelastic material behavior are likely to exhibit a limit load with a loss of load carrying capacity in the post-limit regime. In the previous sections, through a set of various problems, it was demonstrated that the proposed optimization technique does result in structures with improved overall stability.

Most currently used optimization methods are set to minimize the volume or the cost of a framed structure under some displacement and stress constraints. Displacement constraint optimization methods have been used to limit displacement of a design to minimize damage or perhaps to force a design to remain in the elastic range. Unfortunately, such an approach does not assure overall structural stability. Under severe loading or in the presence of imperfections in the structure, the displacement constrained optimal structure may not have desirable global stability characteristics. To demonstrate this point, the initial design from the previous examples was optimized using an optimality criterion optimization method to minimize the volume subjected to displacement constraints. The detailed formulation of the displacement constraint optimization algorithm used is given in Appendix A. The achieved optimum design then was analyzed and the results are discussed and compared with optimized designs found earlier based on the stability criteria.

### 5.4.2. Example Problems

The frame MRF was optimized under displacement constraint optimization algorithm with minimizing volume as the objective function. Four design variables were used: two for the columns and two for the girders. A rectangular cross section was assumed. Three inches was assumed for the minimum allowable design variables ( $\underline{b} = \underline{h} = 3.0$ ). A combination of load case I and II were applied to the structure throughout the course of optimization. The properties of the optimum design is given in Table 5.6.

Using a displacement constraint of 0.25 inches for the top story displacement resulted in an optimized design with the same volume as the initial design. The optimized design obtained is then analyzed under both load case I and II.

So far, we have optimized an initial design with two different approaches and have come up with two optimized designs. One optimized design was based on displacement control optimization (opt-d) and one was based on the stability criteria optimization technique (opt-s). The resulting load-deformation curve for opt-d is given in Fig. 5.28 and the load-deformation curve for opt-s was given in Fig. 5.16. One can see that under load case I both optimized designs have a much better load carrying capacity and the larger area under the load-deformation curve. Under load case II the optimized design opt-s has better performance than the initial design but the optimized design opt-d has much poorer performance compared to the initial design.

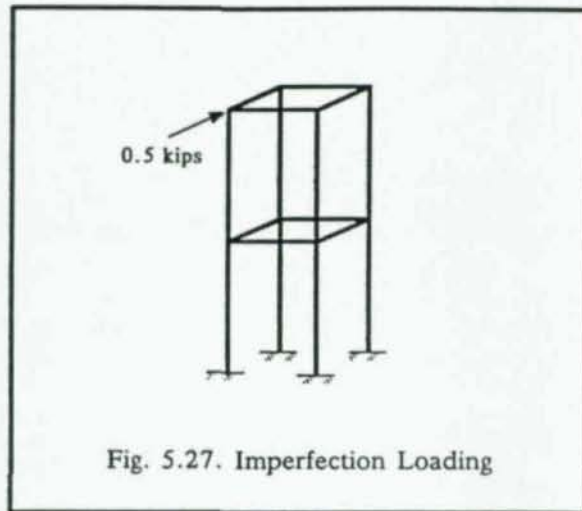
Looking at performance of the both optimized design opt-d and opt-s one can conclude that displacement control optimization did not result in a globally stable structure whereas the proposed the optimization technique did result in a design with a better overall stability characteristics.

#### 5.4.3. Performance of the Optimized Designs Under an Unexpected Loading Condition

Assume that there is an imperfection in the constructed frame or there is an unexpected loading, for example 0.5 kips applied at the top of the one of the second story columns (see Fig. 5.27). Neither of the optimum designs based on displacement constraints or stability criteria are designed for this type of the loading. This loading is used to see how the optimized designs will behave in such an unexpected environment.

Both of the optimum designs using the stability criteria opt-s and the optimum design using displacement constraints opt-d are analyzed under load case I plus the loading give in Fig. 5.27. The result of the load-deformation curves are given in Fig. 5.29. One can see that the optimized design opt-d shows a higher limit load, and is much stiffer than the initial design and the optimized design opt-s. However, the optimized design opt-d has a very steep post-limit curve showing that the load-carrying capacity of structure drops very quickly compared to the initial design or the optimized design opt-s. The same type of behavior is observed for the load versus deformation in both X- and Z-directions. The optimized design based on the stability criteria has slightly better load-carrying capacity than the initial design and has the post-limit degradation of about same as the initial design.





Consequently, based on the examples described, one might conclude that a design based on stability criteria shows better overall stability characteristics compared to one based on a displacement control optimization method, making the former a more attractive design technique. The optimized design based on the displacement constraint may be better if the design is expected to remain in the elastic range.

Table 5.6. Properties of the Optimum Design for the Displacement Constraint Optimization Method

PROPERTY	VALUE
<b>Columns</b>	
Width( <i>in</i> )	10.085
Height( <i>in</i> )	3.000
Area( <i>in</i> <sup>2</sup> )	30.256
Strong Moment of Inertia( <i>in</i> <sup>4</sup> )	22.7
Weak Moment of Inertia( <i>in</i> <sup>4</sup> )	256.4
Torsion( <i>in</i> <sup>4</sup> )	74.2
<b>Girders</b>	
Width( <i>in</i> )	9.693
Height( <i>in</i> )	3.000
Area( <i>in</i> <sup>2</sup> )	29.1
Strong Moment of Inertia( <i>in</i> <sup>4</sup> )	21.8
Weak Moment of Inertia( <i>in</i> <sup>4</sup> )	227.5
Torsion	70.6
<b>Parameters</b>	
Number of iterations	9
$\frac{b}{h}$	3
$\frac{h}{b}$	3



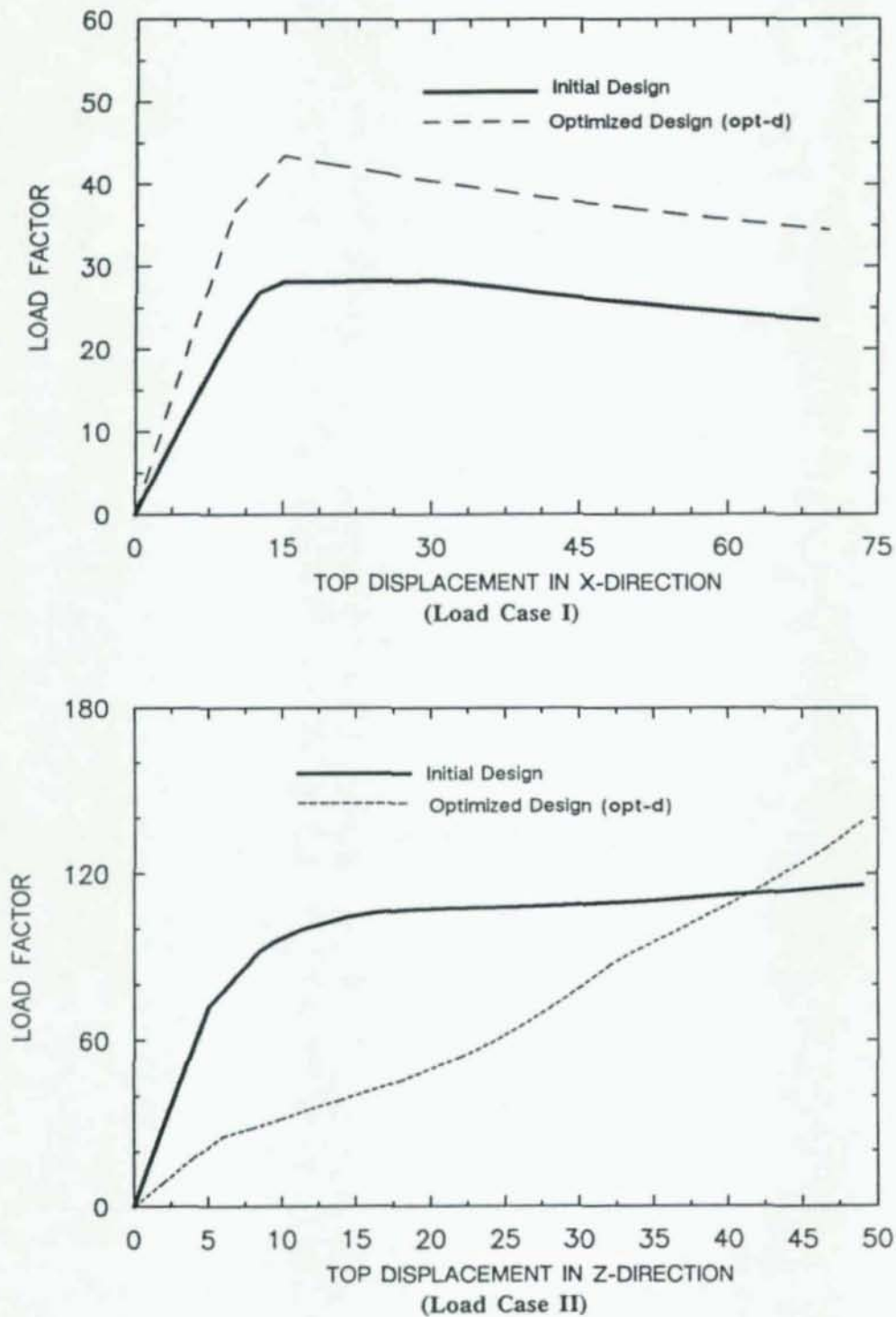


Fig. 5.28. Load-Deformation Curves for Displacement Control Optimization Technique Under Loading Case I and II

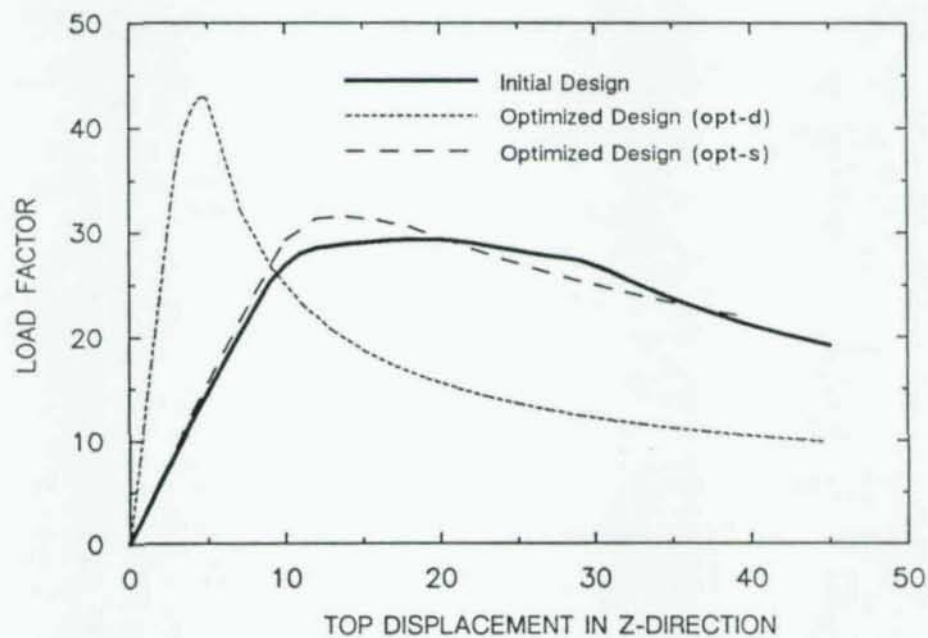
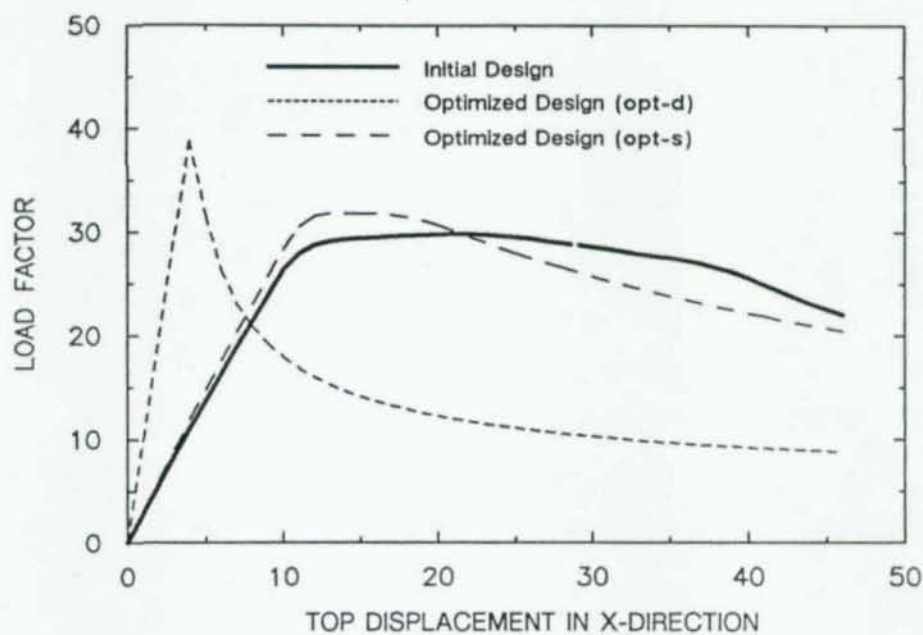


Fig. 5.29. Load-deformation Curves Using Different Optimization Techniques Under Load Case I Plus a Load of 0.5 kips Applied in Z-direction at the Top of One of the Second Story Columns

## CHAPTER 6

### APPLICATION OF 3-D OPTIMIZATION ALGORITHM TO IRREGULAR FRAMED STRUCTURES

#### 6.1. Introduction

It is often difficult to identify the design changes necessary to improve the performance of a structure, especially when the structure is irregular and the response is nonlinear. Trial and error procedures are usually neither effective nor economical due to the fact that the complexity of the problem is beyond the intuition of the designer. An optimization methodology can be efficient and productive for irregular structures. To show the strength and the limitation of the optimization methodology as applied to irregular structures, a setback building is optimized and the result of the optimization presented and discussed.

It is important to remind the reader that the proposed optimization procedure is designed to improve the stability characteristics of a building. The optimization methodology is specially effective for taller buildings when the geometry effect is important. The SETBACK building optimized here is not a tall building, yet the optimization procedure improves the overall performance and stability characteristics of the building.

#### 6.2. Description Of SETBACK Example Problem

SETBACK building considered here is a two-story setback frame with topology as given in Fig. 6.1. First story of the SETBACK frame has two bays and the second story has one bay. The topology of the SETBACK frame was picked from a report by Cheng and Truman (1985). Frame SETBACK is designed based on ATC-3-06 earthquake design recommendation (1978).

The loads on the structure were:

<i>Dead load:</i>	<i>80 psf</i>
<i>Live load:</i>	<i>40 psf</i>



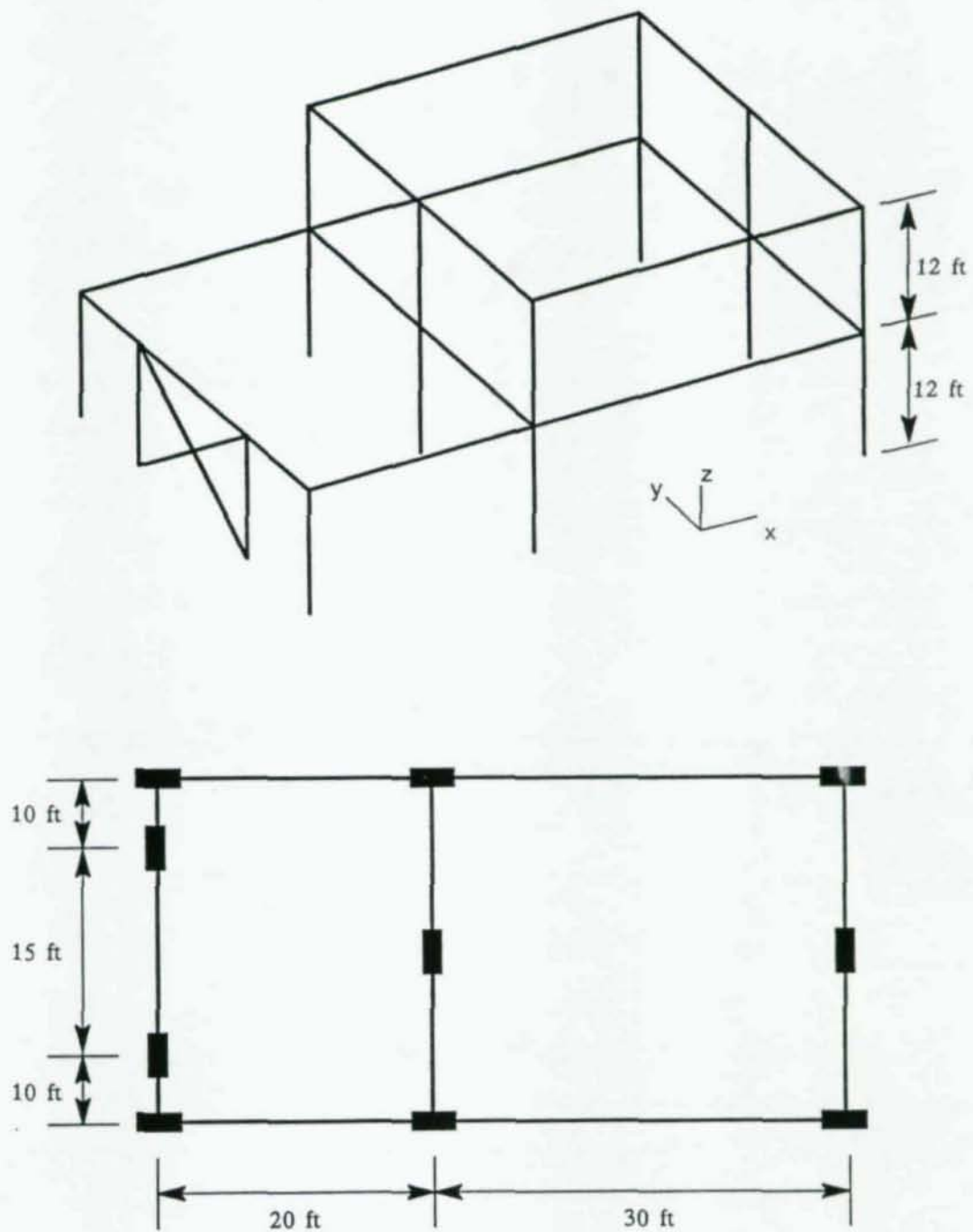


Fig. 6.1. Topology of the SETBACK Frame

A preliminary design was performed using full dead and live load in all members, using approximate coefficients to determine maximum moments in girder sections.

Because SETBACK is an irregular structure, a modal analysis procedure was employed to determine earthquake loads. The building was modeled as a system of masses lumped at the floor levels. A rigid floor diaphragm is modeled as a rigid plane parallel to the horizontal plane, so that all the points on any one floor diaphragm can not displace relative to each other in horizontal plane. Program SAP80 (Wilson and Habibullah, 1984) was used to determine member forces and to perform the frequency analysis. SAP80 has the capability of modeling rigid floor diaphragm systems where each floor diaphragm is established by a rigid joint in the plane of the diaphragm called *master joint* of the diaphragm. All other joints that exist on the diaphragm connected to the master joint by rigid links. SETBACK was modeled by space frame beam elements and two master joints. Each master joint had 3 degrees of freedom. Therefore, a total of 6 frequency eigenpairs can be calculated.

The mass property of each rigid floor diaphragm was determined and is given Table 6.1.

Table 6.1. Mass Properties

Floor Level	Mass ( $k \cdot \text{sec}^2 / \text{in}$ )	Mass Moment of Inertia ( $k \cdot \text{sec}^2 \text{in}$ )
Bottom Story	0.362	16196
Top Story	0.217	5534

#### 6.2.1. Seismic Coefficients

The following seismic coefficients in accordance with ATC-3-06 were used:

$A_d = 0.4$  (Effective peak acceleration)

$A_v = 0.4$  (Effective peak velocity-related acceleration)

$S_2 = 1.2$  (Soil profile characteristics of site)

$R = 4.5$  (Reduction factor to account for effects of inelastic behavior)

Seismic Category C

Seismicity Index of 4

### 6.2.2. Modal Base Shear

The portion of the base shear contributed by the  $m$ th mode,  $V_m$ , according to ATC-3-06 shall be determined as:

$$V_m = C_{sm} \bar{W}_m = C_{sm} \frac{\left[ \sum_{i=1}^n w_i \psi_{im} \right]^2}{\sum_{i=1}^n w_i \psi_{im}^2} \quad m = 1, \dots, N \quad (6.1)$$

Where  $\bar{W}_m$  is the effective modal gravity load,  $w_i$  is the portion of total gravity load of the building at or assigned level  $i$ ,  $\psi_{im}$  is the displacement amplitude at the  $i$ th level of the building when vibrating in  $m$ th mode, and  $C_{sm}$  is the modal seismic design coefficient determined according to Eqn. (6.2) below:

$$C_{sm} = \frac{1.2 A_v S}{R T_m^{2/3}} \leq \frac{2.5 A_a}{R} \quad (6.2)$$

### 6.2.3. Modal Forces

The modal force,  $F_{xm}$ , at each level shall be determined as the following:

$$F_{xm} = \frac{w_x \psi_{xm}}{\sum_{i=1}^n w_i \psi_{im}} V_m \quad m = 1, \dots, N \quad (6.3)$$

A computer program was written to perform modal analysis and to calculate earthquake forces applied to the building according to the Eqn. (6.1) through Eqn. (6.3).

A set of eight combinations of load effects, as recommended by ATC-3-06, was considered:

$$\begin{cases} 1.2Q_D + 1.0Q_L \pm 1.0Q_E \\ 0.8Q_D \pm 1.0Q_E \end{cases} \quad (6.4)$$



where  $Q_D$  is the effect of the dead load,  $Q_L$  is the effect of live load, and  $Q_E$  is the effect of the earthquake load. The critical load effect due to the application of seismic forces on the building are determined as a combination of prescribed loads: 100 percent of the force for one direction plus 30 percent of the force for the perpendicular direction. Therefore, load  $Q_E$  consists of a set of two forces making the total number of the load combinations given in Eqn. (6.4) eight.

The eight different loads were applied to the building and the stresses and the displacements of each load combination were determined. Members of the building were checked for the worst loading case and were redesigned if necessary. This procedure of analysis and redesign was carried out for several iterations until all the requirements were satisfied.

The member properties of the final design were checked against the AISC (1978) specification and all the requirements were satisfied. The properties of the design are given in Table 6.2.

Table 6.2. Properties of the Final Design

Member	Section	Equivalent Rectangle	
		Width (in)	Height (in)
Bottom columns	W10X68	5.5	9.5
Top columns	W10X68	4.0	8.6
Bottom columns	W12X19	1.7	9.8
Top columns	W10X12	1.6	7.5
Braces	W10X12	1.6	7.5

The optimization algorithm for 3-D problem was implemented for rectangular cross sections with height and width of the cross section as the design variables. Therefore, equivalent rectangular sections representing the W-sections of the design were determined and are presented in Table 6.2. Also, Table 6.4 and Table 6.3 give vibration frequency and mode shapes of the final design.

Table 6.3. Mode Shapes of the Final Design

$\psi_1$	$\psi_2$	$\psi_3$	$\psi_4$	$\psi_5$	$\psi_6$
0.384	0.000	0.000	2.112	0.000	0.000
0.000	0.284	-0.356	0.000	1.541	-1.424
0.000	0.000	0.000	0.000	0.000	0.000
1.635	0.000	0.000	-0.297	0.000	0.000
0.001	1.622	0.282	0.000	-0.228	0.006
0.000	0.000	0.000	0.000	0.000	0.000

Table 6.4. Periods of the Final Design

Mode	Period (seconds)
1	0.933
2	0.800
3	0.338
4	0.181
5	0.167
6	0.050

An equivalent set of static forces were obtained using a square-root-of-the-sum-of-the-square (SRSS) method resulting in the forces given in Fig. 6.2. and Fig. 6.3.

#### 6.2.4. A Note on Analysis Procedure

The finite element discretization of the initial and the optimized design consisted of two elements between each structural joints for all the members except for girders with 30 feet length where three elements were used between each structural joints.  $C^0$  quadratic interpolation was used throughout. 5% isotropic hardening was used for all the material properties. Rigid bars were used to model rigid floor behavior for the frame without changing the overall elastic stiffness properties of the structure.

Displacement control load incrementing, as described by Batoz and Dhatt (1979), was used throughout the analyses. One of top story nodes, where the load is applied, was used as the control point. All the deformation history curves presented in this chapter are given in terms of load factors versus lateral top displacements. For irregular frames, specially for 3-D structures, is not clear that if the displacement of a single point would give a good representation of the whole structure displaced configuration. For the SETBACK frame it was decided that the lateral top displacement of the structure does present an accurate displaced characteristics of the whole structure by examining the initial design. As the initial design was analyzed, two sets of information were stored: (1) top displacement versus load factors and (2) the norm of the nodal displacement versus the load factors. The norm of all the nodal displacements were calculated using the formula:

$$\|U\| = U^T K U \quad (6.5)$$



where  $U$  is vector of nodal displacements and  $K$  is the linear elastic stiffness matrix of the structure. Since the problem is nonlinear, the stiffness matrix changes after each displacement increment, therefore, the initial elastic stiffness matrix was stored to be used for the calculation of the norm of nodal displacements as the deformation progressed. The norm  $\|U\|$  is a scalar representing the norm of the nodal displacement of the whole structure. The plot of the lateral top displacement versus load factor and the norm of the displacements versus the load factor is given in Fig. 6.4. Observe that both load-deformation curves present the same behavior. Therefore, for the presentation of load-deformation curves, a plot of load factor versus top displacements is adopted and used for the remainder of this chapter.

### 6.3. Discussion of the Optimization Algorithm as Applied to SETBACK Frame

Six different examples are considered in this section, five under a single loading condition and one under multiple loading condition. Parameter studies have been performed on the number of design variables, the number of buckling eigenvalues and eigenvectors, and the minimum and maximum allowable values of the design variables. Table 6.5 gives a summary of the parameters studied.

Table 6.5. Parameter Properties of the Example Problems

Case Studied	Parameters				
	Mat	$\underline{b}$	$\underline{h}$	N	L
(1)	5	4.0	4.0	5	1
(2)	5	4.0	4.0	10	1
(3)	8	4.0	4.0	5	1
(4)	5	1.8	7.5	5	1
(5)	5	1.8	7.5	10	1
(6)	5	1.8	7.5	5	2

Mat = No. of Material Sets  
 $\underline{b}$  = Min. Permissible Width  
 $\underline{h}$  = Min. Permissible Height

N = Number of eigenpairs  
L = Number of Loading Cases



(1) (5M-1L),  $N=5$ ,  $\underline{b}=4.0$ ,  $\underline{h}=4.0$

The five design variables used are: bottom story columns, top story columns, bottom story girders, top story girders, and braces. The spectral evolution for this case is given in Fig. 6.5. The optimization converged in 41 iterations with the properties of the optimized design summarized in Table 6.7. About iterations 17 and 18, it appears that optimization is diverging but after iteration 18 the algorithm recovers and works its way toward a smooth convergence. To avoid setting design variables as passive artificially, for the first 20 iterations all the design variables were set to active after each iteration. If we had not reactivated the design variables, the algorithm might not have recovered after iteration 17. The reason for this behavior is that modes 1 and 2 coalesced in iteration 16 resulting in undefined eigenvector sensitivities.

The important conclusion drawn from this example is that the optimization is robust in the sense that it is independent of the initial design. In other words if one chooses the initial design as the design found in iteration 17, which is obviously a bad design and far from optimal, the optimization still can reach the optimal design with no problem.

At optimum the height and width of the first story girders and braces with the width of the second story girder became passive and adopted the minimum permissible sizes of 4.0 inches. At the optimum, all the eigenvalues of the structure were distinct and evenly spaced.

Looking at nonlinear static analyses of the optimized design and the initial design, Fig. 6.5, one can see that the limit-load capacity of the structure has increased and although the post-limit slope of the optimized design is steeper than the initial design post-limit slope, it always bounds it from above.

(2) (5M-1L),  $N=10$ ,  $\underline{b}=4.0$ ,  $\underline{h}=4.0$

The difference between the case (2) and case (1) is in the number of the buckling eigenvalues and eigenvectors used in the objective function. Ten buckling eigenpairs were used to see how the result of the optimized design changes compared to the previous case where 5 buckling eigenpairs were used.

The spectral evolution and the result of the nonlinear static analysis of the optimized design for case (5M-1L),  $N=10$ ,  $\underline{b}=4.0$ ,  $\underline{h}=4.0$  is given in Fig. 6.6. The optimization process converged in 45

iterations with properties of the optimized design tabulated in Table 6.7. Nonlinear static behavior of the optimized design is similar to the nonlinear static behavior of the optimized design obtained in case (1), except that the optimized design here is slightly stiffer elastically. The reason for similar performances can be explained by investigating the spectral history plot where one can observe that the participation of the first buckling mode in the overall response of the structure,  $\beta_{ij}$ , for both cases are almost the same. The participation of the higher modes in the objective function were much smaller compared to the first mode.

(3) (8M-1L),  $N=5$ ,  $\underline{b}=4.0$ ,  $\underline{h}=4.0$

The case (8M-1L),  $N=5$ ,  $\underline{b}=4.0$ ,  $\underline{h}=4.0$  is optimized using 8 different material properties with a total of 16 design variables. The distribution of the material properties used is shown in Fig. 6.7. As can be seen from Fig. 6.8 of the spectral evolution, optimization converged in 29 iterations with the properties of the optimized design given in Table 6.8. The dominant buckling eigenvalue of the optimized design was mode 1 with the magnitude of 30.0, (150% higher than cases (1) and (2)). Having a higher dominant buckling eigenvalue, it is expected that the optimized design to behave better than cases (1) and (2). Looking the nonlinear static analysis of the optimized design, it is obvious that indeed it does behave better than the optimized designs of cases (1) and (2) and the initial design. The limit-load capacity of the optimized design was 163% higher than the initial design limit-load, with post-limit strength degradation about the same as the initial design.

(4) (5M-1L),  $N=5$ ,  $\underline{b}=1.8$ ,  $\underline{h}=7.5$

Minimum design variables of  $\underline{b}=1.8$ ,  $\underline{h}=7.5$  of the cross section were chosen for the case (4) and the following two cases. Such a selection of minimum permissible design variables has a twofold purpose: (I) to investigate the effect of different minimum permissible sizes on the outcome of the optimization, and (II) to have minimum sizes comparable to the initial design.

The spectral evolution and the nonlinear load-deformation curves for the optimized design is given in Fig. 6.8. Observe that a lot of mode shifting takes place during the optimization with large changes in the magnitude of the buckling eigenvalues. After iteration 25 the step length was increased from 10 to 25, where the optimization settled down and finally converged in 45 iterations. The properties of the optimized design is given in Table 6.9.



Observe that the limit-load capacity of the optimized structure improved considerably with the post-limit slope of about the same as the initial design. The performance of the optimized design is an improvement over the optimized designs found in cases (1) and (2) where the same objective function was employed with different limits on the size of the design variables.

(5) (5M-1L),  $N=10$ ,  $\underline{b}=1.8$ ,  $\underline{h}=7.5$

For the case studied here, (5M-1L),  $N=10$ ,  $\underline{b}=1.8$ ,  $\underline{h}=7.5$ , 10 buckling eigenvalues were used in the objective function compared to 5 buckling eigenvalues for the case (4). The result of the spectral evolution and the nonlinear static load-deformation curves are given in Fig. 6.10. The optimized design performed quite well, with limit-load carrying capacity and improved post-limit behavior compared to the initial design. Looking at the property table, one can see that the optimized design for case (4) has about the same properties as case (5) except that the second story girder is smaller for the present optimized design and the columns are slightly heavier, causing a better post-limit behavior and slightly smaller load carrying capacity. The dominant mode started as mode 1 and switched to mode 4 at optimum with a magnitude of 41.3 compared to the previous case of 23.6.

(6) (5M-2L),  $N=5$ ,  $\underline{b}=1.8$ ,  $\underline{h}=7.5$ ,  $\Pi=\{1,1\}$

Last case studied was the optimization of the initial design under loading cases (I) and (II). The objective function  $\sum_{i=1}^{10} \sum_{j=1}^2 \mu_i \beta_{ij} \mu_j$  was used with  $\underline{b}=1.8$ ,  $\underline{h}=7.5$ ,  $\Pi=\{1,1\}$ . The two loading cases considered are not necessarily expected to act at the same time. The result of optimization is given in Fig. 6.11 in terms of spectral evolution and nonlinear static load-deformation curve for the design. Optimization converged in 39 iteration with first mode as the dominant mode and modes 4 and 5 coalescing. Properties of the optimized design are given in Table 6.10. Looking at the load-deformation curve, one can see that optimization improved the performance of the optimized design under both loading cases. The optimized design has higher load carrying capacity under both loading conditions compared to the initial design. The post-limit behavior of both designs are about the same.

To investigate the integrity of the optimized design under dynamic loading conditions it was decided to excite both the optimized and the initial designs under a sinusoidal base acceleration. To



make the comparison fair, both initial and the optimized designs were excited under a sinusoidal ground motion of the same frequency but different amplitudes. The amplitude of the base sinusoidal acceleration was chosen to give the same dynamic magnification factor for both initial and the optimized designs. An equivalent of 0.65g base acceleration was considered. Table 6.6 gives the dynamic properties of the initial and the optimized designs along with the applied sinusoidal base acceleration.

Table 6.6. Dynamic Properties of the Applied Sinusoidal Loading

Parameters	Initial Design	Optimized Design
Fundamental Period, $T_1$ , (sec)	0.78	0.85
Base Acceleration Period, $T$ (sec)	0.50	0.50
Period Ratio: $\beta = \frac{T_1}{T}$	1.49	1.70
Dynamic Magnification Factor	0.82	0.53
Base acceleration	$A_g = 250 \sin(25.13t)$	$A_g = 161 \sin(25.13t)$

The response history of the both initial design and the optimized design are give in Fig. 6.12. Observer that the optimized design has smaller drift and smaller base shear compared to the initial design. Both designs are stable structures and both behaved well under the applied dynamic excitation.

#### 6.4. Displacement Constraint Optimization

The initial design was optimized under a displacement constraint with properties of the optimized design given in Table 6.11. The formulation and discussion on the displacement constraint optimization can be found in Appendix A. The volume of the structure was minimized under a top displacement constraint of 1.2 inches. A combination of the load cases I and II was considered as the applied loading. The optimized obtained under displacement constraint (opt-d) had a volume of close to the initial design.

The nonlinear response of **opt-d** design under both loading cases I and II along with the load-deformation response of the optimized design based on a stability criterion, **opt-s**, are given in Fig. 6.13. Observe that under load case I, the design **opt-d** is stiffer and has higher load carrying capacity compared to the initial design but has a lower load carrying capacity compared to **opt-s** design. The design **opt-d** has a steeper post-limit slope compared to **opt-s**. Under load case II, the **opt-d** design has much lower load carrying capacity than the initial design whereas **opt-s** has higher load carrying capacity compared the initial design.

### 6.5. General Comments

Through several different example applications, it was shown that the optimization procedure can efficiently produce designs with improved limit strength, stability, and ductility characteristics. The method can effectively be used to handle multiple loading cases.

Based on the parameter studies it was concluded that in general: (1) using more design variables will result in optimized designs with better overall performance; (2) using more eigenpairs in the objective function will improve the performance of the optimized design if one or more of the eigenvectors in the range chosen have the same shape as the displaced configuration of the structure under one of the loading cases; (3) the performance of the design in the post-limit regime is dependent on the minimum design variables.

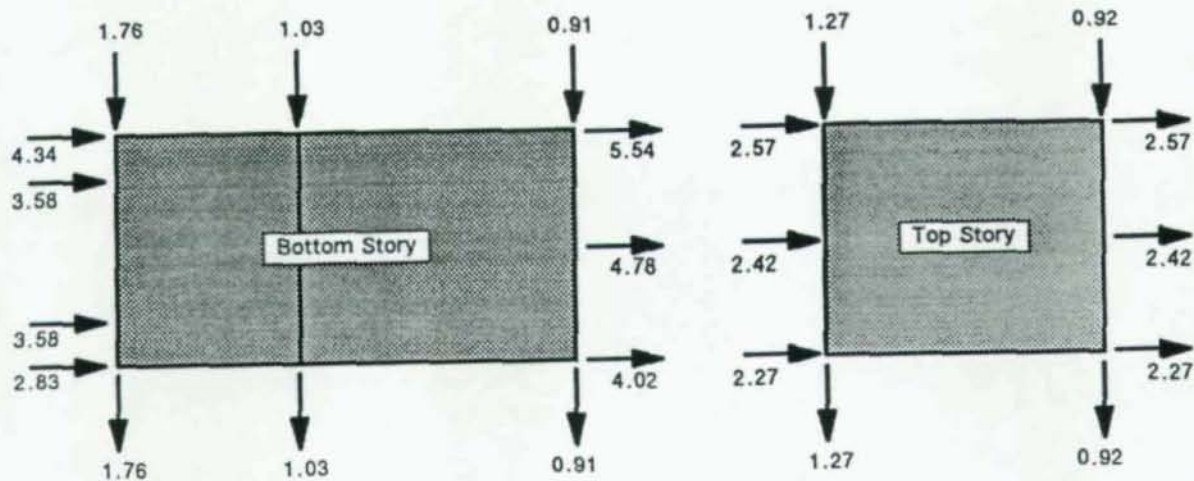


Fig. 6.2. Load Case I (100%  $Q_E$  in X-direction plus 30%  $Q_E$  in Y-direction)

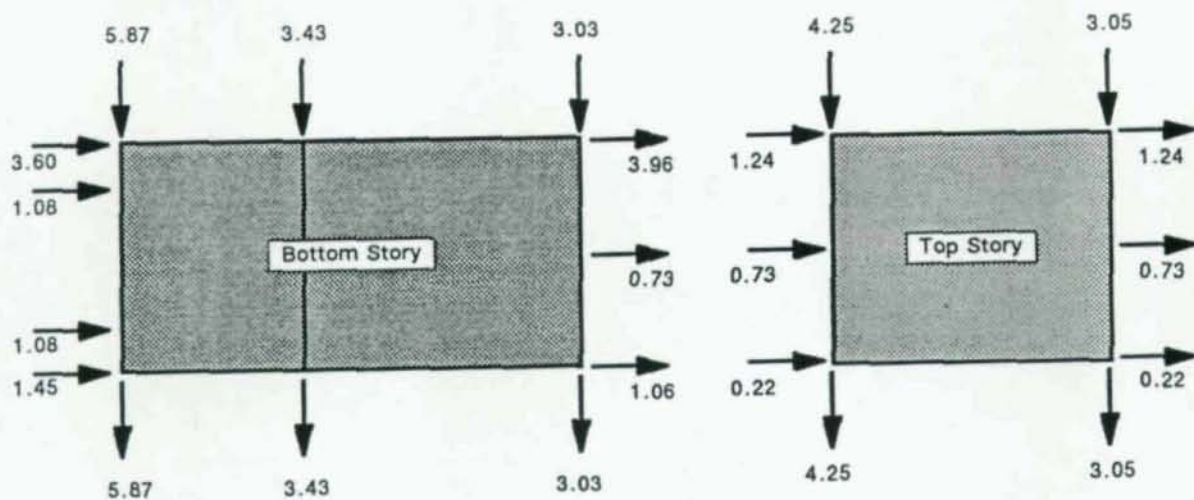


Fig. 6.3. Load Case II (100%  $Q_E$  in Y-direction plus 30%  $Q_E$  in X-direction)



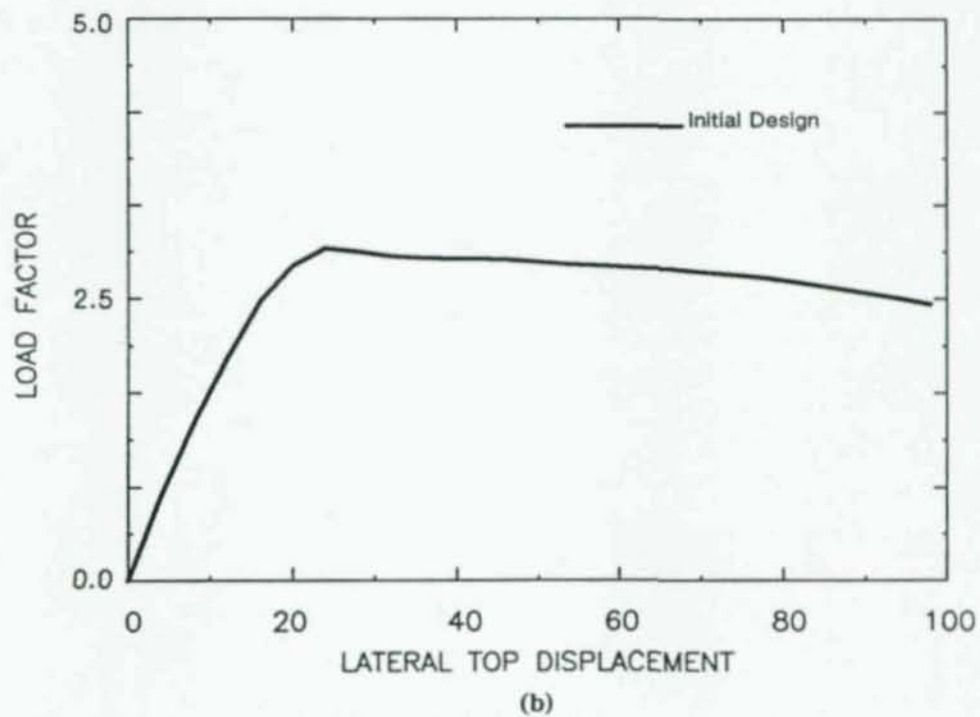
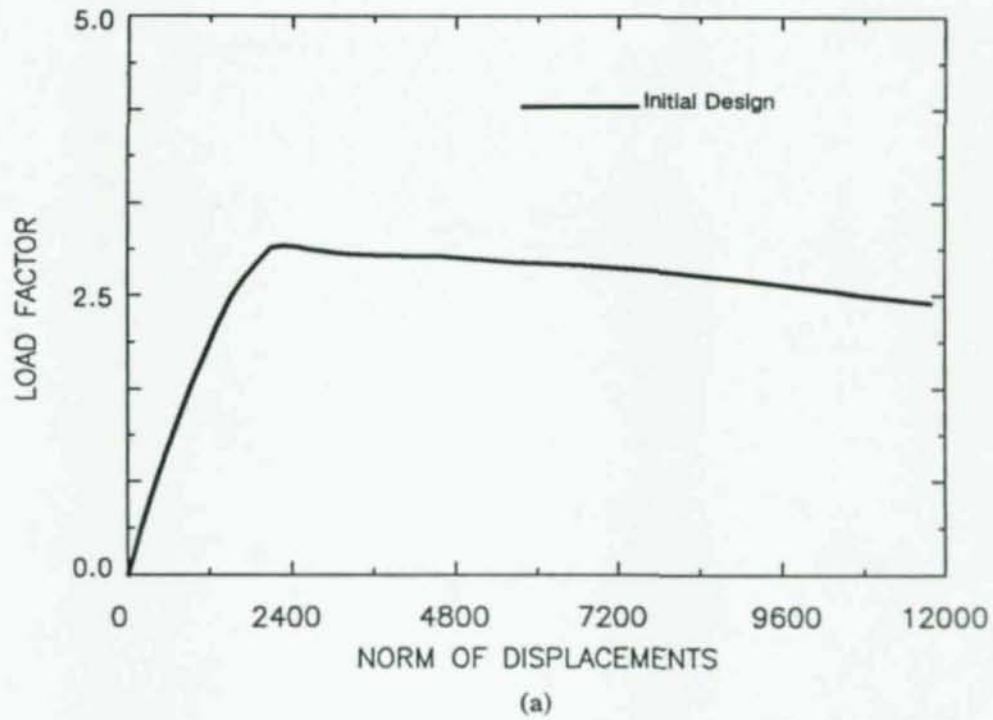


Fig. 6.4. Nonlinear Static Analysis of the Initial Design: (a) Load Factor Versus Norm of Nodal Displacements; (b) Load Factor Versus Lateral Top Displacement

Table 6.7. Properties of the Optimized Designs for the  
Case (5M-1L) & N=5, and  $b = 4.0, \underline{h} = 4.0$  and  
Case (5M-1L) & N=10, and  $b = 4.0, \underline{h} = 4.0$

PROPERTY	Case (1) (5M-1L) & N=5	Case (2) (5M-1L) & N=10
<b>1st Story Columns</b>		
Width	7.029	9.559
Height	5.988	4.000
Area	42.11	38.2
Strong Moment of Inertia	125.8	51.0
Weak Moment of Inertia	173.3	291.2
Torsion	247.3	150.5
<b>2nd Story Columns</b>		
Width	4.896	7.376
Height	6.208	6.861
Area	30.4	50.6
Strong Moment of Inertia	97.6	198.5
Weak Moment of Inertia	60.7	229.5
Torsion	127.1	361.0
<b>1st Story Girders</b>		
Width	4.000	4.000
Height	4.000	4.000
Area	16.0	16.0
Strong Moment of Inertia	21.3	21.3
Weak Moment of Inertia	21.3	21.3
Torsion	36.2	36.2
<b>2nd Story Girders</b>		
Width	4.000	4.000
Height	6.636	8.731
Area	26.5	34.9
Strong Moment of Inertia	97.4	221.9
Weak Moment of Inertia	35.4	46.6
Torsion	88.6	132.0
<b>Braces</b>		
Width	4.000	4.000
Height	4.000	4.000
Area	16.0	16.0
Strong Moment of Inertia	21.3	21.3
Weak Moment of Inertia	21.3	21.3
Torsion	36.2	36.2

Mode No.	Eigenvalues at Optimum
1	20.6 <sup>†</sup>
2	27.3
3	31.0
4	34.8
5	40.2

Case (1)  
(5M,1L) & N=5

Mode No.	Eigenvalues at Optimum
1	21.0 <sup>†</sup>
2	25.0
3	39.0
4	44.0
5	47.0
6	55.0
7	56.0
8	77.0
9	91.0
10	92.0

Case (2)  
(5M,1L) & N=10

<sup>†</sup> Dominant mode at convergence

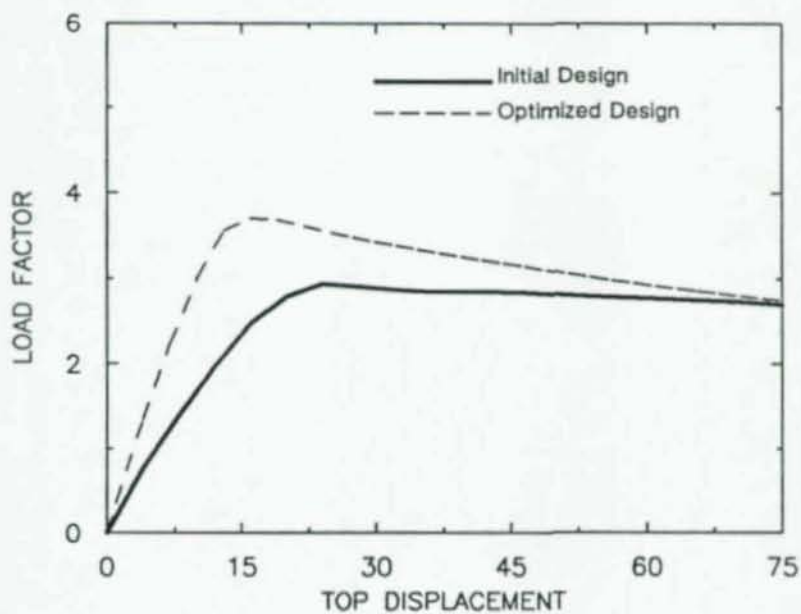
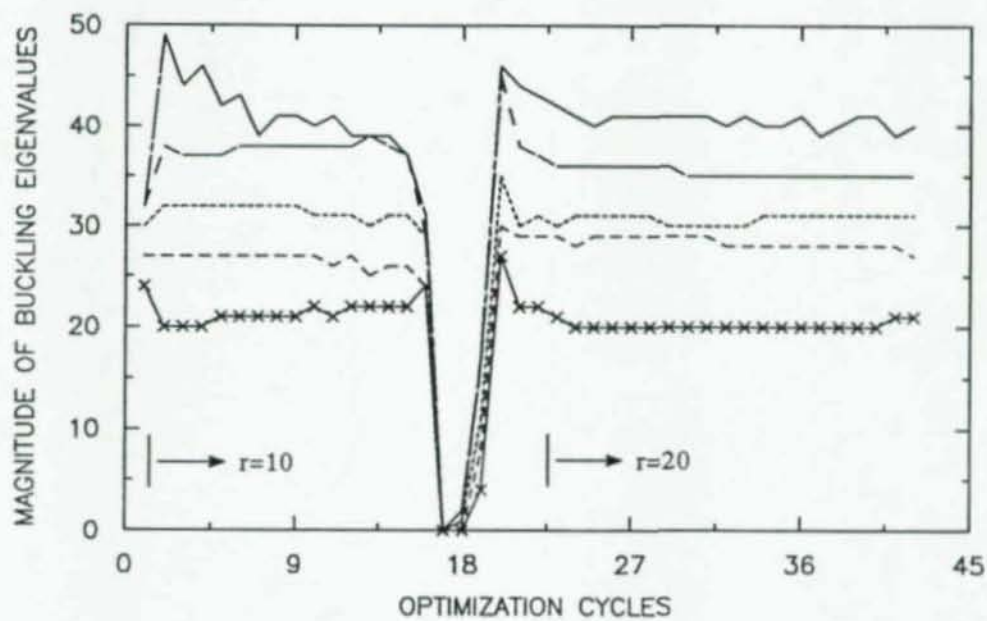


Fig. 6.5. Case (1): with (5M-11) &  $N=5$ , and  $\underline{b} = 4.0$ ,  $\underline{h} = 4.0$



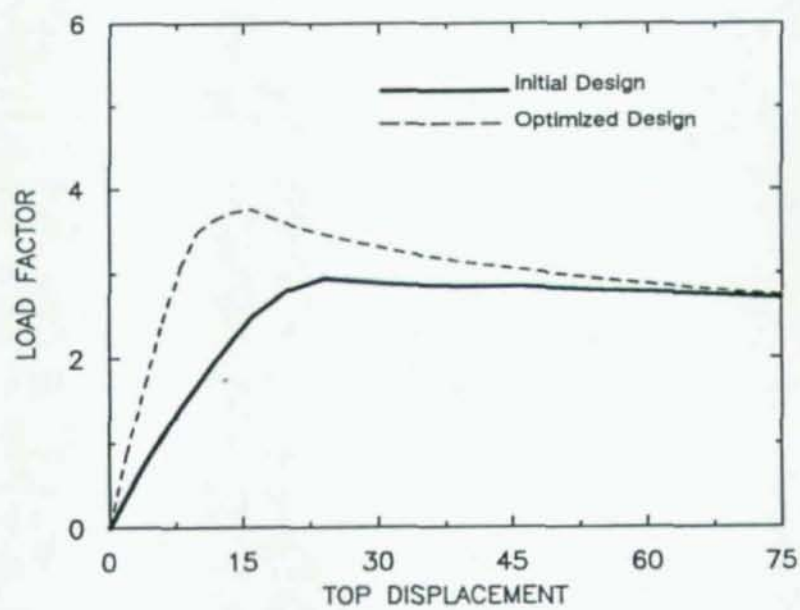
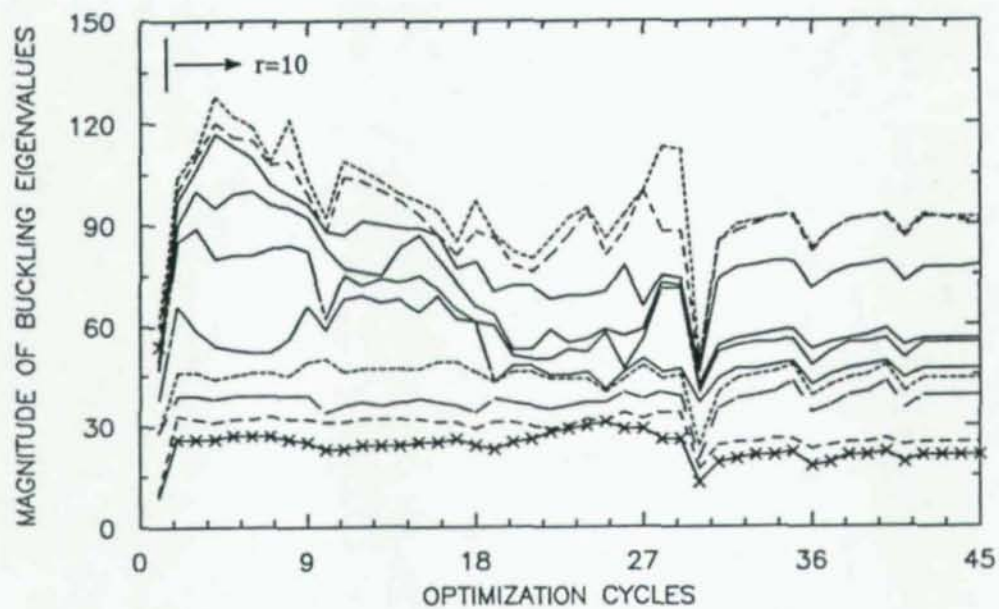


Fig. 6.6. Case (2): with (5M-1) &  $N=10$ , and  $\underline{b} = 4.0, \underline{h} = 4.0$

Table 6.8. Properties of the Optimized Design for the Case (8M-1L) & N=5, and  $\underline{b} = 4.0, \underline{h} = 4.0$

PROPERTY	case (3) (8M-1L) & N=5
<b>Material Set 1</b>	
Width	4.000
Height	4.000
Area	16.0
Strong Moment of Inertia	21.3
Weak Moment of Inertia	21.3
Torsion	36.2
<b>Material Set 2</b>	
Width	10.687
Height	4.000
Area	42.7
Strong Moment of Inertia	406.9
Weak Moment of Inertia	57.0
Torsion	175.9
<b>Material Set 3</b>	
Width	5.306
Height	13.669
Area	88.4
Strong Moment of Inertia	1129.3
Weak Moment of Inertia	170.2
Torsion	519.5
<b>Material Set 4</b>	
Width	5.224
Height	5.472
Area	28.6
Strong Moment of Inertia	65.0
Weak Moment of Inertia	71.3
Torsion	
<b>Material Set 5</b>	
Width	4.846
Height	7.956
Area	38.6
Strong Moment of Inertia	203.4
Weak Moment of Inertia	75.5
Torsion	158.3
<b>Material Set 6</b>	
Width	4.000
Height	4.000
Area	16.0
Strong Moment of Inertia	21.3
Weak Moment of Inertia	21.3
Torsion	36.2
<b>Material Set 7</b>	
Width	4.000
Height	6.450
Area	25.8
Strong Moment of Inertia	89.4
Weak Moment of Inertia	34.4
Torsion	86.6
<b>Material Set 8</b>	
Width	4.000
Height	4.000
Area	16.0
Strong Moment of Inertia	21.3
Weak Moment of Inertia	21.3
Torsion	36.2

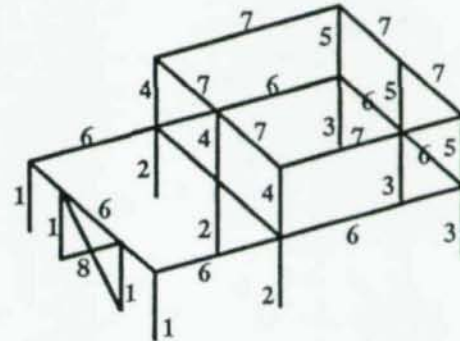


Fig. 6.7. Distribution of Material Sets for (8M-1L) & N=5

Mode No.	Eigenvalues at Optimum
1	30.0 <sup>†</sup>
2	21.5
3	31.0
4	33.5
5	37.0

case (3)  
(8M,1L) & N=5

<sup>†</sup> Dominant mode at convergence

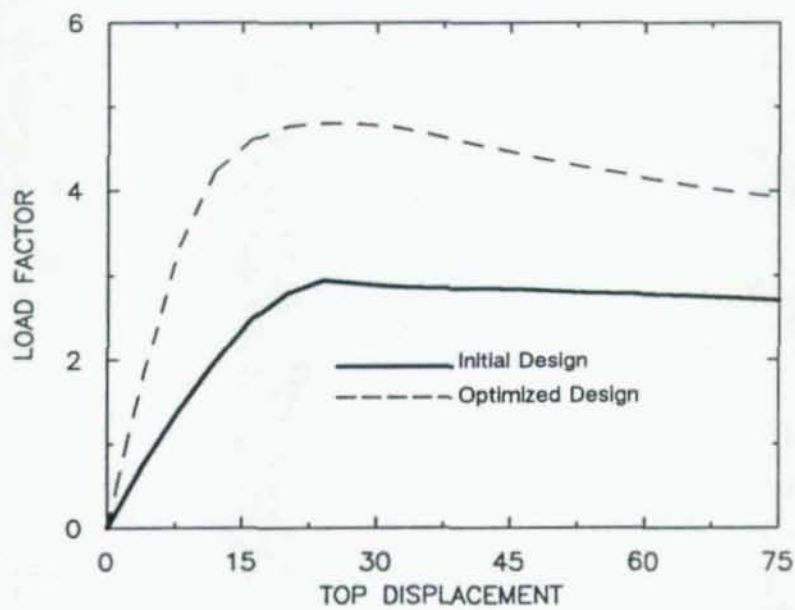
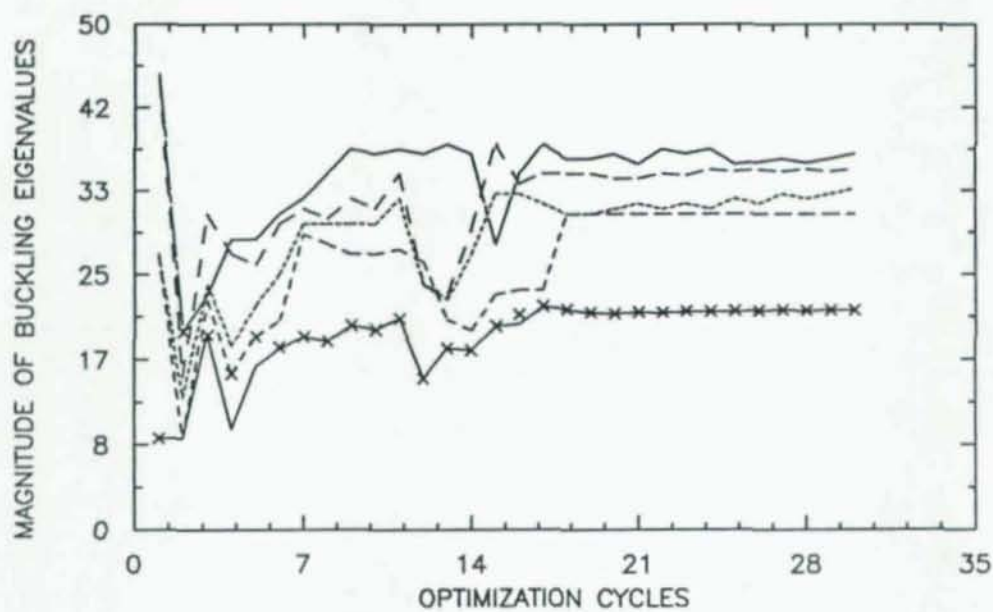


Fig. 6.8. Case (3): with (8M-1L) &  $N=5$ , and  $\underline{b} = 4.0$ ,  $\underline{h} = 4.0$



Table 6.9. Properties of the Optimized Designs for the  
Case (5M-1L) & N=5, and  $\underline{b} = 1.8, \underline{h} = 7.5$  and  
Case (5M-1L) & N=10, and  $\underline{b} = 1.8, \underline{h} = 7.5$

PROPERTY	Case (4) (5M-1L) & N=5	Case (5) (5M-1L) & N=10
<b>1st Story Columns</b>		
Width	5.687	6.919
Height	7.500	7.500
Area	42.6	51.9
Strong Moment of Inertia	200.0	243.3
Weak Moment of Inertia	115.0	207.1
Torsion	247.0	379.6
<b>2nd Story Columns</b>		
Width	5.045	6.145
Height	7.500	7.500
Area	37.8	46.1
Strong Moment of Inertia	177.4	216.0
Weak Moment of Inertia	80.3	145.0
Torsion	188.0	294.5
<b>1st Story Girders</b>		
Width	1.800	1.800
Height	7.500	7.500
Area	13.5	13.5
Strong Moment of Inertia	63.3	63.3
Weak Moment of Inertia	3.6	3.6
Torsion	12.0	3.6
<b>2nd Story Girders</b>		
Width	3.578	1.800
Height	7.500	7.500
Area	26.8	13.5
Strong Moment of Inertia	125.8	63.3
Weak Moment of Inertia	28.6	3.6
Torsion	80.3	3.6
<b>Braces</b>		
Width	1.800	1.800
Height	7.500	7.500
Area	13.5	13.5
Strong Moment of Inertia	63.3	63.3
Weak Moment of Inertia	3.6	3.6
Torsion	12.0	3.6

Mode No.	Eigenvalues at Optimum
1	23.59 <sup>†</sup>
2	31.50
3	35.00
4	37.41
5	38.23

Case (4)  
(5M,1L) & N=5

Mode No.	Eigenvalues at Optimum
1	15.16
2	15.57
3	41.07
4	41.26 <sup>†</sup>
5	41.86
6	41.96
7	63.33
8	63.35
9	79.29
10	94.24

Case (5)  
(5M,1L) & N=10

<sup>†</sup> Dominant mode at convergence

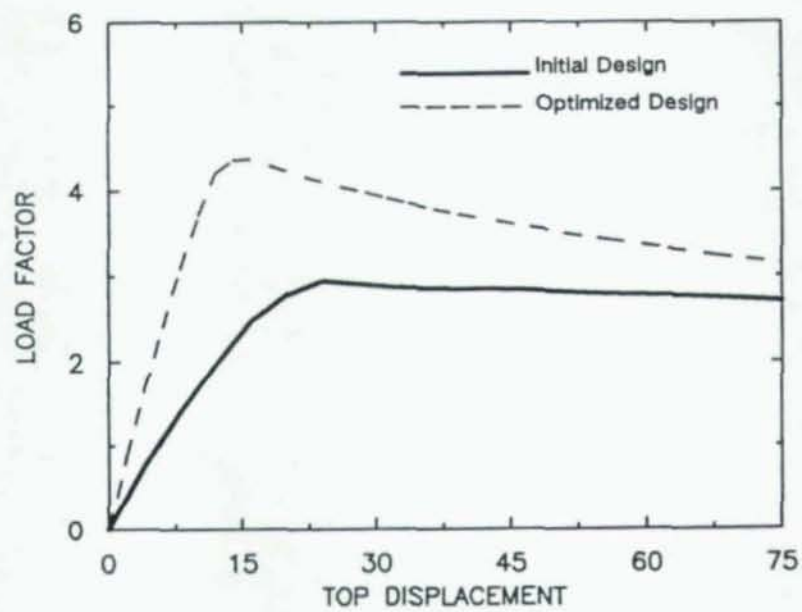
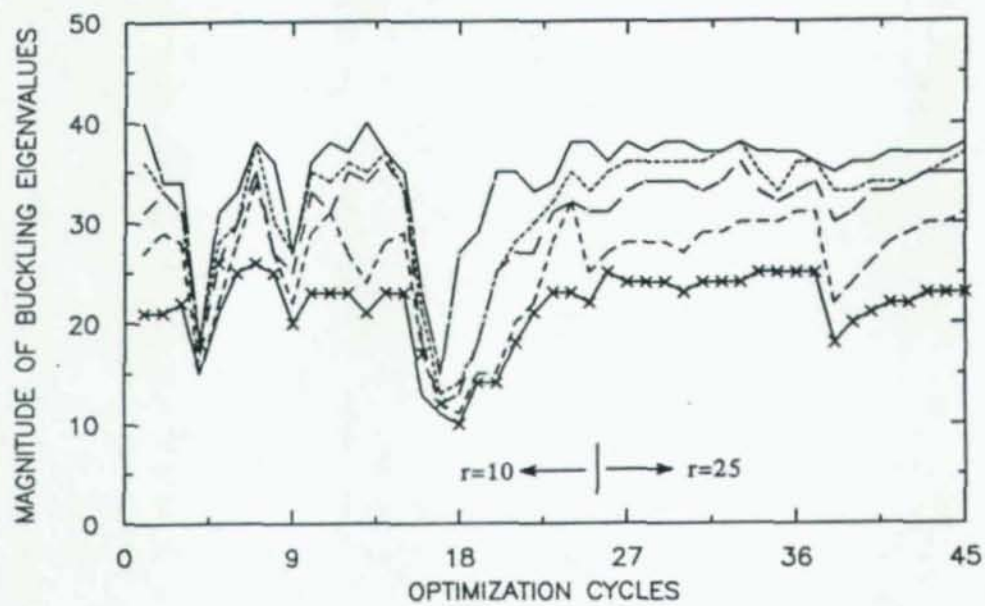


Fig. 6.9. Case(4): with (5M-1L) &  $N=5$ , and  $\underline{b} = 1.8, \underline{h} = 7.5$

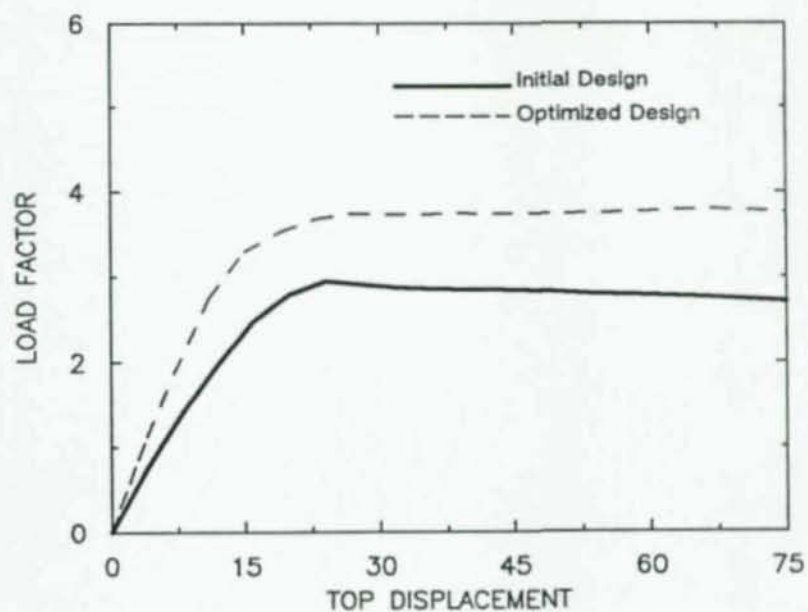
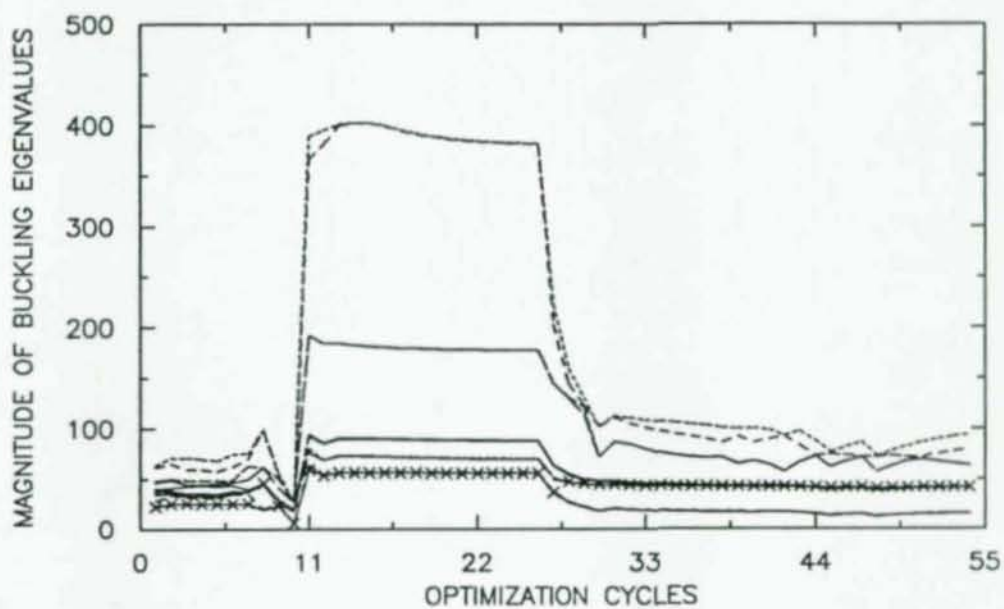


Fig. 6.10. Case (5): with (5M-1L) &  $N=10$ , and  $\underline{b} = 1.8, \underline{h} = 7.5$



Table 6.10. Properties of the Optimized Design for the  
Case (5M-2L) & N=5, and  $\underline{b} = 1.8, \underline{h} = 7.5$

PROPERTY	Case (6) (5M-L) & N=5
<b>1st Story Columns</b>	
Width	5.619
Height	7.500
Area	42.1
Strong Moment of Inertia	197.5
Weak Moment of Inertia	110.9
Torsion	241.2
<b>2nd Story Columns</b>	
Width	4.141
Height	7.500
Area	31.1
Strong Moment of Inertia	145.6
Weak Moment of Inertia	44.4
Torsion	116.4
<b>1st Story Girders</b>	
Width	1.800
Height	7.500
Area	13.5
Strong Moment of Inertia	62.3
Weak Moment of Inertia	3.6
Torsion	12.4
<b>2nd Story Girders</b>	
Width	4.113
Height	7.500
Area	30.9
Strong Moment of Inertia	144.6
Weak Moment of Inertia	43.5
Torsion	114.5
<b>Braces</b>	
Width	1.800
Height	7.500
Area	13.5
Strong Moment of Inertia	62.3
Weak Moment of Inertia	3.6
Torsion	12.4

Mode No.	Eigenvalues at Optimum
1	22.8 †
2	39.2
3	34.9
4	37.1
5	37.2

Case (6)  
(5M,1L) & N=10

† Dominant mode at convergence

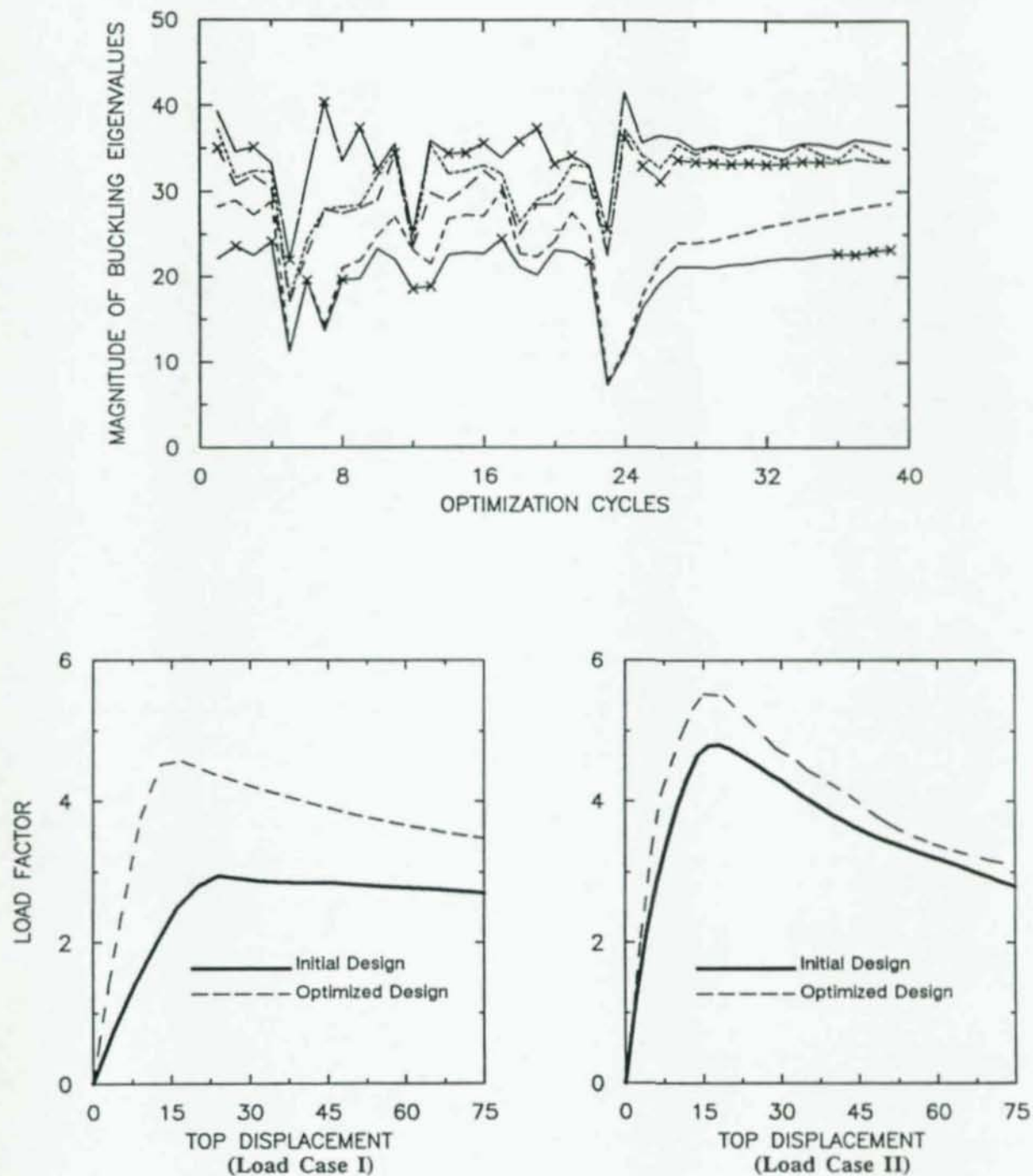


Fig. 6.11. Case (6): with (5M-2L) &  $N=5$ ,  $\Pi=[1,1]$ , and  $\underline{b} = 1.8$ ,  $\underline{h} = 7.5$

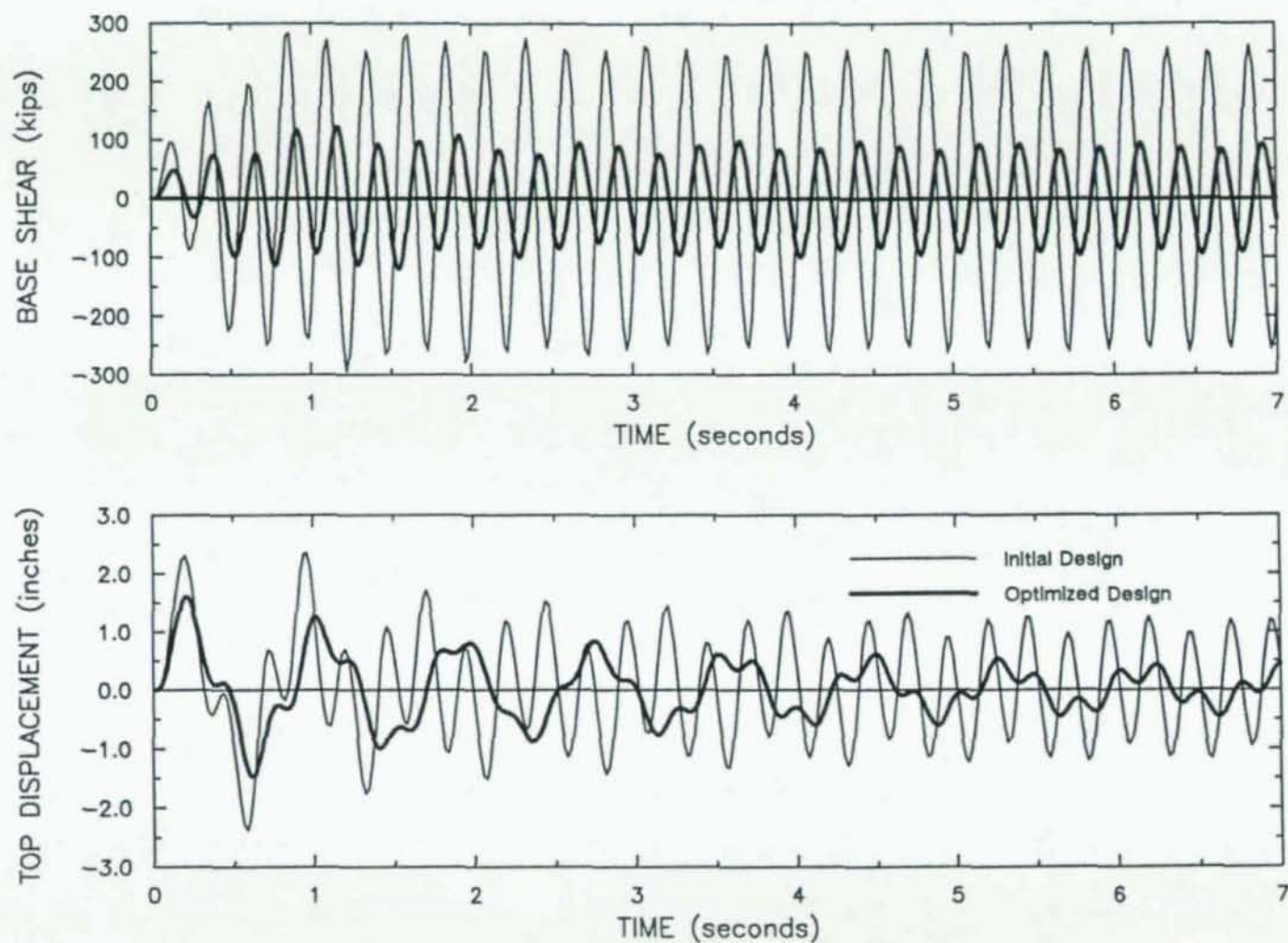


Fig. 6.12. SETBACK Frame under Sinusoidal Base Acceleration with Amplitude and Frequency of the Base Acceleration Chosen to Give the Same Dynamic Magnification Factor for Both Designs



Table 6.11. Properties of the Optimized Design Using a Displacement Constraint Approach to Minimize Volume under a Top Displacement Constraint of 1.2 Inches

PROPERTY	DISPLACEMENT CONSTRAINT OPTIMIZATION
<b>1st Story Columns</b>	
Width	1.800
Height	19.020
Area	34.2
Strong Moment of Inertia	1302.0
Weak Moment of Inertia	9.2
Torsion	34.8
<b>2nd Story Columns</b>	
Width	1.800
Height	11.865
Area	21.4
Strong Moment of Inertia	250.1
Weak Moment of Inertia	5.8
Torsion	20.9
<b>1st Story Girders</b>	
Width	1.800
Height	7.500
Area	13.5
Strong Moment of Inertia	62.3
Weak Moment of Inertia	3.6
Torsion	12.4
<b>2nd Story Girders</b>	
Width	5.4640
Height	7.500
Area	38.25
Strong Moment of Inertia	156.2
Weak Moment of Inertia	95.2
Torsion	201.6
<b>Braces</b>	
Width	1.800
Height	7.500
Area	13.5
Strong Moment of Inertia	62.3
Weak Moment of Inertia	3.6
Torsion	12.4

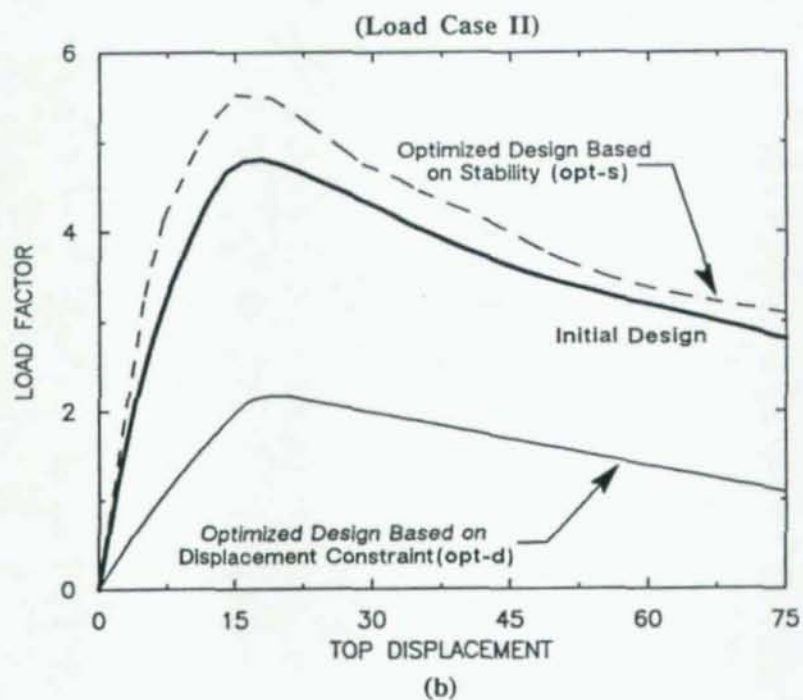
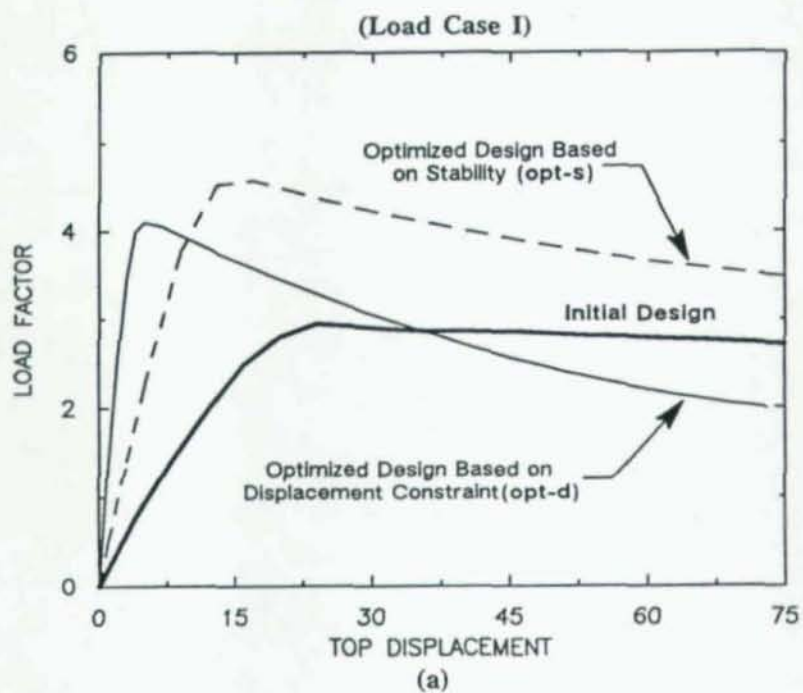


Fig. 6.13. Analyses of Optimized Design Based on Stability Criterion and Optimized Design Based on Displacement Constraint; (a) Under Load Case I; (b) Under Load Case II

## CHAPTER 7

### APPLICATION OF 3-D OPTIMIZATION ALGORITHM TO HIGH-RISE FRAMED STRUCTURES

#### 7.1. Overview

The purpose of the design procedure introduced in this study is to improve the overall stability and strength of structures. The taller is the structure the more important is the role of stability in the performance of the design. In this chapter, the optimization procedure is applied to a tall framed structure to show that when stability is important, the design procedure generates optimized designs with better overall performance.

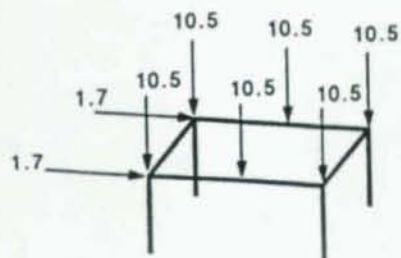
#### 7.1. Application of the Optimization to KORN Frame

The frame KORN considered here was picked from a paper by Korn and Galambos (1968). The topology of the frame along with the loading condition applied to the frame is given in Fig. 7.1. Frame KORN is a fifteen story one bay frame with width in both direction of 12 feet and story height of 14 feet. The properties of the initial design are given in Table 7.1.

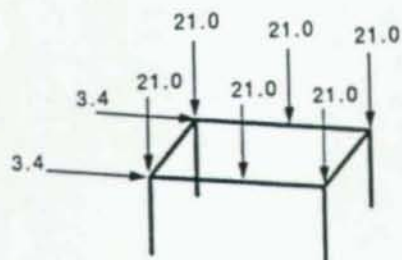
The initial design was optimized under a lateral and vertical loading conditions shown in Fig. 7.1. The optimization converged in 38 iterations with mode three as the dominant mode and the height of all the girders becoming passive. The properties of the optimized design is given in Table 7.1. A minimum permissible size of 3 inches was chosen for both width and height of the cross section. The spectral evolution and the nonlinear load-deformation curves for both initial and the optimized designs are given in Fig. 7.2. Observe that the performance of the optimized design has improved tremendously compared to the initial design. The limit strength of design improved by a factor of 12 with post-limit slope of the structure staying the same as the initial design.

Based on parameter studies done on the minimum permissible dimensions in earlier chapters, it was noticed that the performance of the optimized design can be improved by decreasing the minimum sizes. Therefore, it is possible to improve the performance of design even more by changing the permissible sizes on the design variables.





Loading applied to the top story (kips)



Loading applied to the other stories (kips)

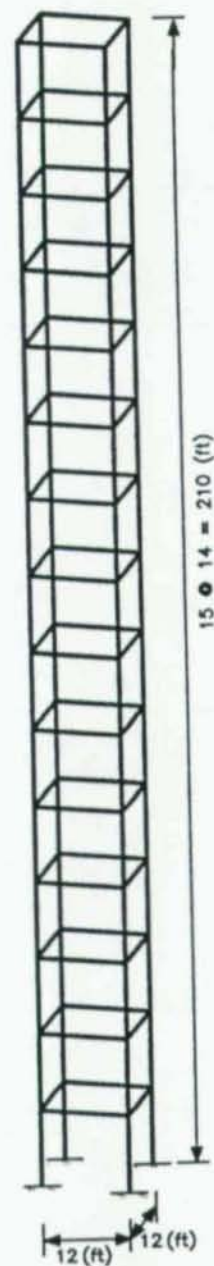


Fig. 7.1. Topology of KORN Frame and Loading Conditions

Table 7.1. Properties of the Initial and Optimized Designs  
( $\underline{b} = 3.0, \underline{h} = 3.0$ ) under Single Loading Case

PROPERTY	Initial Design		Optimized Design	
	Column	Girder	Column	Girder
1st Story				
Width <sup>‡</sup>	6.579	6.914	13.89	3.000
Height <sup>‡</sup>	0.762	0.852	3.000	3.000
2nd Story				
Width	7.069	8.397	11.92	9.733
Height	1.164	0.876	3.000	3.000
3rd Story				
Width	8.592	8.099	12.32	6.800
Height	1.338	0.982	3.000	3.000
4th Story				
Width	8.592	10.29	11.11	7.705
Height	1.338	1.031	3.000	3.000
5th Story				
Width	9.966	10.29	6.175	5.580
Height	1.184	1.031	4.832	3.000
6th Story				
Width	10.58	10.28	6.837	5.391
Height	1.389	1.284	3.960	3.000
7th Story				
Width	10.48	11.15	6.115	5.259
Height	1.572	1.399	4.048	3.000
8th Story				
Width	11.71	11.87	5.397	5.588
Height	1.528	1.508	4.111	3.000
9th Story				
Width	12.37	11.87	4.843	5.828
Height	1.762	1.508	4.121	3.000
10th Story				
Width	12.26	12.37	4.542	5.793
Height	2.014	1.762	3.930	3.000
11th Story				
Width	12.63	12.00	4.296	5.457
Height	2.589	1.909	3.671	3.000
12th Story				
Width	12.63	12.26	4.035	4.953
Height	2.589	2.014	3.364	3.000
13th Story				
Width	12.63	13.77	3.680	4.273
Height	2.589	1.889	3.041	3.000
14th Story				
Width	13.131	14.70	3.000	3.000
Height	2.841	1.918	3.000	3.000
15th Story				
Width	13.37	15.31	3.000	3.000
Height	2.992	1.842	3.000	3.000

Mode No.	Eigenvalue at Optimum
1	0.57
2	1.77
3	3.01
4	3.19
5	3.74
6	3.96

Initial Design

Mode No.	Eigenvalue at Optimum
1	17.27
2	19.43
3	20.05 <sup>†</sup>
4	34.22
5	38.44
6	43.81

Optimized Design

<sup>†</sup> Dominant mode at convergence

<sup>‡</sup> measured in inches

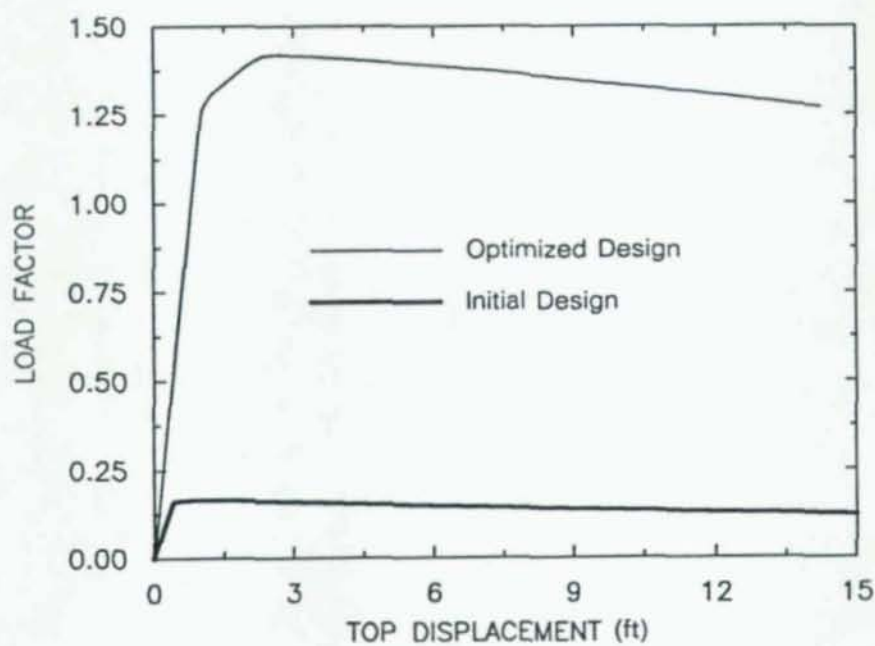
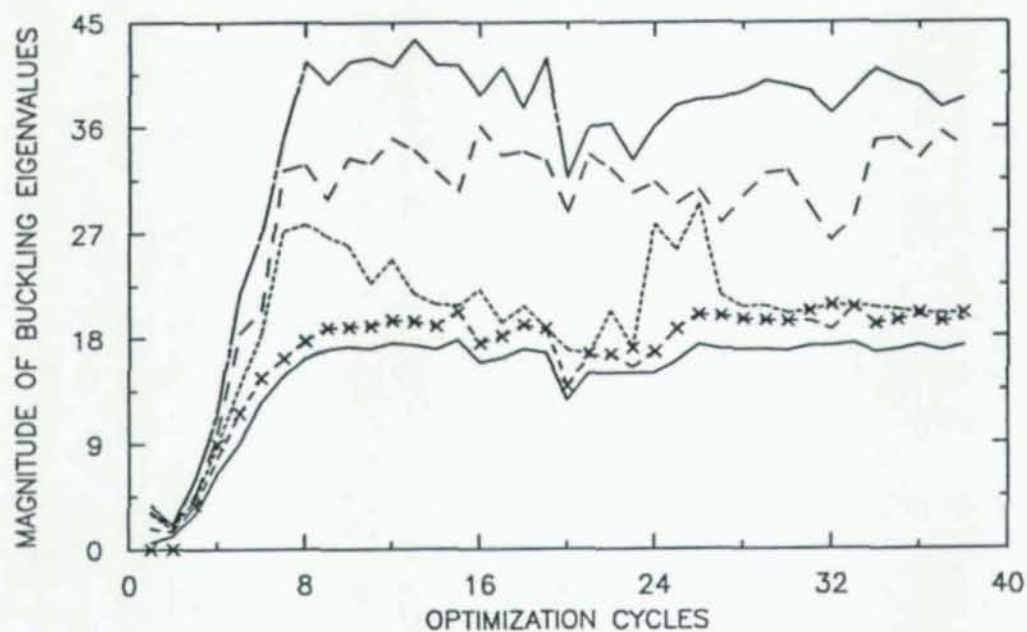


Fig. 7.2. Spectral Evolution and the Load Deformation Curves for Frame KORN



## CHAPTER 8

### SUMMARY, CONCLUSIONS, AND RECOMMENDATIONS FOR FUTURE RESEARCH

#### 8.1. Summary

The overall focus of this study has been centered on the development of a new optimal design methodology to improve strength, stability, and ductility characteristics of structures under single and multiple loading cases.

Most existing optimal design procedures are based on an "accepted design philosophy". The design procedure studied in this report is novel in the sense that it is based directly on stability considerations and is motivated by observations made on the real nonlinear behavior of structures. The design procedure dictates what the "design philosophy" should be in order to improve the performance of the design, and provides a consistent means for studying different aspects of design.

The development of the optimization procedure for planar structures was presented in Chapter 2. The choice of objective was motivated by observations made on the limit and post-limit behavior of elasto-plastic frames and was based on an approximate model of the nonlinear behavior of framed structure. The performance of the optimization algorithm was investigated through two example problems which showed that the procedure not only improves the static response but also can produce improved designs for resisting strong ground shaking. The optimized designs were analyzed under a variety of dynamic excitations to demonstrate that the procedure improves the strength, ductility, and overall stability of a structure. Also, the concept of frequency penalty, which is a useful tool in avoiding undesirable dynamic effects such as resonance, was introduced.

The design procedure was extended to handle three-dimensional structures under multiple loading cases with multiple design variables. Three-dimensional design problems yield insight into the real behavior of the structure and can help avoiding some of the problems that might appear in planar design procedure such as the need for an out-of-plane buckling constraint. The design methodology presented was a multiple-objective optimization procedure whose objective function involved the applied loading vectors, buckling eigenvalues, and eigenvectors of the structure. The three-dimensional optimization technique proposed was solved using a weighting method. The weighting parameters  $\beta_{ij}$  were automatically generated from the loading conditions and the buckling

modes. Multiple objective design optimization results in set of optimized designs that are referred to as the noninferior design set. The designer can then choose the best design from the noninferior set. This choice is generally made using information which is not included in the objective function; for example nonlinear and dynamic analyses. The formulation of the three-dimensional design procedure was presented in Chapter 4. Several issues concerning the implementation of the design procedure were also presented and discussed.

One of the novelties of the procedure presented in Chapter 4 is its ability to efficiently model and optimize structures under multiple loading conditions. This is a very useful tool for design engineers that are faced with many different loading conditions in every day design problems.

Chapters 5 through 7 are the application three-dimensional optimization procedure to a two-story frame, a setback frame, and a fifteen-story high-rise building. These frames were optimized under different loading conditions and various parameter studies were performed which demonstrated that optimization methodology is a strong tool in obtaining designs with better overall performance.

## 8.2. Conclusions

The following conclusions can be drawn from the preceding chapter:

- Maximizing the buckling eigenvalues increases the static limit-load of a structure without degrading the post-limit behavior, increasing overall toughness.
- The optimization procedure based on stability consideration results in a more robust design compared to an optimization procedure with displacement constraint.
- The optimization procedure developed here improves the performance of the initial design under multiple loading conditions.
- The bigger the magnitude of the dominant eigenvalue (one with maximum  $\beta_{ij}$ ) at convergence, the better the final optimized design will behave.
- In general, using more design variables will result in a better behaved optimized design. From practical point view, however, it makes sense to group elements together to save on labor, detailing, and fabrication costs.



- The frequency penalty function can help control the vibration spectrum and can be thought of as a flexible constraint imposed on a design. The frequency penalty may be important in some applications.
- Statically based optimal design results in an optimized design that behaves well under dynamically applied loads. The optimization method is directly aimed at improving the limit-load and post-limit slope response of a statically loaded structure but has the consequence of improving the performance of the structure under dynamic loads.
- Maximizing the buckling modes that have a shape similar to the displaced configuration of the structure will improve the stability performance of the design. Since a large amount of mode shifting takes place during the first few iterations, it is not possible to know which modes will be similar to the displaced configuration from the buckling mode shapes of the initial design. If there is a specific mode that one needs to maximize, it is recommended that a subspace of size several modes more than the desired mode be chosen.
- In general, the more eigenpairs used in the objective function, the better was the performance of the optimized design.
- If a combination of the loading conditions was used to formulate the eigenvalue problem, the final modes came out distinct. However, if one loading condition was used to formulate the buckling eigenvalue problem, then the optimum had multiple eigenvalues.
- The optimized space frames were interesting in the sense that they usually have passive girder depth. The tendency is probably due to the fact that deep girders do not add much to the lateral stiffness of the structure. Physically, the structure is telling us that the optimum configuration is like having columns tied together with simple beams.
- The study on the minimum permissible design variables exposes the fact that the minimum dimension is important on the post-limit degradation of the structures. The observation reveals the fact that the post-limit robustness might be weakened with a poor choice of minimum design variables.
- Slender buildings are particularly well suited to the proposed optimization procedure. Since their behavior is more greatly influenced by geometric effects ( $P-\Delta$  effect). Thus, stability, which is the basis of the optimization methodology, becomes more important.



### 8.3. Recommendations for Future Research

There are two major directions that can be pursued for further research: (1) investigating ways to improve the optimization algorithm, and (2) investigating the application of the optimization method to practical problems.

One of the components of the optimization procedure is the solution of the eigenvalue problem which takes a big portion of the computing time of the whole process. To expedite the optimization process we need to improve the eigenvalue problem solution technique. One possibility would be to make use of the new generation of supercomputers and their multiprocessing capabilities by modifying and implementing the solution of the eigenvalue problem and the other parts of the optimization procedure for such environment. Other possibility would be to develop a new procedure that can use, instead of the eigenvalues and eigenvectors, some other means which would be computationally less expensive such as a modified version of Ritz vectors.

To preserve the numerical stability of the optimization algorithm during and after reaching the optimal design, there is a need for a general procedure that can accurately and efficiently calculate the derivative of the eigenvectors in the case of the repeated eigenvalue. In literature there have been some work in this area but there is a need for refinement and generalization of the existing methods to handle cases that one might encounter during optimization in an efficient and systematic manner.

Other fruitful areas for further investigation will be to develop an optimization procedure that considers material and geometrical nonlinearities in the optimization phase. The present form of the optimization procedure considers only linear elastic behavior of the structures with aim at improving the nonlinear behavior of the design. The present optimization procedure is not always robust in improving the post-limit strength degradation of the structures. Therefore, an optimization algorithm that can incorporate geometry nonlinearities and inelasticity in the optimization phase might enhance the robustness of the method in improving the post-limit behavior.

The second direction of the future investigation could be focused on the application of the optimization to the practical problems.

So far we have developed a working optimization-based design procedure that can produce designs with enhanced overall structural stability and strength. This design procedure can be used effectively as a strong research tool to perform computational experimentation and to conduct parameter studies on various aspects of design for different types of structures from moment-resisting

frames to eccentrically braced frames, from regular to irregular, from low-rise to high-rise, from planar to space frames to possibly come up with ways that some the existing design concepts can be massaged and perhaps lead to simpler and better design criteria to improve stability, strength, and ductility characteristics of the design.

The following would be some of the possible investigations that can be pursued:

- Using different earthquake design codes, find the equivalent static lateral load distributions and apply them to the structure and optimize. Perform this task for various structures with different sizes, shapes, and types. Investigate the effect of the load distribution on the performance of the optimized designs and possibly come up with recommendations on how the load distribution must be in order to achieve a design with better strength, stability, and ductility characteristics.
- ATC-3-06 gives a guideline on when to ignore and how to incorporate the effect of large deformation or the  $P-\Delta$  on story shear and moments referred to as the stability coefficient (equation 4-10 of ATC-3-06). This criterion is very important from stability point of view and needs more investigation. By using the optimization procedure we can perform parameter studies on different structures to determine the accuracy of the guideline and possibly improve it.
- Using the multiple loading capability of the developed optimization method the effect of multicomponent earthquake loads on the structures can be investigated to understand and make recommendations on how to design structures for multicomponent earthquakes. One of the areas that needs more investigation is the effect of vertical component of the earthquakes on the buildings. By using the multiple loading capability of the developed optimization method we can investigate the effect of vertical earthquake in conjunction with the other earthquake components on the structures by optimizing and examining different structures.



# APPENDIX A

## 3-D DISPLACEMENT CONSTRAINT OPTIMIZATION PROBLEM

### A.1. Introduction

The aim of this appendix is to develop a structural optimization algorithm based on optimality criteria to achieve a minimum weight structure that satisfies the displacement constraint. This formulation is an extension of the work done by Khot *et al.* (1979) where multiple design variables are considered for cross sectional properties. Since the optimization problem is a nonlinear problem, an iterative scheme is needed to obtain an optimal design. The optimization algorithm consists of two main steps. The first step is to analyze the structure to determine its response to the applied loads. The second step is to reallocate the material in the members so that the weight of the structure is reduced. The second step is carried out by using a recurrence relation derived from appropriate optimality criteria methods. The recurrence relation contains unknown Lagrange multiplier that corresponds to the displacement constraint. To be able to use the recurrence relation the Lagrange multiplier must be determined. The numerical method to determine the Lagrange multiplier is developed based on the constraint equations.

### A.2. Formulation

The minimum weight displacement constraint optimization problem to be solved is

MINIMIZE

$$V = \sum_{m=1}^M A_m(x_m)L_m \quad (\text{A.1})$$

SUCH THAT

$$D_j - \bar{D}_j \leq 0 \quad (\text{A.2})$$

$$\underline{x}_{mn} < x_{mn} < \bar{x}_{mn} \quad (\text{A.3})$$

where  $M$  = number of groups of elements with identical cross sectional properties;  $n = 1, \dots, N_v$  where  $N_v$  = the number of the independent design variables,  $J$  = number of displacement constraints;  $D_j$  = nodal displacement for  $j$ th constraint;  $\bar{D}_j$  = assigned  $j$ th nodal displacement constraint;  $A_m$  = area of elements in group  $m$  (elements in each group have identical cross sectional properties);  $L_m$  = length of the  $m$ th element;  $x_{mn}$  =  $n$ th design variable for  $m$ th group;  $\bar{x}_{mn}$  = maximum permissi-



ble height of the  $n$ th design variable for  $m$ th group;  $\underline{x}_{mn}$  = minimum permissible height of the  $n$ th design variable for  $m$ th group.

Similar to Chapter 4 this formulation is given in general form that can be specialized for either rectangular or I-beam cross sections.

Using Eq. (A.1) and Eq. (A.2) the Lagrangian functional can be cast as:

$$L(x, \xi_j) = \sum_{m=1}^M A_m(x_m) L_m - \sum_{j=1}^J \xi_j (D_j - \bar{D}_j) \quad (A.4)$$

where  $\xi_j$  is the Lagrange multiplier corresponding to the  $j$ th constraint. It should be pointed out here that the constraints on the size of the elements given in Eq. (A.3) are not included in deriving Eq. (A.4). The size constraints are handled efficiently by treating them as active/passive design variables.

Differentiating Eq. (A.4) with respect to design variable  $x_{mn}$  and setting the corresponding equations to zero will result in:

$$\frac{\partial L}{\partial x_{mn}} = \frac{\partial A_m}{\partial x_{mn}} L_m - \sum_{j=1}^J \xi_j \frac{\partial D_j}{\partial x_{mn}} = 0 \quad (A.5)$$

To determine the sensitivity of  $D_j$  with respect to the design variable the pseudo-load technique is used where:

$$D_j = \sum_{m=1}^M U_m^t K_m U_m^j \quad (A.6)$$

where  $K_m$  is the stiffness matrix of  $m$ th element, superscript "t" indicates transpose,  $U_m$  are the nodal displacement of  $m$ th element under of the action of the applied design loads, and  $U_m^j$  are the displacements of the same nodes due to the action of a unit load applied at node  $j$  in the direction of  $U_j$ . Taking the derivative of the Eq. (A.6) gives:

$$\frac{\partial D_j}{\partial x_{mn}} = U_m^t \frac{\partial K_m}{\partial x_{mn}} U_m^j \quad (A.7)$$

Substituting Eq. (A.7) in Eq. (A.5) and simplifying will result in the *optimality criteria*

$$\frac{U_m^t \frac{\partial K_m}{\partial x_{mn}} \sum_{j=1}^J U_m^j \xi_j}{\frac{\partial A_m}{\partial x_{mn}} L_m} = 1 \quad (A.8)$$

To make the formulation easier to understand, simplify Eq. (A.8) as

$$\sum_{j=1}^J B_{mnj} \xi_j = 1 \quad (\text{A.9})$$

where  $B_{mnj}$  is strain energy density defined as

$$B_{mnj} = \frac{U_m^t \frac{\partial K_m}{\partial x_{mn}} U_m^j}{\frac{\partial A_m}{\partial x_{mn}} L_m} \quad (\text{A.10})$$

In Chapter 4, the sensitivity of the stiffness matrix with respect to the design variables was derived in general form is used here also.

### A.3. Recurrence Relations

The optimality criteria are used to modify the design variables in each iteration in terms of recurrence relations similar to that used in Chapter 4 as:

$$x_{mn}^{\kappa+1} = x_{mn}^{\kappa} \left[ 1 + \frac{1}{r} \left( \sum_{j=1}^J B_{mnj} \xi_j - 1 \right) \right] \quad (\text{A.11})$$

where  $\kappa$  is the iteration number and  $r$  is the step size parameter. The method of choosing the step length to help with convergence was explained in detail in section 2.5.1.

### A.4. Equations to Determine Lagrange Multipliers

In order to be able to use the recurrence Eqn. (A.9), the Lagrange multipliers  $\xi_j$  have to be determined. The Lagrange multipliers are determined by using the condition that after each iteration the design moves on the constraint surface so that the constraint is satisfied. A set of equations to determine the Lagrange multiplier can be obtained by linearizing the constraint equation about current iterate.

The displacement constraint can be expanded as:

$$C(\mathbf{x}) = \sum_j^J (D_j - \bar{D}_j) = 0 \quad (\text{A.12})$$

Linearizing about the configuration  $x^e$  one obtains:

$$L[C]_{x=x^e} = C(x^e) + \sum_{j=1}^J \sum_{m=1}^M \sum_{n=1}^{N_v} \frac{\partial C}{\partial x_{mn}} (x_{mn} - x_{mn}^e) \quad (A.13)$$

where the partial derivative of constraint with respect to the design variable  $x_{mn}$  can be evaluated by taking derivative of Eqn. (A.12):

$$\frac{\partial C}{\partial x_{mn}} = \frac{\partial D_j}{\partial x_{mn}} = U_m \frac{\partial K_m}{\partial x_{mn}} U_m^j \quad (A.14)$$

The Lagrange multiplier can be obtained by satisfying the linearized constraint equation at the new iterate  $x^{e+1}$ . Substituting Eqn. (A.14) and Eqn. (A.12) into Eqn. (4.35) and making use of Eqn. (A.10) one gets:

$$\begin{aligned} \sum_{j=1}^J \sum_{k=1}^J \sum_{m=1}^M \sum_{n=1}^{N_v} \xi_k B_{mnj} B_{mnk} \frac{\partial A_m}{\partial x_{mn}} x_{mn} L_m = \sum_{j=1}^J \sum_{m=1}^M \sum_{n=1}^{N_v} B_{mnj} \frac{\partial A_m}{\partial x_{mn}} L_m x_{mn} \\ - r \sum_{j=1}^J \left( \sum_{m=1}^M U_m^t K_m U_m^j - \bar{D}_j \right) \end{aligned} \quad (A.15)$$

where the Lagrange multipliers have to be positive, otherwise the corresponding constraints are set as passive.

#### A.5. Scaling Procedures

After each iteration to satisfy the constraint relationship, it is necessary to scale the design variables to bring the displacements that violate the constraint to the level of the assigned displacements ( $\bar{D}$ ).

The following is a scaling procedure for rectangular members. The same procedure can be developed for I-beam cross sections. The scaling factor  $\xi$ , such that  $x_{ij} \leftarrow x_{ij} \xi$ , is determined by the equation:

$$\xi = \sqrt{\frac{\bar{D}}{D}} \quad (A.16)$$

where  $D$  is the displacement of the node that the displacement constraint is violated the most and  $\bar{D}$  is the assigned displacement at that node.



## APPENDIX B

### SOME PRACTICAL IMPLEMENTATION ISSUES NECESSARY TO SOLVE THE BUCKLING EIGENVALUE PROBLEM

#### B.1 Introduction

Subspace iteration is a standard tool for solving the eigenvalue problems which occur in vibration and buckling analysis of structures. The buckling eigenvalue problem is given as

$$K\Psi = G\Psi\Lambda \quad (B.1)$$

Where  $K$  is positive definite elastic stiffness matrix, and  $G$  is the (possibly indefinite) geometric stiffness matrix.  $\Lambda$  is a diagonal matrix containing the buckling eigenvalues, and  $\Psi$  is a matrix whose columns are the eigenvectors.

The goal of this appendix is to present an overall view of the subspace iteration algorithm and to address some practical implementation issues necessary to solve the buckling eigenvalue problem. For detailed discussion on the subject of subspace iteration the reader is referred to Bathe (1982).

The basic objective in subspace iteration method is to solve for the lowest  $p$  eigenvalues and the corresponding eigenvectors satisfying Eqn. (B.1).

The first step in subspace iteration is the selection of the initial subspace vectors. Initial subspace vectors can be generated from an identity matrix, the diagonals of the  $G$  matrix, or from a Krylov basis. The subspace iteration method is used to solve for the eigenpairs to be incorporated into the optimization algorithm where a combination of the eigenvalues is maximized. As a structure is being optimized, from one iteration to another the buckling eigenvectors of the previous iteration can be used as the initial subspace vectors of the current iteration.

As subspace iteration progresses the Ritz vectors tend to lose orthogonality. The loss of orthogonality among the Ritz vectors can result in floating point overflows or delay in convergence. Performing a modified Gram-Schmidt orthogonalization on the eigenvectors keeps the subspace vectors linearly independent and orthogonal. The modified Gram-Schmidt orthogonalization algorithm employed can be found in Dahlquist *et al.* (1974).

The vector  $\Psi$  can be written in terms of initial subspace starting vectors as

$$\Psi = ZP \quad (B.2)$$

where  $Z$  is the vector storing the  $p$  starting vectors, and  $P$  is a vector. Substituting Eqn. (B.2) into Eq. (B.1) and multiplying both sides by transpose of  $Z$  results in

$$Z^T K Z P = Z^T G Z P A \quad (B.3)$$

Eqn. (B.3) is equivalent to an eigenvalue problem of reduced size obtained by projecting  $K$  as  $\tilde{K} = Z^T K Z$  and  $G$  as  $\tilde{G} = Z^T G Z$ :

$$\tilde{K} P = \tilde{G} P A \quad (B.4)$$

The eigenvalue problem (Eqn. (B.4)) must now be transformed to a standard form. Since  $G$  matrix is usually indefinite the Choleski factorization is performed on the reduced stiffness matrix as  $\tilde{K} = C C^T$ .

Substitute  $P = C^{-1} U$  and  $\tilde{K} = C C^T$  in Eqn. (B.4) and simplify

$$U = C^{-1} G C^{-1} U A \quad (B.5)$$

Next simplify Eqn. (B.5) by defining  $\tilde{\tilde{G}}$  as

$$\tilde{\tilde{G}} = C^{-1} \tilde{G} C^{-T} \quad (B.6)$$

Substitute Eqn. (B.6) in Eqn. (B.5) and reorder terms

$$U \Lambda^{-1} = \tilde{\tilde{G}} U \quad (B.7)$$

Equation (B.7) is a standard eigenvalue problem which can be solved, for example, by the QL method to find eigenvectors  $U$  and eigenvalues  $\Lambda^{-1}$ . The eigenvectors  $\Psi$  can be found from  $\Psi = ZP = ZC^{-1}U$ . Eigenvalues are simply found by inverting the matrix  $\Lambda^{-1}$ .

Subspace iteration algorithm is converged when the change in all the eigenvalues from one iteration to the previous iteration is less than the specified tolerance.

The recommended size of the subspace to improve the convergence of subspace iteration algorithm is  $q = \min\{2p, p+8\}$ . This recommendation is based on vibration eigenvalue problems. Through experience in solving the buckling eigenvalue problem, it became apparent that a larger subspace (such as  $q = 3p$ ) is needed to promote convergence

After convergence the sign of the eigenvectors are checked. If the work as calculated by multiplying the applied forces on the structure by the corresponding displaced mode shapes is negative the sign of the eigenvector is changed. This is important from the optimization point view, because if the sign of the buckling mode shape is not checked after each iteration it will cause difficulties in convergence of the optimization problem due to flip-flop of the sign.

Steps for a subspace iteration algorithm as defined above is summarized in Table B.1 below.

Table B.1. Subspace Iteration

- |  |
|--|
| <p>Step 1. Compute initial subspace vectors <math>Z</math></p> <p>Step 2. Perform Modified Gram-Schmidt orthogonization<br/>on vector <math>Z</math> (if necessary)</p> <p>Step 3. Project <math>G</math> to form <math>\tilde{G} \leftarrow Z^T G Z</math></p> <p>Step 4. Project <math>K</math> to form <math>\tilde{K} \leftarrow Z^T K Z</math></p> <p>Step 5. Solve eigenvalue problem <math>\tilde{K} P = \tilde{G} P \Lambda</math></p> <ol style="list-style-type: none"> <li>Factor <math>\tilde{K} = C C^T</math> (Choleski factorization)</li> <li>Project <math>\tilde{G} \leftarrow C^{-1} \tilde{G} C^{-T}</math></li> <li>Solve the standard eigen-problem <math>\Lambda^{-1} U = \tilde{G} U</math><br/>by QL algorithm.</li> <li>Compute <math>U = C^T P</math> and <math>\Lambda \leftarrow \Lambda^{-1}</math> (Invert)</li> </ol> <p>Step 6. Compute approximate eigenvectors <math>\Psi = Z P</math></p> <p>Step 7. Check convergence, if not converged go to Step 2.</p> |
|--|

## B.2 References

- Bathe, K.J., *Finite Element Procedures in Engineering Analysis*, Prentice-Hall, Inc., Englewood Cliffs, 1982.
- Dahlquist, A.B., A. Bjorck, and N. Anderson, *Numerical Methods*, Prentice-Hall, Inc., Englewood Cliffs, 1974.



## APPENDIX C

### APPROXIMATE ANALYSIS OF THE POST-LIMIT RESPONSE OF FRAMES

#### C.1. Introduction

Elastoplastic structures subjected to gravity loads generally exhibit a limit point with degrading post-limit behavior when subjected to overloads. Therefore, geometric effects play a fundamental role in determining the maximum capacity of a structure and its rate of failure. Recent advances in computational mechanics have made it possible to carry out fully nonlinear analyses of structures, and effective algorithms exist for tracing limit points and post-limit behavior. However, these methods give little qualitative insight into the behavior of complex structures.

The approximate method to be developed in this chapter was inspired and generalizes Horne's approach (Horne 1963) in estimating the nonlinear response of frames. Also, it is to be shown that an estimate similar to Horne can be obtained without solving an eigenvalue problem. The approximate method is also an extension of Horne's method to the case of non-proportional loading for structures in wind and earthquake environments. The formulation presented here is distinguished by clear statements of both the approximations involved and the sense in which the method approximates the exact solution. Qualitative insight into the behavior of framed structures is gained both through the success of the approximation as well as through a spectral analysis of the results.

This chapter starts with the general ideas and features of the nonlinear equations governing the response of framed structures. The empirical relationships for estimating nonlinear response of framed structures from geometrically linear response is then derived from a simple decomposition of the nonlinear equations in conjunction with a hypothesis about the way the internal forces are distributed in framed structures. Then the strength and the limitation of the method is tested as it is applied to several example problems. Finally, from the behavioral observations made on the nonlinear response of the structures and the from the empirical relationships derived a conclusion is arrived at in which it will show how one needs to combine and maximize the buckling eigenvalues of a structure to achieve better designs.

## C.2. Nonlinear Analysis of Frames

The theory and the background material used for the present development can be found in references by Simo (1982) where he developed a consistent second order approximation to the fully nonlinear equations governing the response of plane beams; by Simo, Hjelmstad, and Taylor (1984) where they extended the formulation of Simo (1982) for the nonlinear response of beam theory to account for inelasticity; and by Hjelmstad and Popov (1983) where they treated the second order theory explicitly and developed the constitutive equations for I-beam type members. Some aspects of the theory as is used explicitly for the development of this chapter is explained in the following sections.

### C.2.1. Equilibrium

The equations governing the equilibrium of a beam can be expressed in their weak or variational form as a statement of the principle of virtual displacements. Accordingly one can define the following functional for all the admissible variations  $\eta$ , of the displacement field as:

$$G(u, \eta) = \int_{\Gamma} B^T \Xi(u) R(u) ds - \int_{\Gamma} \eta^T q ds = 0 \quad (C.1)$$

where  $u = \{u, v, \psi\}^T$  denotes the vector of generalized displacements,  $B(u) = \{1 + u', v', \psi', \psi\}^T$  is the strain displacement operator that acts on real displacements  $u$  or their variation  $\eta$ , and  $R = \{N, V, M\}$  is the vector of the internal stress resultants where  $N$  is the axial force,  $V$  is the shear force, and  $M$  is the bending moment.  $q = \{p, q, m\}^T$  is the vector of the applied forces with  $p$  being the applied axial force,  $q$  being the applied shear force, and  $m$  being the applied moment.  $\Xi(u)$  is a matrix of strain gradient operator which reflects the effect of geometry on the equilibrium of the internal resisting forces  $R$  and is approximated to second order as:

$$\Xi(u) = \begin{bmatrix} 1 & (v' - \kappa\beta) & 0 & \kappa\beta \\ -\psi & 1 & 0 & -(1 + u') \\ 0 & 0 & 1 & 0 \end{bmatrix} \quad (C.2)$$



where  $\kappa$  is the shear coefficient. Note that prime means differentiation with respect to the argument, and superscript "t" means the transpose of the argument. The integral in Eqn. (C.1) is taken over the entire volume,  $\Gamma$ , of the structure and is generally accomplished by summing the integrals over each element. Equilibrium is satisfied for any configuration in which  $G(u, \eta) = 0$  for all  $\eta$ . Errors in equilibrium are measured in a weak sense by non-zero values of  $G(u, \eta)$ .

### C.2.2. Constitutive Equations

Constitutive equations for stress resultants are discussed in Simo, Hjelmstad, and Taylor (1984), where the strain resultants,  $\epsilon$ , is decomposed into an elastic part,  $\epsilon^e$ , and an inelastic part,  $\epsilon^p$  (Hodge, (1959)). The elastic strains are then related to the stress resultants through the elastic moduli  $R = D\epsilon^e$ , where  $D = \text{diag}[EA, \kappa GA, EI]$ . The inelastic part is assumed to evolve according to rate equations of the form:

$$\dot{\epsilon}^p = \xi \frac{\partial \mathcal{Y}(R)}{\partial R} \quad (C.3)$$

where  $\mathcal{Y}(R)$  is the yield potential of the member and  $\xi$  is a scalar multiplier which can be determined from consistency condition. Constitutive relationships having the form described are capable of representing generalized yielding due to the interaction of all stress resultants. They can be specialized for particular cross sections.

### C.2.3. Nonlinear Analysis of Structures

The equations of equilibrium can be discretized using the finite element method and can be solved using an incremental procedure with Newton-Raphson iteration at each step. Ramm (1980) has presented a general summary of algorithms for tracing the response of a structure, including passage through limit load points. A displacement control procedure was used to carry out the exact analysis of the example problems.

### C.2.4. Approximation of the Nonlinear Load Factor

The aim of the development in this chapter is to estimate the nonlinear response of a structure subjected to proportional and non-proportional loads from a geometrically linear response. In short,



it is attempted to approximate the load factor which gives an estimate of the loads equilibrated by the nonlinear system. The approximate formulation developed here is based on the observation that each configuration satisfying the linear equations is close to an associated configuration which satisfies the nonlinear equations. Hence, as the linear behavior is traced, a series of load factors can be determined which estimates the true external loads that the structure can take as given by the nonlinear theory.

### C.2.5. Decomposition of the Nonlinear Operator

The strain gradient operator which reflects the geometry on the equilibrium of the internal resisting forces can be split into a linear and a nonlinear operator:  $\Xi(u) = \Xi(0) + \hat{\Xi}(u)$ .

Therefore, the nonlinear form of the equilibrium equation, expressed by Eqn. (C.1), can be decomposed into linear part and a nonlinear part as:

$$G(u, \eta) = \int_{\Gamma} B^t(\eta) [\Xi_0 + \hat{\Xi}(u)] R(u) ds - Q(q, \eta) \quad (C.4)$$

where  $Q(q, \eta) = \int \eta^t q ds$  represents the virtual work associated with the external loading and for simplicity the notation  $\Xi(0) = \Xi_0$  and  $\hat{\Xi} = \Xi(u) - \Xi_0$  has been introduced.

A matrix of  $A_g$  can be defined in terms of forces  $R$  as:

$$A_g(R) = \begin{bmatrix} 0 & 0 & 0 & -V \\ 0 & (1-\kappa)N & 0 & \kappa N \\ 0 & 0 & 0 & 0 \\ -V & \kappa N & 0 & -\kappa N \end{bmatrix} \quad (C.5)$$

where  $N$  and  $V$  are the axial forces and shear force respectively, and  $\kappa$  is the shear coefficient. Now with these definitions the equilibrium equation can be rewritten as:

$$G(u, \eta) = \int_{\Gamma} B^t(\eta) \Xi_0 R(u) ds + \int_{\Gamma} B^t(\eta) A_g(R(u)) B(u) ds - \lambda Q_0 - Q_1 = 0 \quad (C.6)$$

where the external loading  $Q = \lambda Q_0 + Q_1$  has been divided into fixed part,  $Q_1 = Q(q_1, \eta)$ , (dead loading) and a part,  $Q_0 = Q(q_0, \eta)$ , which is driven by the proportionality factor  $\lambda$ . The expression given Eqn. (C.6) is a simple statement of the nonlinear equilibrium equations which is used for the following developments.

Eqn. (C.6) can be linearized about the initial configuration to yield the associated linear equation of equilibrium:

$$\int_r B^t(\eta) \Xi_0 R(\dot{u}) ds - \lambda_L Q_0 - Q_1 = 0 \quad (C.7)$$

where by solving the linear equilibrium equations a sequence of geometrically linear load factors,  $\lambda_L$ , and the corresponding linear displacement  $\dot{u}$  can be obtained.

Substitute  $\lambda_L$  and  $\dot{u}$  into the nonlinear operator, the expression for the residual takes the form:

$$G(\dot{u}, \eta) = \int_r B^t(\eta) \Xi_0 R(\dot{u}) ds + \int_r B^t(\eta) A_g(R(\dot{u})) B(u) ds - \lambda_L Q_0 - Q_1 \quad (C.8)$$

The best value of the parameters  $\lambda$  is the one that corresponds to the smallest error, i.e.  $G(u, \eta) = 0$ . By setting the Eqn. (C.8) equal zero and by assuming that  $\int_r B^t(\eta) \Xi_0 R(\dot{u}) ds = \lambda Q_0 + Q_1$ , one can obtain:

$$(\lambda - \lambda_L) Q_0 + \int_r B^t(\eta) A_g(R(\dot{u})) B(u) ds = 0 \quad (C.9)$$

Eqn. (C.9) simply states that the difference between the load carrying capacity represented by the linear versus nonlinear operator is given by the term associated with the nonlinear part of the deformation gradient. This expression is approximate because the linear and nonlinear configurations are generally not identical.

#### C.2.6. Derivation of the Approximate Load Factor

For most structures with the exception of triangulated structures, it can be observed that the distribution of axial forces in a structure does not change appreciably as inelasticity progresses. On

other hand, the moment field can change considerably as the structure strains inelastically. The key to the success of the approximation is that the bending moment does not appear in the second term of the Eqn. (C.9) and thus, the redistribution of moment does not affect the approximation. The internal shear force will change in accordance with their equilibrium relation to the changing moments. However, the importance of shear is small for most structures. Even for structures such as eccentrically braced frames, in which shear is important, only few of the members are affected by high shear and hence the aggregate effect of shear on the structure as whole is small.

Assume that the internal axial and shear forces as designated by  $\hat{R} = \{N, V\}$  can be approximately represented in terms of their initial linear values and a proportionality factor as:

$$\hat{R}(u) = \lambda \hat{R}_0 + \hat{R}_1 \quad (C.10)$$

Where  $\hat{R}_0$  is a vector of internal forces in equilibrium with  $[q_0, \eta]$ ; and  $\hat{R}_1$  which is vector of internal forces in equilibrium with  $[q_1, \eta]$ . Since  $A_g$  is linear in terms of stress resultants  $N$  and  $V$ , it too can be decomposed into a part contributing to the dead loading and a part contributing to the proportional loading as:

$$A_g = \lambda A_g(\hat{R}_0) + A_g(\hat{R}_1) = \lambda A_g^0 + A_g^1 \quad (C.11)$$

Substituting Eqn. (C.11) into Eqn. (C.9) and solving for  $\lambda$ , the following estimate of the actual nonlinear load factor is obtained:

$$\lambda = \frac{\lambda_L Q_0 - \int_r B^t(\eta) A_g^1 B(\hat{u}) ds}{Q_0 - \int_r B^t(\eta) A_g^0 B(\hat{u}) ds} \quad (C.12)$$

The variational form found in Eqn. (C.12) is suitable for computation and can be discretized with a finite element approximation. Therefore, the discrete representation of Eqn. (C.12) can be obtained as:



$$\lambda = \frac{\lambda_L Q_0 - \mathbf{H}' \mathbf{G}_1 \dot{\mathbf{U}}}{Q_0 + \mathbf{H}' \mathbf{G}_0 \dot{\mathbf{U}}} \quad (\text{C.13})$$

where  $\mathbf{U}$  and  $\mathbf{H}$  are the discrete nodal displacements and their variations, respectively; and  $\mathbf{G}_0$  and  $\mathbf{G}_1$  are the geometric stiffness matrices and are obtained in the standard way from element shape functions and direct assembly procedures. Note that  $\mathbf{G}_0$  is the linearized geometric stiffness resulting from the action of only the forces  $Q_0$ , whereas  $\mathbf{G}_1$  is the linearized geometric stiffness resulting from the action of only the forces  $Q_1$ .

It will be convenient to characterize the variation in the displacement field as being proportional to some displaced configuration of the structure ( $\mathbf{H} \propto \mathbf{U}$ ). An advantage of making the variation proportional to a displacement vector is that one can define a natural way of measuring the displaced configuration of the structure with a scalar quantity,  $\|\mathbf{U}\|^2 = \mathbf{U}' \mathbf{G} \mathbf{U}$ . In general  $\mathbf{G}$  is not guaranteed to be positive-definite, and thus  $\|\mathbf{U}\|$  does not define a true norm. However, it does have the advantage of treating the displacements in a dimensionally consistent manner, and it has been used as measure of the deformed state of the structure.

Eqn. (C.13) with  $\mathbf{H}=\mathbf{U}$  provide a formula for computing the nonlinear load factor from the sequence of linear configurations generated from Eqn. (C.7). The second term in the numerator of the Eqn. (C.13),  $\mathbf{H}' \mathbf{G}_1 \dot{\mathbf{U}}$ , vanishes in the absence of dead loading.

### C.2.7. Spectral Analysis

Eqn. (C.13) can be studied through a spectral analysis of the system. One consequence of performing a spectral analysis is the ready identification of the special case studied by Horne (1963). In addition, the spectral approach provides a convenient framework for characterizing the behavior of complex systems. By referring to response of a structure to an associated eigenbasis, it is possible to follow the progress of a few generalized components of the system, and from this information evaluate some of the approximations that has been made.

The eigenbasis is determined from considering the buckling eigenvalue problem:

$$\mathbf{K}\phi = \mu \mathbf{G}\phi \quad (\text{C.14})$$

where  $K$  is the initial elastic stiffness matrix and  $G$  is the geometric stiffness matrix of the system. The method of finding eigenvalues and eigenvectors are discussed in Appendix B. A discrete system with  $n$  degrees-of-freedom will yield  $n$  eigenpairs by solving the Eqn. (C.14). In accordance with standard practice, the eigenpairs are ordered such that  $|\mu_1| < |\mu_2| < \dots$ , and the eigenvectors are normalized such that  $\phi_i^T G \phi_j = \delta_{ij}$  where  $\delta_{ij}$  is the Kronecker delta. Note that since tensile axial forces are positive, the eigenvalues of Eqn. (C.14) will be negative when forces in the structure are generally compressive.

For proportionally loaded structures there is only one initial geometric stiffness and therefore, there is only one associated eigenvalue problem. A non-proportionally loaded structure has an associated eigenvalue problem corresponding to the proportional loads and one corresponding to the dead loads. A set of non-proportional loads are considered which gives rise to a family of associated eigenvalue problems with  $G = \gamma G_0 + G_1$ , in which  $\gamma$  is the parameter of the family. As  $\gamma \rightarrow 0$  the eigenvalue problem is governed by dead loads only and as  $\gamma \rightarrow \infty$  the eigenvalue problem is governed by proportional loads only. Through example problems, it will be shown that the specific choice of  $\gamma$  is crucial to the success of some of the approximations.

The displacement vector  $U$  can be decomposed into components along the eigenbasis induced by the eigenvalue problem. The displacements can be expressed in terms of spectral ordinates as:

$$U = \sum_{i=1}^n a_i \phi_i \quad (C.15)$$

where  $a_i$  is identified as the modal participation factors, measuring the components of the displacement relative to the basis  $\{\phi_i\}$ . The participation factors can be computed from the displacement  $U$  using the formula:

$$a_i = \frac{U_i^T G \phi_i}{\phi_i^T G \phi_i} \quad (C.16)$$

If the basis  $\{\phi_i\}$  is normalized with respect to the matrix  $G$ , then the denominator of Eqn. (C.16) is unity.

Substituting Eqn. (C.15) into the expression for the nonlinear load factor (C.13), noting that  $Q_0 = U^T R_0 = U^T K U_0$ , one obtains the following expression:



$$\lambda = \frac{\lambda_1 \sum a_{0i} a_{ij} \mu_i - \sum \sum a_i a_j \gamma_{ij}^1}{\sum a_{0i} a_{ij} \mu_i + \sum \sum a_i a_j \gamma_{ij}^0} \quad (C.17)$$

where the  $a_{0i}$  are the initial linear participation factors, i.e.  $U_0 = \sum a_{0i} \phi_i$ , and the  $\mu_i$  are the eigenvalues of the Eqn. (C.14). Earlier it was noted that the eigenvalue problem has been normalized such that  $\phi_i^T G \phi_j = \delta_{ij}$ . However,  $G$  need not to be either  $G_0$  or  $G_1$ , and hence the parameters  $\gamma_{ij}^0 = \phi_i^T G_0 \phi_j$  and  $\gamma_{ij}^1 = \phi_i^T G_1 \phi_j$  have been introduced in Eqn. (C.17).

If the first buckling mode behavior is assumed to dominate the response, i.e.,  $a_1 \neq 0$ ,  $a_i = 0$ ,  $i = 2, \dots, n$ , then under these restrictions the Eqn. (C.17) simplifies as:

$$\lambda(a) = \frac{\lambda_1(a) a_0 \mu - a \gamma_1}{a_0 \mu + a \gamma_0} \quad (C.18)$$

where the subscripts on  $a$ ,  $a_0$ , and  $\mu$  are understood to be one;  $\gamma_0 = \gamma_{11}^0$  and  $\gamma_1 = \gamma_{11}^1$ . Note also that an approximation having the form of Eqn. (C.18) can be achieved using any of the eigenvectors in the expression for the nonlinear load factor. This observation is important because the fundamental mode will not always dominate the limit response of the frame.

Eqn. (C.18) degenerates to the expression given by Horne (1963) if only proportional loads are considered ( $\gamma_1 = 0$ ,  $\gamma_0 = 1$ ). Horne has suggested that Eqn. (C.18) provides lower bound on the nonlinear load factor for moment-resisting frames. However, as demonstrated in one of the examples, it is found that lower bound character can be spoiled if the selected mode does not actually dominate the response.

If the displacement of the structure is approximated as proportional to a constant vector,  $U = a v$  (not an eigenvector), the preceding derivations apply, except that  $\mu$  is simply the Rayleigh quotient and not an eigenvalue. The reason for choosing the vector  $v$  is that the initial displaced configurations of the structure under load ( $U_0$ ) will be examined in the examples later. One might expect that when the chosen assumed shape is representative of the shape at the limit load, then a good estimate of the limit load can be achieved. Such approximation has the computational advantage of avoiding the solution of an eigenvalue problem.



### C.2.8. Rankine-Type Formula for Limit Load

The limit load plays a significant role in the limit design of structures, and hence its estimation is of fundamental importance. Plastic design is predicted based on the knowledge of the "limit" load without any knowledge of the response history. In this section it will be shown that the limit load can be estimated from Eqn. (2.18). The success of the estimate depends both on an appropriate choice of the displaced shape and on the invariance of that shape during the course of deformation. The validity of the estimate will be investigated by examining the spectral analyses of the example structures presented later.

The limit load occurs when the slope of the load-defamation curve become zero,  $\lambda' = 0$ . Differentiating Eqn. (2.18) with respect to parameter  $a$  and setting the result equal to zero gives:

$$(a_0\mu + a\gamma_0)\lambda'_L(a) - \gamma_0\lambda_L(a) - \gamma_1 = 0 \quad (C.19)$$

where by solving the expression of Eqn. (C.19) limit displacement ( $\bar{a}$ ) can be evaluated. Substituting the Eqn. (C.19) into Eqn. (C.18) and simplifying the expression, one can arrive at the limit load expression in terms of the slope of the linear response curve evaluated at the limit displacement:

$$\lambda_{cr} = \frac{1}{\gamma_0} [a_0\mu\lambda'_L(\bar{a}) - \gamma_1] \quad (C.20)$$

For proportional loading cases  $\gamma_1$  is zero and  $\gamma_0$  is one which simplifies the Eqn. (C.20) to

$$\lambda_{cr} = a_0\mu\lambda'_L(\bar{a}) \quad (C.21)$$

which is the formula given by Horne (1963). Thus Eqn. (C.20) generalizes Horne's formula for the case of non-proportional loading.

For some structures, the transition from elastic to plastic behavior covers a reasonably short range of displacement values, as shown in Fig C.1. As the structure passes through this region the slope  $\lambda'_L$  changes dramatically from the large elastic slope to a very small post-yield slope. The slope of the linear response at the limit displacement is certainly contained within these bounds. For these structures, failure will occur at or near the "knee" of the linear curve, which has an approximately identifiable displacement  $a_p$  and load level  $\lambda_p$  (the linear plastic capacity of the structure).

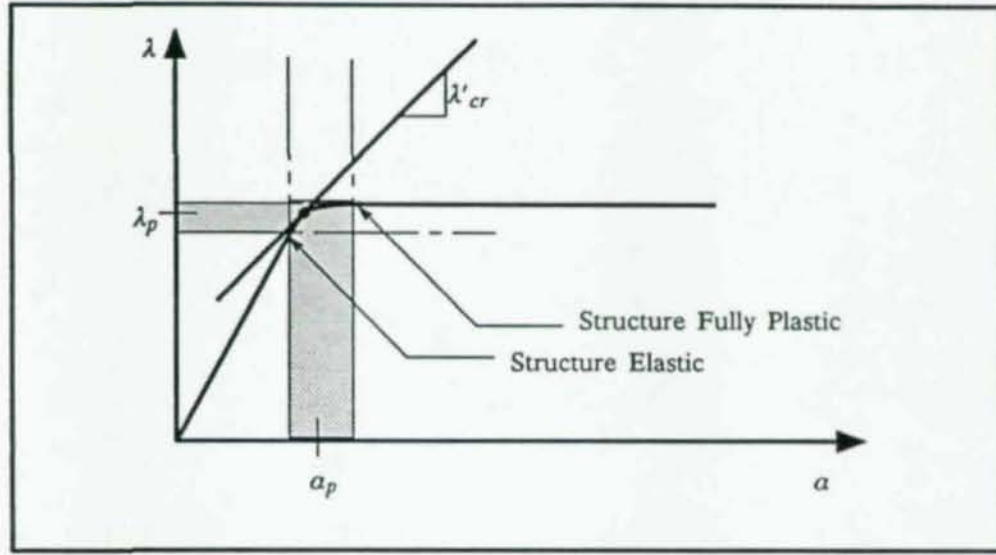


Fig C.1 Idealized Structural Behavior for Rankine-Type Estimate

The known values of force and displacements can be substituted into Eqn. (C.19) to solve for the indeterminate slope  $\lambda'_L$ . Solving for  $\lambda'_L$  from Eqn. (C.19) gives

$$\lambda'_L \approx \frac{\gamma_1 + \gamma_0 \lambda_p}{a_0 \mu + \gamma_0 a_p} \quad (C.22)$$

By noting that  $a_p = a_0 \lambda_p$ , and substituting Eqn. (C.22) into the Eqn. (C.20), one can obtain an estimate of the limit load as

$$\lambda_{cr} \approx \lambda_p \frac{\mu - \gamma_1}{\mu + \gamma_0 \lambda_p} \quad (C.23)$$

If the loading condition is proportional, the Eqn. (C.23) reduces to the so called Merchant-Rankine load of the structure:

$$\frac{1}{\lambda_R} = \frac{1}{\mu} + \frac{1}{\lambda_p} \quad (C.24)$$

where  $\mu$  is the fundamental linear elastic buckling eigenvalue of the structure and  $\lambda_R$  is the Merchant-Rankine estimate of the limit-load.



### C.3. Application to Framed Structures

The remainder of this chapter is devoted to application of the methods derived previously to a set of examples. The examples will serve to demonstrate the effectiveness of the approximate methods of tracing the limit behavior of framed structures and to indicate the limitations of the approximate formulas. Furthermore, the examples will demonstrate that the approximate methods provide a useful framework for estimating the limit performance of framed structures in general. From all these example problems one can get insight into the performance of the method and into the behavior of framed structures.

Six structures covering a wide range of types including moment-resisting and eccentrically braced frames, low rise and high-rise buildings, proportionally and non-proportionally loaded structures are analyzed. For simplicity the designation of MRF is used for moment-resisting frames and EBF is used for eccentrically braced frames. The properties of the most of members used in example structures are tabulated in Table C.1.

For each example problem an exact nonlinear analysis is performed using the methodology and finite elements developed by Simo, Hjelmstad, and Taylor (1984). For each of these "exact" analyses, the solution has been decomposed along the eigenbasis  $\{\phi_i\}$ , where the basis vectors are generated from the eigenvalue problem defined by Eqn. (C.14) with  $G$  selected from the family of initial geometric stiffness matrices. The modal participation factors  $a_i$  are evaluated according to Eqn. (C.16).

Evolution of modal participation factors as the nonlinear progresses permits one to estimate the change in the character of the displaced configuration as the nonlinearities take place. One can also compare the different bases by observing how the same nonlinear response curve reflects on each basis. Viewing the results in this manner provides an indication as to why and how the approximate methods work well in some cases but not in the others. A modal decomposition provides a good qualitative representation of the progress of the solution.

For each frame, the nonlinear load versus displacement history is presented for several cases: (1) the actual computed nonlinear response designated as "Exact Nonlinear" in the figures; (2) the actual computed response without nonlinear geometric effect as designated by "Exact Linear"; (3) an approximation to the nonlinear response using Eqn. (C.13); and (4) an approximation of the nonlinear response using Eqn. (C.18).



The finite elements used in these analyses were all  $C^0$  quadratic elements. Each structural member was discretized using two of these elements. Inelasticity of the elements accrue due to the interaction of shear force, axial force, axial force, and bending moment. The computational model is a viscoplastic penalty approach to model perfect elastoplasticity. The yield function used in these computations was:

$$q(n, v, m) = |m| + n^2(1+v^2) + v^4 - 1 \quad (C.25)$$

where  $n = N/N_0$ ,  $v = V/V_0$ , and  $m = M/M_0$  are the axial force, shear force, bending moment normalized by their fully plastic values. Each stage of computation is iterated using a Newton-Raphson iteration scheme to satisfy the equilibrium within a specified tolerance of the Euclidean norm of the out-of-balance forces. The following is a discussion on the result of the analyses.

MRF-1 is the first frame studied which is a two-story, single bay, moment-resisting frame with tall stories. The beam members with W14X53 and columns are of type "column". The frame MRF-1 was proportionally loaded as shown in Fig. C.2 with two vertical loads of  $5\lambda$  applied to the top story and one lateral top story load of magnitude  $\lambda$ . Fig. C.2 presents the results of various analyses as were performed on MRF-1 along with the spectral evolution of the exact nonlinear solution.

The linear elastoplastic response of the structure shows a typical multilinear force-deformation behavior, with the changes in slope corresponding to the formation of plastic zones in the structure. Because of the heavy vertical loads and slender columns, the actual capacity of the structure is greatly reduced from the linear "collapse load". Both Eqn. (2.13) and Eqn. (2.18) gave excellent approximations of the nonlinear behavior of the frame. Note in particular the accuracy with which the post-limit behavior of the frame is traced by the approximate methods. From the figure of the spectral evolution of the participation factors, observe that the first buckling mode dominates the response throughout the analysis.

MRF-2 is a five story, single bay, moment resisting frame with W14X53 beams and W14X48 columns. The loading of the frame was similar to that of frame MRF-1 with the loading applied to the top level of the building. The response of MRF-2 is shown in Fig 2.3. Again, both approximate methods worked well. Eqn. (2.13) gave a more accurate estimate of the response near the limit load than does Eqn. (2.18). Since the columns are not as slender as the ones in MRF-1, the reduction in load carrying capacity due to geometric effects is not as dramatic as it was for MRF-1. However, the

slope of the post-limit response curve is steeper indicating poorer post-limit behavior. The initial response was dominated by the first mode and the second mode contributes more as the structure settles into its final collapse deformation mode.

MRF-3 is also a moment resisting frame and has the same topology as MRF-1. This frame is different from the previous frames in that the vertical loads are gravity loads instead of proportional loads. The lateral loads at the two-story levels were equal and increased monotonically in accordance with the proportionality factors. Such a loading would be representative of a building structure subjected to earthquake or wind loads.

The response of the structure under the applied loading is shown in Fig 2.4. The initial displacement is due to presence of the dead loading, while the proportionality factor is still zero. Two different approximations as applied to the Eqn. (2.13) were considered. Two different approximations differ only in the choice of the form of the variation in displacements  $H$ . In one case,  $H$  is taken to be proportional to the initial displaced configuration  $U$ . Both approximations gave good estimate of exact nonlinear results but demonstrated that the method depends on the choice of the vector representing the variation in displacements.

The results obtained from Eqn. (2.18) are shown in Fig. C.4(b and c). Three different methods of calculation were used: (P)  $\alpha$  and  $\{\mu, \phi\}$  were computed using only the proportional part of the geometric stiffness; (D)  $\alpha$  and  $\{\mu, \phi\}$  were computed using only the dead part of the geometric stiffness; (P+D)  $\alpha$  and  $\{\mu, \phi\}$  were computed using the geometric stiffness  $G = \lambda_{cr}G_0 + G_1$ , where  $\lambda_{cr}$  is the actual limit load of the structure. Case (P+D) worked well for this problem whereas cases (P) and (D) did not. The reason that the case (P) and (D) performed so poorly can be seen by examining the spectral evolution of the modal participation factors. Three different versions of this history are shown in Fig 2.4(d-f), corresponding to geometric stiffness matrices and associated eigenvectors of cases (P), (D), and (P+D). The first eigenvector for the case (P) contributes very little to the response. The first eigenvector for the case (D) is orthogonal to the displaced configuration of the structure. Eqn. (2.13) was also tried using mode five for the (P) case and mode six for the (D) case. The results for these cases were also poor. It is interesting to observe that, while mode one of the (P) and (D) cases did not contribute to the response, mode one of the (P+D) case dominated the response as it passed through the limit load. The obvious shortcoming of the method represented by case (P+D) is that the limit load is not known in advance. However, it is possible to estimate the limit



load from the Rankine approximation. The method that uses Eqn. (2.13) does not suffer from ambiguity that Eqn. (2.18) does and does not require an advance knowledge of the limit load.

One conclusion that can be made is that it is not the vector  $\mathbf{v}$  that is important to the approximation, but the matrix  $\mathbf{G}$  used in computing the norm of the displacements. To verify this conclusion, the initial displacement  $\mathbf{v}=\mathbf{U}_0$  was employed in Eqn. (2.18) with (P+D) geometric stiffness. The results for this case were found to be indistinguishable for the curve  $\mathbf{H}=\mathbf{U}_0$  shown in Fig. C.4(a).

MRF-4 is an eight-story, single bay moment resisting frame similar to the one analyzed by Korn and Galambos (1968). Similarly to MRF-3, this frame was subjected to both proportional and non-proportional loads. The member types used are tabulated in Table C.2. The topology and the loading used along with the response of the structure are shown in Fig. C.5. MRF-4 was subjected to the same analyses as was MRF-3.

Observe from Fig. C.5(a) that Eqn. (2.13) estimated the true nonlinear solution well. As was true for MRF-3, Eqn. (2.18) gave meaningful results only for the case (P+D) where the geometric stiffness matrix has  $\gamma$  equal to the limit load of the structure. Contrary to MRF-3, this frame had a good result for the case (D) in which only dead loads were used for the geometric stiffness. The reason for this behavior is clear upon observing the modal participation histories for the various cases as shown in Fig. C.5(d and e). The case (D) showed a history of modal participation factors almost identical to the (P+D) case. The first mode did not contribute significantly to the response. The success of case (D) can be considered coincidental. Again the initial displacement  $\mathbf{v}=\mathbf{U}_0$  was used in conjunction with the (P+D) case and was found to give excellent results.

EBF-1 is a three-story, single bay, eccentrically braced frame with an eccentricity of  $e=22$  inches. The frame was subjected to proportional loads at the top level. The topology along with the various computed response of the frame to the applied loading are shown in Fig. C.6. Both approximate methods gave a reasonable representation of the actual nonlinear behavior of the structure. Eqn. (2.13) slightly overestimated the response, while Eqn. (2.18) slightly underestimated the response. Both methods accurately reproduce the post-limit slope of the response curve, and give a correct representation of the rate of loss of carrying capacity of the structure. The method based on Eqn. (2.18) can be improved by noting that the structure responds predominantly in the third mode. The result of using the third mode in Eqn. (2.18) is also shown in Fig 2.6.

EBF-2 is a three-story, two bay, eccentrically braced frame having W14X43 beams, ST8X8X(5/6) braces, and W14X132 columns except for the bottom story interior column which is a



W14X426 section. The topology of the frame along with the proportion loads and the result of the different analyses are shown in Fig. C.7. The eccentricity of the frame was  $e=48$  inches. Observe that Eqn. (2.13) gave good estimate of the exact nonlinear behavior of the structure.

An interesting feature of the response of this structure is that modes four through nine has the greatest participation to the displacement field. In addition, modes four and five shift in importance as the deformation passed the limit-point. The computation using Eq. (2.18) were carried using mode one, four, and nine. It is clear that used of mode one does not give good results, and in fact, violates the lower-bound character suggested by Horne. Using either mode four or mode nine gave a better representation of the response than mode one.

#### C.4. Conclusions

An approximate method for tracing the nonlinear behavior of framed structures has been developed. The validity of the approximate method was shown through several examples with wide variety of types and properties under proportional and non-proportional loading cases. The approximate method is an extension and an improvement over the previous work done by Horne (1963).

The approximate method not only can trace the nonlinear behavior of a framed structure accurately, but also gives an insight into real nonlinear behavior of structures. The approximate method and the subsequent spectral analyses of the example problems demonstrated the role of geometric stiffness matrix in the nonlinear response and clarified the issue for non-proportional load case.

Table C.1. Member Properties

Frame	Stiffness Properties ( $\times 10^{-3}$ )			Yield Properties		
	EA (k)	$\kappa GA$ (k)	EI (k-ft <sup>2</sup> )	$N_0$ (k)	$V_0$ (k)	$M_0$ (k-ft <sup>2</sup> )
W14X43	365	183	86.2	449	83	206.3
W14X48	410	205	97.2	510	90	233.3
W14x53	425	266	108.9	560	102	260.4
W14x132	1125	563	308.1	1409	183	71.0
W14X426	3625	1813	1329	4705	610	2726.0
ST8X8X	1200	600	208.3	1650	500	583.3
"Column"	1200	600	208.3	1650	500	583.3

Table C.2. Frame MRF-4 Properties

Story	Column	Beam
1	W14X99	W14X38
2	W14X90	W14X34
3	W12X79	W14X30
4	W10X49	W12X26
5	W8X35	W12X22
6	W8X31	W10X22
7	W8X31	W8X21
8	W6X20	W8X18

Table C.3. Summary of Results

Frame	$\frac{\text{Approximate } \lambda_{cr}}{\text{Exact } \lambda_{cr}}$	Normalized Rankine Estimates of Limit Loads		$\frac{\text{Approximate } \Delta_{cr}}{\text{Exact } \Delta_{cr}}$
		$v = U_0$	$v = \phi_1$	
MRF-1	1.009	1.187	1.164	0.881
MRF-2	1.001	1.041	1.004	1.000
MRF-3	0.997	1.412	1.407	0.942
MRF-4	1.005	1.095	1.064	0.916
EBF-1	1.045	1.123	1.086	1.499
EBF-2	0.984	1.047	0.998	0.929



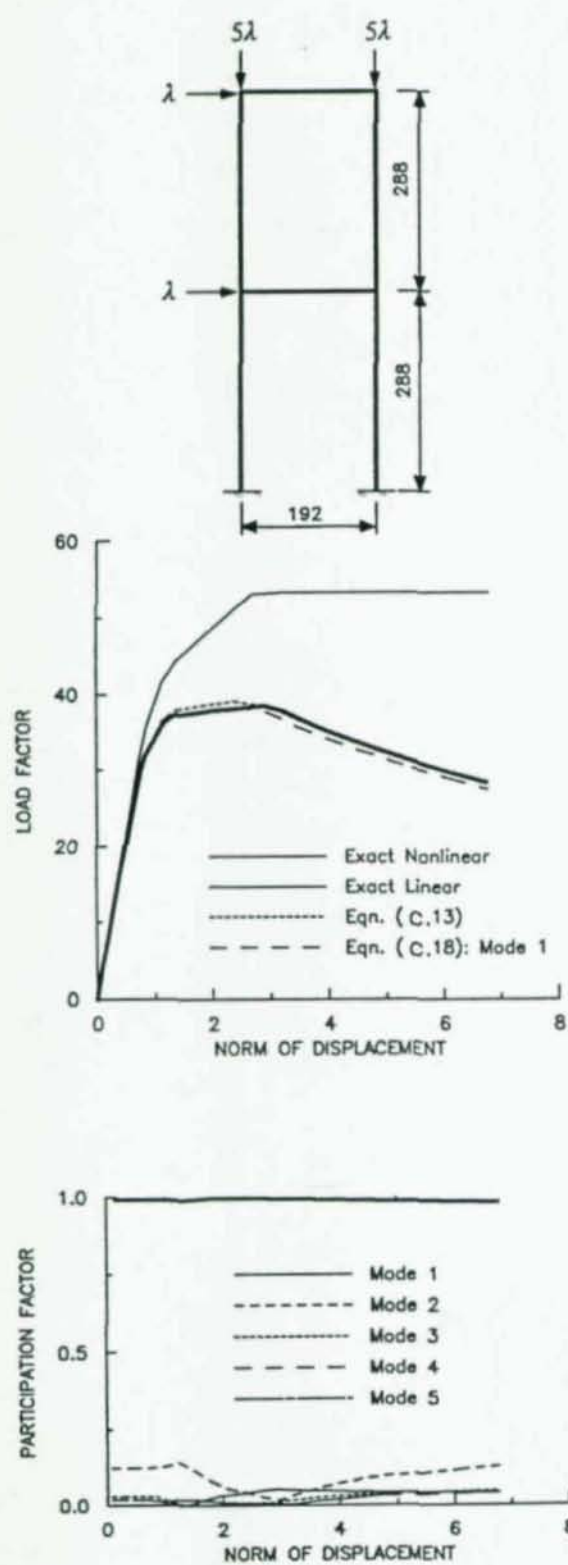


Fig. C.2. Response of MRF-1

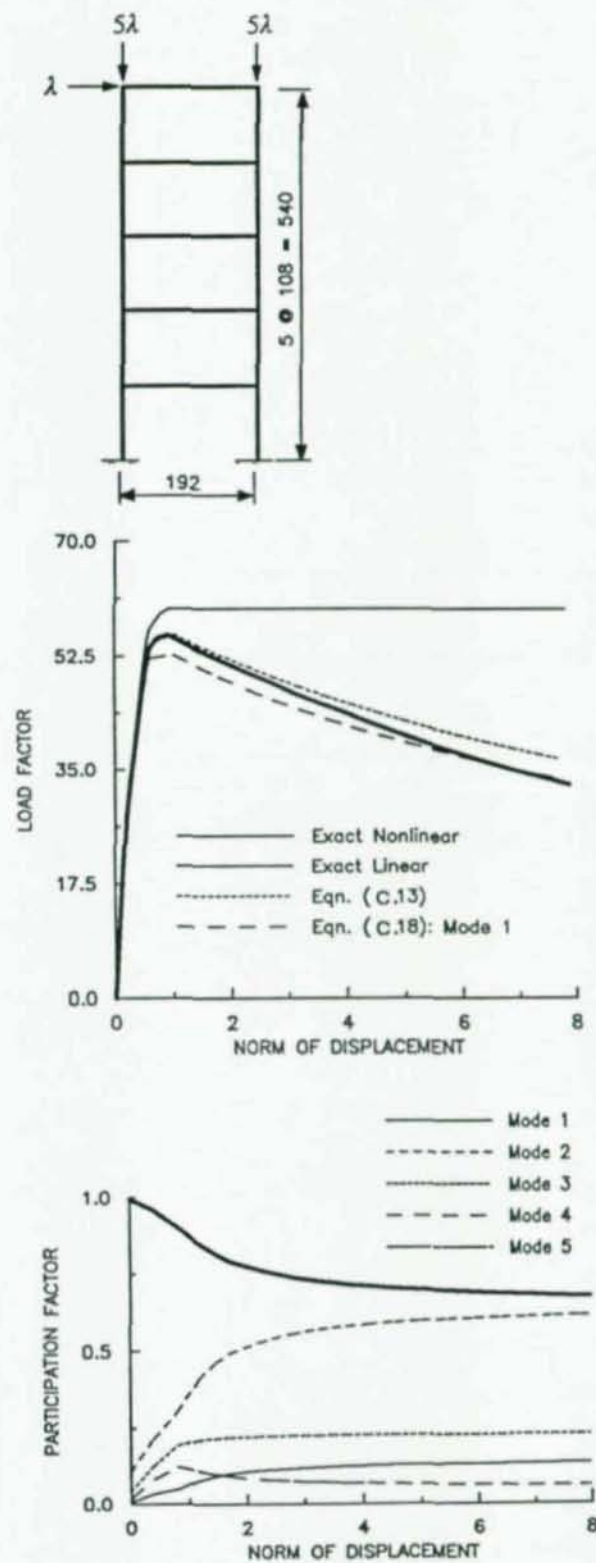


Fig. C.3. Response of MRF-2

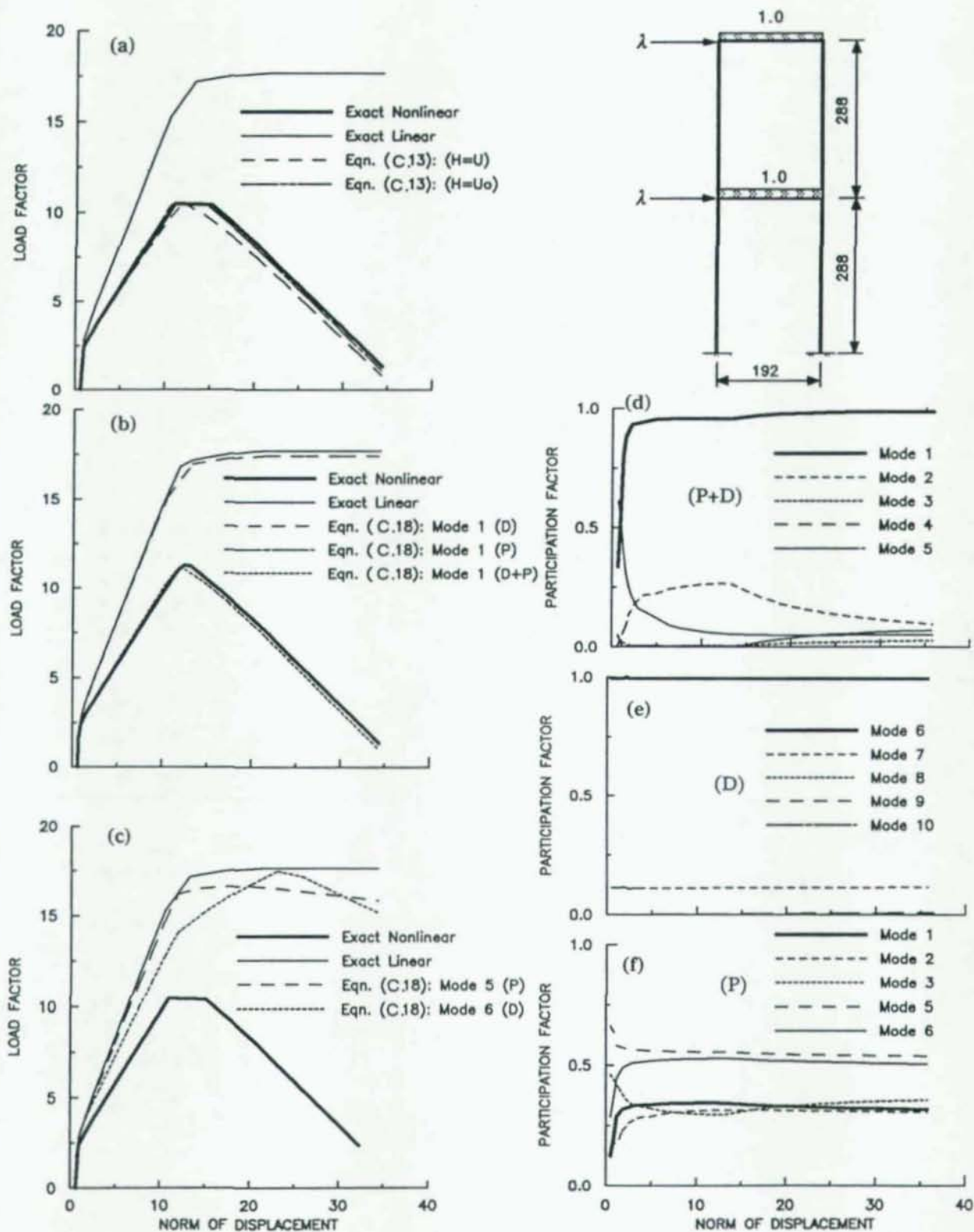


Fig. C.4. Response of MRF-3: (a) Estimates Based on Eqn. (2.13); (b) Estimates Based on Eqn. (2.18) Using Mode One; (c) Estimates Based on Eqn. (2.18) Using Other Modes; (d) Evolution of Participation Factors: (P+D) Case; (e) Evolution of Participation Factors: (D) Case; (f) Evolution of Participation Factors: (P) Case

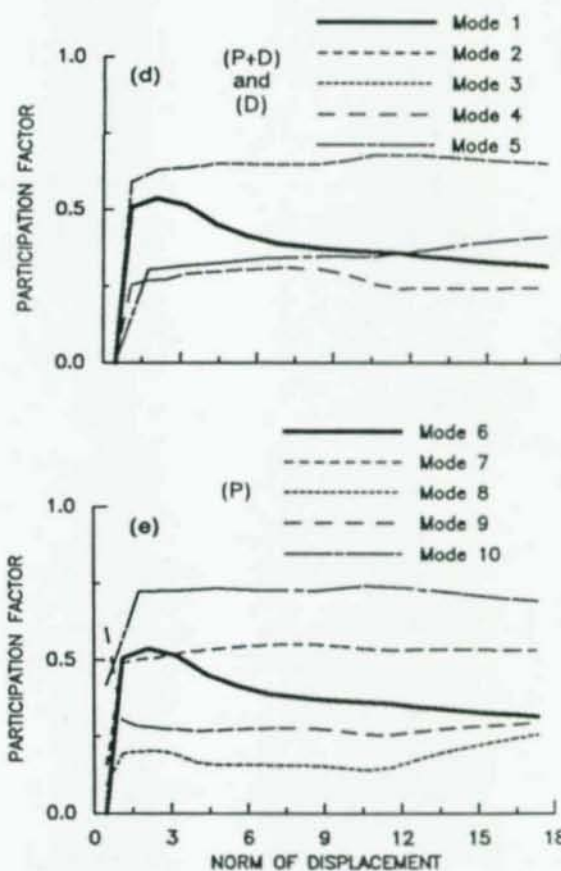
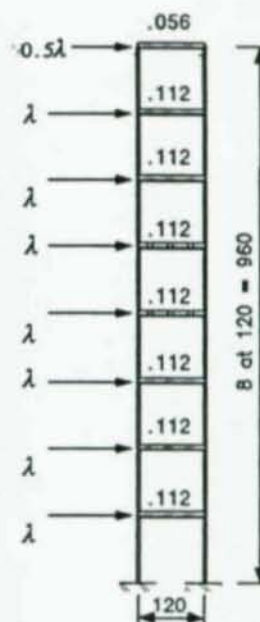
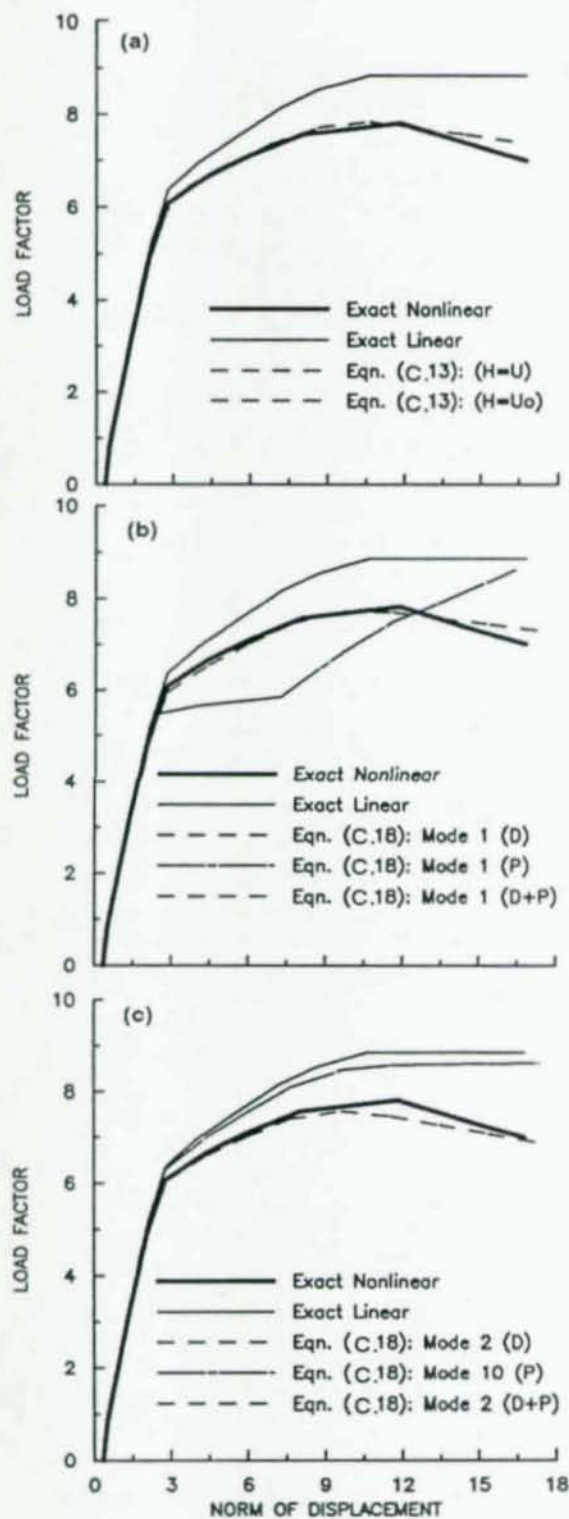


Fig. C.5. Response of MRF-4: (a) Estimates Based on Eqn. (2.13); (b) Estimates Based on Eqn. (2.18) Using Mode One; (c) Estimates Based on Eqn. (2.18) Using Other Modes; (d) Evolution of Participaton Factors: (P+D) and (D) Cases; (e) Evolution of Participation Factors: (P) Case



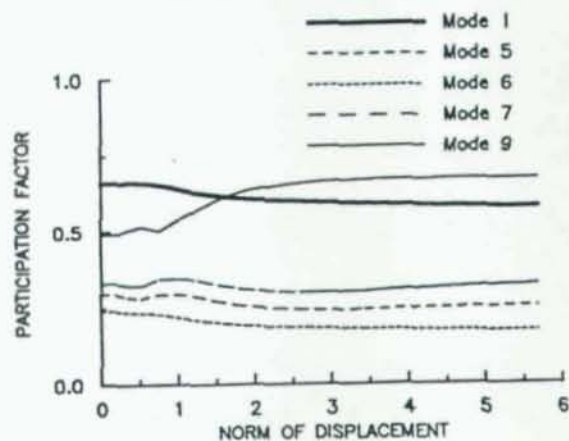
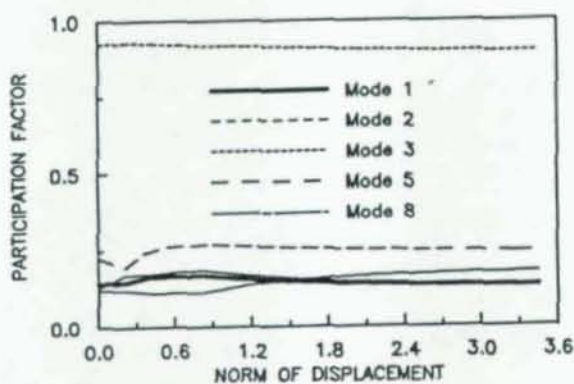
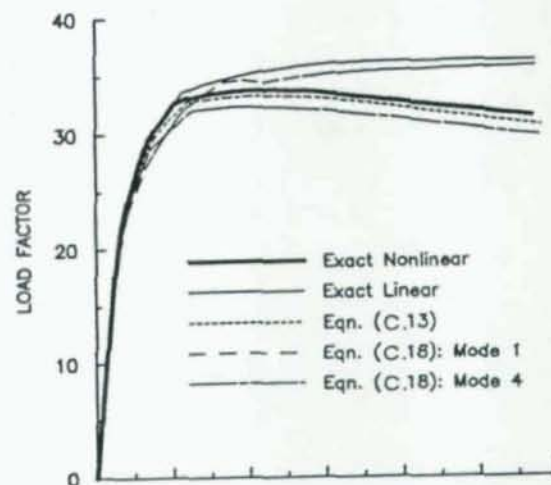
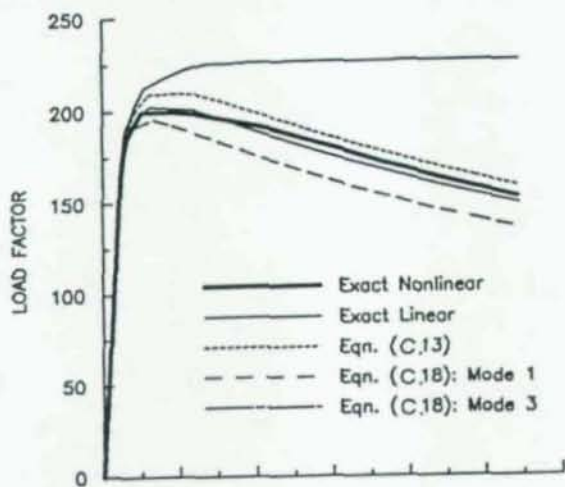
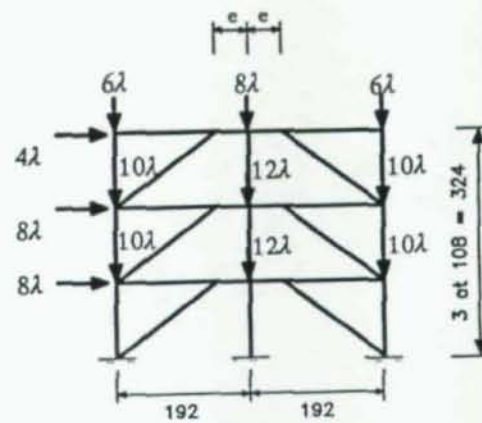
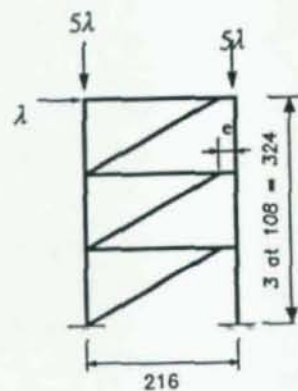


Fig C.6. Response of EBF-1

Fig C.7. Response of EBF-2

## APPENDIX D

### SENSITIVITY OF GEOMETRIC STIFFNESS MATRIX

#### D.1. Formulation

The weak form of the equilibrium equations can be expressed as (Simo *et al.* 1985):

$$G(u, \eta) \equiv \int_0^L R \cdot D\lambda \cdot \eta dx - \int_0^L q \eta_2 dx - [\eta \cdot \hat{R}]_{\partial R} \quad (D.1)$$

where  $u = [u, v, \psi]^t$  denotes the vector of generalized displacements,  $\partial R$  denotes those directions at  $x = 0$  and  $x = L$  subject to applied tractions,  $q$ , is the transversally applied load,  $\eta$  is a displacement field satisfying the displacement boundary conditions, and  $R \equiv [N, V, M]^t$  denotes the stress resultants conjugate to the strain measures  $\lambda \equiv [\lambda_n, \lambda_v, \lambda_\psi]^t$  which is expressed as:

$$\begin{aligned} \lambda_n &= u' + \frac{1}{2}(v')^2 - \frac{1}{2}\kappa\beta^2 \\ \lambda_v &= v' - (1 + u')\psi \\ \lambda_\psi &= \psi' \end{aligned} \quad (D.2)$$

where  $\beta \equiv v' - \psi$  and  $\kappa$  is the shear coefficient.

By defining the operator  $w \rightarrow B(w) \equiv [u', v', \psi', \psi]^t$  and noting (D.2), the expression for directional derivative of the strain measures can be written in the explicit form:

$$D\lambda \cdot \eta = \Xi(u)B(\eta) \quad (D.3)$$

where the matrix  $\Xi(u)$  is a matrix of strain gradient operator which reflects the effect of geometry on the equilibrium of the internal resisting forces  $R$  and is approximated to second order and was given in Eqn. (C.2) of Appendix C.

The geometric stiffness matrix was obtained by linearizing the weak form In Appendix C as:

$$G = \int_0^L B^t(\eta)A_g(R)B(u)dx \quad (D.4)$$

where  $A_g$  is given in Eqn. (C.5) and can be split into shear and axial parts as:

$$A_g^N = \begin{bmatrix} 0 & 0 & 0 & 0 \\ 0 & (1-\kappa) & 0 & \kappa \\ 0 & 0 & 0 & 0 \\ 0 & \kappa & 0 & -\kappa \end{bmatrix} \quad A_g^V = \begin{bmatrix} 0 & 0 & 0 & -v \\ 0 & 0 & 0 & 0 \\ 0 & 0 & 0 & 0 \\ -v & 0 & 0 & 0 \end{bmatrix} \quad (D.5)$$

Therefore, the geometric stiffness matrix can be written as:

$$G = N \int_0^L B^t(\eta) A_g^N B(u) dx + V \int_0^L B^t(\eta) A_g^V B(u) dx \quad (D.6)$$

Using a numerical integration scheme the geometric stiffness matrix  $G$  can be found as:

$$G_i = \frac{L}{2} \sum_{j=1}^{NGP} \left[ N_{ij} B^t(\xi_j) A_g^N B(\xi_j) + V_{ij} B^t(\xi_j) A_g^V B(\xi_j) \right] w_j \quad (D.7)$$

where  $N_{ij}$  = axial stress resultant of element  $i$  at gauss point  $j$ ,  $\xi_j$  = normalized coordinate at gauss point  $j$ ,  $w_j$  = numerical integration weighting factor, and  $NGP$  = the number of gauss points.

Taking the derivative of the geometric stiffness Eqn. (D.7) with respect to the design variables gives:

$$\frac{\partial G_i}{\partial x_k} = \frac{L}{2} \sum_{j=1}^{NGP} \left[ N_{ij,k} B^t(\xi_j) A_g^N B(\xi_j) + V_{ij,k} B^t(\xi_j) A_g^V B(\xi_j) \right] w_j \quad (D.8)$$

In order to determine the sensitivity of the geometric stiffness with respect to the design variables, we need to determine the sensitivity of the axial and shear resultant forces ( $N_{ij,k}$  and  $V_{ij,k}$ )

The resultant forces can be written as:

$$R = D \Xi B(\eta) \quad (D.9)$$

where  $D = \text{diag}[EA, \kappa GA, EI]$  being the elastic compliance matrix. Following the standard finite element discretization procedure, the displacement  $u = [u, v, \psi]^t$  can be interpolated as:

$$u(x) = \sum_{\alpha=1}^{nel} h_{\alpha} U_{\alpha} \quad (D.10)$$



where  $nel$  is the number of the nodes per element,  $h_a(x)$  are the  $C^0$  interpolation functions, and  $U_a = [U, V, \Psi]^t$  are the nodal displacements. From the interpolation (D.10) the operator  $B$  is given by:

$$B = \sum_{a=1}^N \hat{B}(x) U_a \quad (D.11)$$

where  $\hat{B}(x)$  is given by:

$$\hat{B}(x) = \begin{bmatrix} h'_a & 0 & 0 \\ 0 & h'_a & 0 \\ 0 & 0 & h'_a \\ 0 & 0 & h_a \end{bmatrix} \quad (D.12)$$

Substituting Eqs. (D.11) and (D.10) into (D.9) and taking the derivative gives:

$$R_{,k} = D_{,k} \Xi \sum_p^{nel} \hat{B}_p(x) U_p + D \Xi \sum_p^{nel} \hat{B}_p(x) U_{p,k} \quad (D.13)$$

To determine the derivative of the nodal displacement vector consider the discrete form of force displacement relationship:

$$KU = F \quad (D.14)$$

where  $K$  is the elastic stiffness matrix, and  $F$  is the nodal force vector. Taking the derivative of Eqn. (D.14) gives:

$$U_{,k} = K^{-1} K_{,k} U \quad (D.15)$$

Substituting Eqn. (D.15) into Eqn. (D.13) we can determine the derivative of the stress resultant forces as:

$$R_{,k} = D_{,k} \Xi \sum_p^{nel} \hat{B}_p(x) U_p + D \Xi \sum_p^{nel} \hat{B}_p(x) (K^{-1} K_{,k} U)_p \quad (D.16)$$

where  $R_{,k} \equiv [N_{,k}, V_{,k}, M_{,k}]^t$ . Having (D.16) the sensitivity of the geometric stiffness matrix can easily be determined from Eqn. (D.8).

## LIST OF REFERENCES

- ATC-3-06, Tentative Provisions for Development of Seismic Regulations for Buildings, Prepared by the Applied Technological Council, National Science Foundation, and National Bureau of Standards, NBS Special Publication, NSF Publication 78-8, June 1978.
- Adeli, H., H.M. Gere, and W. Weaver (February 1978). "Algorithms for Nonlinear Structural Dynamics." *Journal of Structural Division*, ASCE, 104(ST2), 263-280.
- Allwood, R.J., and Y.S. Chung (1984). "Minimum-Weight Design of Trusses by an Optimality Criteria Method." *International Journal for Numerical Methods in Engineering*, 20, 697-713.
- Ariarantnam, S.T. (1961). "The Southwell Method for Predicting Critical Loads of Elastic Structures." *Quarterly Journal of Mechanics and Applied Mathematics*, 14, 137-154.
- Atrek, E., R.H. Gallagher, K.M. Ragsdell, and O.C. Zienkiewics (1984). *New Directions in Optimum Structural Design*, John Wiley & Sons Ltd., New York.
- Balling, R.J., V. Ciampi, K.S. Pister, and E. Polak (1981). "Optimal Design of Seismic-Resistant Planar Steel Frames." *Report No. UBC/SESM-81/20*, University of California, Berkeley.
- Barnett, R.L. (Feb. 1961). "Minimum Weight Design of Beams for Deflection." *Journal of Engineering Mechanics Division*, Proceedings of ASCE, 87(EM1) 75-109.
- Batoz, J.-L. and G. Dhatt (1971). "Incremental Displacement Algorithms for Nonlinear Problems." *International Journal for Numerical Methods in Engineering*, 14, 1262-1267.
- Belytschko, T. and D.F. Schoeherle (Dec. 1975). "On the Conditional Stability of an Implicit Algorithm for Nonlinear Structural Dynamics." *Journal of Applied Mechanics*, 42, 865-969.
- Bendsoe, M.P., N. Olhoff, and J.E. Taylor (1983-1984). "A Variational Formulation for Multicriteria Structural Optimization." *J. Struct. Mech.*, 11(4), 523-544.
- Bendsoe, M.P., and J.E. Taylor (1984). "An Interpretation for Min-Max Structural Design Problems Including a Method for Relaxing Constraints." *Int. J. Solids Structures*, 20(4), 301-314.
- Berke, L. (July 1970). "An Efficient Approach to the Minimum Weight Design of Deflection Limited Structures." *AFFDL-TM-70-4-FDTR*, Flight Dynamics Laboratory, Wright-Patterson AFB, Ohio.
- Bertero, V.V. and H. Kamil (1975). "Nonlinear Seismic Design of Multistory Frames." *Can. J. Civ. Eng.* 2, 494-516.
- Carmichael, D.G. (1980). "Computation of Pareto Optima in Structural Design." *Int. J. Num. Meth. Engrg.*, 925-929.
- Cheng, F.Y. and K.Z. Truman (1985). "Optimal Design of 3-D Reinforced Concrete and Steel Buildings subjected to Static and Seismic Loads Including Code Provisions." *Structural Series 85-20*, Department of Civil Engineering, University of Missouri, Rolla, Missouri.



Chern, J.M., and W. Prager (June 1970). "Optimal Design of Beams for Prescribed Compliance under Alternative Loads." *Journal of Optimization Theory and Applications*, 5(6), 424-431.

Chern, J.M. (May 1971). "Optimal Design of Beams for Alternative Loads and Constraints on Generalized Compliance and Stiffness." *International Journal of Mechanical Science*, 13, 661-674.

Chern, J.M. and J.P. Martin (1971). "The Multipurpose Optimal Design of Elastic Structures with Piecewise Uniform Cross Section." *Journal of Applied Mathematics and Physics*, 22, Fasc. 5, 834-855.

Chern, J.M., and W. Prager (1971). "Minimum-Weight Design of Statically Determinate Trusses Subject to Multiple Constraints." *International Journal Solids & Structures*, 7, 931-940.

Clausen, T., *Über die Form architektonischer Säulen*. Bulletin physico-mathématique de l'Académie 9, 368-379 (St. Petersburg 1851). Also *Mélanges Mathématiques et Astronomiques*, Tome I (1849-1853), 279-294. St. Petersburg 1853. This work is summarized in Todhunter, I. and Pearson K., *A History of the Theory of Elasticity and of the Strength of Materials*, 2, 325-329, Cambridge 1893.

Cohon, L.C. (1979). *Multiobjective Programming and Planning*, Academic Press, New York.

Dailey, R.L. (April 1989). "Eigenvector Derivatives with Repeated Eigenvalues." *AIAA J.*, 27(4), 486-491.

Dlesk, D.C. and J.S. Liebman (1983). "Multi-objective Engineering Design." *Engineering Optimization*, 6.

Fluery, C., and C. Sanders (1977). "Relations Between Optimality Criteria and Mathematical Programming in Structural Optimization." *Proc. Symp. Application of Computer Methods in Engineering*, University of Southern California, Los Angeles, 507-520.

Fluery, C., and C. Sanders (1983). "Dual Method for Optimizing Finite Element Flexural Systems." *Computer Methods in Applied Mechanics and Engineering*, 37, 249-275.

Gajewski, A. and M. Zyczkowski (1988). *Optimal Structural Design Under Stability Constraints*, Kluwer Academic Publishers, Dordrecht, The Netherlands.

Galambos, T.V. and L.G. Maxwell L.G. (Aug. 1965). "Studies of the Ductility of Steel Structures." *Journal of the Structural Division*, No. (ST4), 125-151.

Gellatly, R.A., and L. Berke L. (April 1971). "Optimal Structural Design." *AFFDL-TR-70-165*, Air Force Flight Dynamics Laboratory, Wright-Patterson AFB, Ohio.

Goicoechea, A., D.R. Hansen D.R., and L. Duckstein (1982). *Multi-Objective Analysis with Engineering and Business Applications*, J. Wiley and Sons, New York.

Haug, E.J., K.K. Choi, and V. Konkov (1986). *Design Sensitivity Analysis of Structural Systems*, Academic Press, New York.



- Haug, E.J. and B. Rousselet (1980). "Design Sensitivity Analysis in Structural Mechanics II." *J. Struct. Mech.*, 8(2), 161-186.
- Hjelmstad, K.D. and E.P. Popov (July 1983). "Seismic Behavior of Active Beam Links in Eccentrically Braced Frames." *Report No. UBC/SESM-83/15*, University of California, Berkeley.
- Hjelmstad, K.D. and S. Pezeshk (May 1987). "Improving the Limit Behavior of Earthquake Resistant Steel Framed Structures." *ASCE EMD 6th Specialty Conference*, Buffalo, New York.
- Hjelmstad, K.D. and S. Pezeshk (Feb. 1988). "Approximate Analysis of Post-Limit Response of Frames." *J. of Struct. Eng.*, ASCE, 114(2).
- Hodge, P.G. (1959). *Plastic Analysis of Structures*, McGraw-Hill Book Company, New York.
- Horne, M. and L.J. Morris (Jan. 1962). "Optimum Design of Multi-Story Rigid Frames." *University of Wales at Swansea Conference*.
- Horne, M. (1962). "The Effect of Finite Deformations in Elastic Stability of Plane Frames." *Proceeding of the Royal Society of London, Series A*, 266, 47-68.
- Horne, M. (July 1963). "Elastic-Plastic Failure Loads of Plane Frames." *Proceedings of the Royal Society of London*, 274(1358).
- Horne, M., and W. Merchant W. (1965). *The Stability of Frames*, Pergamon Press, Oxford, Great Britain.
- Hughes, T.J.R. and K.S. Pister (1978). "Consistent Linearization in Mechanics of Solids and Structures." *Computers and Structures*, 8(2).
- Kamat, M.P., and P. Ruangsilasingha (1985). "Optimization of Space Trusses Against Instability Using Design Sensitivity Derivatives." *Eng. Opt.*, 177-188, 8.
- Kamat, M.P. (1987). "Optimization of Shallow Arches Against Instability Using Design Sensitivity Derivatives." *Finite Element in Analysis and Design*, 3, 277-284.
- Keller, J.B. (1960). "The Shape of the Strongest Column." *Archive for Rational Mechanics and Analysis*, 5(4), 275-285.
- Keller, J.B. and F.I. Niordson (1966). "The Tallest Column." *J. Math. Mech.*, 433-446.
- Kim, S.H. and Y.-K. Wen (Feb 1987). "Reliability-Based Structural Optimization under Stochastic Time Varying Loads." *Structural Research Series No. 533*, UILU-ENG-87-2003, Civil Engineering Studies, Univ. of Illinois, Urbana, IL.
- Kirch, U. (1981). *Optimum Structural Design*, McGraw Hill, New York.
- Khot, N.S. (1981). "Algorithm Based on Optimality Criteria to Design Minimum Weight Structures." *Engineering Optimization*, 5, 73-90.

Khot, N.S., V.B. Venkayya, and L. Berke (Dec. 1973). "Optimization of Structures for Strength and Stability Requirements." *AFFDL-TR-73-89*, Air Force Flight Dynamics Laboratory, Wright-Patterson AFB, Ohio.

Khot, N.S., V.B. Venkayya, and L. Berke (1976). "Optimum Structural Design with Stability Constraints." *International Journal for Numerical Methods in Engineering*, 10, 1097-1114.

Khot, N.S., L. Berke, and V.B. Venkayya (Feb. 1979). "Comparison of Optimality Criteria Algorithms for Minimum Weight Design of Structures." *AIAA Journal*, 17(2), 182-190.

Khot, N.S. (Aug. 1981). "Optimality Criteria Methods in Structural Optimization." *Technical Report AFWAL-TR-81-3124*.

Khot, N.S. and M.P. Kamat (May 1983). "Minimum Weight Design of Structures with Geometric Nonlinear Behavior." *24th Structural Dynamics and Material Conference*, Lake Tahoe, Nevada.

Korn, A., and T.V. Galambos (1968). "Behavior of Elastic-plastic Frames." *ASCE, Journal of the Structural Division*, 94(ST5).

Koski, J. (1979). "Truss Optimization with Vector Criterion." Tampere University of Technology, Publications 6, Tampere, Finland.

Koski, J. (1981). "Multi-Criterion Optimization in Structural Design." *Proceeding, Int'l Symp. on Optimum Structural Design*, Tuscon, Arizona.

Koski, J., and R. Silvennoinen (1982). "Pareto Optima of Isostatic Trusses." *Comp. Meth. Appl. Mech. Engrg.*, 265-279.

Lagrange, H.L. (1770-1773). *Sur La figure des colonnes*, Miscellanea Taurinensia (Royal Society of Turin), 123.

Levy, R. and H.-S. Perng (1988). "Optimization for Nonlinear Stability." *Computers & Structures*, 30(3), 529-535.

Lin, C.C. and I.W. Liu (1989). "Optimal Design Based on Optimality Criterion for Frame Structures Including Buckling Constraint." *Computers & Structures*, 31(4), 535-544.

Manual of Steel Construction, American Institute of Steel Construction, New York, 8th Edition.

Marsden, J.E., and T.J.R. Hughes (1983). *Mathematical Foundation of Elasticity*, Prentice-Hall, Inc., Englewood Cliffs, New Jersey.

Matrin, J.B. (Sept. 1969). "The Optimal Design of Beams and Frames with Compliance Constraints." *Division of Engineering, Brown University*, DA-ARO-D-31-124-G1025, Providence, R.I.

Martin, J.B. Communicated by W. Prager (July 1970). "Optimal Design of Elastic Structures for Multi-Purpose Loadings." *Journal of Optimization Theory and Applications*, 6(1), 22-40.



Masur, E.F., and Z. Mroz (1980). "Singular Solution in Structural Optimization Problems." *Proceedings IUTAM Symposium on Variational Methods in Mechanics of Solids* (S. Nemat-Nasser, ed.), Pergamon, New York, 337-343.

Menegotto, M., and P. Pinto (1973). "Method of Analysis for Cyclically Loaded Reinforced Concrete Frames Including Changes on Geometry and Nonelastic Behavior of Elements Under Combined Normal Force and Loadings." *IABSE Symposium on the Resistance of Ultimate Deformability of Structures Acted on by Well-Defined Repeated Loads*, Lisbon.

Molhem, Z. (1989). "A Geometrically Exact Elasto-Plastic 3-D Beam Element." CE-498 Class project, Dept. of Civil Engineering, University of Illinois, Urbana, IL.

Morris, A.J. (1982). *Foundations of Structural Optimization: A Unified Approach*, John Wiley and Sons, Inc., New York.

Nelson, R.B. (Sept. 1976). "Simplified Calculation of Eigenvector Derivatives." *AIAA Journal*, 14(9), 1201-1205.

Nguyen, D.T. and J.L. Roger, Jr. (1986). "Optimal Design of structures with Multiple Design Variables per Group and Multiple Loading Conditions on the Personal Computer." *Computers & Structures*, 22(2), 179-184.

Nikolai, E.L. (1955). "The Problem of Lagrange on Optimal Shapes of Columns." (in Russian), *IZV, Petersburg, Polit, Inst. 8, Trudy po mekhanike, Moskva*, 9-44.

No, M., and J.M. Aguinalalde (1987). "Finite Element Method and Optimality Criterion Based Structural Optimization." *Computers & Structures*, 27(2), 287-295.

Ojalvo, I.U. (Oct. 1987). "Efficient Computation of Mode-Shape Derivatives for Large Dynamic Systems." *AIAA journal*, 25(10), 1386-1390.

Ojalvo, I.U. "Gradients for Large Structural Models with Repeated Frequencies." *Aerospace Technology Conference and Exposition*, Society of Automotive Engineers, Warrendale, PA, Paper 86-1789.

Olhoff, N. and S.H. Rasmussen (1977). "On a Single and Bimodal Optimum Buckling Loads of Clamped Columns." *Int. J. Solids and Structures*, 13(7), 605-614.

Park, Y-J., and A.H.-S. Ang (1985). "Mechanistic Seismic Damage Model for Reinforced Concrete Buildings." *J. Struct. Engrg.*, ASCE, 111(4), 722-739.

Polak, E. and Y. Wardi (1982). *Computational Methods in Optimization: A Unified Approach*, Academic Press, New York.

Prager, W. (Nov. 1968). "Optimality in Structural Design." *Proceeding of National Academic of Sciences*, University of California (San Diego), 61(3), 794-796.



Prager, W. and R.T. Shield (1968). "Optimal Design of Multi-Purpose Structures." *International Journal of Solids & Structures*, 4, 469-475.

Prager, W. (July 1971). "Optimal Design of Statically Determinate Beams for Given Deflection." *International Journal of Mechanical Science*, 13, 893-895.

Prager, W. (March 1973). "Minimum Weight Design of a Statically Determinate Truss Subjected to Constraints on Compliance, Stress, and Cross Sectional Area." *Journal of Applied Mechanics*.

Prager, S. and W. Prager (1979). "A Note on Optimal Design of Columns." *Int. J. Mech. Sci.*, 21, 249-251.

Prager, W. and J.E. Taylor (March 1968). "Problems of Optimal Structural Design." *J. Applied Mechanics*, 35(1), Series E, 102-106.

Pique, R.J., and J.M. Roeset (Sept. 1976). "On the Use of Simple Models in Nonlinear Dynamic Analysis." *Report No. R76-43 Dept. of Civil Engineering*, MIT, Cambridge, Mass.

Popov, E.P., and V.V. Bertero (Sept. 1975). "Hysteretic Behavior of Steel Columns." *Report No. EERC 75-11*, University of California, Berkeley.

Rosenblueth, E. (1971). *Design of Earthquake Resistant Structures*, John Wiley & Sons Ltd., New York.

Sheu, C.Y., W. Prager, and communicated by H. Halkin (1968). "Minimum Weight Design with Piecewise Constant Specific Stiffness." *Journal of Optimization Theory and Applications*, 2(3), 179-186.

Simitses, G.J., M.P. Kamat, and C.V. Smith (1973). "The Strongest Column by the Finite Element Displacement Method." *AIAA Journal*, (10), 1409-1412.

Simo, J.C. (1982). "A Consistent Formulation of Nonlinear Theories of Elastic Beams and Plates." *Report No. UBC/SESM-82/06*, University of California, Berkeley.

Simo, J.C., K.D. Hjelmstad, and R.L. Taylor (1983). "Finite Element Formulations for Problems of Finite Deformation of Elasto-Viscoplastic Beams." *Report No. UBC/SESM-83/01*, University of California, Berkeley.

Simo, J.C. (1984). "On a One-Dimensional Finite Strain Beam Theory: The 3-Dimensional Dynamic Problem." *Report No. UBC/SESM-84/02*, University of California, Berkeley.

Simo, J.C. and R.L. Taylor (1985). "A Consistent Return Mapping Algorithm for Plane Stress Elasto-Plasticity." *Report No. UBC/SESM-85/04*, University of California, Berkeley.

Simo, J.C. and L. Vu-Quoc (1986). "A Three-Dimensional Finite Strain Rod Model. Part II: Computational Aspects." *Comput. Meth. Appl. Mech. Engng.*, 58,79-116.

Tada, Y. and Seguchi (1989). "Structural Shape Determination under Uncertain Loading Conditions." *Computational Mechanics*, (4), 219-228.

Tadzbakhash, I. J.B. Keller (1962). "Strongest Columns and Isoparametric Inequalities for Eigenvalues." *Journal of Applied Mechanics*, 29, 159-164.

Taylor, J.E. (1967). "The Strongest Column: An Energy Approach." *Journal of Applied Mechanics*, 34, 487-487.

Turner, H.T. and R.H. Plaut R.H. (Dec. 1980). "Optimal Design for Stability under Multiple Loads." *J. of Eng. Mech., ASCE*, 106(EM6), 1365-1382.

Uniform Building Code, International Conference of Building Officials, Whittier, CA, 1979 Edition.

Venkayya, V.B., N.S. Khot, V.A. Tischler, and R.F. Taylor (1971). "Design of Optimum Structures for Dynamic Loads." *Presented at the Third Air Force Conference on Matrix Methods in Structural Mechanics*, WPAFB, Ohio.

Venkayya, V.B., N.S. Khot, and L. Berke (April 1973). "Application of Optimality Criteria Approaches to Automated Design of Large Practical Structures." *Second Symposium on Structural Optimization*, AGARD Conference proceedings, (123), Milan, Italy, April.

Walker, N.D. Jr. (1977). "Automated Design of Earthquake Resistant Multistory Steel Building Frames." *Report No. UBC/SESM-77/12*, University of California, Berkeley.

Wardi, Y.Y. and E. Polak (1984). "A Nondifferentiable Optimization Algorithm for Structural Problems with Eigenvalue Inequality Constraints." *J. Struct. Mech.*, 11(4), 561-577.

Wen, Y.-K. (May 1977). "Statistical Combination of Extreme Loads." *J. Struct. Div., ASCE*, 103(ST5), 1079-1093.

Wen, Y.-K. (1980). "Methods for Reliability of Structures under Multiple Time Varying Loads." *Nuclear Engineering and Design*, 61-71, 60.

Wen, Y.-K. (Sept. 1980). "Reliability Analysis under the Combination of Stochastic Loads." *Proc. International Specialty Conf. on the Probabilistic Safety of Structures*, Paris, France.

Wen, Y.-K. and H.T. Pearce (March 1981). "Stochastic Models for Dependent Load Processes." *Structural Research Series No. 489*, UILU-ENG-81-2002, Civil Engineering Studies, Univ. of Illinois, Urbana, IL.

Wilson, E.L. and A. Habibullah (1984). "SAP80 Structural Analysis Programs, A Series of Computer Programs for Static and Dynamic Finite Element Analysis of Structures." Berkeley, California.

Zhong, W., and G. Cheng (1986). "Second-Order Sensitivity Analysis of Multimodal Eigenvalues and Related Optimization Techniques." *J. Struct. Mech.*, 14(4), 421-436.

Zienkiewicz, O.C. (1982). *The Finite Element Method*, McGraw Hill Book Company (UK) Limited, London, 3rd Edition.



